Vasco Miguel Graça Lopes

Licenciado em Engenharia Informática

Seeded Region Growing Methods for Automatic Upwelling Detection from Sea Surface Temperature Images

Dissertação para obtenção do Grau de Mestre em

Engenharia Informática

Orientadora: Susana Nascimento, Profª. Auxiliar, Faculdade de Ciências e Tecnologia
da Universidade Nova de Lisboa

Júri

Presidente: Doutor Pedro Abílio Duarte de Medeiros
Arguente: Doutor Victor José de Almeida e Sousa Lobo
Vogal: Doutora Susana Maria dos Santos Nascimento Martins de Almeida

FACULDADE DE CIÊNCIAS E TECNOLOGIA
UNIVERSIDADE NOVA DE LISBOA

Outubro, 2015

Seeded Region Growing Methods for Automatic Upwelling Detection from Sea Surface Temperature Images

Este documento foi gerado utilizando o processador (pdf)LaTeX, com base no template "unlthesis" [1] desenvolvido no Dep. Informática da FCT-NOVA [2]. [1] https://github.com/joaomlourenco/unlthesis [2] http://www.di.fct.unl.pt

Acknowledgements

Agradeço à orientadora, Profª. Susana Nascimento, pelo acompanhamento que prestou ao longo de todo o trabalho desta dissertação e pelo rigor que foi exigido em todas as etapas.

Agradeço também o auxílio que foi prestado pelo Prof. Boris Mirkin para encontrar soluções de controlo de explosões na segmentação de imagens das Canárias, e ao Sérgio Casca pela assistência que foi dada na implementação do algoritmo SEC.

Ao Instituto de Oceanografia da Universidade de Lisboa pela cedência das imagens de Portugal, bem como aos Professores Paulo Relvas e Joaquim Luís da Faculdade de Ciências e Tecnologia da Universidade do Algarve, pela preparação e cedência das imagens das Canárias.

Também quero referir o papel importante que os professores do Departamento de Informática da FCT-UNL tiveram no meu desenvolvimento ao longo do curso.

Resta agradecer aos meus amigos e colegas por me terem acampanhado nas exigências da experiência académica, bem como nos seus muitos aspectos positivos.

Abstract

Coastal upwelling is a phenomenon of ocean dynamics which the Oceanographers are very interested in detect and delimitate. However, it is a tedious work to manually extract the boundaries of the upwelling area, so automatic recognition is necessary. Recently it has been proposed a new algorithm for automatic upwelling detection and delineation of its fronts, the One Seed Expanding Clustering (SEC) (Nascimento et al. (2015)). The novel features of this algorithm, compared to Seeded Region Growing (SRG) methods, include a novel homogeneity criterion in the format of a product rather than the conventional difference between a pixel value and the mean of the values over the region of interest and, the automatic threshold of the homogeneity criterion which is mathematically derived from the criterion, used in the self-tuning version of the method.

The main goal of this dissertation was to advance in the development of this algorithm in the following aspects: to make a comparative study between distinct automatic thresholding techniques and the self-tuning version of the SEC algorithm, and also one between the SEC and several SRG algorithms selected from the literature. It was developed an iterative version of the SEC algorithm which allowed to correctly and automatically recognize discontinuous upwelling areas. The experimental results were analyzed using supervised evaluation measures, for images with ground-truth map, and unsupervised measures for images without ground-truth.

For the images with ground-truth map the SEC-SelfTuning achieved good results (F-measure ≥ 0.7) in 62.3% of the images, the SEC-Kittler was the most reliable of the SEC versions with 78.7% positive evaluations and, the method of Adams and Bischof (1994) was best of the SRG methods with 83.6% good scores, but with manual seed selection. For images without ground-truth, the mean rate of positive classifications, using the selected evaluation measures, was 69.7% for the SEC-SelfTuning, 72.4% for the best SEC version, SEC-Ridler, and 89.5% for the Adams and Bischof (1994) method.

Keywords: Automatic detection of upwelling, seeded region growing, automatic thresholding, evaluation methods for image segmentation.

Resumo

Afloramento costeiro é um fenómeno relacionado com a dinâmica dos oceanos que os oceanógrafos estão muito interessados em detectar e delimitar. No entanto, é um trabalho repetitivo e aborrecido de fazer, de modo que é necessário um sistema automático. Recentemente, foi proposto um novo algoritmo para a detecção automática de afloramento e delimitação das suas frentes, o *One Seed Expanding Clustering* (SEC) (Nascimento et al. (2015)). As novas características deste algoritmo, em comparação com os métodos *Seeded Region Growing* (SRG), incluem um novo critério de homogeneidade, no formato de um produto, em vez da habitual diferença entre um valor de um pixel e a média dos valores dentro da região de interesse e também, o *threshold* do critério de homogeneidade é derivado matematicamente deste critério, e é utilizado na versão auto-afinada do método.

O objetivo principal desta dissertação foi avançar no desenvolvimento deste algoritmo nos seguintes aspectos: fazer um estudo comparativo entre diversas técnicas de *thresholding* automático e a versão auto-afinada do algoritmo SEC, e também desenvolver um estudo entre o algoritmo SEC e vários algoritmos SRG selecionados da literatura. Foi desenvolvida uma versão iterativa do algoritmo SEC que permitiu reconhecer correctamente e automaticamente áreas de afloramento descontínuas. Os resultados experimentais foram analisados utilizando medidas de avaliação supervisionadas, em imagens com mapa de *ground-truth*, e medidas não supervisionadas para imagens sem *ground-truth*.

Para as imagens com *ground-truth*, o *SEC-SelfTuning* alcançou bons resultados (*F-measure* $\geq$ 0,7) em 62,3% das imagens, o *SEC-Kittler* foi o mais fiável das versões do SEC com 78,7% avaliações positivas, o método de Adams e Bischof (1994) foi o melhor método SRG com 83,6% de boas pontuações, mas com a selecção manual de sementes. Para imagens sem *ground-truth*, a taxa média de classificações positivas, utilizando as medidas não supervisionadas seleccionadas, foi de 69,7% para o *SEC-SelfTuning*, 72,4% para a melhor versão do SEC, o *SEC-Ridler*, e 89,5 % para o método de Adams e Bischof (1994).

Palavras-chave: Detecção automática de afloramento costeiro, *seeded region growing*, *thresholding* automático, métodos de avaliação de segmentação de imagem.

Contents

List of Figures **x**

List of Tables **xxii**

1 Introduction **1**
1.1 Motivation 1
1.2 Description and Context 3
1.3 Main Contributions 6
1.4 Document Organization 6

2 Related Work **7**
2.1 Introduction to Image Segmentation 7
2.2 Seeded Region Growing (SRG) 8
2.2.1 Overview of SRG methods 9
2.2.2 Domains of Applications 15
2.2.3 Selected SRG Methods for Sea Surface Temperature (SST) Image Analysis 17
2.3 Automatic Thresholding Techniques 22
2.3.1 Ridler and Calvard's method 24
2.3.2 Otsu's method 24
2.3.3 Kittler and Illingworth's method 24
2.4 Evaluation Measures for Image Segmentation 25
2.4.1 Supervised Evaluation Measures 25
2.4.2 Unsupervised Evaluation Measures 26

3 Proposed Approach **28**
3.1 The Seed Expanding Cluster (SEC) 28
3.1.1 The SEC method 28
3.1.2 The SEC Algorithm 28
3.1.3 Self-tuning version of SEC 32
3.2 Iterative Seed Expanding Cluster (I-SEC) 32
3.2.1 Termination condition 37
3.2.2 Threshold definition 39

3.3 Applying the SRG Methods to SST Image Analysis 42
3.3.1 Applying the Adams and Bischof Seeded Region Growing 43
3.3.2 Applying the Verma Seeded Region Growing 43
3.3.3 Applying the Shih and Cheng Seeded Region Growing 44
3.3.4 Applying the Gambotto Seeded Region Growing 45
3.3.5 Applying the Zanaty and Asaad Seeded Region Growing 45

4 Experimental Study **46**
4.1 Goals of the Study 46
4.2 Imagery Data 47
4.3 Setting of the Experiments 49
4.4 Supervised Analysis of SEC versions 51
4.4.1 SEC Automatic thresholding vs Self-tuning 51
4.4.2 SEC versions vs other SRG Methods 59
4.4.3 Study for SST Images of Canary 64
4.5 Unsupervised Analysis of SEC versions 71
4.5.1 Comparing the Unsupervised Evaluation Measures 71
4.5.2 SEC Automatic thresholding vs Self-tuning 75
4.5.3 SEC versions vs other SRG Methods 76
4.6 Tuning the Density Threshold of the SEC Algorithm 79
4.7 Outlook of the Results 79

5 Conclusion and Future Work **82**

Bibliography **84**

A Analysis of Experimental Results **90**
A.1 Discontinuity in the Upwelling Region 90
A.2 Validation of SRG methods 92
A.2.1 Validation of SRG methods with the F-measure 92
A.2.2 Validation of SRG methods with ARI index 99
A.2.3 Validation of SRG methods with unsupervised evaluation measures 101
A.3 Thresholds of the Unsupervised Evaluation Measures 111
A.4 Empirical Study of Density Threshold 112
A.5 Iterative Procedure Segmentation Study 113
A.5.1 Iterative Procedure for the SEC-Otsu 113
A.5.2 Iterative Procedure for the SEC-Kittler 116
A.5.3 Iterative Procedure for the SEC-Ridler 118
A.5.4 Iterative Procedure for the SEC-SelfTuning 120
A.5.5 Iterative Procedure for the OtsuVermaSRG 123
A.5.6 Iterative Procedure for the MeanVermaSRG 126
A.5.7 Iterative Procedure for the ShihSRG 129

A.5.8 Iterative Procedure for the GambottoSRG 130
A.5.9 Iterative Procedure for the ZanatySRG 133

B Segmentation Results **135**
B.1 SST Images with GT / Strong Gradients from 1998 135
B.2 SST Images with GT / Weak Gradients from 1998 141
B.3 SST Images with GT / Noisy from 1998 151
B.4 SST Images with GT from 1999 155
B.5 SST Images without ground-truth (NGT) from 1998 159
B.6 SST Images NGT from 2000 161
B.7 SST Images NGT from 2001 163
B.8 SST Images NGT from 2002 165
B.9 SST Images from the Canary 167

List of Figures

1.1 SST image of the portuguese coast (1 August 1998). The temperature values are codified in a color scale, where blue represents colder waters and red warmer waters. The white pixels represent land in the continental area, or noise derived from clouds or transmission errors from the satellite in the ocean area. 2

3.1 SST image of the portuguese coast (12 June 1998). At least two relatively large, not contiguous, upwelling areas can be distinguished in this image, one in the north and other in the south, which are separated by warmer waters in the middle of the image. 32
3.2 1998-08-05 SEC-SelfTuning 37
3.3 1998-08-05 ground-truth map 37
3.4 1998-09-24 SEC-Kittler 37
3.5 1998-09-24 ground-truth map 37
3.6 The plot shows the percentage for each termination possibility of the iterative procedure, organized by sets of images, in this case for the results of the SEC-SelfTuning. 38
3.7 Data related to the iterative procedure applied to the SEC-SelfTuning for the SST images of 1998 with ground-truth. The graphic which includes the values for the difference between the mean of the first region and the minimum of one relevant cluster, the relevant cluster has different meanings depending of which category described in the legend. It also includes, for each SST image, the number of the iteration that the last region of upwelling was extracted and the reason why the iterative procedure ended. 41
3.8 Data related to the iterative procedure applied to the SEC-SelfTuning for the SST images of 1999 with ground-truth. 42

4.1 Two SST images of Portugal, the one in the left was captured in 2 August 1998 and the one in the right in 28 July 1998. 48
4.2 The ground-truth images correspondent to the SST images of 2 August 1998 in the left and of 28 July 1998 in the right. The white area represents noise, land or clouds, the light blue area contains the waters that are not part of the upwelling zone, and the dark blue area is the upwelling area. 49

4.3 SST Image from the Canary, named *img*_58, in the left, and the correspondent ground-truth in the right. 49
4.4 F-measure results for the comparative study between the SEC algorithm versions. The segmentation results are from the SST images of the portuguese coast from the year 1998, which was divided into subsets of images with strong gradients in the frontier of the upwelling area, weak gradients and images with noise, from left to right in the graphic correspondingly. 53
4.5 Similarity thresholds that were calculated for each of the SEC algorithm versions. Higher thresholds will contain more the growth of the clusters than smaller ones. The segmentation results are from the SST images of the portuguese coast from the year 1998, which was divided into subsets of images with strong gradients in the frontier of the upwelling area, weak gradients and images with noise, from left to right in the graphic correspondingly. 54
4.6 F-measure results for the comparative study between the SEC algorithm versions. The segmentation results are from the SST images of the portuguese coast from the year 1999. 55
4.7 Similarity thresholds that were calculated for each of the SEC algorithm versions. Higher thresholds will contain more the growth of the clusters than smaller ones. The segmentation results are from the SST images of the portuguese coast from the year 1999. 56
4.8 The graphic shows the improvements that the fine-tuning of the density threshold can have in the F-measure score. It is compared the SEC-Otsu and SEC-SelfTuning versions with their own versions, but with the fine-tuning of the density threshold. The segmentation results are from the SST images of the portuguese coast from the year 1998, which was divided into subsets of images with strong gradients in the frontier of the upwelling area, weak gradients and images with noise, from left to right in the graphic correspondingly. 57
4.9 The graphic shows the improvements that the fine-tuning of the density threshold can have in the F-measure score. It is compared the SEC-Otsu and SEC-SelfTuning versions with their own versions, but with the fine-tuning of the density threshold. The segmentation results are from the SST images of the portuguese coast from the year 1999. 58
4.10 SST Image from 18 of June 1998, in the left, and the correspondent ground-truth map in the right. 59
4.11 SST Image from 18 of June 1998, in the left without the fine-tuning of the density threshold, and in the right the fine-tuning version, with the density threshold set to 0.3878. It is an example of how the quality of the segmentation result can be improved. The extracted upwelling region is the pink area and the initial seed is at the black marker. 59

4.12 F-measure results for each of the SRG methods visualized in a box plot, making it possible to understand the variation of the results in the set of SST images from 1998. The box represents 50% of the data and its lower and upper lines are at the 25% and 75% quantile of the data. The remaining results are inside the vertical lines, with exception for the outliers that are represented by the plus symbols. 63
4.13 F-measure results for each of the SRG methods visualized in a box plot, making it possible to understand the variation of the results in the set of SST images from 1999. 64
4.14 F-measure results for the comparative study between the SEC algorithm versions. The segmentation results are from the SST images of the Canary. . . . 66
4.15 Similarity thresholds that were calculated for each of the SEC algorithm versions. Higher thresholds will contain more the growth of the clusters than smaller ones. The segmentation results are from the SST images of the Canary. 67
4.16 The graphic shows the improvements that the fine-tuning of the density threshold can have in the F-measure score. It is compared the SEC-Otsu and SEC-SelfTuning versions with their own versions, but with the fine-tuning of the density threshold. The segmentation results are from the SST images of the Canary. 68
4.17 F-measure results for each of the SRG methods visualized in a box plot, making it possible to understand the variation of the results in the set of SST images of the Canary. 71
4.18 Correlation factors between the F-measure and the unsupervised evaluation measures, for each of the versions of the SEC algorithm. It is important to have into consideration which methods should have positive and negative correlation values. 73
4.19 Correlation factors between the F-measure and the unsupervised evaluation measures, for each of the SRG methods. It is important to have into consideration which methods should have positive and negative correlation values. . 73

A.1 SST Image from 29 of July 1999, in the left, and the correspondent ground-truth in the right. It is an example of how noise, in this case clouds, can interfere and make necessary to the region growing algorithms to extract more than one cluster for just one continuous upwelling area. In this case, there are only one upwelling region, but the algorithm must extract two continuous regions. 91
A.2 SST Image from 21 of July 1999, in the left, and the correspondent ground-truth in the right. This image has a type of noise that is not caused by clouds, which cuts the upwelling area in two and make it necessary to the region growing algorithms to extract more than one cluster. There are only one upwelling region, but the algorithm must extract two continuous regions. . . 91

A.3 ARI results for the comparative study between the SEC algorithm versions. The segmentation results are from the SST images of the portuguese coast from the year 1998, which was divided into subsets of images with strong gradients in the frontier of the upwelling area, weak gradients and images with noise, from left to right in the graphic correspondingly. 99
A.4 ARI results for the comparative study between the SEC algorithm versions. The segmentation results are from the SST images of the portuguese coast from the year 1999. 100
A.5 ARI results for the comparative study between the SEC algorithm versions. The segmentation results are from the SST images of the Canary. 100
A.6 Inter-Otsu results for each of the SRG methods visualized in a box plot, making it possible to understand the variation of the results in the set of SST images from 1998 with no ground-truth map. 101
A.7 Inter-Otsu results for each of the SRG methods visualized in a box plot, making it possible to understand the variation of the results in the set of SST images from 2000 with no ground-truth map. 101
A.8 Inter-Otsu results for each of the SRG methods visualized in a box plot, making it possible to understand the variation of the results in the set of SST images from 2001 with no ground-truth map. 102
A.9 Inter-Otsu results for each of the SRG methods visualized in a box plot, making it possible to understand the variation of the results in the set of SST images from 2002 with no ground-truth map. 102
A.10 Inter-FRC results for each of the SRG methods visualized in a box plot, making it possible to understand the variation of the results in the set of SST images from 1998 with no ground-truth map. 103
A.11 Inter-FRC results for each of the SRG methods visualized in a box plot, making it possible to understand the variation of the results in the set of SST images from 2000 with no ground-truth map. 103
A.12 Inter-FRC results for each of the SRG methods visualized in a box plot, making it possible to understand the variation of the results in the set of SST images from 2001 with no ground-truth map. 104
A.13 Inter-FRC results for each of the SRG methods visualized in a box plot, making it possible to understand the variation of the results in the set of SST images from 2002 with no ground-truth map. 104
A.14 Intra-FRC results for each of the SRG methods visualized in a box plot, making it possible to understand the variation of the results in the set of SST images from 1998 with no ground-truth map. 105
A.15 Intra-FRC results for each of the SRG methods visualized in a box plot, making it possible to understand the variation of the results in the set of SST images from 2000 with no ground-truth map. 105

A.16 Intra-FRC results for each of the SRG methods visualized in a box plot, making it possible to understand the variation of the results in the set of SST images from 2001 with no ground-truth map. 106
A.17 Intra-FRC results for each of the SRG methods visualized in a box plot, making it possible to understand the variation of the results in the set of SST images from 2002 with no ground-truth map. 106
A.18 CalinskiHarabasz results for each of the SRG methods in a box plot, making it possible to understand the variation of the results in the set of SST images from 1998 with no ground-truth map. 107
A.19 CalinskiHarabasz results for each of the SRG methods in a box plot, making it possible to understand the variation of the results in the set of SST images from 2000 with no ground-truth map. 107
A.20 CalinskiHarabasz results for each of the SRG methods in a box plot, making it possible to understand the variation of the results in the set of SST images from 2001 with no ground-truth map. 108
A.21 CalinskiHarabasz results for each of the SRG methods in a box plot, making it possible to understand the variation of the results in the set of SST images from 2002 with no ground-truth map. 108
A.22 Differences between the best density threshold and the empirically selected thresholds for the SEC-SelfTuning in 1998 images. Lower differences are best. 112
A.23 Differences between the empirically selected thresholds and 0.0204 for the SEC-SelfTuning in 1998 images. Higher differences are best. 112
A.24 Data related to the iterative procedure applied to the SEC-Otsu for the SST images from 1998 with ground-truth. 113
A.25 Data related to the iterative procedure applied to the SEC-Otsu for the SST images from 1999 with ground-truth. 114
A.26 Data related to the iterative procedure applied to the SEC-Otsu for the SST images of the Canary with ground-truth. 114
A.27 The plot shows the percentage for each termination possibility of the iterative procedure, organized by sets of images, in this case for the results of the SEC-Otsu. 115
A.28 Data related to the iterative procedure applied to the SEC-Kittler for the SST images from 1998 with ground-truth. 116
A.29 Data related to the iterative procedure applied to the SEC-Kittler for the SST images from 1999 with ground-truth. 116
A.30 Data related to the iterative procedure applied to the SEC-Kittler for the SST images of the Canary with ground-truth. 117
A.31 The plot shows the percentage for each termination possibility of the iterative procedure, organized by sets of images, in this case for the results of the SEC-Kittler. 117

A.32 Data related to the iterative procedure applied to the SEC-Ridler for the SST images from 1998 with ground-truth. 118
A.33 Data related to the iterative procedure applied to the SEC-Ridler for the SST images from 1999 with ground-truth. 118
A.34 Data related to the iterative procedure applied to the SEC-Ridler for the SST images of the Canary with ground-truth. 119
A.35 The plot shows the percentage for each termination possibility of the iterative procedure, organized by sets of images, in this case for the results of the SEC-Ridler. 119
A.36 Data related to the iterative procedure applied to the SEC-SelfTuning for the SST images from 1998 with ground-truth. 120
A.37 Data related to the iterative procedure applied to the SEC-SelfTuning for the SST images from 1999 with ground-truth. 120
A.38 Data related to the iterative procedure applied to the SEC-SelfTuning for the SST images of the Canary with ground-truth. 121
A.39 The plot shows the percentage for each termination possibility of the iterative procedure, organized by sets of images, in this case for the results of the SEC-SelfTuning. 122
A.40 Data related to the iterative procedure applied to the OtsuVermaSRG for the SST images from 1998 with ground-truth. 123
A.41 Data related to the iterative procedure applied to the OtsuVermaSRG for the SST images from 1999 with ground-truth. 123
A.42 Data related to the iterative procedure applied to the OtsuVermaSRG for the SST images of the Canary with ground-truth. 124
A.43 The plot shows the percentage for each termination possibility of the iterative procedure, organized by sets of images, in this case for the results of the OtsuVermaSRG. 125
A.44 Data related to the iterative procedure applied to the MeanVermaSRG for the SST images from 1998 with ground-truth. 126
A.45 Data related to the iterative procedure applied to the MeanVermaSRG for the SST images from 1999 with ground-truth. 126
A.46 Data related to the iterative procedure applied to the MeanVermaSRG for the SST images of the Canary with ground-truth. 127
A.47 The plot shows the percentage for each termination possibility of the iterative procedure, organized by sets of images, in this case for the results of the MeanVermaSRG. 128
A.48 Data related to the iterative procedure applied to the ShihSRG for the SST images from 1998 with ground-truth. 129
A.49 Data related to the iterative procedure applied to the ShihSRG for the SST images from 1999 with ground-truth. 129

A.50 Data related to the iterative procedure applied to the ShihSRG for the SST images of the Canary with ground-truth. 130
A.51 Data related to the iterative procedure applied to the GambottoSRG for the SST images from 1998 with ground-truth. 130
A.52 Data related to the iterative procedure applied to the GambottoSRG for the SST images from 1999 with ground-truth. 131
A.53 Data related to the iterative procedure applied to the GambottoSRG for the SST images of the Canary with ground-truth. 131
A.54 The plot shows the percentage for each termination possibility of the iterative procedure, organized by sets of images, in this case for the results of the GambottoSRG. 132
A.55 Data related to the iterative procedure applied to the ZanatySRG for the SST images from 1998 with ground-truth. 133
A.56 Data related to the iterative procedure applied to the ZanatySRG for the SST images from 1999 with ground-truth. 133
A.57 Data related to the iterative procedure applied to the ZanatySRG for the SST images of the Canary with ground-truth. 134
A.58 The plot shows the percentage for each termination possibility of the iterative procedure, organized by sets of images, in this case for the results of the ZanatySRG. 134

B.1 1998-08-02 135
B.2 1998-08-02 ground-truth map 135
B.3 1998-08-02 SEC-Otsu 135
B.4 1998-08-02 SEC-Kittler 135
B.5 1998-08-02 SEC-Ridler 136
B.6 1998-08-02 SEC-SelfTuning 136
B.7 1998-08-02 AdamsSRG 136
B.8 1998-08-02 OtsuVermaSRG 136
B.9 1998-08-02 MeanVermaSRG 136
B.10 1998-08-02 ShihSRG 136
B.11 1998-08-02 GambottoSRG 137
B.12 1998-08-02 ZanatySRG 137
B.13 1998-08-05 137
B.14 1998-08-05 ground-truth map 137
B.15 1998-08-05 SEC-Otsu 137
B.16 1998-08-05 SEC-Kittler 137
B.17 1998-08-05 SEC-Ridler 138
B.18 1998-08-05 SEC-SelfTuning 138
B.19 1998-08-05 AdamsSRG 138
B.20 1998-08-05 OtsuVermaSRG 138

B.21 1998-08-05 MeanVermaSRG 138
B.22 1998-08-05 ShihSRG 138
B.23 1998-08-05 GambottoSRG 139
B.24 1998-08-05 ZanatySRG 139
B.25 1998-09-15 139
B.26 1998-09-15 ground-truth map 139
B.27 1998-09-15 SEC-Otsu 139
B.28 1998-09-15 SEC-Kittler 139
B.29 1998-09-15 SEC-Ridler 140
B.30 1998-09-15 SEC-SelfTuning 140
B.31 1998-09-15 AdamsSRG 140
B.32 1998-09-15 OtsuVermaSRG 140
B.33 1998-09-15 MeanVermaSRG 140
B.34 1998-09-15 ShihSRG 140
B.35 1998-09-15 GambottoSRG 141
B.36 1998-09-15 ZanatySRG 141
B.37 1998-06-14 141
B.38 1998-06-14 ground-truth map 141
B.39 1998-06-14 SEC-Otsu 141
B.40 1998-06-14 SEC-Kittler 141
B.41 1998-06-14 SEC-Ridler 142
B.42 1998-06-14 SEC-SelfTuning 142
B.43 1998-06-14 AdamsSRG 142
B.44 1998-06-14 OtsuVermaSRG 142
B.45 1998-06-14 MeanVermaSRG 142
B.46 1998-06-14 ShihSRG 142
B.47 1998-06-14 GambottoSRG 143
B.48 1998-06-14 ZanatySRG 143
B.49 1998-07-11 143
B.50 1998-07-11 ground-truth map 143
B.51 1998-07-11 SEC-Otsu 143
B.52 1998-07-11 SEC-Kittler 143
B.53 1998-07-11 SEC-Ridler 144
B.54 1998-07-11 SEC-SelfTuning 144
B.55 1998-07-11 AdamsSRG 144
B.56 1998-07-11 OtsuVermaSRG 144
B.57 1998-07-11 MeanVermaSRG 144
B.58 1998-07-11 ShihSRG 144
B.59 1998-07-11 GambottoSRG 145
B.60 1998-07-11 ZanatySRG 145
B.61 1998-07-15 145

B.62 1998-07-15 ground-truth map . . . 145
B.63 1998-07-15 SEC-Otsu . . . 145
B.64 1998-07-15 SEC-Kittler . . . 145
B.65 1998-07-15 SEC-Ridler . . . 146
B.66 1998-07-15 SEC-SelfTuning . . . 146
B.67 1998-07-15 AdamsSRG . . . 146
B.68 1998-07-15 OtsuVermaSRG . . . 146
B.69 1998-07-15 MeanVermaSRG . . . 146
B.70 1998-07-15 ShihSRG . . . 146
B.71 1998-07-15 GambottoSRG . . . 147
B.72 1998-07-15 ZanatySRG . . . 147
B.73 1998-08-23 . . . 147
B.74 1998-08-23 ground-truth map . . . 147
B.75 1998-08-23 SEC-Otsu . . . 147
B.76 1998-08-23 SEC-Kittler . . . 147
B.77 1998-08-23 SEC-Ridler . . . 148
B.78 1998-08-23 SEC-SelfTuning . . . 148
B.79 1998-08-23 AdamsSRG . . . 148
B.80 1998-08-23 OtsuVermaSRG . . . 148
B.81 1998-08-23 MeanVermaSRG . . . 148
B.82 1998-08-23 ShihSRG . . . 148
B.83 1998-08-23 GambottoSRG . . . 149
B.84 1998-08-23 ZanatySRG . . . 149
B.85 1998-09-08 . . . 149
B.86 1998-09-08 ground-truth map . . . 149
B.87 1998-09-08 SEC-Otsu . . . 149
B.88 1998-09-08 SEC-Kittler . . . 149
B.89 1998-09-08 SEC-Ridler . . . 150
B.90 1998-09-08 SEC-SelfTuning . . . 150
B.91 1998-09-08 AdamsSRG . . . 150
B.92 1998-09-08 OtsuVermaSRG . . . 150
B.93 1998-09-08 MeanVermaSRG . . . 150
B.94 1998-09-08 ShihSRG . . . 150
B.95 1998-09-08 GambottoSRG . . . 151
B.96 1998-09-08 ZanatySRG . . . 151
B.97 1998-07-07 . . . 151
B.98 1998-07-07 ground-truth map . . . 151
B.99 1998-07-07 SEC-Otsu . . . 151
B.100 1998-07-07 SEC-Kittler . . . 151
B.101 1998-07-07 SEC-Ridler . . . 152
B.102 1998-07-07 SEC-SelfTuning . . . 152

B.103 1998-07-07 AdamsSRG . . . 152
B.104 1998-07-07 OtsuVermaSRG . . . 152
B.105 1998-07-07 MeanVermaSRG . . . 152
B.106 1998-07-07 ShihSRG . . . 152
B.107 1998-07-07 GambottoSRG . . . 153
B.108 1998-07-07 ZanatySRG . . . 153
B.109 1998-09-30 . . . 153
B.110 1998-09-30 ground-truth map . . . 153
B.111 1998-09-30 SEC-Otsu . . . 153
B.112 1998-09-30 SEC-Kittler . . . 153
B.113 1998-09-30 SEC-Ridler . . . 154
B.114 1998-09-30 SEC-SelfTuning . . . 154
B.115 1998-09-30 AdamsSRG . . . 154
B.116 1998-09-30 OtsuVermaSRG . . . 154
B.117 1998-09-30 MeanVermaSRG . . . 154
B.118 1998-09-30 ShihSRG . . . 154
B.119 1998-09-30 GambottoSRG . . . 155
B.120 1998-09-30 ZanatySRG . . . 155
B.121 1999-09-01 . . . 155
B.122 1999-09-01 ground-truth map . . . 155
B.123 1999-09-01 SEC-Otsu . . . 155
B.124 1999-09-01 SEC-Kittler . . . 155
B.125 1999-09-01 SEC-Ridler . . . 156
B.126 1999-09-01 SEC-SelfTuning . . . 156
B.127 1999-09-01 AdamsSRG . . . 156
B.128 1999-09-01 OtsuVermaSRG . . . 156
B.129 1999-09-01 MeanVermaSRG . . . 156
B.130 1999-09-01 ShihSRG . . . 156
B.131 1999-09-01 GambottoSRG . . . 157
B.132 1999-09-01 ZanatySRG . . . 157
B.133 1999-09-10 . . . 157
B.134 1999-09-10 ground-truth map . . . 157
B.135 1999-09-10 SEC-Otsu . . . 157
B.136 1999-09-10 SEC-Kittler . . . 157
B.137 1999-09-10 SEC-Ridler . . . 158
B.138 1999-09-10 SEC-SelfTuning . . . 158
B.139 1999-09-10 AdamsSRG . . . 158
B.140 1999-09-10 OtsuVermaSRG . . . 158
B.141 1999-09-10 MeanVermaSRG . . . 158
B.142 1999-09-10 ShihSRG . . . 158
B.143 1999-09-10 GambottoSRG . . . 159

B.144 1999-09-10 ZanatySRG . . . 159
B.145 1998-08-04 . . . 159
B.146 1998-08-04 SEC-Otsu . . . 159
B.147 1998-08-04 SEC-Kittler . . . 159
B.148 1998-08-04 SEC-Ridler . . . 160
B.149 1998-08-04 SEC-SelfTuning . . . 160
B.150 1998-08-04 AdamsSRG . . . 160
B.151 1998-08-04 OtsuVermaSRG . . . 160
B.152 1998-08-04 MeanVermaSRG . . . 160
B.153 1998-08-04 ShihSRG . . . 160
B.154 1998-08-04 GambottoSRG . . . 161
B.155 1998-08-04 ZanatySRG . . . 161
B.156 2000-08-08 . . . 161
B.157 2000-08-08 SEC-Otsu . . . 161
B.158 2000-08-08 SEC-Kittler . . . 161
B.159 2000-08-08 SEC-Ridler . . . 162
B.160 2000-08-08 SEC-SelfTuning . . . 162
B.161 2000-08-08 AdamsSRG . . . 162
B.162 2000-08-08 OtsuVermaSRG . . . 162
B.163 2000-08-08 MeanVermaSRG . . . 162
B.164 2000-08-08 ShihSRG . . . 162
B.165 2000-08-08 GambottoSRG . . . 163
B.166 2000-08-08 ZanatySRG . . . 163
B.167 2001-08-04 . . . 163
B.168 2001-08-04 SEC-Otsu . . . 163
B.169 2001-08-04 SEC-Kittler . . . 163
B.170 2001-08-04 SEC-Ridler . . . 164
B.171 2001-08-04 SEC-SelfTuning . . . 164
B.172 2001-08-04 AdamsSRG . . . 164
B.173 2001-08-04 OtsuVermaSRG . . . 164
B.174 2001-08-04 MeanVermaSRG . . . 164
B.175 2001-08-04 ShihSRG . . . 164
B.176 2001-08-04 GambottoSRG . . . 165
B.177 2001-08-04 ZanatySRG . . . 165
B.178 2002-07-31 . . . 165
B.179 2002-07-31 SEC-Otsu . . . 165
B.180 2002-07-31 SEC-Kittler . . . 165
B.181 2002-07-31 SEC-Ridler . . . 166
B.182 2002-07-31 SEC-SelfTuning . . . 166
B.183 2002-07-31 AdamsSRG . . . 166
B.184 2002-07-31 OtsuVermaSRG . . . 166

B.185 2002-07-31 MeanVermaSRG 166
B.186 2002-07-31 ShihSRG 166
B.187 2002-07-31 GambottoSRG 167
B.188 2002-07-31 ZanatySRG 167
B.189 *img_262* 167
B.190 *img_262* ground-truth map 167
B.191 *img_262* SEC-Otsu 167
B.192 *img_262* SEC-Kittler 167
B.193 *img_262* SEC-Ridler 168
B.194 *img_262* SEC-SelfTuning 168
B.195 *img_262* AdamsSRG 168
B.196 *img_262* OtsuVermaSRG 168
B.197 *img_262* MeanVermaSRG 168
B.198 *img_262* ShihSRG 168
B.199 *img_262* GambottoSRG 169
B.200 *img_262* ZanatySRG 169
B.201 *img_336* 169
B.202 *img_336* ground-truth map 169
B.203 *img_336* SEC-Otsu 169
B.204 *img_336* SEC-Kittler 169
B.205 *img_336* SEC-Ridler 170
B.206 *img_336* SEC-SelfTuning 170
B.207 *img_336* AdamsSRG 170
B.208 *img_336* OtsuVermaSRG 170
B.209 *img_336* MeanVermaSRG 170
B.210 *img_336* ShihSRG 170
B.211 *img_336* GambottoSRG 171
B.212 *img_336* ZanatySRG 171

List of Tables

1.1 Table that contains the abbreviations for the different methods that were used in the studies, divided in separated categories and with the reference to the section of the dissertation document where the correspondent method was presented. 5

2.1 Definitions and notation necessary to describe thresholding algorithms (Prieto et al. (2012)): 24

4.1 Table that accounts for how frequent each version of the SEC algorithm, excluding the fine-tuning version, had the best score when segmenting an SST image of the portuguese coast. It is also accounted the frequency that each version had F-measure scores superior or equal to 0.7, which was empirically identified has a threshold for separating good from bad segmentation results. The best versions scores are bold in the table, for each of the sets of images and information that is being analyzed. 52

4.2 Table that accounts for how frequent SRG method had the best score when segmenting an SST image of the portuguese coast. 61

4.3 Table that accounts for how frequent each version of the SEC algorithm, excluding the fine-tuning version, had the best score when segmenting an SST image of the Canary. It is also accounted the frequency that each version had F-measure scores superior or equal to 0.7, which was empirically identified has a threshold for separating good from bad segmentation results. The best versions scores are bold in the table, for each of the sets of images and information that is being analyzed. 66

4.4 Table that accounts for how frequent each version of the SEC algorithm, excluding the fine-tuning version, and each SRG method had the best score when segmenting an SST image of the Canary. It is also accounted the frequency that each version had F-measure scores superior or equal to 0.7, which was empirically identified has a threshold for separating good from bad segmentation results. The best versions scores are bold in the table, for each of the sets of images and information that is being analyzed. 69

4.5 Accuracy that each unsupervised evaluation measure had when applied to each SRG method. Underlined are the three most accurate evaluation measures for each of the SRG methods. In the bottom line it can be seen the percentage of times that each unsupervised evaluation measure was in the three most accurate for each SRG method (Success Rate). The values in bold are the ones where the correlation to the F-measure was better, meaning higher or lower than 0.2 or -0.2, depending if for the given unsupervised evaluation measure the ideal correlation should be positive or negative correspondingly. 75
4.6 Table that accounts for how frequent each version of the SEC algorithm and each SRG method had positive scores given by each unsupervised evaluation measures, when segmenting SST image without ground-truth. The best SRG methods scores are bold in the table. In the bottom lines it can be seen the mean rate of positive classifications given by the select four best unsupervised evaluation measures, and the correspondent standard deviation. 78

A.1 Images with discontinuity that need more than one iteration to extract the full upwelling area and the correspondent cause of the discontinuity. 92
A.2 Table with the F-measure results for the comparative study between the SEC algorithm and the SRG methods applied to the extraction of upwelling context. The segmentation results are from the SST images of the portuguese coast from the year 1998, with strong gradients in the frontier of the upwelling area. The best scores for each SST image are highlighted in bold. 93
A.3 Table with the F-measure results for the comparative study between the SEC algorithm and the SRG methods applied to the extraction of upwelling context. The segmentation results are from the SST images of the portuguese coast from the year 1998, with weak gradients in the frontier of the upwelling area. The best scores for each SST image are highlighted in bold. 94
A.4 Table with the F-measure results for the comparative study between the SEC algorithm and the SRG methods applied to the extraction of upwelling context. The segmentation results are from the SST images of the portuguese coast from the year 1998, with noise interfering with the segmentation process. The best scores for each SST image are highlighted in bold. 95
A.5 Table with the F-measure results for the comparative study between the SEC algorithm and the SRG methods applied to the extraction of upwelling context. The segmentation results are from the SST images of the portuguese coast from the year 1999. The best scores for each SST image are highlighted in bold. (Part 1/2) 96

A.6 Table with the F-measure results for the comparative study between the SEC algorithm and the SRG methods applied to the extraction of upwelling context. The segmentation results are from the SST images of the portuguese coast from the year 1999. The best scores for each SST image are highlighted in bold. (Part 2/2) 97
A.7 Table with the F-measure results for the comparative study between the SEC algorithm and the SRG methods applied to the extraction of upwelling context. The segmentation results are from the SST images of the Canary. The best scores for each SST image are highlighted in bold. 98
A.8 Table that accounts for how frequent each version of the SEC algorithm, excluding the fine-tuning version, and each SRG method had good score, relatively to the correspondent threshold, when segmenting SST image without ground-truth. The best SRG methods scores are bold in the table, for each of the sets of images and information that is being analyzed. (Part 1/2) 109
A.9 Table that accounts for how frequent each version of the SEC algorithm, excluding the fine-tuning version, and each SRG method had good score, relatively to the correspondent threshold, when segmenting SST image without ground-truth. The best SRG methods scores are bold in the table, for each of the sets of images and information that is being analyzed. (Part 2/2) 110
A.10 Table with the produced thresholds using the Information Gain method. For each region growing algorithm, different thresholds were calculated for the many unsupervised evaluation measures. The values in bold text are the ones where the correlation to the F-measure was better, meaning higher or lower than 0.2 or -0.2, depending if for the given unsupervised evaluation measure the ideal correlation should be positive or negative correspondingly. 111
A.11 Table with the produced thresholds using the Otsu's method. For each region growing algorithm, different thresholds were calculated for the many unsupervised evaluation measures. The values in bold text are the ones where the correlation to the F-measure was better, meaning higher or lower than 0.2 or -0.2, depending if for the given unsupervised evaluation measure the ideal correlation should be positive or negative correspondingly. 111

CHAPTER 1

INTRODUCTION

1.1 Motivation

Coastal upwelling is an oceanographic phenomenon characterized by the presence, at the sea surface, of colder and nutrient rich waters which are driven by the wind force over the continental shelf, and by filaments of upwelled waters extended for a large area. It is expressed by alterations in the movement of surface water masses perpendicular to the coast line, which come to replace warmer waters, usually surface water with low nutrient levels. Diverse ecological effects derive from upwelling, but one impact is especially noteworthy. When upwelling brings nutrient-rich waters to the surface, it supports blooms of phytoplankton which are the energy base for large animal populations higher in the food chain, making its detection indispensable to fisheries. Delimitation of this phenomenon is also important to the development of climate models, detection of pollutants and general coastal monitoring.

Remote sensing is a widely applied technique in the detection of the upwelling phenomenon. Obtained with the thermal infrared channels of the Advanced Very High Resolution Radiometer (AVHRR) sensor on board NOAA-n satellite series, images of sea surface temperature (SST) are used by the oceanographers, as described by Nascimento and Franco (2009) and Nascimento et al. (2012), to identify the transition zone between the colder upwelled waters and warmer oceanic waters. SST images must be processed by the Oceanographers and a high resolution color scale is applied to each one. It is a very time-consuming process to manually tune the color scale in large volumes of images, which is a important step to get the best contrast definition for a good visualization of the phenomenon. The identification and continuing monitoring of upwelling might be an expensive process, so automatic detection tools are a demand, not only because of the large quantity of data daily collected, which puts an enormous load of work on

Oceanographers hands, but also because of the subjectivity inherent to visual inspection, so an objective approach to extract the upwelling is necessary. Also, it is too difficult to deal with upwelling regions with transition zones characterized by smooth thermal boundaries, where it is hard to make the distinction between the objects of interest and the background.

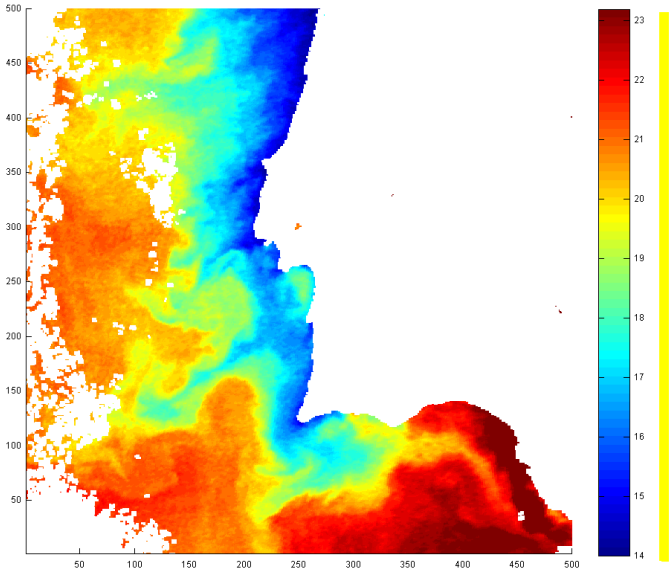

Figure 1.1: SST image of the portuguese coast (1 August 1998). The temperature values are codified in a color scale, where blue represents colder waters and red warmer waters. The white pixels represent land in the continental area, or noise derived from clouds or transmission errors from the satellite in the ocean area.

Different approaches have been proposed in the past to do automatic upwelling detection from remote sensing images, like the example image in Figure 1.1, where the upwelling areas are represented by blue tones corresponding to colder waters and, the lateral yellow bar represents contains the color that codifies the temperature at the boundary.

In (Kriebel et al. (1998)) artificial neural networks were applied to wind data and remotely sensed SST data, for the analysis and prediction of coastal upwelling; after that in (Arriaza et al. (2003)) artificial neural networks were also used for basic pre-processing tasks such as cloud masking, and an connectionist technique, using regional features, identified ocean structures like upwelling areas; while in (Chaudhari et al. (2008)) detection and segmentation of upwelling regions was made using neural networks, which are trained using K-means clustering results and a statistical coefficient used to determine the presence of upwelling; in (Marcello et al. (2005)) it was proposed an automatic upwelling extraction approach based on a coarse-segmentation methodology followed by a fine-detail growing process; Plattner et al. (2006) developed a semi-automated method to classify upwelling areas, which derives from wind measurements, and it is based on statistical characterization; Nieto et al. (2012) proposed an improved automatic detection

of mesoscale frontal activity based on the edge detection algorithm initially presented by Cayula and Cornillon (1992); also in (Tamim et al. (2013)) for automatic detection and extraction of upwelling areas an approach is presented, based on the evaluation and comparison between two unsupervised classification methods, Otsu's method and Fuzzy C-means. However, these approaches require, to achieve an admissible segmentation, a more or less complex pre-processing stage, with exception for the work of Tamim et al. (2013).

In (Nascimento et al. (2005)) the segmentation of SST images was successfully achieved using the fuzzy c-means algorithm, however it did not provide an automatic mechanism to make the delimitation of the frontier of upwelling areas. This problem was solved, as described in (Nascimento and Franco (2009)), by adding a step of frontier detection after the segmentation phase. Nascimento et al. (2012) developed a fully automated fuzzy clustering method to solve the problem of automatic recognition of upwelling areas in SST images. The system presented, FuzzyUPWELL, provides a framework for an unsupervised segmentation and delimitation of upwelling areas. The FuzzyUPWELL system integrates an unsupervised fuzzy clustering algorithm, the Anomalous Pattern Fuzzy Clustering (AP-FCM), a threshold procedure to determine the upwelling fronts that combines a variety of features extracted from the obtained clusters, a mechanism to delimitate the upwelling areas by fuzzy boundaries defined from measures of classification uncertainty, and a Graphical User Interface (GUI). Although the FuzzyUPWELL had shown to be a reliable system, it only operates over the temperature data during the segmentation process, not taking directly into account the geographic information about the clusters it creates. Moreover, the delineation of the upwelling front is a stage separated from the segmentation process.

Therefore, in (Nascimento et al. (2015)) it was proposed a new method, the Seed Expanding Cluster algorithm (SEC) inspired on the popular Seeded Region Growing (SRG) algorithm (Adams and Bischof (1994)), and that takes into account not only the temperature value of the pixel, but also its spacial context, in order to model the process of upwelling formation as a process of combining pixels, into a progressive bigger region, according to the similarity of their temperatures to the temperature of a seed point at the beginning, which is chosen as the pixel with lower temperature. The SEC algorithm has shown promising results in its ability to automatically recognize upwelling area and its frontline from SST images.

The SEC algorithm does not require posterior steps of delimitation of the frontier of upwelling areas. In each iteration of the algorithm a new frontier to the cluster is being defined, so the final frontier contains the pixels that delimit the upwelling area.

1.2 Description and Context

The Seed Expanding Cluster (SEC), presented in the context of solving the problem of coastal upwelling detection considering spacial information, is inspired in the Seeded

Region Growing method introduced by Adams and Bischof (1994), but is a considerably modified version of it, and it belongs to the region growing family of algorithms. The SRG algorithms are characterized by growing a region whenever its interior is homogeneous according to a certain feature of interest, and the region growing begins from one initial seed or multiple seeds if the objective is to segment into multiple areas, by adding similar neighboring pixels according to a homogeneity criterion.

The SEC algorithm is conceptually similar to most of SRG methods, but it is important to salient its specifications. The algorithm starts its growing process from one seed only and adds pixels to the region using a novel homogeneity criteria, in the form of a product rather than a difference as usual in most of the approaches of SRG algorithms. Other important characteristic of this algorithm is that the threshold of the homogeneity criterion is mathematically derived from this criterion, which is a unique feature as compared to other adaptive thresholding SRG algorithms presented in the literature. This last characteristic is used in the Self-tuning Seeded Expanding Clustering (SEC-SelfTuning, for short) version. To control the expansion of the region, a threshold value for the homogeneity criterion must be set, however it is sometimes a difficult and tedious work to the user to do, so to fully automate the SEC algorithm a self-tuning version was proposed. It is important to compare this self-tuning version with other versions of the algorithm, where automatic thresholding techniques can be used to find an adequate threshold value without user intervention. This methods to tune the threshold value are already applied in image segmentation, where the calculated threshold value is used to separate an object from the background of the image. Different thresholding methods must be tested and their effectiveness evaluated. The self-tuning version of the algorithm will be compared with other version of the algorithm where the homogeneity threshold value is established by the selected automatically thresholding methods (Ridler and Calvard (1978); Otsu (1979); Kittler and Illingworth (1986)).

An iterative version of the algorithm is also to be produced. The SEC algorithm only grows one region, however an extension of it will extract several regions of the phenomenon under study, which sometimes does not cover a contiguous area of ocean.

The new SEC algorithm not only requires that methods to tune the threshold value are tested, but it is also important to benchmark its segmentation results comparing them to other results from SRG methods present in the literature. So, it will be possible to validate the effectiveness of the algorithm and also learn about its behavior on different sets of images, evaluating its segmentation results. So, an experimental study will be executed to measure the effectiveness of the chosen automatic thresholding methods (Ridler and Calvard (1978); Otsu (1979); Kittler and Illingworth (1986)) to tune the similarity threshold of the SEC algorithm, as well as to validate the performance of the SEC algorithm to segment upwelling images in contrast with a representative sample of SRG algorithms (Adams and Bischof (1994); Gambotto (1993); Shih and Cheng (2005); Verma et al. (2011); Zanaty and Asaad (2013)). There are different methods for evaluating segmentation algorithms, even so there is no generally accepted methodology. Some images, of the database

of images to be analyzed, have assigned to them a binary ground-truth map, delineated by expert oceanographers, representing areas of upwelling and non-upwelling. For these images, supervised techniques to evaluate image segmentation can be applied, which compare the ground-truth to the segmentation result (Zhang (1996)). However, many images can not have a reference image to evaluate the quality of the segmentation, and for fully automate the process and avoid tedious pre-processing by the experts, it is necessary to use unsupervised evaluation techniques (Zhang et al. (2008)).

Many methods are necessary to complete the proposed study, and for convenience short names were attributed for each one, and can be seen in the Table 1.1. The abbreviated names are divided in the the categories of SEC versions, SRG methods used in the comparative study and unsupervised evaluation measures that were used to test the quality in images that did not had ground-truth map associated to them.

Table 1.1: Table that contains the abbreviations for the different methods that were used in the studies, divided in separated categories and with the reference to the section of the dissertation document where the correspondent method was presented.

Category	**Method Abbreviation**	**Described In**
SEC Versions	SEC-Otsu	Section 3.1.1 and 2.3.2
	SEC-Kittler	Section 3.1.1 and 2.3.3
	SEC-Ridler	Section 3.1.1 and 2.3.1
	SEC-SelfTuning	Section 3.1.1 and 3.1.3
	SEC-FineTuning	Section 3.1.1 and 4.3
SRG Methods	AdamsSRG	Section 2.2.3.1
	OtsuVermaSRG	Section 2.2.3.2
	MeanVermaSRG	Section 2.2.3.2
	ShihSRG	Section 2.2.3.3
	GambottoSRG	Section 2.2.3.4
	ZanatySRG	Section 2.2.3.5
Unsupervised Evaluation Measures	Intra_LN	Section 2.4.2, Measure (i)
	Inter_Otsu	Section 2.4.2, Measure (vi)
	Inter_FRC	Section 2.4.2, Measure (iv)
	Intra_FRC	Section 2.4.2, Measure (iii)
	Intra_Liu	Section 2.4.2, Measure (ix)
	CalinskiHarabasz	Section 2.4.2, Measure (vii)
	DaviesBouldin	Section 2.4.2, Measure (viii)

1.3 Main Contributions

The main contributions of this dissertation are three-fold:

1. To make a comparative study among distinct automatic thresholding techniques (Ridler and Calvard (1978); Otsu (1979); Kittler and Illingworth (1986)) and the self-tuning version of the SEC algorithm in order to find the best thresholding method to guide the growing of the cluster;

2. To realize an extensive comparative experimental study between several SRG algorithms established in the literature (Adams and Bischof (1994); Gambotto (1993); Shih and Cheng (2005); Verma et al. (2011); Zanaty and Asaad (2013)) and the SEC algorithm, to study its effectiveness on the automatic upwelling detection for several years of images;

3. To develop an iterative version of the SEC algorithm that allows to recognize discontinuous upwelling regions. This iterative version of SEC sequentially extracts clusters one by one until a pre-specified number of clusters be recognized. The iterative procedure will be used on the two previous comparative studies.

   Transversal to the former contributions is the comparative evaluation of the experimental results. For that, several supervised and unsupervised validation indices will be applied.

1.4 Document Organization

The rest of the document is organized as follows. Chapter 2 essentially describes the state of the art in themes related to this work. It starts with a general description of image segmentation techniques and, after that has an overview on Seeded Region Growing methods, which include an analysis on the reference SRG algorithm (Adams and Bischof (1994)) and other SRG methods, as well as their applications presented in the recent literature. Several automatic thresholding techniques are also analyzed and evaluation measures for image segmentation algorithms are also studied. In Chapter 3, the SEC algorithm is characterized, the approach for the iterative version is presented and, the application of the SRG methods to the detection of the upwelling phenomenon is described. The experimental study is described in the Chapter 4 and, the different comparative studies as well as the necessary complementary studies are exposed.

Chapter 2

Related Work

2.1 Introduction to Image Segmentation

The process of partitioning an image into multiple segments, with the objective of changing the representation of an image into something meaningful and easier to analyze is called image segmentation. It is the low-level operation that targets to partitioning images by determining disjoint and homogeneous regions or, equivalently, by finding edges or boundaries and, it is a first step before applying to images higher-level operations such as recognition, semantic interpretation, and representation. This was explained in Luccheseyz and Mitray (2001), which presented a survey on color image segmentation since most of the methods till that time were focused on segmentation of gray-level images.

There are a lot of different segmentation techniques present in the literature (Haralick (1983); Pal and Pal (1993); Szeliski (2010)). Some methods perform better on different kinds of images, so there is no universal method accepted and it is still a challenging problem to achieve good image segmentation.

Segmentation process is classified into different methods based on the user interaction level needed. There are manual segmentation, semi-automatic segmentation and automatic segmentation. For this work the most relevant method is the automatic image segmentation which is divided in four techniques (Fan et al. (2001); Dass and Devi (2012); Preetha et al. (2012); Dantulwar and Krishna (2014)):

- **Thresholding techniques** are based on the assumption that adjacent pixels whose value (gray intensity, color, etc.) lies within a certain range belong to the same class. This technique performs better with images that include only two opposite components. These techniques ignore all the spatial relationship information of the images, and so they do not deal well with noise, blur at object boundaries, or multiple component image segmentation.

- **Boundary-based techniques** use the assumption that pixel values change rapidly at the boundary between two regions. The basic principle is to apply some of the gradient operators convolving them with the image. The edges are rapid transitions between two different regions and can be detected when high values of the gradient magnitude are found. After finding edges, they have to be linked to form closed boundaries of the regions. This might involve some post-procedures which can be very time-consuming.

- **Region-based techniques** partition an image into regions that are similar according to a criterion of homogeneity. Homogeneity criteria are based on some threshold value which can be difficult to specify, because it depends on the image data. It is in this category that the Seeded Region Growing (SRG) technique is inserted and it will be largely discussed further on.

- **Hybrid techniques** which integrate the results of boundary detection and region growing techniques expecting to obtain better overall results in segmentation. There is a great variety of ways to mix different techniques, but they might be expensive in computational power sometimes. More about this combination of methods can be seen in the survey of Freixenet et al. (2002).

2.2 Seeded Region Growing (SRG)

The Seeded Region Growing (SRG), which is the reference method in the literature, is presented by Adams and Bischof (1994) is a robust, rapid and free of tuning parameters algorithm for segmentation of intensity images. The method requires the input of a number of seeds that can be individual pixels or a set of them, which will control the formation of regions where the image will be segmented. The algorithm grows these seeded regions until all the image pixels have been allocated to a specific region. This is made iteratively and all those pixels at the border of growing regions are examined at each iteration. The pixel that is most similar to a region that it borders is assigned to that region.

The algorithm works well for a great variety of images and it is also very attractive for semantic image segmentation by involving the high-level knowledge of image components in the seed selection procedure, it allows to separate regions that have the same properties taking into account the spacial information of the pixels. Unfortunately the SRG algorithm suffers from some problems, namely his inherent dependency on the order of processing of the image pixels, as well from not having an automatic seed generation. So the obvious way to improve the SRG technique is to provide a better pixel labeling method and automate the process of seed selection (Mehnert and Jackway (1997) ; Fan et al. (2001)).

A great variety of SRG algorithms had appeared in order to achieve better segmentation results and to adapt to many specific problems of some kinds of images. So, when

analyzing a SRG growing algorithm there are some questions that are important to answer:

1. How to select the seeds and how critical is the seed selection to get a good segmentation result?
2. What is the homogeneity criterion for the region growing and how to specify the corresponding threshold?
3. How to manage the pixel labeling procedure efficiently?

The SRG methods have several advantages, but also some disadvantages, as stated by Kamdi and Krishna (2011):

Advantages

1. Can correctly separate regions with the same properties following an homogeneity criterion.
2. Perform well in images that have clear edges.
3. To grow a region it is only necessary to place a seed inside of it.
4. The seed can be chosen by the user to extract some object.
5. It performs well when dealing with noise.

Disadvantages

1. The computation might be consuming.
2. Noise or variation of intensity in the image may result in holes or over-segmentation.
3. It may not distinguish the shading of the image.

2.2.1 Overview of SRG methods

After the reference Seeded Region Growing algorithm has been proposed by Adams and Bischof (1994), a great variety of works related to this algorithm emerged. All of them tried to improve the method in different ways, and from the main ideas, many adaptations were done in order to better solve problems in specific applications, or to simply create a better algorithm in general. Most of the research works do not solve all the problems at once, rather they focus on improving some aspects of this kind of algorithms, like order dependency in pixel processing, selection of the initial seed, establishment of threshold of the homogeneity criterion, and definition of the homogeneity criterion itself.

Some variations of the algorithm, as well as the one from Adams and Bischof (1994), are greedy algorithms, meaning that all pixels in the image are processed and assigned

with a label while satisfying a connectivity constraint. What happens is that if only one seed is provided, then the region corresponding to that single seed will grow until all pixels in the image are allocated to it. So, algorithms that use a threshold value to constraint the growth of the region, appeared in order to solve this problem. Another problem is the one of finding noise in the images which can lead an over-segmentation of the image.

2.2.1.1 Strategies for order dependency

The order dependency in pixel processing leads to different final segmentation results, so it is a problem that was addressed in some earlier works (Mehnert and Jackway (1997); Wan and Higgins (2003); Shih and Cheng (2005); Fan et al. (2005)) and, was also a worry in most of the other works even so it was not the main focus of their research. In the reference SRG paper from Adams and Bischof (1994) , one of the reasons the order dependency was tolerated was because in their implementation, the speed was enhanced greatly, besides knowing that order dependency leads to a negligible difference in the results.

Mehnert and Jackway (1997) came with a solution for the two problems of order dependency that are inherent in the SRG algorithm proposed by Adams and Bischof (1994). The first problem of order dependency is called inherent order dependency and occurs whenever several pixels have the same difference measure to their neighboring regions and, the second is called implementation order dependency and occurs when one pixel has the same difference measure to several regions. The solution to the first problem was achieved by processing pixels with the same difference measure in parallel. This means that pixels can only be labeled and region means updated, when all other pixels at that priority have been examined. To solve the second order dependency, the pixels with same difference measure to several regions are assigned with a special label and take no further part in the region growing process, only in the end, after all the pixels have been labeled, the problematic pixels are independently re-examined to see what region they belong to. This fix was important because a different order of processing pixels leads to different final segmentation results. In (Wan and Higgins (2003)) a generic Symmetric Region Growing method that is insensitive to the initial input seeds was theoretically described. The objective, which they aimed to achieve, was to define the theoretical criteria necessary for region growing algorithms, to be insensible to the initial seeds selection and to be still efficient, in any dimensionality.

2.2.1.2 Strategies to select the initial seeds

An obvious way to extend the SRG algorithms is to make the selection of initial seeds automatic, a process that can produce good seed sets without to have semantic knowledge of the domain or having explicit criterion. However, the seed selection process can take

into account that one advantage of SRG is the high-level knowledge of semantic image components and this can be exploited to select the suitable seeds for obtaining meaningful region growing. Melouah and Amirouche (2014) regarding automatic seed selection, classified the different works in three axes: region extraction approach, features extraction approach and edges extraction approach.

Fan et al. (2001) contributed to improve the seeded region growing algorithms by proposing an automatic form of selecting the initial seeds. Doing this requires the extraction of the major geometric structures of the image using color edges. The centroids between the adjacent edge regions are taken as the initial seeds for seeded region growing. Initial seeds are then replaced by the centroids of the generated homogeneous regions. After, Fan et al. (2005) presented an automatic SRG algorithm with a boundary-oriented efficient parallel pixel labeling technique and, three automatic seed selection methods: one center-oriented seed generation method and two edge-oriented seed generation methods. They also present a seed tracking algorithm for automatic moving object extraction, where the seeds located inside the temporal change mask are selected for generating the regions of moving objects. In other work, of Shih and Cheng (2005), an automatic seeded region growing for color image segmentation was created. They defined that for automatic seed selection, three criteria must be fulfilled. The first one is that the seed pixel must have high similarity to its neighbors, the second one says that at least one seed must be generated in order to create a certain region and the last one obligates that seeds from different regions must be disconnected. The candidate pixels must pass the test of two conditions, one that checks whether the seed pixel has high similarity to its neighbors and another that makes sure that the seed pixel is not on the boundary of two regions. After this process, a proposed SRG algorithm is used to segment the color image using the set of seeds automatically generated before. It is possible that several seeds are generated to split a region into several small ones, causing over-segmentation, so a region merging procedure is executed using some threshold value on similarity. Using other algorithms to help selecting suitable seeds is also a possibility and, in (Tang (2010)) the selection of the initial seeds was automatic, using watershed algorithm to segment the image and extract the seeds from the regions created. This seeds automatically generated are then the input for an SRG algorithm, that improves the original gray image segmentation method according to color image segmentation needs. Preetha et al. (2012) proposed a new method for color image segmentation based on region growing and region merging. Based on the same three criteria described in (Shih and Cheng (2005)), the seeds were automatically generated. The merging of regions is done by considering the size and the Euclidean distance of regions. Tilton et al. (2012) improved the described HSeg algorithm, which begins by initializing the segmentation and assigning each image pixel a region label. If a pre-segmentation is provided, each pixel is labeled according to the pre-segmentation results. This avoids the need to have the seeds as input. Then, it calculates a dissimilarity criterion value, based on minimizing the increase of mean squared error between the region mean image and the original image data, or based on the spectral similarity

between two spectral vectors. After this, pairs of spatially adjacent regions are merged based on a threshold criterion equal to the smallest dissimilarity criterion value between pairs of spatially adjacent regions. The process is repeated until a chosen convergence criterion is achieved, usually this being a specified number of regions to be reached. Also, Dantulwar and Krishna (2014) created an algorithm to overcome the problem of initial seeds selection, which might be costly. So, a single seeded region growing technique is presented, which always selected the initial seed as the central pixel of the image. After that, it grows the region according to a grow formula with a intensity based similarity index, calculated by Euclidean distance between labeled pixel and a non labeled pixel. It selects the next seed from a connected pixel to the region. The stopping criterion for the grow formula is determined using the Otsu's thresholding method (Otsu (1979)).

2.2.1.3 Types of homogeneity criteria

The homogeneity criteria are a very important part of the SRG algorithms, because choosing appropriate criteria is the key in extracting the desired regions. Pohle and Toennies (2001) has categorized the selection of different homogeneity criteria into three methods: criteria selection based on intensity level properties of the current points; comparison of segmentation with different homogeneity criteria; criteria selection for a complete segmentation of the scene with potentially varying criteria for different regions. Stopping criteria should be efficient to discriminate neighbor elements in non-homogeneous domains. Most of the SRG approaches involve a homogeneity criterion based on a dissimilarity measure defined by the difference between the pixel to be labeled and the mean of the region of interest, initially described in (Adams and Bischof (1994)). However, there are other works that use alternative homogeneity criteria in order to obtain better quality in segmentation, and trying to solve some problems of SRG methods like cases of explosion in the segmented area provoked by weak boundaries of the regions. Regarding homogeneity, the region growing formula should be capable of guarantee that pixels inside one region must be homogeneous with respect to some properties, and that pixels from different regions must have distinct properties.

The method proposed by Gambotto (1993) controls which of the pixels should enter the region by using a hybrid strategy that combines region growing with edge detection algorithm. The adjacent pixels to the region are hierarchically clustered and the groups of pixels that are closer to the region model are merged to the region. Gradient information is used to find the optimum region boundary and the growth stops. Hojjatoleslami and Kittler (1998) proposed a new region growing method by pixel aggregation that used novel similarity measure has homogeneity criterion. A boundary pixel is joined to the current region if it has the highest grey level among the neighbors of the region. Something that was new about this method is that at each step, at most one pixel exhibits the required properties to join the region. Pohle and Toennies (2001) stated that homogeneity

criterion specification depends on image formation properties that are not known to the user, so they developed a region growing algorithm that learns its homogeneity criterion from characteristics of the region to be segmented. Two runs of SRG are necessary, the first with the objective of estimate the parameters of the homogeneity criterion that will be applied to the second run. Learning the criterion requires to estimate mean and two different standard deviations for grey values from a number of pixels of the region. The algorithm produces results that are only little sensitive to the seed point location. Espindola et al. (2006) stated that the region growing algorithms, which are usually used for remote sensing image segmentation, need the user to supply control parameters, like the similarity threshold and an area threshold (Bins et al. (1996)), so an objective function is proposed for selecting suitable parameters for region-growing algorithms to ensure best quality results. The new objective function must guarantee that each of the resulting segments should be internally homogeneous and should be distinguishable from its neighborhood. The function combines a variance indicator that expresses the overall homogeneity of the regions, with a spatial auto-correlation index that detects separability between regions. Rai and Nair (2010) showed the impact in the quality of segmentation made by the various aspects of homogeneity criterion. A gradient based homogeneity criterion that is characterized by a cost function is used and, it exploits features of the surroundings of the seed. The method is semi-automatic because the seed must be provided as input. With weak boundaries problem in mind, Zanaty and Asaad (2013) presented a new algorithm called Probabilistic Region Growing. This approach automatically sets the similarity threshold value, based on estimating the probability of pixel intensities of the whole image. The homogeneity criterion, similar to the reference one that has the form of a difference between the pixel to be labeled and the mean of the region, is extracted automatically from characteristics of the regions and it might be different for every pixel, since the threshold value is adaptive. In this algorithm the pixels are processed sequentially in a random path starting at the initial seed, and the homogeneity criterion is updated continuously.

2.2.1.4 Thresholding strategies

A problem with some of the SRG algorithms is that the threshold value must be given has input, either way by trial and error experiments, or its value is the output of another algorithm. An improper threshold value can have a considerable impact on the quality of the segmentation result. Sometimes in the same image, there are different levels of threshold that must be taken in consideration in order to extract objects with different characteristics.

Chang and Chen (2007) proposed a multi-scale region growing segmentation method, based on the maximization of the change of edge density. The region growing algorithm is applied successive times with different threshold values, from the smallest to the largest

value, and a tree is create that in each node, a change in edge density is saved. The perfect partition of an observed target is registered when the change of edge density is maximum, meaning that the desired threshold value was captured. The goal of Wu et al. (2008) approach was to achieve automatic texture based segmentation. They start by extract texture features for each pixel in the region of interest. A cost function, based on three sub-functions, is applied to every pixel in the region of interest and the one with minimum value is chosen as seed. The three sub-functions are: the spatial distance from the pixel to the center point of the region of interest; the Euclidean distance on feature space from the pixel to the centroid of the region of interest; the sum of the Euclidean distance on feature space from the pixel to its neighbors. After this the region growing starts using the Euclidian distance of texture features, as homogeneity criterion. If the threshold value is higher than the optimal one, the region grows to a much larger area than it should, this is called explosion. In order to avoid it, it is necessary to find the highest threshold value just before explosion. To accomplish this, the SRG algorithm is executed with a progressively larger threshold value and when the explosion is detected, the optimum threshold value is retrieved from the last execution without explosion. In (Al-Faris et al. (2012)) a modified automatic SRG algorithm was presented and it was based on the Particle Swarm Optimization image clustering system. The modification is made by introducing two automatic approaches for selecting the SRG variable factors. The first one chooses the initial seed automatically from the results of the clustering algorithm, and the seed is selected as the center of the cluster with the highest intensity. The second automatic approach chooses the threshold value, based upon finding the optimum estimated value from the intensities mean values of the clusters. Both approaches are based on the intensities of the clusters which resulted from the Particle Swarm Optimization Image Clustering. Verma et al. (2011) presented a Single Seeded Region Growing Algorithm for Color Image segmentation, which grows from an initial seed in the center of the image. The homogeneity criterion use an intensity based similarity index, calculated by Euclidean distance, between the seed and the 8-neighbor pixels. The stopping criterion is determined from the Otsu's adaptive thresholding method. After a region is grown, the threshold value is calculated again in order to adjust better to the next region to be grown. For color image segmentation, Jain and Susan (2013) came with an adaptive single seed based region growing algorithm. The initial seed is the center pixel of the image. This region growing algorithm uses three different homogeneity criteria, so a pixel is allocated to a region if: it is similar enough to a connected pixel belonging to the region; it is similar enough to the mean value of the region; it is more similar to the mean value of the region than to its 8-neighbors. The third criterion is only analyzed if the first two fail to hold. After one region is completely grown, a new seed is selected from the boundary pixel stack. This algorithm solves the problem of initial seed selection, and also does not need to select a threshold heuristically, however the homogeneity criteria need some similarity values that the authors selected empirically.

2.2.1.5 Dealing with noisy images

Dealing with noisy images can also be a major problem and a technique developed by Carvalho et al. (2010) finds a way of doing it without pre-processing methods. For this they create an algorithm that comprises a statistical region growing procedure combined with hierarchical region merging. A coefficient of variation is the criterion to test homogeneity. The strategy used was to aggregate statistically homogeneous regions until a dissimilarity between the most similar pair of spatially adjacent regions reaches a specified threshold or a certain number of regions is obtained.

2.2.2 Domains of Applications

A great variety of scientific work has been done, which do not necessarily change the SRG algorithm, but used it to solve a complex problem, many times integrating it as a step in a larger and more sophisticated process.

There are some types of applications, referenced in the literature, where Seeded Region Growing algorithms are very popular, like Remote Sensing, Medical Image Processing or Industrial Inspection.

2.2.2.1 SRG in Remote Sensing

In Remote Sensing there are examples like Bins et al. (1996), which presented a region growing method with the objective of assess land use changes in the Amazon region; Bagli et al. (2004)presented an automatic delineation of shoreline and lake boundaries, and is successful in integrating SRG algorithm in the process; Wang and Chen (2012) proposed an algorithm composed in five steps including k-means clustering, segment initialization, seed generation, region growing, and region merging. This algorithm is used to segment remote sensing data, and can be used for a variety of applications, including urban and regional planning; Gao et al. (2011) evaluated different segmentation methods in multispectral Landsat imagery, because image segmentation is a critical step to achieve object-based image classification, and one of the methods is the SRG method; Stroppiana et al. (2012)proposed a method for extracting burned areas, using some techniques which include a region growing algorithm that will, in the end of the process, generate the burned area map; in (Zhang et al. (2013)), where extraction of coastline in aquaculture zones is done, by a process that involves multiple steps to segment the ocean. After this segmentation, objects near aquaculture zones are used as a seed to the SRG algorithm that will segment until detect the desired coastline; Mishra and Susaki (2013) created some methodologies focused on the analysis of multi-temporal Synthetic Aperture Radar images. They use some thresholding techniques, but the threshold value alone cannot give the best results, so they coupled it with a region growing algorithm, and obtained better results.

2.2.2.2 SRG in Medical Image Processing

In Medical Image Processing this kind of algorithms are used in works like segmentation in brain MRI, studied in (Stokking et al. (2000)), which explained that region growing methods, applied to brain MRI images, suffer from problems caused by weak boundaries, because of the fact that the brain tissue under consideration is readily connected to another tissue type, so another techniques must be conjugated with the SRG algorithm to achieve better results; Wang and Chen (2012) established the method of vector seeded region growing suitable for medical images, and after a vector seed selection, a region growing algorithm is used. A new technique was proposed because traditional SRG methods do not work well in Brain MRI image segmentation. Breast MRI images are object of study in works like Al-Faris et al. (2012), which proposed a modified automatic SRG algorithm based on the Particle Swarm Optimization image clustering system. This method resulted in a significant improved performance, but it also avoided the need for manual selection of the suspected region window with the object of interest, seed pixel and threshold value processes; Al-Faris et al. (2013) used a system with automated features for MRI breast tumor segmentation, staged in three stages, being the last one based on a modified version of the SRG method. The first modification is that the algorithm automatically selects the initial seed and, the second is that SRG threshold value is determined by measuring the difference between the initial pixel and its neighbors. This modified method was presented before in (Al-Faris et al. (2012)). Wong and Zrimec (2006) automatically detected lung disease and, used a seeded region growing algorithm to guide the classifier to regions with potential disease patterns. The seeds utilized are selected based in regions of interest in the periphery of the lung. Mat-Isa et al. (2005) improved screening for cervical cancer, using SRG algorithm to extract features of cervical cells and it was proved to be very suitable for resolving this problem. Or applying these techniques to forensic-case analysis, as in (Urschler et al. (2012)), where blood pools are extracted from the MRI scan using SRG because of the good contrast that the blood pool has with the surrounding tissue. There are other works using this kind of algorithm, like Pohle and Toennies (2001), which presented a new self-learning, fully automatic approach for a region-oriented segmentation of medical images. The algorithm learns its homogeneity criterion automatically from characteristics of the region to be segmented; Chen et al. (2006) created a sketch-based interface for seeded region growing volume segmentation. The region of interest is showed in real-time to the user when he places the seed point in the 3D model.

2.2.2.3 SRG in Industrial Applications

Seeded Region Growing algorithms are also used in Industrial Inspection, and Lachance et al. (2004) presented a region growing technique specifically adapted to wear flats segmentation, this was necessary because segmentation of wear flat area from the image background is a difficult task. The new method made possible to recognize wear flats

by their pixels grayscale value as well as their connectivity to reference pixels; Pottmann et al. (2005) used region growing as an aid in the segmentation process for reverse engineering of geometric objects in Industrial Geometry applications; Hadwiger et al. (2008) presented a novel method for interactive exploration of industrial CT volumes, such as cast metal parts, which helps to bridge the gap between visualization and feature detection. The standard approach for defect detection is based on region growing, which requires manually tuning parameters, however a new approach is introduced that allows interactive exploration of the parameter space, in a pre-processing stage separated from the region growing stage; Zhengtao et al. (2011) proposed a region growing technique based on linear scanning in order to do online capsule image segmentation.

2.2.3 Selected SRG Methods for Sea Surface Temperature (SST) Image Analysis

Summary of the SRG methods used to tackled the problem of upwelling delimitation:

- **SEC** (Single seeded)
  Novel homogeneity criterion in the format of a product. The growth is controlled by a threshold and it stops when no more pixels meet the homogeneity criterion.

- **AdamsSRG** (At least two seeds (manual))
  The frontier pixel that has the smaller difference of intensity to the mean of its neighbor region is added to it. The growth of the regions stop when all the image pixels were allocated to some region.

- **VermaSRG** (Single seeded)
  Organizes the region pixels in one stack. The pixel in the top of the stack is removed and, allocated to the region if the Euclidean distance of its intensity to the seed is smaller than a pre-defined threshold. The growth stops when the stack is empty.

- **ShihSRG** (At least two seeds (auto))
  Similar to the AdamsSRG, but offers an automatic seed selection mechanism and, a merging procedure that in the end of the segmentation combines regions that are similar to each other.

- **GambottoSRG** (Single seeded)
  Combines the region growing with an edge detection algorithm, in order to detect the optimal region boundary and stop the growth.

- **ZanatySRG** (Single seeded)
  The homogeneity criterion consists in the difference between the pixel and the mean of the region, but the threshold that controls the growth is based on the probability of the pixels and changes dynamically. The growth stops when one of the pixels does not pass the homogeneity criterion.

2.2.3.1 The Adams and Bischof Seeded Region Growing

The first chosen SRG algorithm to be used in the comparison was the Seeded Region Growing algorithm presented by Adams and Bischof (1994). It was chosen exactly because it is the reference algorithm in terms of SRG, and consequently it has been widely studied in many related studies on SRG methods. Even it being an algorithm with some problems, namely order dependency issues, it is also very appropriate to use it in this study, because it is a well referenced work in the literature.

It performs a segmentation of an image in K regions with respect to a set of seed points. Each seed region is a connected set of points or a individual point represented by C_k, where $k = 1, 2, \ldots, K$. Each step involves adding one pixel to one of the regions. We start reasoning about the algorithm by considering the current state of the sets C_k after m steps. Let F be the set of all unallocated pixels that border at least one of the labeled regions C_k:

$$F = \left\{ (i,j) \notin \bigcup_{k=1}^{K} C_k \mid N(i,j) \cap \bigcup_{k=1}^{K} C_k \neq \oslash \right\} \tag{2.1}$$

where $N(i,j)$ represents the immediate neighbors of the pixel (i,j).

For a pixel $(i,j) \in F$, if $N(i,j)$ intersects only one labeled region then, to this pixel, a label represented as $l(i,j) = k$ ($l(i,j) \in \{k = 1, 2, \ldots, K\}$). A measure, $\delta((i,j), C_k)$, is defined as the difference between $(i,j) \in T$ and the intersected region C_k:

$$\delta((i,j), C_k) = |g(i,j) - mean\{g(i_k, j_k)\}| \tag{2.2}$$

where $g(i,j)$ is the intensity value of the testing pixel (i,j), and $g(i_k, j_k)$ are the intensity values for the region C_k.

If $N(i,j)$ intersects more than one region C_k, then (i,j) will be labeled to the region k^* for which $\delta((i,j), C_{k^*})$ is minimized with respect to the neighboring regions C_k, $l(i,j) = k^*$. From all the points in F, one is chosen that satisfies:

$$(i^z, j^z) = argmin_{(i,j) \in F} \left\{ \delta\Big((i,j), C_{l(i,j)}\Big) \right\} \tag{2.3}$$

and (i^z, j^z) is added to $C_{l(i,j)}$.

After this, step $m+1$ is completed. The algorithm continues executing more steps until all the pixels have been allocated.

The definitions at 2.2 and 2.3 guarantee that the final segmentation is into regions as homogeneous as possible given the connectivity constraint.

2.2.3.2 The Verma Seeded Region Growing

Other chosen SRG algorithm was the Single Seeded Region Growing Algorithm for Color Image segmentation presented by Verma et al. (2011). The reason for its selection is that it is a similar algorithm to the SEC algorithm in terms of its architecture, because it is single

seeded and only grows one region at a time, and it also uses thresholding techniques to tune the threshold value, in this case they used the Otsu's adaptive thresholding method.

The method allocates pixels to the cluster C in a growing process that organizes the region pixels in a stack. Starting with only the seed in the stack, $N(i^{'}, j^{'})$ represents the 8-neighbors of the pixel in the top of the stack. If these pixels match the similarity criterion and they are not yet in the cluster C, they are added to the top of the stack and to the cluster C. The similarity criterion consists in:

$$\sqrt{(g(i,j) - g(i_s, j_s))^2} < \pi \tag{2.4}$$

where $g(i,j)$ is the intensity value of the testing pixel $(i,j) \in N(i^{'}, j^{'})$, and $g(i_s, j_s)$ is the intensity value of the seed. The π value is the threshold that controls the growth of the cluster C and it is defined using the Otsu's method of automatic thresholding applied to the image.

When a new pixel has its neighbors $N(i^{'}, j^{'})$ evaluated, this pixel of the cluster C is removed from the top of the stack. The growth of the cluster C stops when there are no pixels left in the stack.

2.2.3.3 The Shih and Cheng Seeded Region Growing

This method presented by Shih and Cheng (2005) is similar to the greedy method of Adams and Bischof (1994) described in the Section 2.2.3.1, so it requires more than two seeds to segment the image. One of the main focus of this method is to overcome the problem that the reference method has in the seed selection, so the growing phase between both methods is very similar, however this method has a mechanism to automatically select adequate seeds and a merging procedure that in the end of the segmentation combines regions that are similar to each other. For this method the homogeneity condition is defined by:

$$\delta((i,j), C_k) = \sqrt{(g(i,j) - mean\{g(i_k, j_k)\})^2} \tag{2.5}$$

instead of what is defined at 2.2.

The automatic seed selection process consists in evaluating which of the the image pixels pass in two conditions. The first condition checks if the pixel is similar to its neighbors and the second condition check if the pixel is not on the boundary of two regions. Each spatially connected set of pixels will be used as seed to the growth of the different regions.

In the first condition starts defining the similarity of a pixel by calculating the standard deviation σ to its 8-neighbors. The standard deviation is normalized to [0,1] by:

$$\sigma_N = \frac{\sigma}{\sigma_{max}} \tag{2.6}$$

where σ_{max} is the maximum of the standard deviation in the image. The similarity of a pixel to its neighbors is:

$$H = 1 - \sigma_N \tag{2.7}$$

A seed pixel candidate must have the similarity H higher than a pre-defined threshold value.

For the second condition it is calculated the Euclidean distance of the candidate pixel to its 8-neighbors. Then it is calculated the maximum distance to its neighbors:

$$d_{max} = max_{i=1}^{8}(d_i) \tag{2.8}$$

where d_i is the distance between the pixel and one of its neighbors. A seed pixel candidate must have the maximum distance d_{max} below a pre-defined threshold.

The automatic seed selection process can generate too much regions and after the growth phase the image can be over-segmented, so to overcome the problem it is applied region-merging. Two criteria are used, the first is about merging similar regions, if the mean intensity difference between two neighboring regions is less than a threshold value, the regions are merged and the mean re-computed. The process is repeated until no region has the distance less than the threshold. The other criterion merges regions until there are no regions left with size smaller than a pre-defined threshold.

2.2.3.4 The Gambotto Seeded Region Growing

Another method was selected, proposed by Gambotto (1993), and it is single seeded, however the reason to be chosen for this study is because it combines the region growing with an edge detection algorithm, in order to detect the optimal region boundary and stop the growth. This approach can be specially efficient for images with weak gradients in the upwelling frontier, where it is difficult to avoid explosions.

Initially the cluster C is composed only by the seed, but more pixels are merged to the cluster in a iterative growing until the maximum of a global contrast function is detected.

Let C^+ be the set of pixels which are frontier to the cluster C and, C^- be the set of pixels which are adjacent to C^+ and belong to the cluster. The pixels in the frontier C^+ are joined into segments using an hierarchical clustering algorithm, and all the segments S_k of the region boundary C^+ are merged with the cluster C if they satisfy the following criterion:

$$|d(S_k, C)| < \alpha \cdot thg \tag{2.9}$$

where $d(S_k, C)$ is the distance of intensities between the cluster and a segment, α is a preset parameter and, thg is a threshold that is recomputed dynamically through the growing process, and consists in calculating the mean of the values in an histogram of Euclidean distances between pixels of the cluster C and the mean intensity of the

cluster. If none of the segments S_k satisfy the condition, the closest to the cluster is merged, meaning that the stopping criterion depends on the contour detection function to avoid an infinite number of iterations. The growing termination function depends on the average gradient of the boundary:

$$F(n) = \sum \frac{G(k,l)}{P(n)} \tag{2.10}$$

where $P(n)$ is the perimeter of region C, for the iteration n, and $G(k,l) = \left|Y_{i,j} - Y_{k,l}\right|$, where $Y_{i,j}$ and $Y_{k,l}$ are two adjacent pixels such that $Y_{i,j} \in C^+$ and $Y_{k,l} \in C^-$.

The function $F(n)$ is computed at each iteration and growing stops when two criteria are satisfied, the first one being:

$$Fmax - F(n) = \lambda \cdot thg \tag{2.11}$$

where λ is a pre-defined parameter. The second criterion is computed whenever the first one is satisfied:

$$Fmax - F^+(n^*) = \lambda \cdot thg \tag{2.12}$$

where n^* is the optimal iteration according to the first criterion and, $F^+(n^*)$ is the average gradient computed over the boundary of the cluster on the optimal iteration.

After stopping the growth, the algorithm has an de-growing phase in which the final cluster C contains the pixels that it had when the maximum of the function $F(n)$ was reached.

2.2.3.5 The Zanaty and Asaad Seeded Region Growing

The Probabilistic Region Growing algorithm presented by Zanaty and Asaad (2013) has also been chosen, since the homogeneity criterion is based on a different approach, the probability of pixels, also it presents a different approach to solve the problem of weak boundaries on images, and yet its thresholding strategy is adaptive, by varying over the image as a function of intensity probability.

The method normalizes each pixel intensity in the image to values between 0 and 1. It starts the growth with a seed pixel and transfers to the cluster C, from the frontier F of the cluster, one pixel at a time the until one of them does not pass in the homogeneity criterion. The pixel Z that will be analyzed next is the one selected by the function:

$$\delta(F,C) = |mean\{g(i_C, j_C)\} - g(i,j)| \tag{2.13}$$

where $(i,j) \in F$ and $g(i_C, j_C)$ is the mean intensity of the pixels in the cluster C. The selected pixel is:

$$Z = argmin_{(i,j)\in F}\{\delta(F,C)\} \tag{2.14}$$

The pixel Z is added to the cluster C if it passes the following homogeneity criterion:

$$|I_Z - mean\{g(i_C, j_C)\}| \leq T(I_Z, Pr(I_Z)) \tag{2.15}$$

where I_Z is the intensity of the pixel Z and $Pr(I_Z)$ is the probability of that intensity value in the image. The threshold is dinamically calculated for each pixel and is defined as:

$$T(I_Z, Pr(I_Z)) = T1(I_Z) \cdot T2(Pr(I_Z)) \tag{2.16}$$

which is defined by two thresholds $T1$ and $T2$. $T1$ is defined by:

$$T1(I_Z) = \begin{cases} I_Z^{2\gamma} & I_Z \leq \theta \\ (1 - I_Z)^{2\alpha} & I_Z > \theta \end{cases} \tag{2.17}$$

where $\gamma = \gamma_1 \cdot I_Z^{1/2}$ and $\alpha = \alpha_1(1 - I_Z)^{1/2}$. γ_1, α_1 and θ are pre-defined values. The threshold $T2$ is defined by:

$$T2(Pr(I_Z)) = e^{\beta} \tag{2.18}$$

where $\beta = -\beta_1 [log(Pr(I_Z))]^{-1}$ with β_1 being a pre-defined value.

2.3 Automatic Thresholding Techniques

Automatic thresholding techniques are very useful tool to separate objects from the background. These thechniques work especially well in images where the intensity values of pixels belonging to the object are substantially different from the intensity values of the pixels belonging to the background. The output of the thresholding operation is a binary image, usually represented with black and white pixels which are allocated to one or other color if their intensity is higher or lower to a threshold value. There is a range of factors that can interfere with the result of the threshold operation, such as nonstationary and correlated noise, ambient illumination, busyness of gray levels within the object and its background, inadequate contrast and object size not commensurate with the scene. The thresholding methods can be categorized into six groups according to the information they are exploiting (Sezgin and Sankur (2004)):

1. **Histogram shape-based methods**, where the smoothed histogram is analyzed in some features like the peaks, valleys and curvatures.

2. **Clustering-based methods**, which include algorithms where either gray-level samples are clustered in two parts as background and foreground or are modeled as a mixture of two Gaussians that represent the background and foreground.

3. **Entropy-based methods**, analyze some features of the image related to entropy, such as the entropy of the background and foreground regions, the cross-entropy between the original and the binary image, and others.

4. **Object attribute-based methods**, search a measure of similarity between the gray-level and the binary image, using the fuzzy shape similarity, edge coincidence and others.

5. **The spatial methods**, based on the analysis of higher-order probability distribution and/or correlation between pixels.

6. **Local methods**, calculate a threshold for each pixel adapted to the local image characteristics.

Threshold techniques are used for image segmentation, but they can also be used for optimization of threshold values used by other segmentation methods. Since, besides producing a binary image, they can also return the threshold value that leads to that segmentation, this value can be used afterwards in other algorithms. In the Seed Expanding Cluster algorithm the returned value of the thresholding techniques will be used in the similarity condition test. If a good threshold value is provided to the algorithm, then the segmentation achieved will be better.

Prieto et al. (2012) presented results for 12 fully automatic threshold methods. Their work analyses 40 algorithms studied in Sezgin and Sankur (2004), and excluded 19 algorithms with user-adjustable parameters. After this, they selected only 12 of them, the ones that provided good results in the tests performed. Analyzing Sezgin and Sankur (2004) and Prieto et al. (2012) studies, three threshold methods were selected, based on their performance. Since no experimental study was done, using most of the thresholding techniques studied on the surveys applied to the segmentation of coastal upwelling images, the results to be achieved might not be the best, but for an initiating the study the threshold methods presented by Ridler and Calvard (1978), Otsu (1979) and Kittler and Illingworth (1986), which belong to the category of clustering-based algorithms, look like a good bet. If good segmentation results fail to exist, then other methods might have to be considered.

There are a close relationship between the three popular methods of image thresholding, which is explained in (Xue and Zhang (2012)). The authors derived that the Ridler and Calvard's iterative-selection method is an iterative version of Otsu's method; Otsu's method can be viewed as a special case of Kittler and Illingworth's minimum-error-thresholding method.

The definitions necessary to understand this three thresholding algorithms are described in the Table 2.1.

Table 2.1: Definitions and notation necessary to describe thresholding algorithms (Prieto et al. (2012)):

		Segmented Image	
	Original Image	**Background**	**Foreground**
Fraction of pixels	1	$\omega_1(T) = \sum_{i=1}^{T} p(i)$	$\omega_2(T) = \sum_{i=T+1}^{L} p(i)$
Probability of level i	$p(i)$	$p_1(i) = \frac{p(i)}{\omega_1}$	$p_2(i) = \frac{p(i)}{\omega_2}$
Average	$\mu = \sum_{i=1}^{L} i \cdot p(i)$	$\mu_1(T) = \sum_{i=1}^{T} i \cdot p_1(i)$	$\mu_2(T) = \sum_{i=T+1}^{L} i \cdot p_2(i)$
Variance	$\sigma^2 = \sum_{i=1}^{L} (i-\mu,)^2 \cdot p(i)$	$\sigma_1^2(T) = \sum_{i=1}^{T} (i-\mu_1(T))^2 \cdot p_1(i)$	$\sigma_2^2(T) = \sum_{i=T+1}^{L} (i-\mu_2(T))^2 \cdot p_2(i)$

2.3.1 Ridler and Calvard's method

Ridler and Calvard (1978) presented an iterative process, based on two-class Gaussian mixture models, to select the optimum threshold value automatically, as successive iterations provide increasingly cleaner extractions of the object region. For the next iteration, optimum threshold is defined as the average of the foreground and background class means. Iterations stop when the difference between the current iteration threshold and next iteration threshold is sufficiently small.

$$T_{n+1} = \frac{\mu_1(T_n) + \mu_2(T_n)}{2}$$

where $\mu_i(T_n)$ are the means of the background and foreground defined by the threshold T_n of the previous iteration.

2.3.2 Otsu's method

Otsu (1979) proposed a nonparametric and unsupervised method of automatic threshold for image segmentation. This method is suitable for segmentation of classes, in the histogram, with approximate or equal within-class variances. This technique consists in minimizing the weighted sum of within-class variance of the foreground and background to extract an optimum threshold. Minimizing the within-class variance is equivalent to maximizing the between-class variance. This is a very popular method and it has been applied to tune threshold values in works developed by Shih and Cheng (2005), Verma et al. (2011) and Dantulwar and Krishna (2014).

$$T = argmax\left\{\omega_1(T)(\mu_1(T) - \mu)^2 + \omega_2(T)(\mu_2(T) - \mu)^2\right\}$$

where weights $\omega_i(T)$ are the probabilities of the two classes separated by a threshold T, $\mu_i(T)$ are the class means and, μ is the mean value of the complete image.

2.3.3 Kittler and Illingworth's method

Kittler and Illingworth (1986) presented a method that starting at an initial threshold value, the two resulting pixel populations, in the histogram, are modeled by Normal

distributions. One formed by the pixels which the brightness level is smaller than the initial threshold and the other formed by the pixels which the brightness level is bigger than the threshold. A criterion function is calculated for each brightness threshold and the better the models fit the data, the smaller the criterion. So, the output will be the threshold value that minimizes the criterion function.

$$T = argmin\{1 + 2[\omega_1(T)log(\sigma_1(T)) + \omega_2(T)log(\sigma_2(T))] \\ -2[\omega_1(T)log(\omega_1(T)) + \omega_2(T)log(\omega_2(T))]\}$$

where weights $\omega_i(T)$ are the probabilities of the two classes separated by a threshold T and, foreground and background standard deviations are represented by $\sigma_i(T)$.

2.4 Evaluation Measures for Image Segmentation

Many different approaches and algorithms for image segmentation were proposed, but it is still difficult to assess if an algorithm produces good segmentation results (Zhang et al. (2008)). Subjective evaluation is a very common method for evaluating the effectiveness of a segmentation method, in which a human visually analyze the results, but it might be a tedious process and inherently limits the depth of evaluation to a limited amount of images, other disadvantage is its inherent subjective nature. Another common method is supervised evaluation, which operates by comparing the resulting segmented image against a manually-segmented reference image, often referred to as gold standard or ground-truth. The advantage of this method is that direct comparison between image and reference image provides solid quality evaluation. However this method also has disadvantages, namely the need to generate the reference image, which might be difficult, subjective and time-consuming. Both this methods require user assistance, so sometimes they are unfeasible in many applications, so unsupervised methods are necessary. This methods are quantitative, objective and do not require a reference image, but instead evaluate a segmented image based on how well it matches a broad set of characteristics of segmented images as desired by humans. Unsupervised methods are uniquely suitable for automatic systems, which do not include beforehand knowledge about the content of the image and no ground truth is available.

2.4.1 Supervised Evaluation Measures

Zhang (1996) classified segmentation evaluation into three groups: the analytical, the empirical goodness and the empirical discrepancy groups. For images with ground-truth made by the experts, supervised evaluation approach, also known as empirical discrepancy method, can be used taking into account the difference between the segmented and reference image. This author stated that the discrepancy measures are based on: the

number of mis-segmented pixels; the position of mis-segmented pixels; the number of objects in the image; the feature values of segmented objects; miscellaneous quantities.

A commonly used measure that combines precision and recall, calculated from the values in a confusion matrix that crosses the results with a ground-truth, is the harmonic mean of precision and recall, the F-measure (Van Rijsbergen (1979)). Precision is the proportion of predicted positive cases that are correctly real positives, while recall is the proportion of real positive cases that are correctly predicted positive. This method produces results between 0 and 1, being the highest score the best result.

Other supervised measure is the Adjusted Rand Index (ARI), presented by Hubert and Arabie (1985) , which measures the similarity between two data clusterings, starting by calculating a confusion matrix as in the F-measure measure. This method can score from negative values until 1, and the highest the score better the result.

These two supervised measures, the F-measure and the ARI, were the selected ones for evaluate the quality of the segmentation produced by the different segmentation methods applied in these study.

2.4.2 Unsupervised Evaluation Measures

Zhang et al. (2008) examined unsupervised objective evaluation methods that have been proposed in the literature and experiment the performance of nine evaluation metrics, founded suited to general image segmentation. This metric can be largely divided into three categories: those for measuring intra-region uniformity, those for measuring inter-region disparity, and those for measuring semantic cues of objects, such as shape. These metrics are then combined to give a composite effectiveness measure.

The selected unsupervised evaluation measures were the intra-region and inter-region measures of Levine and Nazif, intra-region and inter-region measures of Rosenberger and Chehdi, Otsu's within-class and between-class variances, Calinski-Harabasz criterion, Davies-Bouldin criterion and intra-region of Liu and Yang.

The following notation was used to describe the unsupervised evaluation measures. Let I be the segmented image divided in N regions. The number of pixels in the image is S_I, and it is used R_j to denote the set of pixels in the region j, so S_j is the number of pixels of the region. Let x be the temperature and p a pixel. $C_x(p)$ is the temperature associated to the pixel p.

The average temperature in the region j is:

$C_x^{'}(R_j) = \left(\sum_{p \in R_j} C_x(p) \right) \Big/ S_j$

The squared color error of region j is denoted as:

$e_x^2(R_j) = \sum_{p \in R_j} (C_x(p) - C_x^{'}(R_j))^2$

(i) **Intra-region of Levine and Nazif (1985):**

$Eval = \sum_{j=1}^{N} \frac{e_x^2(R_j) \cdot W_j}{Z}$

$Z = (maxR_j - minR_j) \cdot S_j$

$W_j = 1$ (weighting factor)

(ii) **Inter-region of Levine and Nazif (1985):**

For an area α, the adjacency value p_{ij} is used for weighting the contrast between regions, and the weight for the region R_j is v_j.

$Eval = \left(\sum_{R_j \in \alpha} v_j \sum_{adjR_i} p_{ij} \frac{\left|C^{'}(R_i) - C^{'}(R_j)\right|}{C^{'}(R_i) + C^{'}(R_j)} \right) \Big/ \sum_{R_j \in \alpha} v_j$

(iii) **Intra-region of Rosenberger and Chehdi (2000):**

$Eval = \frac{1}{N} \sum_{j=1}^{N} \frac{S_j}{S_I} e_x^2(R_j)$

(iv) **Inter-region of Rosenberger and Chehdi (2000):**

Let B_j be the barycenter of region R_j and $d(B_i, B_j)$ be the Euclidean distance between two different regions.

$Eval = \frac{d(B_i, B_j)}{\|B_i\| + \left\|B_j\right\|}$

(v) **Intra-region of Otsu (1979):**

$Eval = \frac{S_i}{S_I} \cdot e_x^2(R_i) + \frac{S_j}{S_I} \cdot e_x^2(R_j)$

(vi) **Inter-region of Otsu (1979):**

$Eval = \frac{S_i}{S_I} \cdot \frac{S_j}{S_I} \cdot (C_x^{'}(R_j) - C_x^{'}(R_i))^2$

(vii) **Intra-inter-region of Caliński and Harabasz (1974):**

Let SS_B be the overall between-cluster variance, SS_W the overall within-cluster variance, O the number of observations and m be the overall mean.

$Eval = \frac{SS_B}{SS_W} \cdot \frac{(O-N)}{N-1}$

$SS_B = \sum_{i=1}^{N} n_i \left\| C_x^{'}(R_i) - m \right\|^2$

$SS_W = \sum_{i=1}^{N} \sum_{x \in R_i} \left\| x - C_x^{'}(R_i) \right\|^2$

(viii) **Intra-inter-region of Davies and Bouldin (1979):**

Let $d^{'}$ be the average distance between each pixel temperature in a region and the centroid of that region. The Euclidean distance between the centroids of two regions is denoted by d_{ij}.

$Eval = \frac{1}{N} \sum_{i=1}^{N} max_{j \neq i} \left\{ D_{ij} \right\}$

$D_{ij} = \frac{(d_i^{'} + d_j^{'})}{d_{ij}}$

(ix) **Intra-region of Liu and Yang (1994):**

$Eval = \sqrt{N} \sum_{i=1}^{N} \frac{e_x^2(R_j)}{S_i}$

Chapter 3

Proposed Approach

3.1 The Seed Expanding Cluster (SEC)

3.1.1 The SEC method

In order to do automatic detection of coastal upwelling from Sea Surface Temperature images, a clustering algorithm was proposed as a new version of Seeded Region Growing. One Seed Expanding Cluster (SEC), as it was named by Nascimento et al. (2015), takes the concept of approximate clustering due to Mirkin (1996) and Mirkin (2013) to derive a homogeneity criterion different from the conventional difference between a pixel value and the mean of the values over the region of interest. The proposed homogeneity criterion has the format of a product and it is mathematically equivalent.

Basically, the algorithm checks for the coldest pixel in the image and uses it as the initial seed. Then, it involves a boundary-oriented pixel labeling, and expanding its boundary iteratively so that the cluster can grow.

This method overcomes the problem of dependence of pixel sorting order, and the boundary-oriented pixel labeling can be done in parallel to speed up the procedure.

3.1.2 The SEC Algorithm

As described in Nascimento et al. (2015), the algorithm receives as input a temperature map $T(R,L)$, where R is the set of rows and L the set of columns, and elements of $R \times L$ are pixels. It also receives the size of the exploring window W, and two threshold values π and α. The exploring window $W(i,j)$ is centered at pixel $(i,j) \in R \times L$. π represents the temperature similarity threshold and α describes the cluster density threshold. The Output is a cluster $C \subseteq R \times L$ in the format of a binary map $Z(R,L)$ with elements z_{ij} where $z_{ij} = 1$ if $(i,j) \in C$ and $z_{ij} = 0$ if $(i,j) \notin C$.

A Pre-Processing stage, which is the step one, is executed, and for each pixel in the image, the average temperature $t^* = mean(T(R,L))$ is subtracted. The values after the subtraction are denoted as $t(i,j)$.

The second step of the algorithm is the Cluster Initialization, which will initially be a cluster containing only the pixel with minimum temperature value, the initial seed $o = (i_o, j_o)$. If there is more than one pixel that has the same minimum temperature, then o is chosen randomly among them. With the exploring window W centered at the seed pixel o, for every pixel (i,j) inside the window $W(i_o, j_o)$, the pixel is added or not to the cluster C, if the similarity condition holds:

$$c \times t(i,j) \geq \pi \tag{3.1}$$

where c is the temperature in the seed pixel, $t(i,j)$ the temperature in the tested pixel and π is the temperature similarity threshold.

In the third step, Set Cluster Boundary, it is defined the cluster boundary set F containing the unlabeled pixels $(i^{'}, j^{'})$ within the map $R \times L$ which are adjacent to the cluster C. The boundary pixels do not belong to the cluster but have an 8-neighborhood set of pixels intersecting the cluster. The boundary set F is defined as:

$$F = \left\{(i^{'}, j^{'}) \notin C | N(i^{'}, j^{'}) \cap C \neq \oslash\right\} \tag{3.2}$$

where $N(i^{'}, j^{'})$ is the 8-neighborhood set of the pixel.

Then, in the fourth step, Expansion, the cluster C will be expanded step by step in an iterative way, until the boundary F is empty or the boundary does not change between consecutive iterations. So, for each boundary pixel $(i^{'}, j^{'})$ in F the boundary expand region, for that pixel, is defined as the subset of pixels in the exploring window $W(i^{'}, j^{'})$ that intersect the pixels (i,j) of the cluster, that is $(i,j) \in W(i^{'}, j^{'}) \cap C$. Let c^* be defined as the mean temperature of those pixels.

The homogeneity criterion is defined by two conditions, the temperature similarity condition and the density condition. The first one guarantees that the expansion of the cluster evolves smoothly according to the variation of temperatures, and the second one guarantees the special continuity of the cluster.

First, the similarity condition which compares the product of c^* by $t(i^{'}, j^{'})$ to the similarity threshold:

$$c^* \times t(i^{'}, j^{'}) \geq \pi \tag{3.3}$$

with the temperature c^* defined as $c^* = mean(T(W(i^{'}, j^{'}) \cap C))$ and $t(i^{'}, j^{'})$ representing the current boundary pixel temperature.

Second, the density condition tests if the number of pixels of cluster C that intersect the exploring window $W(i^{'}, j^{'})$ divided by the number of total pixels within $W(i^{'}, j^{'})$, is higher than the given density threshold:

$$\frac{|W(i^{'}, j^{'}) \cap C|}{|W(i^{'}, j^{'})|} \geq \alpha \tag{3.4}$$

If both homogeneity tests hold true, then the boundary pixel $(i^{'}, j^{'})$ is inserted in an auxiliary cluster $C^{'}$ and the corresponding boundary pixels $N(i^{'}, j^{'})$, that do not belong already to the cluster C or to the current boundary F, are allocated to the auxiliary boundary set $F^{'}$. Both the auxiliary sets $C^{'}$ and $F^{'}$ are emptied in every iteration of this fourth step. Until all boundary pixels of F have been tested, the process continues. After this, the new labeled pixels in $C^{'}$ are merged with cluster C and the pixels in the auxiliary set $F^{'}$ are merged with the boundary set F, and the pixels which the result in both homogeneity tests was positive, meaning the new members of the cluster saved in $C^{'}$, are removed from the new boundary set F.

Treating all frontier pixels before updating the cluster and the new boundary set, guarantees that there will not be a dependency on the order of processing boundary pixels. This also permits the parallel processing of similarity and density conditions, as well of the different boundary pixels.

It is important to salient that in the self-tuning version of the SEC algorithm the density condition 3.4 was abolished and the similarity threshold π in conditions 3.1 and 3.3 does not need to be given as input and is specified as $mean(T(W(i^{'}, j^{'}) \cap F))$.

The SEC algorithm can be formally described in the following scheme:

Input: $T(R, L)$ - A temperature map, where R is the set of rows and L the set of columns;
w - The size of the exploring window W;
π - The temperature similarity threshold;
α - The cluster density threshold.

Output: The Output is a cluster $C \subseteq R \times L$ in the format of a binary map $Z(R, L)$ with elements z_{ij} where $z_{ij} = 1$ if $(i, j) \in C$ and $z_{ij} = 0$ if $(i, j) \notin C$.

Step 1 **Pre-processing:** For each pixel in the image, the average temperature $t^* = mean(T(R, L))$ is subtracted. The values after the subtraction are denoted as $t(i, j)$.

Step 2 **Cluster Initialization:** Initially, the cluster contains only the pixel with minimum temperature value, the initial seed $o = (i_o, j_o)$. So, $C = \{(i_o, j_o)\}$. The temperature in the seed pixel (i_o, j_o) is denoted as c. With the exploring window W centered at the seed pixel o, for every pixel (i, j) inside the window $W(i_o, j_o)$, the pixel is added to the cluster C, if the follow similarity criterion holds:

$c \times t(i,j) \geq \pi$

Step 3 **Set Cluster Boundary:** The boundary set F is defined as the unlabeled pixels $(i^{'}, j^{'})$ within the map $R \times L$ which are adjacent to the cluster C:

$$F = \left\{(i^{'}, j^{'}) \notin C | N(i^{'}, j^{'}) \cap C \neq \oslash\right\},$$

where $N(i^{'}, j^{'})$ is the 8-neighborhood set of the pixel.

Step 4 **Expansion: While** boundary set F not empty and the boundary has changed between consecutive iterations:

Step 4.1 Set $C^{'} = \oslash$; $F^{'} = \oslash$

Step 4.2 **For** each boundary pixel $(i^{'}, j^{'}) \in F$:

Step 4.2.1 The *boundary expand region* is defined as the subset of pixels in the exploring window $W(i^{'}, j^{'})$ that intersect the pixels (i, j) of the cluster, that is $W(i^{'}, j^{'}) \cap C$. Let c^{*} be defined as $c^{*} = mean(T(W(i^{'}, j^{'}) \cap C))$.

Step 4.2.2 **If** the *similarity* and *density* criteria hold:

$$c^{*} \times t(i^{'}, j^{'}) \geq \pi$$

$$\frac{|W(i^{'}, j^{'}) \cap C|}{|W(i^{'}, j^{'})|} \geq \alpha$$

then the boundary pixel $(i^{'}, j^{'})$ is inserted in an auxiliary cluster $C^{'}$ and the corresponding boundary pixels $N(i^{'}, j^{'})$, that do not belong already to the cluster C or to the current boundary F, are allocated to the auxiliary boundary set $F^{'}$:

$$C^{'} = C^{'} \cup \left\{(i^{'}, j^{'})\right\};$$

$$F^{'} = F^{'} \cup N(i^{'}, j^{'}) - C - F;$$

Step 4.3 The new labeled pixels in $C^{'}$ are merged with cluster C and the pixels in the auxiliary set $F^{'}$ are merged with the boundary set F, and the pixels which the result in both homogeneity tests was positive, meaning the new members of the cluster saved in $C^{'}$, are removed from the new boundary set F:

$$C = C \cup C^{'}; F = F \cup F^{'} - C^{'}$$

3.1.3 Self-tuning version of SEC

The similarity threshold π has a major impact in the quality of the segmentation produced by the SEC algorithm. The parameter can be tuned using automatic thresholding techniques, meaning that the threshold π is fixed before the growing stage. However, there is an self-tuning version of the SEC algorithm that dinamically calculates the threshold π. Its value changes depending on the state of the cluster C and its interception with the window $W(i^{'}, j^{'})$.

The self-tuning version is similar to the other versions in the structure of the algorithm, except that it is calculated independently for each pixel that is being analyzed to enter the cluster C, meaning that the similarity threshold π in the Condition 3.3 is defined as $(mean(T(W(i^{'}, j^{'}) \cap C)))^2/2$.

3.2 Iterative Seed Expanding Cluster (I-SEC)

The upwelling area sometimes is fragmented by different coastal regions. The SEC algorithm only grows one region, defining a cluster contiguous in space, however for tackling the problem of extracting the upwelling areas composed by more than one single contiguous zone, it is necessary to run the growing procedure more than once. This discontinuity is seen in the Figure 3.1, where the upwelling phenomenon exists in separated areas of water, with the lateral bar of the image containing the colors that codify the temperature at the boundary, of one upwelling area in yellow, and another in green. An iterative version of the SEC algorithm had to be developed to treat the problem of discontinuous upwelling areas.

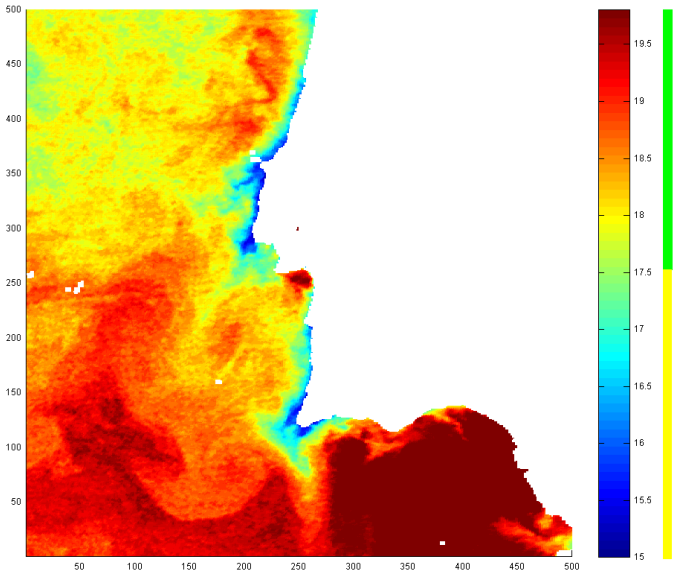

Figure 3.1: SST image of the portuguese coast (12 June 1998). At least two relatively large, not contiguous, upwelling areas can be distinguished in this image, one in the north and other in the south, which are separated by warmer waters in the middle of the image.

In order to extract multiple discontinuous areas it is necessary to have the iterative procedure, which runs the region growing algorithm, and that allocates new regions to the final segmentation result if they meet certain conditions or the stopping criterion is not yet active.

The iterative procedure grows one region at a time, starting in the coldest pixel near the continental coast, where the upwelling occurs, and at each iteration uses the region growing algorithm to extract one more cluster, until a stopping criterion is activated.

All the initial seeds must be inside the seed selection area, near the continental coast where the upwelling occurs, meaning that it was taken advantage of the geographical information and high-level knowledge of the upwelling phenomenon to define the area where the seeds are selected from. After the first region of upwelling is extracted, the next seed will be selected from the residual seed selection area. If there is no available space left in this area, the iterative procedure must stop, because no other further extracted cluster would corresponded to an upwelling region.

It was early defined was that the extracted cluster must have at least a pre-determined size, because it is common that micro groups of pixels are extracted and they usually are created by noise in the image, or alternatively these micro clusters can arise after all the upwelling area is segmented, because the iterative procedure will select the next coldest pixel near the coastal area of the residual image. The defined minimum size of a cluster was defined to 15×15 pixels, because this was a threshold that was small enough to let enter real upwelling areas, but a big enough size to let out of the final result the extracted noise that was irrelevant.

These micro groups of pixels when originated by noise can delay the extraction of the relevant upwelling areas and cause the second upwelling area to only be extracted in the fourth or fifth iteration, for example, and sometimes, after being extracted all the relevant upwelling regions, these micro clusters of noise continue to show up at least until the stopping criteria is reached. It is even possible to the iterative version continue to extract the next coldest pixel that does not grow a big enough cluster for a large number of iterations. To avoid these problems, it was added to the stopping criteria a maximum of iterations, starting at the moment that the first upwelling region is extracted. It was possible to empirically set this maximum number of iterations to 5, which for the full set of SST images in the study was enough to correctly extract the complete area of the upwelling phenomenon.

To define what should be an adequate stopping criterion to the iterative procedure which allows extracting multiple regions that represent upwelling area, it was registered for each of the extracted regions their mean and minimum temperatures and, it was possible do take advantage of the relationship between the mean temperature of the first extracted region and the minimum temperature of the one that is currently being extracted. Giving, as an example, one image with three discontinuous areas of cold waters near the coast that correspond to upwelling, after extracting the first region, the next seed will grow in the second area and the minimum temperature of that region is lower than

the mean temperature of the first extracted cluster. The same thing happens to the third region that still corresponds to an upwelling area, however when the next coldest pixel is selected and the iterative procedure extracts a fourth cluster, because this one does not belong to the coldest waters that represent the upwelling area, its minimum temperature is usually higher than the mean temperature of the first region or at least it is close to that mean temperature. So, knowing this, it is possible to define a stopping criterion that consists in not adding the last extracted cluster to the final segmentation result and stop the extraction of more clusters, if the difference between the mean temperature of the first region and the minimum temperature of the current region is below a pre-defined threshold ε.

An advantage of subtract to the mean of the first extracted cluster is that the difference always decreases at each iteration, and this allows to fix the threshold ε, and knowing for sure that the next extracted region will not enter the final segmentation, because the difference to the the mean of the first extracted region will be even lower, so it makes possible to end earlier the iterative process.

A correct value for the threshold ε is important to guarantee that non upwelling regions will not be added to the final segmentation result and to end the iterative process as soon as possible. In order to correctly define an adequate value for this threshold it was necessary to observe when the mean temperature of the first region subtracted by the minimum temperature of the region that is being analyzed is big enough to let what are upwelling regions to enter the final segmentation and small enough to prevent non upwelling regions to enter the final result.

If the difference between the mean temperature of the first region and the minimum temperature of the cluster that is currently being extracted is higher than the threshold ε, the size of the region that is being extracted is bigger than the minimum size for a cluster to not be considered noise, and the maximum number of iterations was not yet reached, then the extracted region is added to final segmentation. However, sometimes a region can grow with an initial seed pixel which is inside the seed selection area near the coast, but from that growth results an massive explosion that clearly is not part of the upwelling region and, because its seed pixel has a low temperature, the condition that measures the difference between mean of the first and minimum of the current region allows the region to enter the final result. This problem happens mainly when running the self-tuning version of the SEC algorithm in the images of the Canary or, by running some other SRG method that have a tendency to over-segmentation. So, to avoid this improper behavior, an extra condition was defined to reinforce the quality of the final segmentation, by not allowing these explosions to enter the final segmentation result. The condition is of spatial nature and consists in measuring the percentage of pixels of the cluster that fall inside a pre-specified area of the image where the upwelling should be at least partially limited to, and check if it is lower than a certain threshold. This area was defined by observing the segmentation results of all the SST images and, for all types of the images the area of the extracted cluster must have to intercept the pre-defined area

in 20%. In the case of SST images of Portugal the pre-defined area was defined has a rectangle with $1 \leq x \leq 400$ and $175 \leq y \leq 300$. For the SST images of the Canary, the resolution of the SST image is different and the continental coast is not parallel with the sides of the image, so before the pre-defined area where the upwelling should occur at least partially, was defined to $45 \leq x \leq 420$ and $230 \leq y \leq 310$ after rotating the image $+40°$.

In short, the iterative procedure has four conditions that decide if a cluster should or not enter the final segmentation result and when it should stop. First it is checked if the extracted cluster is not noise and big enough to be considered an upwelling region, this parameter was called $minClusterSize$ and set to 15×15 pixels. It was also defined the maximum number of iterations, because even after the correct upwelling regions have been extracted, it can be space left in the residual area for seed selection and, seeds that did not grow continue to naturally appear until $maxIterations = 5$ is reached, as set by the experiments. In the case there is not left space in the seed selection area, then the iterative procedure should end earlier. If the extracted region passes the condition, defined by the difference between the mean of the first extracted cluster and the minimum value of the current one being greater than a threshold ε, the cluster is added to the final segmentation result, otherwise the iterative procedure stops. But if it passes this condition, there is an extra condition of spatiality that puts the extracted region to the final result if it is not a massive explosion that started in cold waters. At least 20% of the area of the extracted cluster must intercept a pre-defined area, which it was called $upwellingLikeliwood$. Besides the configuration of all this parameters and conditions, the one parameter that is more crucial and hard to tune is the threshold ε, and for that matter in Section 3.2.2 the complete study of the setting of this parameter as done.

The code to the iterative procedure is described in the following way:

Data: Image (map with temperature values)
Result: finalJ (binary map with the final segmentation result)

```
finalJ = zeros(size(Image));
iterating = true;
it = 1;
firstExtracted = false;
while iterating do
    [seedX, seedY] = selectSeed(Image);
    J = SEC(Image, seedX, seedY);
    minCluster = calcMinimum(J);
    meanCluster = calcMean(J);
    sizeCluster = calcSize(J);
    Image (J == 1) = NaN;
    if it ≥ maxIterations && firstExtracted then
        iterating = false;
    end
    if sizeCluster > minClusterSize then
        if ¬ firstExtracted then
            if firstMean - min > epsilon && it ≤ maxIterations then
                interception = calcInterceptionWithUpwellingZone(J);
                if interception > upwellingLikeliwood then
                    finalJ(J==1) = 1;
                end
            else
                iterating = false;
            end
        else
            firstExtracted = true;
            firstMean = meanCluster;
            finalJ(J==1) = 1;
        end
    end
    it = it + 1;
end
```

Algorithm 1: Iterative Procedure for the SEC algorithm

In the Figures 3.2 and 3.4 the results of the iterative procedure can be seed. This process allowed the SEC algorithm to successfully extract the correct number of discontinuous upwelling regions.

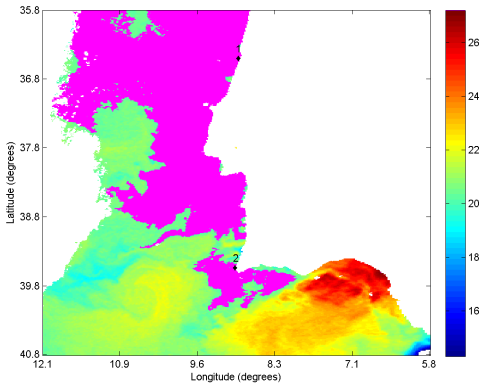

Figure 3.2: 1998-08-05 SEC-SelfTuning

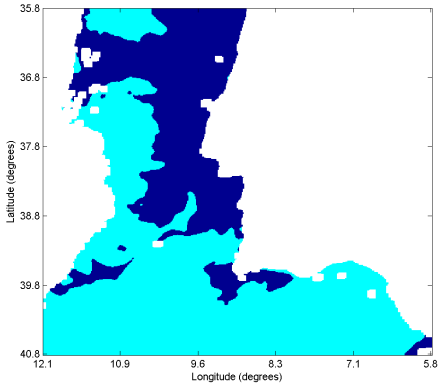

Figure 3.3: 1998-08-05 ground-truth map

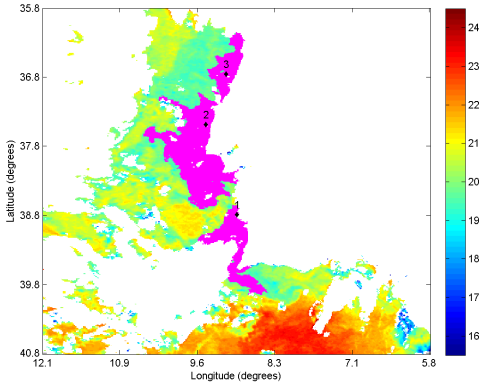

Figure 3.4: 1998-09-24 SEC-Kittler

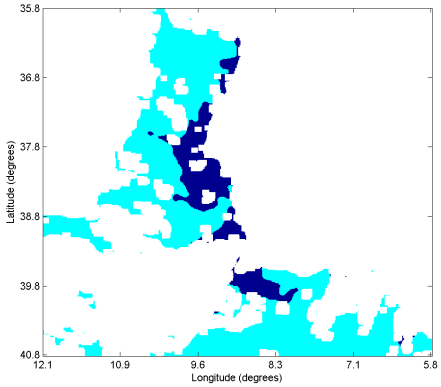

Figure 3.5: 1998-09-24 ground-truth map

3.2.1 Termination condition

The iterative procedure can end its execution by reaching the maximum number of iterations (*Max Iterations Termination*), by not having having enough space in the seed selection area to chose the next seed (*No Seed Termination*) or, by extracting a region that it is not considered to be upwelling and therefore failing in the condition which states that the difference between the mean of the first extracted cluster and the minimum value of the current one must be greater than a threshold ε (*Threshold Termination*), terminating the iterative procedure earlier because it is certain that further extracted clusters will not pass this condition too, due to the difference is always decreasing at each iteration, because the next seed will always be warmer and making the difference smaller.

In the Figure 3.6 it was registered how the iterative procedure terminates, for the results of the SEC-SelfTuning for all the SST images, and it is possible to see the percentage that each termination possibility occurs. In this case, it is possible to see that most of

the times the iterative procedure ends by the maximum number of iterations, which is expected, because most of the images only grow one and only cluster that correspond to a continuous area of upwelling and so, the next clusters that will be extracted are micro groups of pixels that did not grow because they are in warmer waters, and this are ignored because they do not pass in the condition that sets a minimum size for a cluster to represent upwelling. Overall, for the results of the SEC-SelfTuning, there is a good quota of terminations that represents lack of space left in a seed selection area to select another initial seed. This can be perfectly normal when the upwelling area covers all the continental coast and it is correctly extracted, however sometimes this can also be caused by over-segmentation that covers the seed selection area. The remaining reason to termination is not as high as the others and it is because the difference between the mean of the first extracted cluster and the minimum value of the current one is not greater than the threshold ε, so some non upwelling clusters were extracted and should not enter the final segmentation result, and this was detected and the iterative procedure ended earlier, knowing that further extractions would fail in this condition too. The quota from this last cause allows to understand how often a method extracts clusters that should have not been grown to a considerable size out of the upwelling zone.

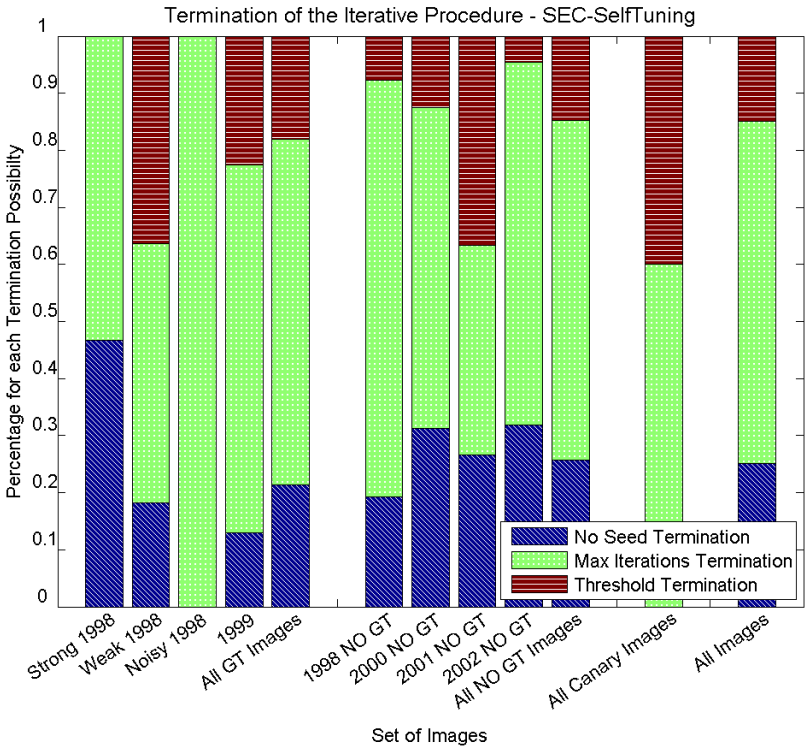

Figure 3.6: The plot shows the percentage for each termination possibility of the iterative procedure, organized by sets of images, in this case for the results of the SEC-SelfTuning.

The remaining graphics for the iterative procedure stopping cause are in the Appendix A.5, and for the other SEC versions, the most similar to the SEC-SelfTuning is

the SEC-Kittler, because is the quota for the *Threshold Termination* cause is also high, contrarily to the other two versions of the SEC algorithm, meaning that this methods are the ones where this condition is more useful to extracting the correct number of upwelling regions. Of the SRG methods, only the ZanatySRG requires frequently of this condition to terminate the iterative procedure. For all the region growing algorithms, *Max Iterations Termination* condition is naturally the most frequent, mostly because after the extraction of the upwelling areas, only micro groups of points that contain the next initial seed are extracted and ignored because of its irrelevant size. For both the Otsu-VermaSRG and MeanVermaSRG, the the quota for *No Seed Termination* is high, because these methods commonly have explosions that cover the entirety of the seed selection area. On the opposite side, the GambottoSRG never stops because of this condition, derived from its problem of under-segmentation, so there area always free space left in the residual seed selection area.

3.2.2 Threshold definition

In this study several data was collected by running the iterative procedure. For each set of SST images it was registered at each iteration the last upwelling region was captured; which termination condition of the iterative procedure was responsible for stopping the process that could be cause by not be any left space in the seed selection area (S), by the maximum number of iterations be reached (M) or by difference between the mean temperature of the first region and the minimum temperature of the cluster that is currently being extracted not being higher than the pre-defined threshold ε (T); and for the SST images of each set it was registered the values for the difference between the mean of the first region and the minimum of one relevant cluster. Relevant cluster can have multiple meanings, and in graphics like the ones of Figure 3.7 or 3.8, for the SEC-SelfTuning for image sets of 1998 and 1999 , the difference value for this relevant cluster is divided in five categories: *Multicluster/OK*, where in this case the SEC-SelfTuning extracted more than one region correspondent to upwelling area correctly, for SST images with discontinuity has listed in the Table A.1, and the relevant cluster which its minimum temperature is subtracted to the mean temperature of the first extracted cluster, in this case represents the last cluster that was extracted and corresponded indeed to an upwelling area. *Multicluster/UnderSegmentation* is similar to *Multicluster/OK*, however it happens in images without discontinuous upwelling regions, what happen in these cases was that besides multiple cluster had to be extracted and effectively correspond to upwelling areas, the multiple regions that were extracted happen because the method produced under-segmented results. For the SEC-SelfTuning this did not happen, however it was common when the SEC-Kittler was applied. *Multicluster/OverSegmentation* represent the cases when the an extracted cluster does not represent an upwelling zone and therefore it must be out of the final segmentation result, the difference in this case is to the first cluster that did not enter to the final segmentation result. Then there are the category

Onecluster/OverSegmentation, that happens in SST images that have discontinuity, but because of over-segmentation all the separated upwelling regions were extracted with only one cluster. *Onecluster/OK* represents the SST images that do not have discontinuity and only one cluster was extracted, meaning that the result was correct. In this case the difference is between the cluster and the residual image.

After the iterative procedure extracts the first region of upwelling, the next extracted regions must be evaluated to see if they should enter or not the final segmentation, in order to guarantee that the correct number of regions of upwelling is extracted. The developed iterative procedure as a condition that focus on this decision and consists in checking if the difference between the mean temperature of the first region and the minimum temperature of the cluster that is currently being extracted is higher than the threshold ε, if it is the region is added to the final result, if it is not then it does not appear in the final segmentation result. The correct tuning of the threshold ε is very important to assure that only upwelling regions enter the result. The threshold ε was calculated with the objective of separating the difference values of the categories *Multicluster/OK* and *Multicluster/UnderSegmentation*, from the values of the category that contains the clusters that do not represent upwelling areas, *Multicluster/OverSegmentation*.

In order to establish the threshold ε to techniques were applied, one supervised and one unsupervised, for each region growing algorithm applied. The Information Gain technique (Han and Kamber (2001)) , which is a entropy-based method that can set a threshold, which has the minimum entropy, to divide two sets . The method is supervised and takes advantage of a ground-truth to find the separation value, in this case the binary ground-truth are the difference values of the categories *Multicluster/OK* and *Multicluster/UnderSegmentation* represented as 1 in the ground-truth, and the *Multicluster/OverSegmentation* represented as 0. Being this method supervised, the ground-truth had to be carefully constructed, by doing the interception of the ground-truth of the SST images with the segmentation results of each algorithm, and seeing what cluster were or not representative of upwelling areas. However because there is no available ground-truth for the many of the images, unsupervised methods to calculate the threshold ε were considered, meaning that a larger amount of difference values could be considered using an unsupervised method, namely the ones from the sets of SST images without ground-truth. Automatic thresholding techniques were applied and, for the SEC-Otsu the method used was the one of Otsu (1979), for the SEC-Kittler the one of Kittler and Illingworth (1986), for the SEC-Ridler the method presented by Ridler and Calvard (1978) and for the SEC-SelfTuning the thresholding method that was used was also the Otsu's method.

In the Appendix A.5 it can be seen all the graphics that describe the behavior of the iterative procedure for the SEC algorithm, as well for the other SRG methods.

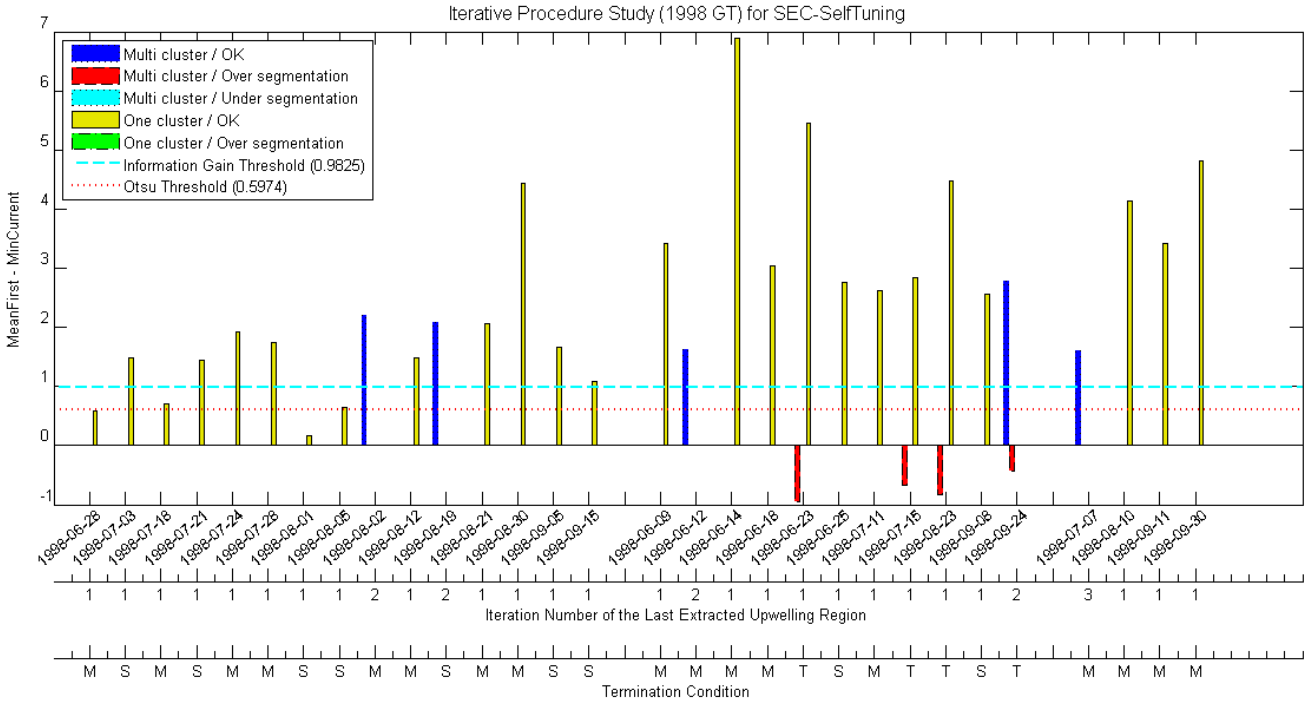

Figure 3.7: Data related to the iterative procedure applied to the SEC-SelfTuning for the SST images of 1998 with ground-truth. The graphic which includes the values for the difference between the mean of the first region and the minimum of one relevant cluster, the relevant cluster has different meanings depending of which category described in the legend. It also includes, for each SST image, the number of the iteration that the last region of upwelling was extracted and the reason why the iterative procedure ended.

For the SEC-SelfTuning segmentation of all images, including the ones without ground-truth map, the Information Gain method defined a threshold that guaranteed that the correct number of regions of upwelling was extracted. The unsupervised measure to define the threshold ε, the Otsu's method in this case, only failed to do it in the image of 1998-09-09 in the set of images with no ground-truth of 1998. For the SEC-Otsu and SEC-Ridler the Information Gain has a misclassification in the 1998-06-16 from the set of images with no ground-truth of 1998, however this is a case where a last third region is extracted and not added to the final segmentation result, but because there is no ground-truth for the image, it is really difficult to say if the region should or not be . For the SEC-Kittler every separation results are fine, and therefore the correct number of upwelling regions is extracted. However, less effective were the results when using the unsupervised methods of thresholding, mainly the Otsu's method for the SEC-Otsu, that misclassified on 8 of the SST images, which is are very poor results. For the SEC-Kittler and SEC-Ridler no misclassifications for the unsupervised thresholding techniques occurred.

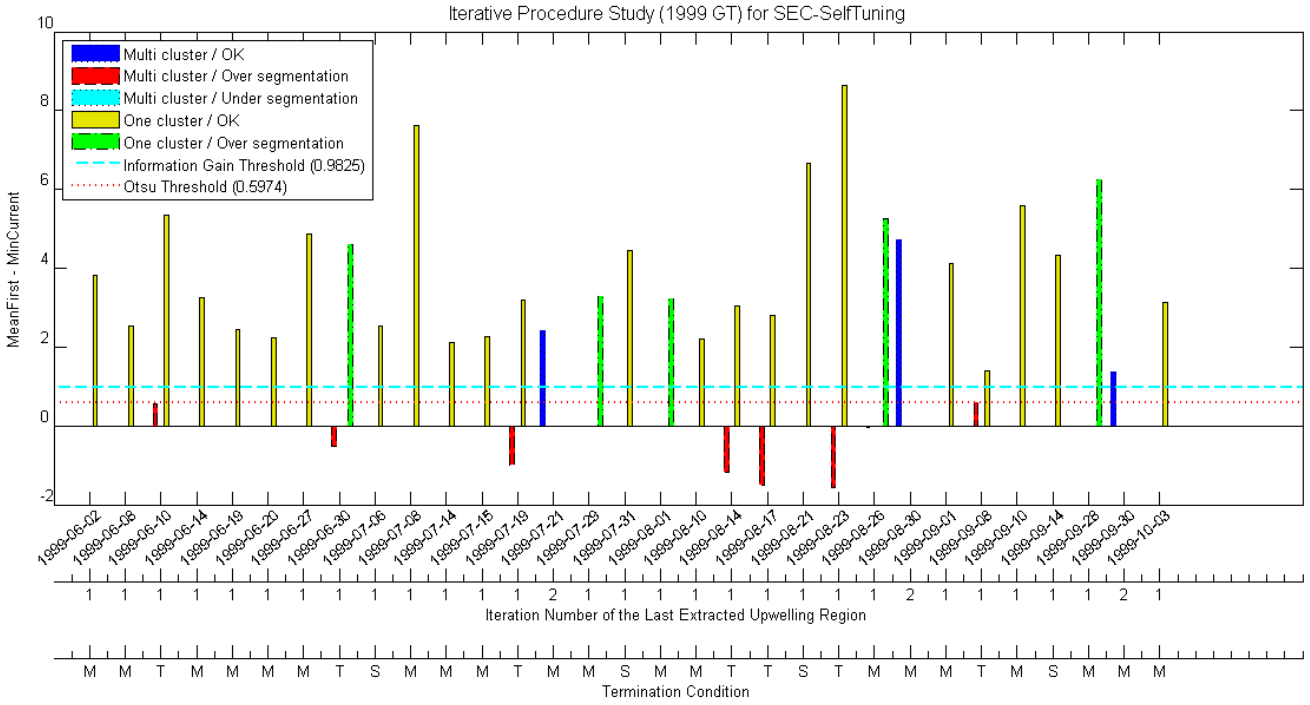

Figure 3.8: Data related to the iterative procedure applied to the SEC-SelfTuning for the SST images of 1999 with ground-truth.

After analyzing the results of the the SEC algorithm versions, it was used the supervised method, Information Gain, for the task of finding the threshold ε . So, after the thresholds have been fixed for the SEC algorithm versions it was also necessary to tune the parameter for the SRG methods that also used the iterative procedure to extract more that one region of upwelling in images with discontinuities, and for this SRG methods study the threshold was defined using the Information Gain only. It is important to point out that for the segmentation results of some of this SRG methods, there was no extracted clusters that did not belonged to the upwelling region, so there was no no groups of values to separate, so in this case the defined threshold was defined has the minimum of the difference values from the *Multicluster/OK* and *Multicluster/UnderSegmentation* categories. For the SRG methods the Information Gain method always correctly delineated thresholds that corresponded to correctly allocating cluster in upwelling zones to the final segmentation result and letting out of it the clusters that should not have entered.

3.3 Applying the SRG Methods to SST Image Analysis

It is important to salient how the different SRG methods, described in the Section 2.2.3 were applied to the domain of upwelling detection, and which settings of their parameters were done. Through testing experiments, the parameters of these SRG methods

were tuned in order to be possible to segment SST images and delimit the upwelling phenomenon.

It was also necessary to allow this methods to correctly segment SST images with discontinuities, and the developed iterative procedure described in the Section 3.2 that allows the SEC algorithm to extract multiple upwelling areas, was also used for the SRG methods that only grow one region starting in an initial seed. Instead of extracting regions with the SEC algorithm, they are extracted by another region growing algorithm. The iterative procedure was also applied for one of the two greedy region growing algorithms, the method of Shih and Cheng (2005), because besides it does not grow a region at a time, it also needs a way to decide which of the regions of the segmentation that it produces, are or not uwpelling regions. This required a slightly modified version of the iterative procedure which is explained in the Section 3.3.3.

3.3.1 Applying the Adams and Bischof Seeded Region Growing

One thing that is different from the SEC algorithm, is that the Adams and Bischof (1994) algorithm is greedy, meaning that it requires at least two seeds, otherwise the image can not be segmented.

One strategy that was tried was to select a seed in the coldest spot of the SST image, which would represent the cluster that is upwelling, and another seed would be placed in the hottest pixel of the image. The training results were not good, many times because one of the seeds grew, but its cluster would be trapped between noisy areas of the image, making the other cluster grow to occupy most of the image. Even if none of the seeds was trapped, using only two seeds placed automatically was generally not enough to extract correctly the upwelling area. Also, in case the image contained discontinuous upwelling areas only two seeds would not be enough.

So, the seed selection strategy chosen consists in placing manually 5 seeds near the continental coast where the upwelling occurs and another 5 seeds far from the continental coast where the upwelling does not occur. The positions of the seeds were identical in most of the images, except for images where the noise would not allow the seeds to grow significantly. The upwelling area extracted is the combination of the regions corresponding to the 5 seeds in the coldest waters.

3.3.2 Applying the Verma Seeded Region Growing

The algorithm of Verma et al. (2011) has to be adapted to the requirements of segmenting SST images, this means that the selection of the initial seed must be the coldest pixel in the image rather than the center pixel used in the original work.

In order to check if a pixel enters or not to the region that is being grown, this method calculates the distance between the intensity of the analyzed pixel and the seed pixel. If this distance is less that a threshold, the pixel is added to the region. The paper mentions that the tuning of the threshold is done using the Otsu's method, however simply applying

this method did not produce results near acceptable, resulting in an explosion covering all the pixels of the image. So two alternatives were tried, one that uses the Otsu's method but to the value it produces, it is subtracted the temperature of the seed pixel. The other alternative consisted in set the threshold to the difference between the mean temperature of the image and the temperature of the seed pixel.

Both the alternatives to tune the threshold proved to be effective, however none of them was consistently better than the other one, so the collection of SST images was segmented using these two versions of the tuning of the threshold.

3.3.3 Applying the Shih and Cheng Seeded Region Growing

This method (Shih and Cheng (2005)) is similar to the one preseted by Adams and Bischof (1994), because it is also a greedy method, requiring more than two seeds to segment the image. The main differences are the capability of this method to automatically select suitable seeds and in the end of the growing phase, merge regions according to how similar they are.

The method has some thresholds that must be tuned for automatically select seeds and for the merging procedure of regions. The different thresholds were tuned empirically, trying to maximize the quality of the results for the different images. In the process of automatically select the initial seeds there were two conditions, in the first, the seed pixel candidate must have the similarity to its neighbors higher than a threshold set to 0.98. The second condition states that a seed pixel candidate must have the maximum relative Euclidean distance to its eight neighbors less than 0.2. There is another threshold that is used for stopping the merging procedure, which merges regions until no region has its distance to its neighbors less that a threshold value of 0.10.

The result after the merging procedure is a segment image in different regions. It is left to decide which ones correspond to upwelling areas and which do not. To define which ones are the upwelling regions it is taken advantage of the iterative procedure developed and used in the other methods. However, in this case, there is not a region that is being extracted at each cycle, but there are a group of regions that will be individually processed to see if they meet the conditions of the developed iterative procedure, and enter the final segmentation image with only correct upwelling regions. The main difference from the iterative version that was applied with the other region growing methods is that the iterative procedure only stops when all the regions, produced by this greedy method, are analyzed and chosen to enter or not the final segmentation result. The first region of upwelling is the one that contains the coldest pixel near the continental coast, the remaining regions are added if they meet the conditions of the iterative procedure, except for the maximum number of iterations that in this case it is necessary to analyze all the regions. If it fails in the condition consisting in the difference between the mean of the first extracted cluster and the minimum value of the current one being greater than a threshold ε, instead of stopping, it simply does not add the current region to the final

segmentation result.

3.3.4 Applying the Gambotto Seeded Region Growing

The merging criterion of the method proposed by Gambotto (1993) selects the boundary regions of one region, if their distance to the region model (mean temperature of the region) is not greater than a threshold multiplied by an α value the regions are merged. The method dynamically calculates the threshold value, but the parameter α must be tuned in order to control the growing pace of the region. A high value might compromise the quality of the segmentation, because it allows pixels to enter the region when it should not. An α that is too small might in the limit not allow any boundary segment to be added to the region, making the growing process too slow because it activates the other mechanism of the method that states that if no merging occurs in the previous verification, only the segment which is closest to the region model is added. This means that at least one boundary segment is merged with the region at each iteration. The most reliable value for this parameter to produce good segmentation results was $\alpha = 6$.

The growth termination consists in check if the difference between the $Fmax$ and the current $F(n)$ is greater that a preset parameter λ multiplied by the threshold that is calculated dynamically. If this condition is true then a second criterion, consisting in the difference between the $Fmax$ and the average gradient computed over the dilated region, is verified to also be greater than the λ value multiplied by the threshold. The parameter λ was empirically defined as $\lambda = 2$.

3.3.5 Applying the Zanaty and Asaad Seeded Region Growing

The method presented by Zanaty and Asaad (2013) makes the assumption that the pixel values along the boundaries usually have lower temperature probability than the pixel temperatures inside the region to be extracted. The method uses the probability of pixel, defined as the number of pixels with the same temperature divided by the size of the image, and uses it to stop the growing of the region by tuning a similarity threshold.

The threshold function is composed by two other threshold functions that have prescribed parameters, $T1$ e $T2$. The first threshold $T1$, takes different values for low temperature pixels and high temperature pixels. In the paper, the separation between high and low intensity pixel values is preset to $\theta = 0.5$, but this value does not work effectively outside the context of segmenting MRI images, like brain tissues, so to tune this parameter adequately to segment upwelling areas, the Otsu's method was used. The threshold $T1$ uses one preset parameter γ for low intensity pixels and an α value to high intensity values, they were set to $\gamma = 1$ and $\alpha = 5$. The threshold $T2$ forces the final threshold to be small at the boundaries using the probabilities of the pixels intensities and it also needs a preset parameter that was defined as $\beta_1 = -2$.

Chapter 4

Experimental Study

4.1 Goals of the Study

The objectives of the experimental study are aligned with the main contributions of the work as described in Section 1.3, plus some complementary studies. In such context the following will be considered:

(i) Comparing the different versions of the SEC algorithm, which differ in how the similarity threshold is calculated. The threshold is calculated using automatic thresholding methods (Ridler and Calvard (1978); Otsu (1979); Kittler and Illingworth (1986)), or can be dynamically calculated in the growing process in the case of the Self-Tuning version. There is also the Fine-Tuning version, in which it is taken advantage of the ground-truth map to maximize the F-measure, by running the SEC algorithm in a range of multiple similarity thresholds, this version purpose is to find out what potential results can be achieved with an optimum tuning of the similarity threshold of the SEC algorithm.

(ii) Comparative study between the SEC method and other SRG methods (Adams and Bischof (1994); Gambotto (1993); Shih and Cheng (2005); Verma et al. (2011); Zanaty and Asaad (2013)), in their ability to correctly segment SST images. The methods were chosen in an attempt to have a representative sample of approaches to tackle the problem of extracting upwelling areas, given the diversity of SRG methods.

(iii) In order to extract the full upwelling region in SST images with discontinuous areas of cold waters, it was developed an iterative method, which region by region evaluates if it should enter or not the final segmentation result. The iterative method was used in all the SRG methods, including the SEC method, with exception for

the algorithm from Adams and Bischof (1994) which the regions corresponding to upwelling were manually selected.

(iv) Some SST images have associated a ground-truth image manually segmented by the Oceanographers, this allows to use supervised evaluation techniques instead of unsupervised methods, because it is believed that direct comparison between a segmented image and a reference image provides a finer resolution of evaluation (Zhang et al. (2008)). However, many SST images do not have a ground-truth associated to them, because this is a time-consuming task for the experts, and the segmentation of those images must be evaluated too. So, in this case, unsupervised evaluation techniques will be applied.

For the images with ground-truth, the evaluation was done using supervised evaluation measures like the F-measure and the Adjusted Rand Index, which provide accurate evaluations, however, for images with no ground-truth, unsupervised evaluation methods were used and their effectiveness had to be studied, including the intra-region and inter-region measures of Levine and Nazif, intra-region and inter-region measures of Rosenberger and Chehdi, Otsu's within-class and between-class variances, Calinski-Harabasz criterion, Davies-Bouldin criterion and intra-region of Liu and Yang.

4.2 Imagery Data

Each SST image is represented by a 500×500 pixels map, for the images of the Portuguese Coast, with a spatial resolution of 1.1 km $\times$ 1.1 km. Most of the images are from Portugal, but the phenomenon of upwelling occurs in other parts of the globe, so there is also a set of images from the African Coast near the Canary islands, which can test the efficiency of the segmentation algorithms for different images with other type of upwelling morphologies. The SST images from the Canary are represented by 350×570 pixels maps.

Each pixel value is a temperature in degrees Celsius, as represented in Figures 1.1 and 3.1, if there are no clouds in the sky and there are no missing data because of errors during satellite transmission. In case some of this two conditions exist or the pixels correspond to a land area, then the pixels where it occurred are represented by NaN's, corresponding to white in the image.

Different types of upwelling situations are presented in different images. Some SST images are characterized by very sharp and well defined upwelling boundaries between cold and warm surface waters along the coast, which will be called images with strong gradients. Some have a much smoother thermal transition zone between what is considered to be upwelling areas and non-upwelling areas, which will be named images with weak gradients. Other images simply have a large amount of noise, from clouds or errors during satellite transmission, which makes it more difficult to extract information about

the full length of the upwelling area. Further explanation for the causes of noise can be seen in the Appendix A.1.

The upwelling is an annual phenomenon and different seasons of have different characteristics, so the images were divided in separated sets. Images from the year of 1998 (30 SST images), 1999 (31 SST images) and from the Canary (10 SST images) are images with ground-truth, and their segmentation results were evaluated using with supervised measures. The SST images of 1998 with ground-truth were divided in three subsets corresponding, has in the paper where the SEC algorithm was presented (Nascimento et al. (2015)) , to images with strong gradients on the upwelling frontier (15 SST images), weak gradients (11 SST images) and noisy images (4 SST images). Complementary to these sets of images with ground-truth, there are more SST images without ground-truth for other years of upwelling. The segmentation results for these images must be evaluated using unsupervised measures that do not require ground-truth, and are divided in different sets, also arranged by year. Without ground-truth there are sets of SST images from 1998 (52 SST images), 2000 (32 SST images), 2001 (30 SST images) and 2002 (22 SST images). There are 71 SST images which the segmentation results can be evaluated using supervised measures, and 136 SST images which the segmentation results can only be evaluated using unsupervised measures, in a total of 207 SST image divided in different sets.

In Figure 4.1 can be seen the SST images of 2 August 1998 and 28 July 1998, and in Figure 4.2 can be seen the correspondent ground-truth images. In the Figure 4.3 it can be seen an example of one of the images from the Canary and its correspondent ground-truth.

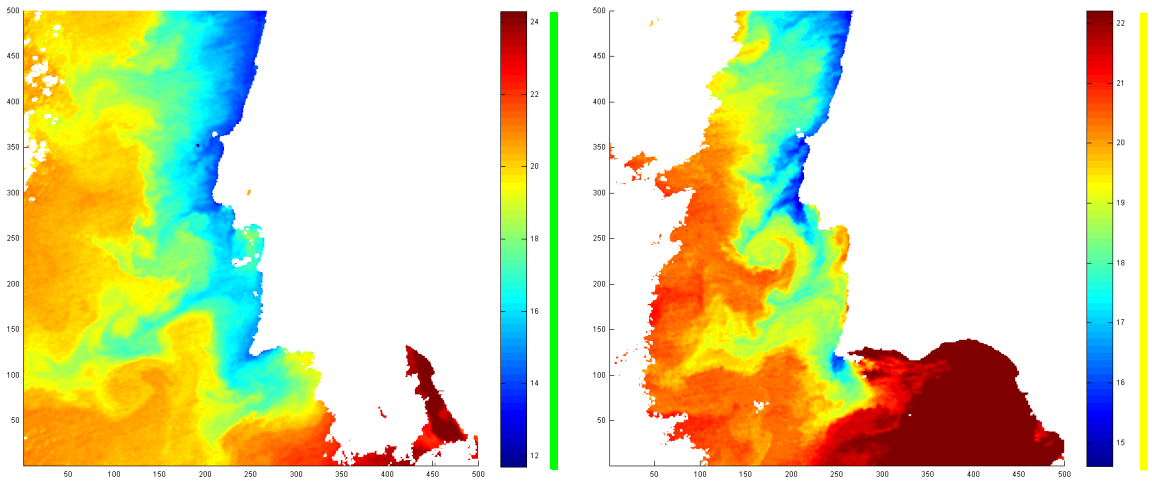

Figure 4.1: Two SST images of Portugal, the one in the left was captured in 2 August 1998 and the one in the right in 28 July 1998.

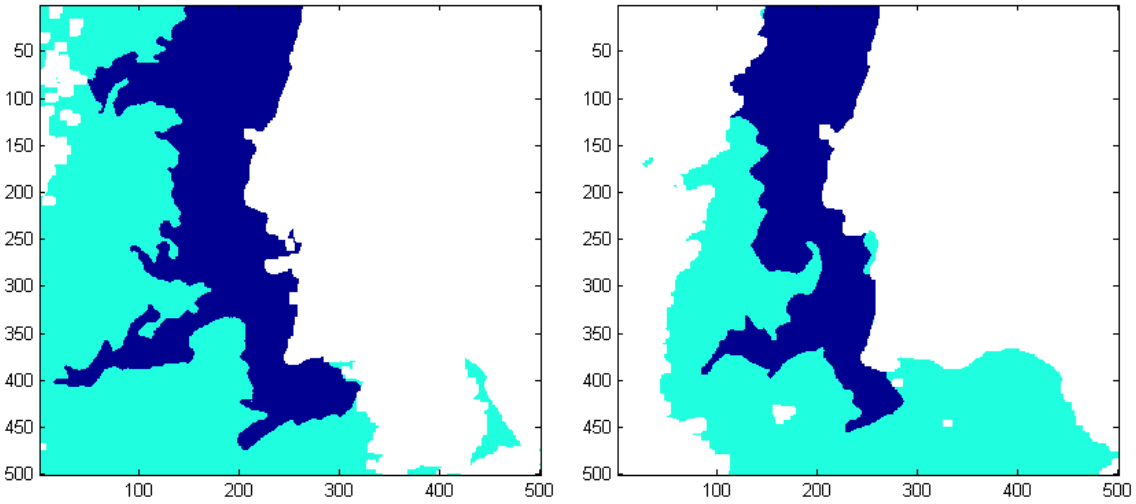

Figure 4.2: The ground-truth images correspondent to the SST images of 2 August 1998 in the left and of 28 July 1998 in the right. The white area represents noise, land or clouds, the light blue area contains the waters that are not part of the upwelling zone, and the dark blue area is the upwelling area.

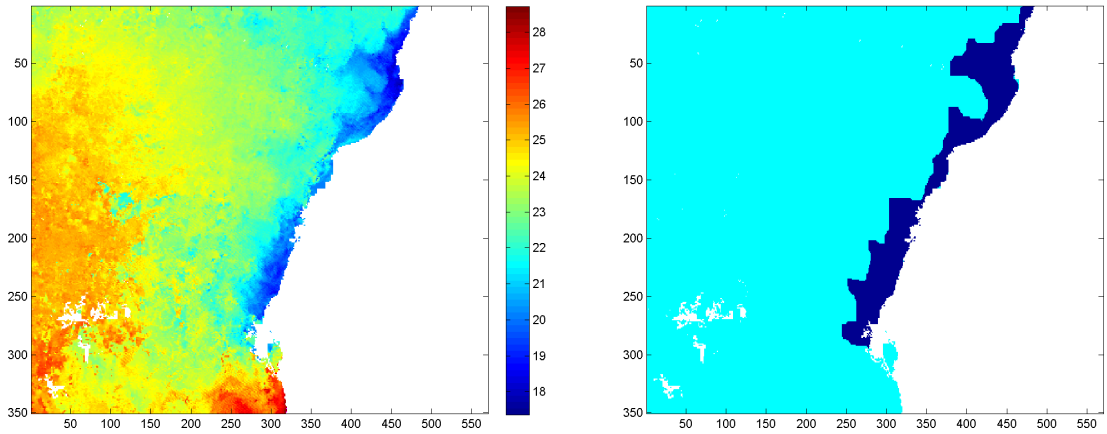

Figure 4.3: SST Image from the Canary, named *img*_58, in the left, and the correspondent ground-truth in the right.

4.3 Setting of the Experiments

The comparative study between the SEC versions as well as the the comparison between the SEC and the other SRG methods, is separated for images of Portugal and Canary because there are very distinct morphological features in the upwelling regions. For the images of Portugal the analysis of the images with ground-truth map allow to have a

very accurate evaluation of the segmentation results, but for the images without ground-truth map, the unsupervised evaluation measures were applied after a complementary comparison study which indicates the measures that can be more reliable in correctly evaluate the segmentation of SST images.

All the the segmentation methods, with the exception of the AdamsSRG, take advantage of the newly developed iterative procedure that allows to extract multiple upwelling regions in the same SST image.

The automatic thresholding methods used to tune the similarity threshold π of the SEC algorithm, Ridler and Calvard (1978); Otsu (1979); Kittler and Illingworth (1986) , were subjected to a small adaptation that forces the output value to be greater than the mean intensity value of the image, which after normalization means that the output must be greater than zero.

This is done because in order to grow the cluster that extracts the coldest waters in the SST image, the similarity threshold value of the SEC algorithm should be positive, this is because the similarity condition of its homogeneity criterion is in a form of a product that has to be bigger than a threshold value to allocate a pixel to the cluster, in an image that is normalized. The initial cluster mean of the seed, in the coldest waters, has a negative value, so a frontier pixel is allocated to the cluster if its temperature value (in the beginning of the growth phase is generally negative) times the mean of the cluster, also with a negative value, is bigger than a threshold. So, it is assumed that the upwelling region is composed by the pixels which their temperature values are below the mean temperature of the image, this means that a similarity threshold set to bigger than zero will prevent that bigger than mean pixels are added to the cluster, which otherwise would result in an massive explosion in the segmentation.

There is the SEC-FineTuning version that allows to put in perspective how good can be the SEC algorithm results when the best similarity threshold is used.

When running the fine-tuning version of the algorithm, it is taken advantage of the ground-truth to maximize the F-measure as it was done in Nascimento et al. (2015).

In the fine-tuning version the similarity threshold was the best of the threshold values between 0 and 1.5, using a step of 0.01.

After the first iteration, the F-measure is maximized taking only into account the residual ground-truth, this is, the ground-truth without the pixels that were allocated to the previous cluster. In the end, the binary image that contains the total upwelling area, composed by more than one region, is compared to the original ground-truth and the final evaluation values are calculated.

On running the SEC algorithm it is necessary to tune the threshold of similarity but also the density threshold. By default the density threshold is fixed at $\frac{1}{windowsSize \times windowsSize}$, with $windowsSize = 7$ defined empirically for these images by Nascimento et al. (2015),

making the pixel that is being evaluated to be connected to the region, property that already is intrinsic to region growing methods. This means that the density threshold is deactivated and the focus is to study the impact of the similarity threshold on the segmentation result, except in the study that compares the SEC algorithm results with and without fine-tuning of the density parameter of the algorithm.

For the study of the density condition of the SEC algorithm, the focus is in studying the impact that the density threshold has in the segmentation results. In order to do this, it was taken advantage of the ground-truth map to maximize the F-measure by fine-tuning the density threshold, in this case, the SEC algorithm was run using values for the density threshold ranging between $\frac{1}{windowsSize \times windowsSize}$ and $\frac{windowsSize \times windowsSize}{windowsSize \times windowsSize}$. The results are compared with the ones achieved without the fine-tuning of the density, in all the versions of the SEC algorithm. And an empirical study was done to also understand if there is a threshold value that can be fixed and that improves the evaluation scores of the segmentation results.

To understand the segmentation results, it is necessary to compare the similarity thresholds produced by the different automatic thresholding techniques. All versions of the SEC algorithm calculate a similarity threshold value, except for the self-tuning that dynamically derives the similarity threshold from the homogeneity criterion, so in order to be able to compare all the similarity threshold values, including for the self-tuning version, a strategy was outlined:

The similarity threshold is different for every frontier pixel that is being analyzed, so first it is calculated the mean of the similarity thresholds from all the frontier pixels, and after that it is calculated the mean of all the mean similarity threshold values of each frontier.

4.4 Supervised Analysis of SEC versions

4.4.1 SEC Automatic thresholding vs Self-tuning

The multiple versions of the SEC algorithm were tested, differing in the way the similarity threshold π is tuned. It was made a comparison study between the segmentation results of the different versions in order to evaluate their performances. The presented results are of the F-measure only, because the ARI measure gave similar evaluation values even if with more variation, even so the results for the ARI can be seen in the Appendix A.2.2.

In the Table 4.1, it was captured the percentage of times that some version had the best segmentation results and that its F-measure scores was 0.7 or higher, a empirically defined threshold that distinguish good for bad segmentation results by Nascimento et al. (2015). For the images with strong gradients, the version that was more times the best was the SEC-Otsu, and all the methods obtained a good extraction of the upwelling area

always or almost always. When seeing the results for the SST images with weak gradients, a method was clearly the best, the SEC-Kittler, because the similarity thresholds that it produced were higher and avoided explosions. For the noisy SST images all methods were good except in one image and the SEC-SelfTuning was more times the best method, as it also was in the SST images from 1999, even if the number of times that it had correctly segmented the upwelling area was lower that the SEC-Kittler. This is because the SEC-Kittler did not failed as much as the other methods when dealing with images with weak gradients at the frontier of upwelling. Overall, none of the methods was the best for all types of images, the SEC-Kittler is well behaved when applied to images with weak gradients, but not as much for the images with strong gradients, contrarily to the other other SEC algorithm versions, which had good results for these images.

Table 4.1: Table that accounts for how frequent each version of the SEC algorithm, excluding the fine-tuning version, had the best score when segmenting an SST image of the portuguese coast. It is also accounted the frequency that each version had F-measure scores superior or equal to 0.7, which was empirically identified has a threshold for separating good from bad segmentation results. The best versions scores are bold in the table, for each of the sets of images and information that is being analyzed.

Image Set	**Information**	**SEC-Otsu**	**SEC-Kittler**	**SEC-Ridler**	**SEC-SelfTuning**
Strong Gradients	% Best Method	**0,467**	0,200	0,133	0,400
(1998) #15	% F-measure $\geq$ 0.7	0,933	0,933	**1**	**1**
Weak Gradients	% Best Method	0,273	**0,455**	0,091	0,182
(1998) #11	% F-measure $\geq$ 0.7	0,636	**0,909**	0,636	0,273
Noisy	% Best Method	0	0,250	0	**0,750**
(1998) #4	% F-measure $\geq$ 0.7	**0,750**	**0,750**	**0,750**	**0,750**
1999	% Best Method	0,097	0,355	0,065	**0,581**
#31	% F-measure $\geq$ 0.7	0,548	**0,677**	0,581	0,548
Overall	% Best Method	0,213	0,328	0,082	**0,475**
#61	% F-measure $\geq$ 0.7	0,672	**0,787**	0,705	0,623

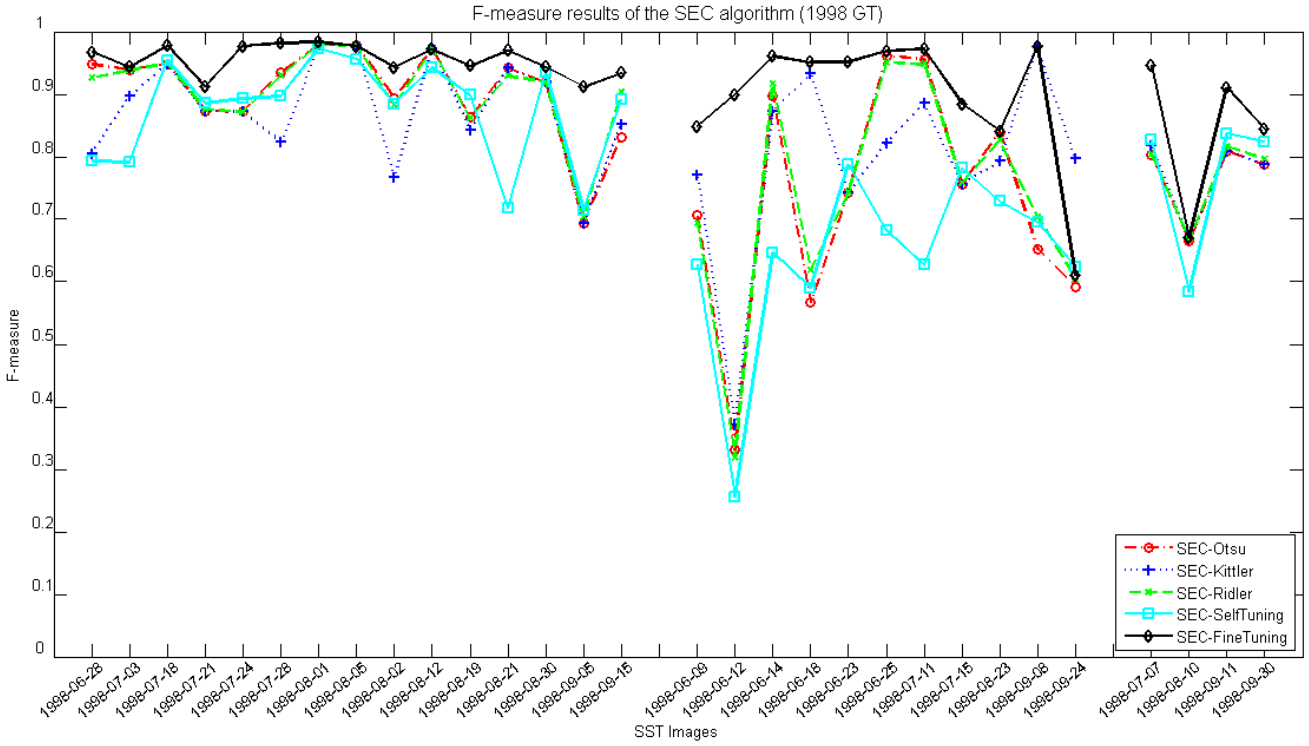

Figure 4.4: F-measure results for the comparative study between the SEC algorithm versions. The segmentation results are from the SST images of the portuguese coast from the year 1998, which was divided into subsets of images with strong gradients in the frontier of the upwelling area, weak gradients and images with noise, from left to right in the graphic correspondingly.

In the Figure 4.4 are presented the results for the segmentation results divided into subsets of images with strong gradients in the frontier of the upwelling area, weak gradients and images with noise.

The SST images with strong gradients in the boundaries of the upwelling area are seen ordered by date in the the subset in the left of the graphic. In the SST image of 1998-07-28 and 1998-08-05 the SEC-Kittler method had worst results then the other versions the cause was under-segmentation, the SEC-SelfTuning achieved lower scores than SEC-Otsu and SEC-Ridler for the those images because of the opposite problem, over-segmentation. The SEC-Otsu and SEC-Ridler versions usually produce similar results. For the other images, the SEC-SelfTuning version follows the good results of the other versions.

The SST images with weak gradients are seen in the the subset in the middle of the graphic and, some bad results bellow the 0.7 score happen for the SEC-Otsu, SEC-Ridler and SEC-SelfTuning because of over-segmentation. For the images of 1998-06-25 and 1998-07-11, the SEC-Otsu and SEC-Ridler have very good scores, almost matching the fine-tuning version, however the SEC-Kittler method and the SEC-SelfTuning version had worst results because, in the case of SEC-Kittler, there is under-segmentation, and by the

contrary, the SEC-SelfTuning produces results with over-segmentation. Compared with images with strong gradients, the difficulties encountered in the images with weak gradients are evident in the results, which in many cases are lower, because of the explosion in the segmented area.

The SST images that are noisy are seen in the the subset in the right of the graphic and, in these SST images the results, all versions stay relatively close to each other, noting that the score of the SEC-SelfTuning is slightly lower in the image of 1998-08-10, but slightly higher in the remaining images than the other versions.

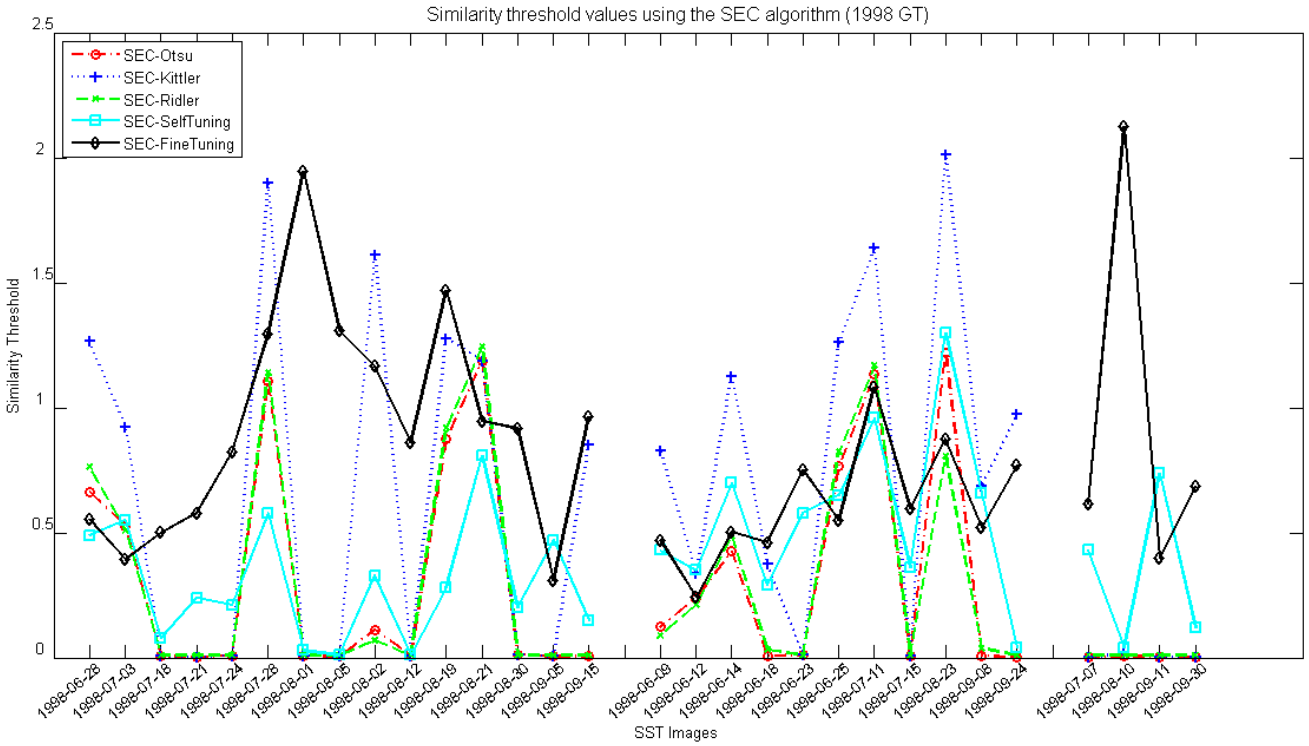

Figure 4.5: Similarity thresholds that were calculated for each of the SEC algorithm versions. Higher thresholds will contain more the growth of the clusters than smaller ones. The segmentation results are from the SST images of the portuguese coast from the year 1998, which was divided into subsets of images with strong gradients in the frontier of the upwelling area, weak gradients and images with noise, from left to right in the graphic correspondingly.

The Figure 4.5 shows the similarity thresholds that originated the results seen in the Figure 4.4.

Dealing with the subset of images with strong gradients, the SEC-Kittler method produced a value to the similarity threshold higher than the other versions, and when the boundaries have strong gradients, an higher threshold will contain the grow and under-segment the SST image, however if the image has weak gradients, an higher threshold is actually preferable to contain explosion, but it is not the case for this set of images.

In most of the SST images with weak gradients in the frontier, the SEC-Kittler tended to produce higher similarity threshold values than the other versions and the fine-tuning version. Higher thresholds can cause under-segmentation, since a bigger threshold value contracts more the size of the cluster. Even so, the SEC-Kittler was the best because when dealing with weak gradients higher thresholds are necessary to contain explosions.

All three automatic thresholding techniques produce similar results for the noisy SST images, close to zero, relatively, but the scores were close to the fine-tuning version.

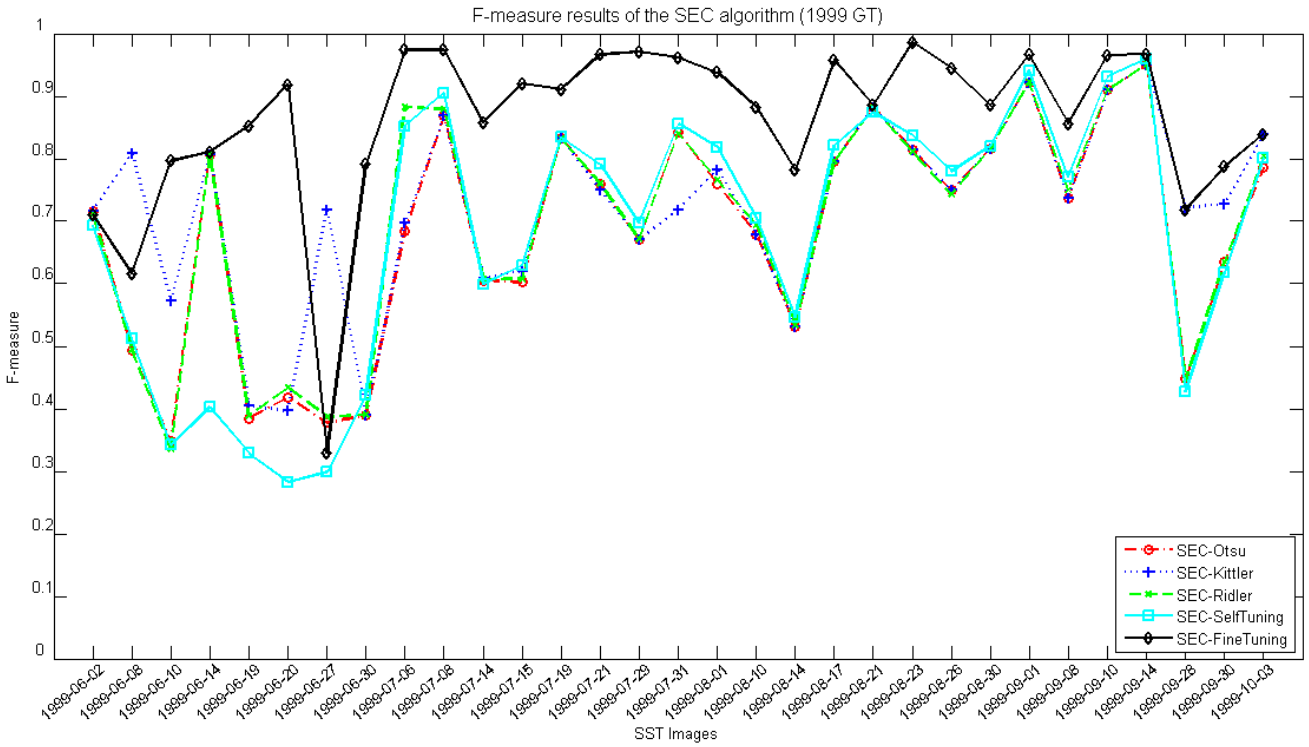

Figure 4.6: F-measure results for the comparative study between the SEC algorithm versions. The segmentation results are from the SST images of the portuguese coast from the year 1999.

There are some SST images from 1999 which the results, can be seen in the Figure 4.6 and, are far from good, because of smooth boundaries that difficult the correct extraction of the upwelling area, resulting in explosions, namely in where lower scores ere achieved. However, for some of these SST images, there is an automatic thresholding method that provides better results, the SEC-Kittler which avoids the explosions. For most of the other SST images from 1999 that have stronger gradients at the boundaries, the SEC-Kittler version behaves similarly to the other versions.

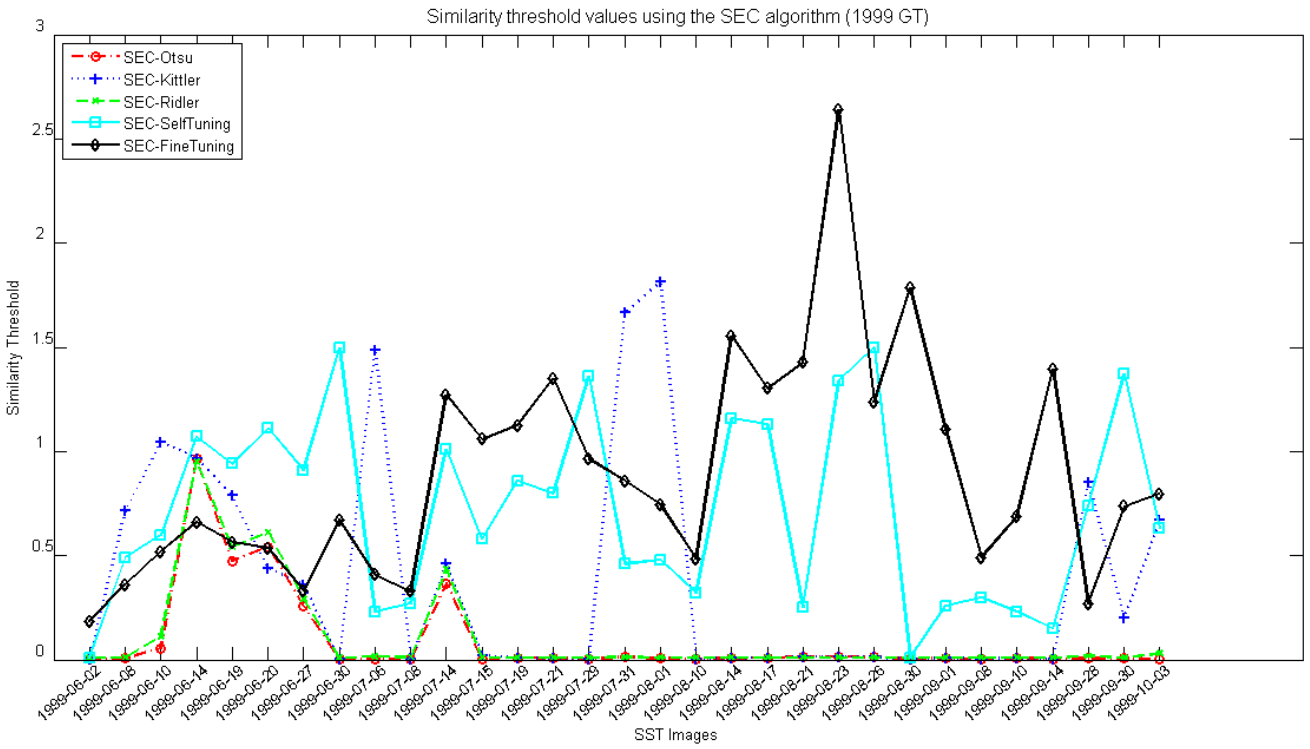

Figure 4.7: Similarity thresholds that were calculated for each of the SEC algorithm versions. Higher thresholds will contain more the growth of the clusters than smaller ones. The segmentation results are from the SST images of the portuguese coast from the year 1999.

The Figure 4.7 contains the calculated similarity thresholds for the different SEC algorithm versions applied to the images from 1999. The explanation for the explosions on many of the SST images is the low similarity threshold produced by the methods. Because the images with worst results have boundaries with smooth gradients, it is necessary to the similarity threshold to be high, in order to contain the growth of the region. For those images, the SEC-Kittler method avoids explosions, because it produces a higher threshold that the other methods.

4.4.1.1 SEC vs SEC-density

The SEC algorithm has two parameters that control the growth of the region, the similarity threshold, which largely influences the segmentation result, as seen in the Section 4.4.1, and the density threshold, which its influence in the final segmentation result is being analyzed here. It order to study its impact it was done the fine-tuning of this parameter taking advantage of the ground-truth to maximize the F-measure score, to see how distinct would be from the versions without this fine-tuning process.

The F-measure scores achieved by using the fine-tuning of the density threshold are always higher or at least equal to the ones using the parameterization of the density

threshold fixed in $\frac{1}{windowsSize \times windowsSize}$. Generally across all sets of images the tuning of this parameter allows to score higher results, sometimes significantly higher, as seen in the Figures 4.8 and 4.9.

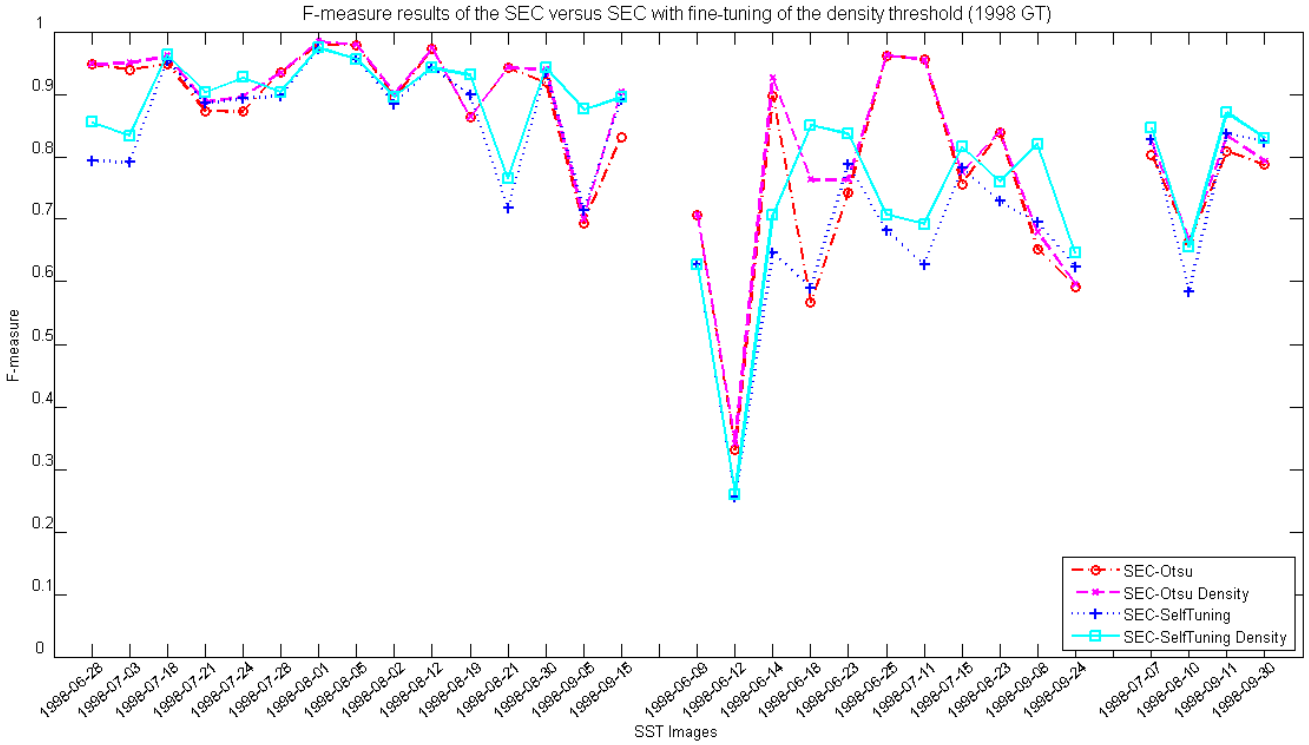

Figure 4.8: The graphic shows the improvements that the fine-tuning of the density threshold can have in the F-measure score. It is compared the SEC-Otsu and SEC-SelfTuning versions with their own versions, but with the fine-tuning of the density threshold. The segmentation results are from the SST images of the portuguese coast from the year 1998, which was divided into subsets of images with strong gradients in the frontier of the upwelling area, weak gradients and images with noise, from left to right in the graphic correspondingly.

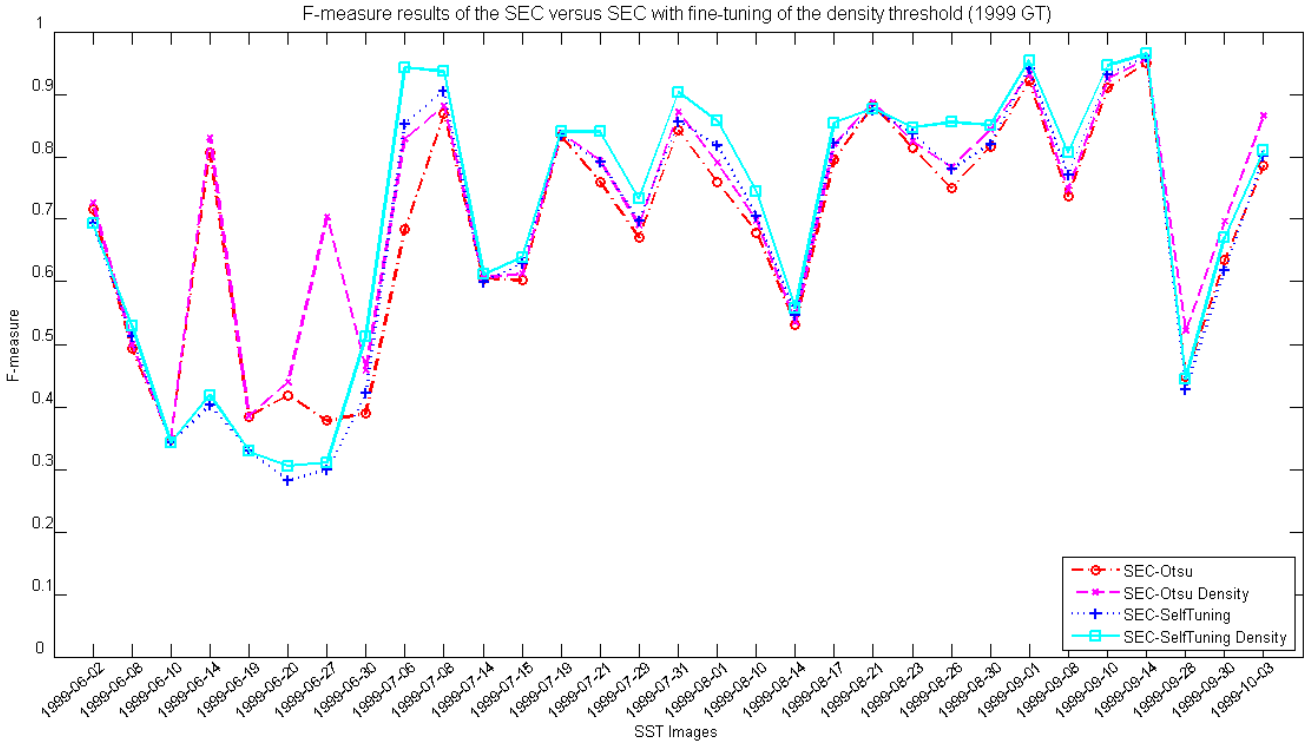

Figure 4.9: The graphic shows the improvements that the fine-tuning of the density threshold can have in the F-measure score. It is compared the SEC-Otsu and SEC-SelfTuning versions with their own versions, but with the fine-tuning of the density threshold. The segmentation results are from the SST images of the portuguese coast from the year 1999.

Using the SEC-SelfTuning and SEC-Otsu versions, in those images where the score is significantly improved, the higher density threshold avoided explosions that would happen with a low density threshold.

For the other SST images, even if this is not enough to control explosions or there are not explosion at all, the correct tuning of this threshold allows to grow the cluster with smooth and better defined boundaries. So, just for allowing the boundaries to be smoother, the F-measure is higher because it matches better the ground-truth map that has smooth and well defined region boundaries.

The smoothness of the boundaries of the region that was extracted using the fine-tuning of the density parameter can be seen and compared with the result for the same image, but without fine-tuning in the Figure 4.11, for the exemplar SST image from 1998-06-18 using the SEC-SelfTuning. The corresponded ground-truth map is displayed in the Figure 4.10. In this case, not only the frontier became smoother, but also an explosion was contained, improving significantly the F-measure score, for this image with weak gradients.

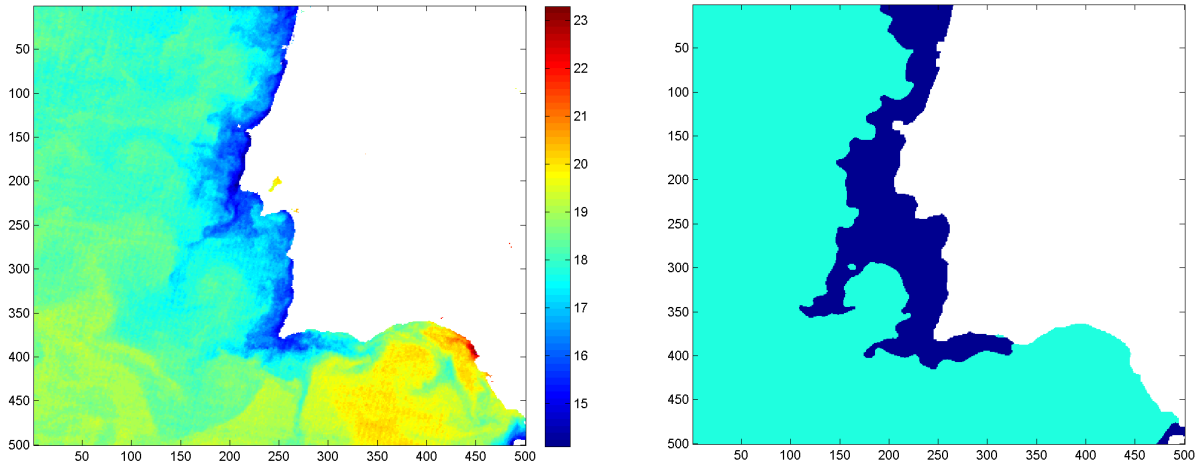

Figure 4.10: SST Image from 18 of June 1998, in the left, and the correspondent ground-truth map in the right.

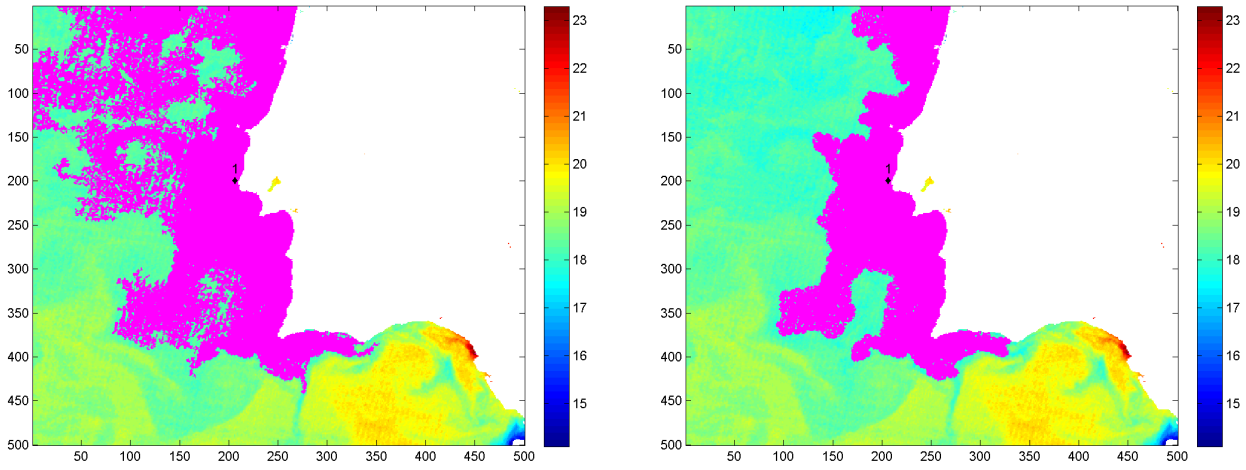

Figure 4.11: SST Image from 18 of June 1998, in the left without the fine-tuning of the density threshold, and in the right the fine-tuning version, with the density threshold set to 0.3878. It is an example of how the quality of the segmentation result can be improved. The extracted upwelling region is the pink area and the initial seed is at the black marker.

4.4.2 SEC versions vs other SRG Methods

The SEC algorithm was developed to delimit the upwelling area in SST images, and its versions were compared in the Section 4.4.1 for images of the portuguese coast. In order to validate its effectiveness to tackle this problem, a comparative study against other SRG methods is here presented. Distinct SRG methods, representative of some of the diversity of SRG methods from the literature, are applied and their performance compared with

the results of the SEC algorithm versions using supervised evaluation measures.

In the Table 4.2 it was captured the percentage of times that some SRG method had the best segmentation results, compared to the others, and that its F-measure scores was 0.7 or higher, a empirically defined threshold that distinguish good for bad segmentation results. Analyzing the set of images with strong gradients, all the methods correctly delimited the upwelling area, with exception to the ShihSRG, GambottoSRG and ZanatySRG, and for the strong gradient images, the SEC versions and the AdamsSRG were the methods that more often had F-measure scores of 0.7 or higher. The SEC-Otsu was more times the best method, even if in only one third of the times. For the SST images with weak gradients the SEC-Kittler was the most reliable method, followed by the AdamsSRG method. The SEC-SelfTuning had difficulties when dealing with this type of images and had the poorest results of the SEC algorithm versions. The remaining SRG methods also performed poorly in most of the images. For the noisy images the AdamsSRG was the best method in half the cases and only the GambottoSRG and ZanatySRG did not scored higher than 0.7 in more than one of the SST images. For the set images from 1999, the good segmentation results were not very frequent, the AdamsSRG was the best method, but even so it did not correctly extracted the upwelling area in nearly one third of the images. Overall the AdamsSRG was the best method followed by the SEC algorithm versions and after that the VermaSRG.

Table 4.2: Table that accounts for how frequent SRG method had the best score when segmenting an SST image of the portuguese coast.

Image Set	Information	SEC-Otsu	SEC-Kittler	SEC-Ridler	SEC-SelfTuning	Adams SRG	OtsuVerma SRG	MeanVerma SRG	Shih SRG	Gambotto SRG	Zanaty SRG
Strong Gradients (1998) #15	% Best Method	**0,333**	0,133	0,133	0,133	0,133	0,200	0	0	0	0,067
	% F-measure ≥ 0.7	0,933	0,933	**1**	**1**	**1**	0,733	0,867	0,533	0,267	0,667
Weak Gradients (1998) #11	% Best Method	0,182	**0,364**	0,091	0	0,273	0	0	0	0,091	0
	% F-measure ≥ 0.7	0,636	**0,909**	0,636	0,273	**0,909**	0,273	0,182	0,182	0,364	0,364
Noisy (1998) #4	% Best Method	0	0,250	0	0,000	**0,500**	0,250	0	0	0	0
	% F-measure ≥ 0.7	**0,750**	**0,750**	**0,750**	**0,750**	**0,750**	**0,750**	**0,750**	0,500	**0,750**	0,250
1999 #31	% Best Method	0,065	0,129	0	0,065	0,290	**0,387**	0	0,032	0,097	0
	% F-measure ≥ 0.7	0,548	0,677	0,581	0,548	**0,742**	0,613	0,484	0,387	0,419	0,323
Overall #61	% Best Method	0,148	0,180	0,049	0,066	**0,262**	**0,262**	0	0,016	0,066	0,016
	% F-measure ≥ 0.7	0,672	0,787	0,705	0,623	**0,836**	0,590	0,541	0,393	0,393	0,410

To all the tested SRG methods, in set of SST images with strong gradients from 1998 which the results are showed in the Table A.2, the SEC versions and AdamsSRG delivered good segmentation results constantly. Between these methods, the SEC-Otsu and SEC-SelfTuning were most of the time very close to each other. The SEC-Ridler had identical results of the ones of SEC-Otsu and, the SEC-Kittler only was lower than the other versions of the SEC in a couple of images. AdamsSRG was relatively close to the other SEC algorithm, in a few images even better, but in half of the images, it was worse than the SEC-SelfTuning and SEC-Otsu, but none the less with good results. Between the two versions OtsuVermaSRG and MeanVermaSRG, for the images in this set, the MeanVermaSRG is clearly the best, achieving almost always good results. Even if the MeanVermaSRG is not the best of all methods, it is still capable of providing quality segmentation results, and in many images it matches the best results. The ShihSRG method and the GambottoSRG also have bad results in half the images, but each in two images achieve results that are very good. The bad results of these methods are all explained by under-segmentation, in the case of the GambottoSRG, stronger under-segmentation. ZanatySRG has good performances in most of the images, matching generally the best results of other methods, however in four images the results are bad, because of big explosions.

For the set of SST images with weak gradients from 1998 which the results are presented in the Table A.3, the main differences to the previous set of images is that the SEC-Kittler was considerably better than the other SEC versions and, that the GambottoSRG is better when dealing with images with weak gradients that with strong gradients. Overall only the SEC-Kittler and the AdamsSRG were robust in segmenting this set of images, but all the other methods had difficulties in achieving good results.

And for these images with a big presence of noise from 1998, as seen in the Table A.4, none of the methods is without a doubt the best across all images, but it is possible to see that all methods, with exception of ShihSRG and ZanatySRG, achieve good results in 3 of the 4 images of the set.

In this set, from the year 1999 with results presented in the Table A.6, there are some images there is one method that does achieve good results in most of the images, even those which the weak gradients make the segmentation difficult, and it is the AdamsSRG method. Even if some segmentation results are bad, it generally is the more reliable method for this set.

Another method that had good results, even many times better than the best of the AdamsSRG method was OtsuVermaSRG. The problem with this method was that contrarily to AdamsSRG it did not perform well on the most difficult images with weak gradients, failing to segment one third of the images. The MeanVermaSRG version had the same problems, but performed well in the same images where OtsuVermaSRG version did, however the scores were lower than the other version.

In between the results of the OtsuVermaSRG and MeanVermaSRG methods, appear very close to each other the SEC-SelfTuning and SEC-Otsu methods, with the first being

a little better in most of the images relatively to SEC-Otsu. For these last four cited methods, the reasons to the bad results are the explosions that over-segment the image. The SEC-Ridler had, as usual, no significant differences in the score relatively to the SEC-Otsu. The SEC-Kittler was better than VermaSRG versions and the other SEC versions in five images because it has tendency to perform better than these methods in images with weak gradients.

The ShihSRG gets bad results in two thirds of the images, even if it in some images behaves very well, in most it fails to have a good performance. The merging procedure ends up merging regions that are very similar to each other and that provokes a decrease in the quality of segmentation. The same to the ZanatySRG method, it performs good in some images, but fails in most of them, in this case because of over-segmentation.

A method that does not have very good results, but has some acceptable ones is the GambottoSRG. The special thing about this method is that achieved good results in images where most of the methods failed. Images of June of 1999 have weak gradients and are very difficult to correctly segment, but in this case this method had acceptable results, because it produced small size regions avoiding explosions.

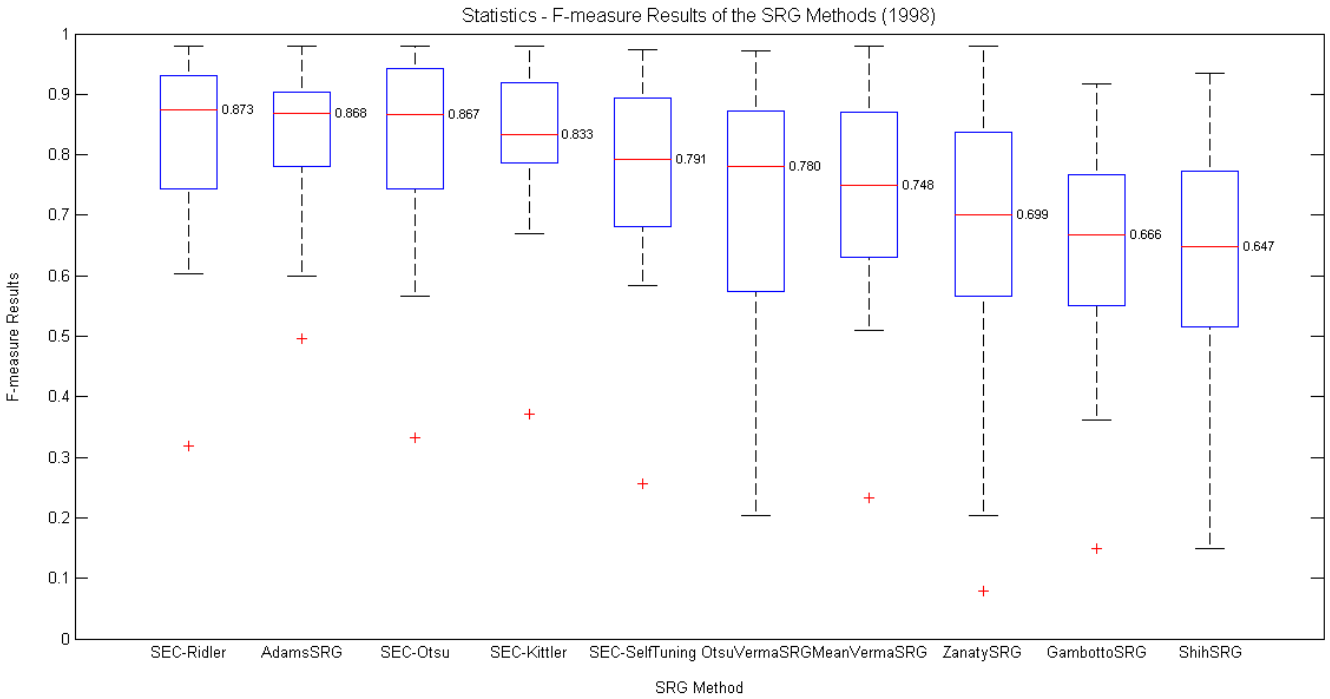

Figure 4.12: F-measure results for each of the SRG methods visualized in a box plot, making it possible to understand the variation of the results in the set of SST images from 1998. The box represents 50% of the data and its lower and upper lines are at the 25% and 75% quantile of the data. The remaining results are inside the vertical lines, with exception for the outliers that are represented by the plus symbols.

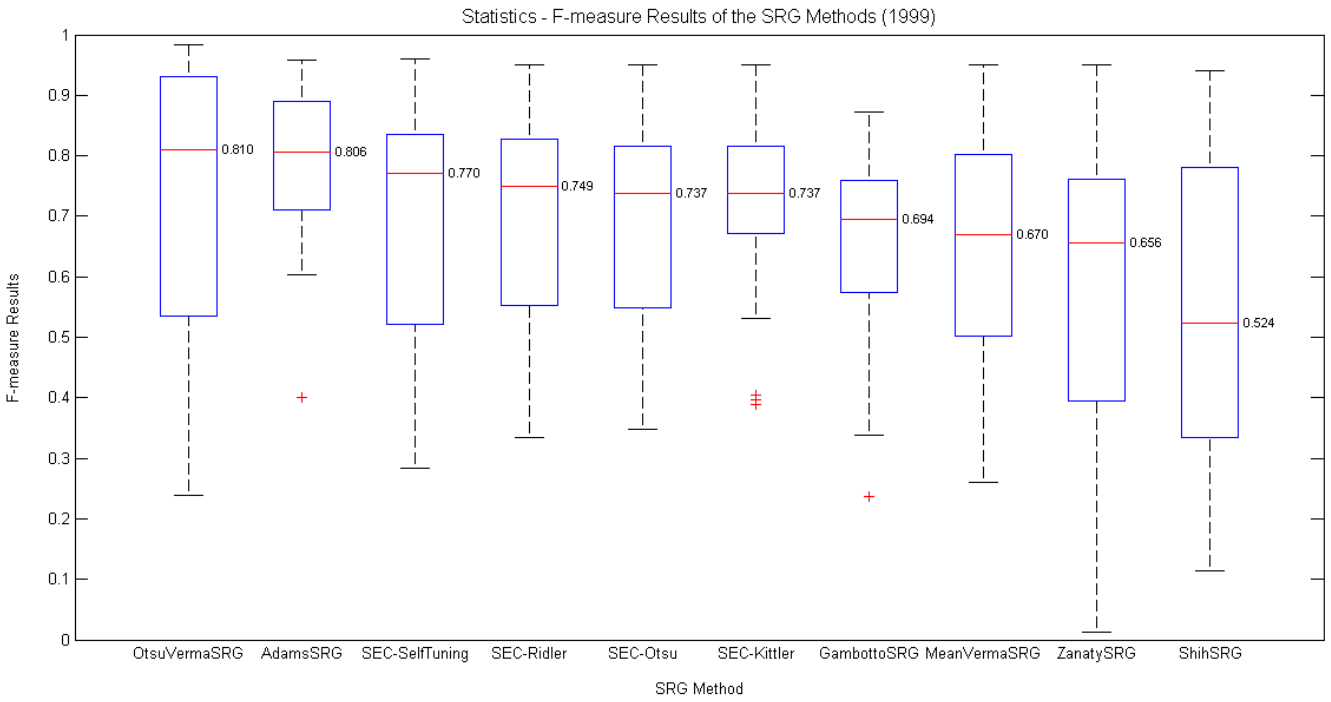

Figure 4.13: F-measure results for each of the SRG methods visualized in a box plot, making it possible to understand the variation of the results in the set of SST images from 1999.

Statistics related to which of the SRG methods was capable of correctly delimit the upwelling region can be seen in the box plots of the Figures 4.12 and 4.13.

The SEC versions do not have very different distributions in the results, however the SEC-Kittler is the method with less variance, because even if it is not the best for images with strong gradients in the frontiers, it is the method that performs better for images with weak gradients. The SEC algorithm versions, the AdamsSRG and the VermaSRG versions had good performances and correctly delimited the upwelling area most of the times. However it is possible to see, mainly for the year of 1999, the variation for these methods was higher, with exception of the SEC-Kittler and AdamsSRG, because a good part of the images had weak gradients and these methods have a tendency to over-segment in these cases. The other SRG methods did not proved to be as robust as the best ones and failed frequently to achieve good segmentation results.

4.4.3 Study for SST Images of Canary

4.4.3.1 Image Normalization for the Canary

The normalization used in the SST images of the Portuguese coast, consisted in subtracting the mean value of the image to all the pixels of the image. However, when using this

normalization in the SST images of Canary, the results were not satisfactory, because of the weak gradients present in those images and very thin upwelling regions. A solution to control the over-segmentation was to change the normalization and instead of subtracting the mean, it was subtracted a value lower than the mean.

Subtracting less than the mean of the temperatures causes the normalized image to have more positive pixels and only the coldest waters to have negative values. Since different images have different temperature histograms, a formula was created to control how much less would be subtracted to each pixel. The value that is subtracted to each pixel is equal to: $meanImage - \frac{meanImage - minImage}{normalizationFactor}$

The normalization factor can be adjusted to maximize the quality of the segmentation.

Additionally to the modified normalization, the SST images of the Canary were cut to a size of 350 × 396, where a chunk of hotter waters in the opposite direction of the continental shelf were removed, meaning that the mean temperature of the SST image decreases and less pixels contain negative temperatures after normalization, which is beneficial to the SST images of the Canary that have upwelling areas very thin and and close to the continental shelf. The SEC algorithm extracts the pixels with negative values and because they are less the explosions are avoided.

4.4.3.2 SEC Automatic thresholding vs Self-tuning

The same comparative study that was done for the the SST images of Portugal in the Section 4.4.1 is done here for the SST images of the Canary. All these SST images have a correspondent ground-truth map associated, so to evaluate the quality of the segmentation results it is only required supervised evaluation measures.

The SEC algorithm with the same normalization done for the SST images of Portugal did not performed well and the result was always over-segmentation in all the images. After coming up with a new normalization formula where the normalization factor was empirically defined to 5, these good results were achieved.

The Table 4.3 summarizes the results and it can be seen that the SEC-SelfTuning correctly extracted the upwelling region for all the SST images of the Canary and, the SEC-Otsu and SEC-Ridler were also very effective. The SEC-Kittler failed to more times, because it under-segmented some images.

Table 4.3: Table that accounts for how frequent each version of the SEC algorithm, excluding the fine-tuning version, had the best score when segmenting an SST image of the Canary. It is also accounted the frequency that each version had F-measure scores superior or equal to 0.7, which was empirically identified has a threshold for separating good from bad segmentation results. The best versions scores are bold in the table, for each of the sets of images and information that is being analyzed.

Image Set	Information	SEC-Otsu	SEC-Kittler	SEC-Ridler	SEC-SelfTuning
Canary	% Best Method	**0,400**	0,100	0,200	0,300
#10	% F-measure $\geq$ 0.7	0,900	0,700	0,900	**1,000**

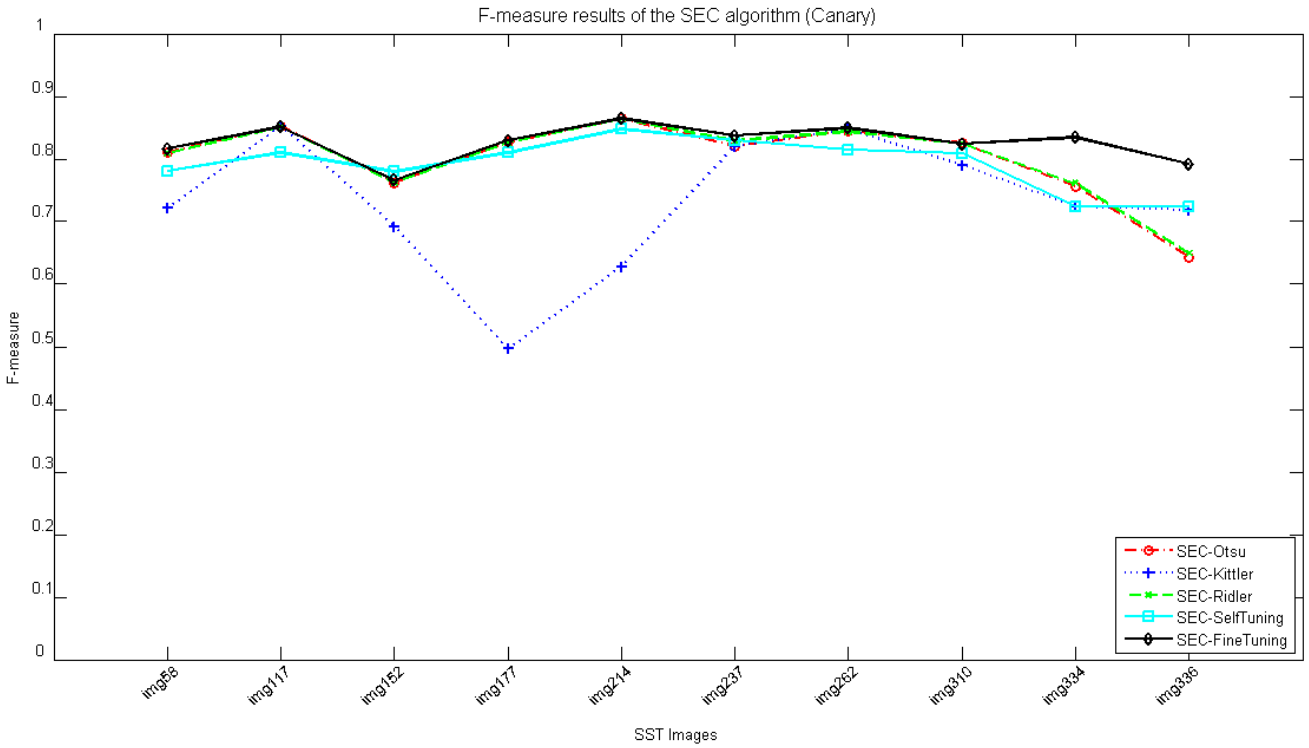

Figure 4.14: F-measure results for the comparative study between the SEC algorithm versions. The segmentation results are from the SST images of the Canary.

For these images the SEC-SelfTuning version had excellent results in all the images and its results were always very close to the SEC-FineTuning version, as it can be seen in the Figure 4.14. For the *img*334 and *img*336, it were not excellent because there were some minor explosions in the north, even if the results were still good.

As good or better than the SEC-SelfTuning was the SEC-Otsu and SEC-Ridler versions, however in one of the images, which the SEC-SelfTuning also had over-segmentation but not big enough to compromise the correct extraction of the upwelling region, the result was not good, because of an explosion in waters of the north degraded the segmentation

result.

The SEC-Kittler version for most of the images adequately segments the upwelling regions as the other versions of the SEC algorithm, however in the *img*177 and *img*214 the results are very poor. This is caused by the come on problem of the SEC-Kittler method, produce threshold values that are too high and constraint the growth of the region to under-segmentation.

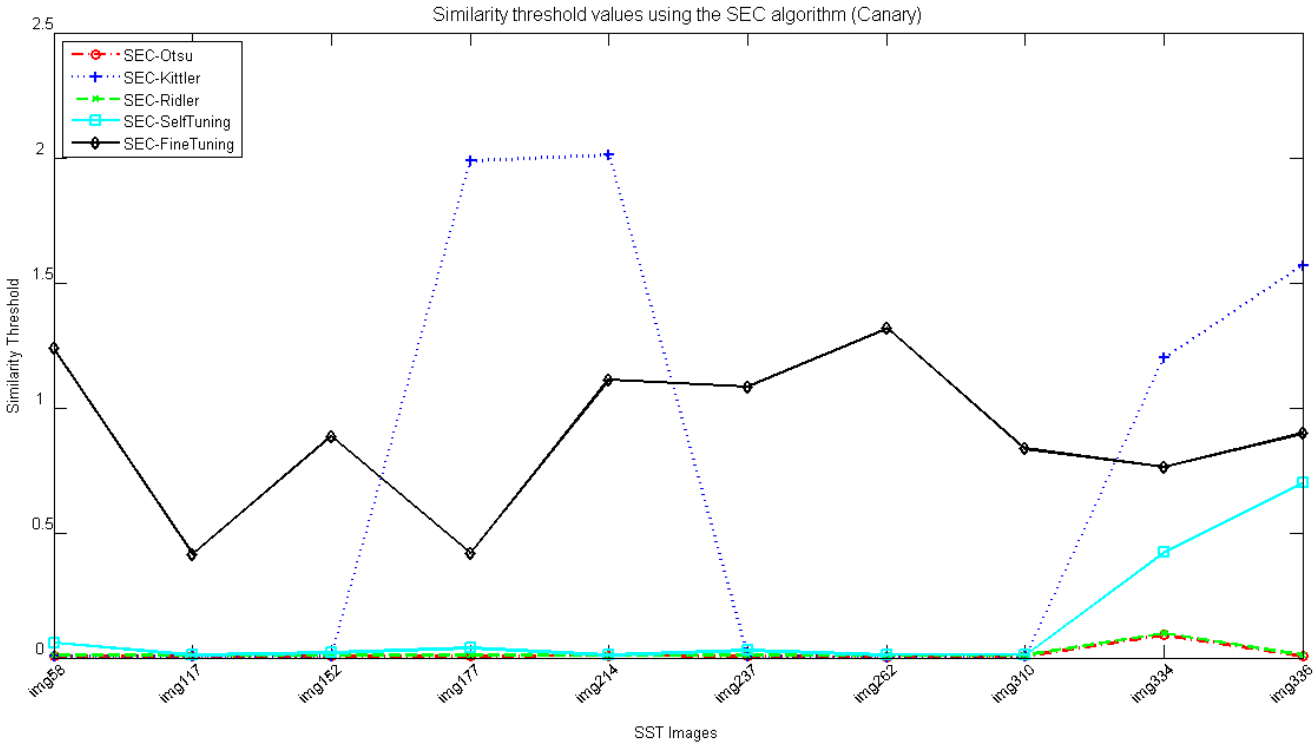

Figure 4.15: Similarity thresholds that were calculated for each of the SEC algorithm versions. Higher thresholds will contain more the growth of the clusters than smaller ones. The segmentation results are from the SST images of the Canary.

The Figure 4.15 reveals that as usual the SEC-Kittler produces the higher similarity thresholds values, and in the case of the *img*177 and *img*214 the results are very poor, because these high thresholds caused under-segmentation. However, in an image like *img*336, a threshold also higher than the ideal set by the SEC-FineTuning was calculated, even so it gave better results than the ones of the SEC-Otsu and SEC-Ridler, because for this image the higher threshold helped to contain an explosion.

SEC vs SEC-density It is also necessary to study the impact that the fine-tuning of the density threshold has in the quality of the segmentation for the SST images of the Canary, and contrast the results with and without the fine-tuning process, as it was done in the Section 4.4.1.1. Only supervised evaluation measures are necessary to this images because they have a ground-truth map that allows it.

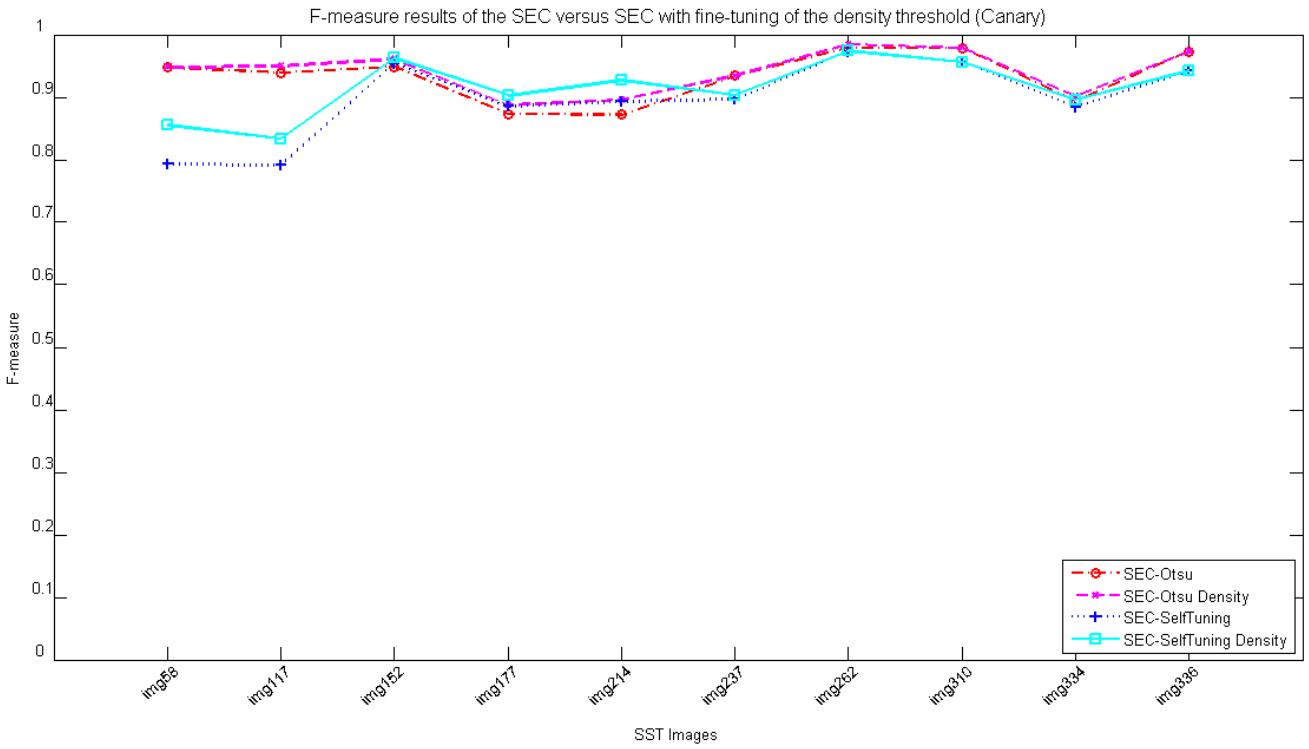

Figure 4.16: The graphic shows the improvements that the fine-tuning of the density threshold can have in the F-measure score. It is compared the SEC-Otsu and SEC-SelfTuning versions with their own versions, but with the fine-tuning of the density threshold. The segmentation results are from the SST images of the Canary.

The gains in the quality of segmentation by doing fine-tuning of the density threshold were very low to most of the images of the Canary, as the Figure 4.16 demonstrate. The only impact that the tuning of this threshold had to the final segmentation results was visible smoother boundaries in some of the images, instead of the usual disperse boundaries that sometimes are delimited by the SEC algorithm without the correct tuning of the density threshold, mainly in images with weak gradients in the frontier of the upwelling area.

4.4.3.3 SEC versions vs other SRG Methods

For the SST images of the Canary, a similar comparative study to the one of the Section 4.4.2 is presented, and the different SRG methods and their segmentation results are evaluated and compared, in order to see which of them are more adequate to delimit correctly the upwelling region.

The Table 4.4 confirms that the SEC algorithm versions and the AdamsSRG method obtained very often a good segmentation result and the SEC-Otsu was, to half of the images, the method that made a better segmentation.

Table 4.4: Table that accounts for how frequent each version of the SEC algorithm, excluding the fine-tuning version, and each SRG method had the best score when segmenting an SST image of the Canary. It is also accounted the frequency that each version had F-measure scores superior or equal to 0.7, which was empirically identified has a threshold for separating good from bad segmentation results. The best versions scores are bold in the table, for each of the sets of images and information that is being analyzed.

Image Set	Information	SEC-Otsu	SEC-Kittler	SEC-Ridler	SEC-SelfTuning	Adams SRG	OtsuVerma SRG	MeanVerma SRG	Shih SRG	Gambotto SRG	Zanaty SRG
Canary #10	% Best Method	**0,500**	0,200	0	0,200	0,200	0	0	0	0	0
	% F-measure ≥ 0.7	0,900	0,700	0,900	**1**	0,900	0,200	0	0,500	0,300	0,100

For these SST images of Canary, with scores showed in the Table A.7, the better methods were the versions of the SEC algorithm using the adequate normalization. The SEC-SelfTuning, SEC-Otsu and SEC-Ridler made adequate segmentations in almost every image, the SEC-Kittler did not perform well in 3 of the 10 images. Along as these two methods the AdamsSRG achieved good results for all the images, even being better in the images $img334$ and $img336$ where the other two methods had over-segmentation and this one not, however for images like $img177$, $img214$ and $img237$ the results from the other SRG methods were clearly inferior to the SEC-SelfTuning, SEC-Otsu and SEC-Ridler, even if they were not bad at all.

Both the OtsuVermaSRG and MeanVermaSRG suffer from the problem that the SEC method suffered before a new normalization method had been experimented, this is very large over-segmented regions. The upwelling area occurs in the coldest of the coldest waters in a thin area near the coast, so these methods extract even the waters that are not as cold as these ones because of the weak gradients in most of the images.

The ShihSRG fails in half the images to obtain good or acceptable segmentation results. Usually these images have at least to separate regions, and the merging procedure of this method sometimes makes one of those regions to be merged with the warmer waters, making the overall result not acceptable. But aside from these cases, it actually can correctly segment some of the images and have good results.

The GambottoSRG also fails to achieve good results in half the images, and in this method the explanation is related to over-segmentation, which in some images it is pretty visible, especially in these last two, where enormous explosions occur in the waters of the north.

By far the worst method for this set of images is the ZanatySRG that does not achieve any good results at all. Bad results that are combination of massive explosions in the segmentation of the region with failing to extract, in some images, a second area of upwelling.

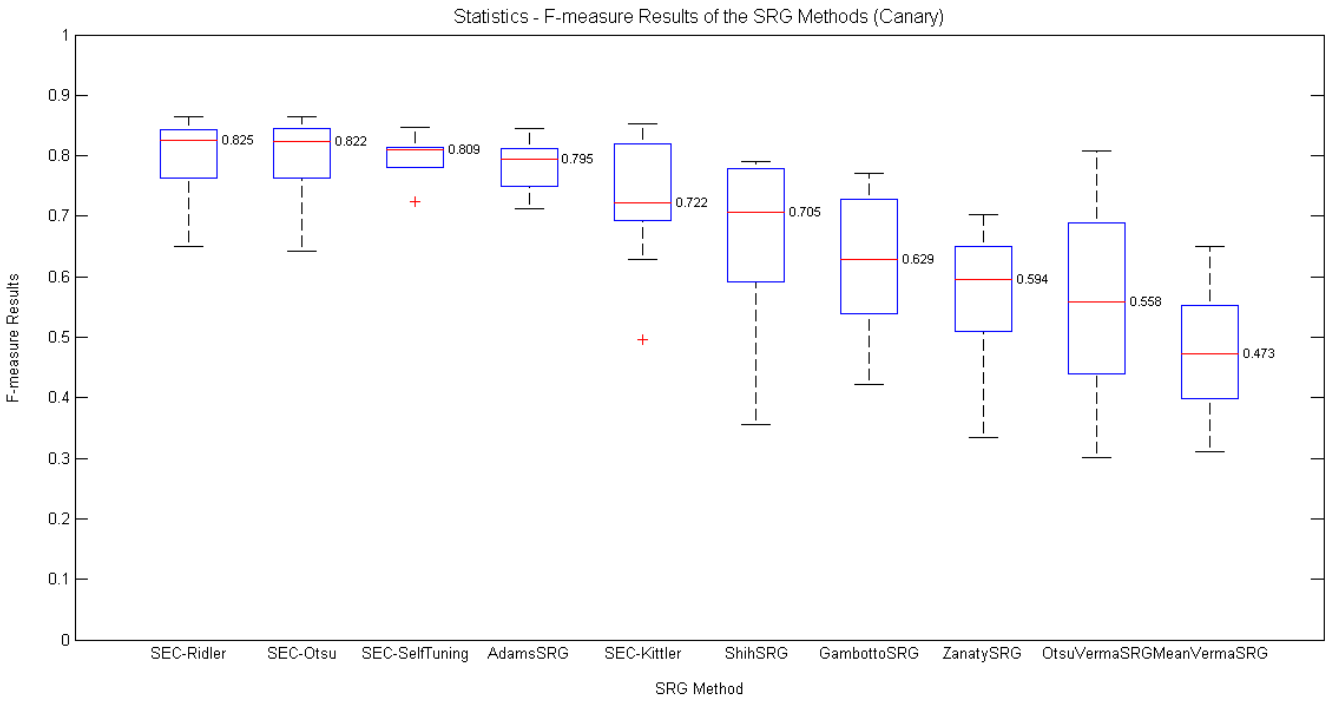

Figure 4.17: F-measure results for each of the SRG methods visualized in a box plot, making it possible to understand the variation of the results in the set of SST images of the Canary.

It were extracted some statistics to see which of the SRG methods were capable of correctly delimit the upwelling region can be seen in the Figure 4.17, and it shows that on pair with the SEC algorithm versions, only the AdamsSRG method created good segmentation results. All the other methods failed to achieve good results.

4.5 Unsupervised Analysis of SEC versions

4.5.1 Comparing the Unsupervised Evaluation Measures

Several unsupervised methods to evaluate the quality of image segmentation or to do clustering evaluation are proposed in the literature. These methods have limitations in correctly distinguish the quality of the segmentation result Zhang et al. (2008) when compared with supervised evaluation methods. Some methods were selected from the literature as being some of the ones with better results, and were applied to evaluate the segmentation of SST images to detect upwelling areas. The selected methods are categorized in intra-region, inter-region and intra-inter-region, and for the purpose of evaluating the SST images with no correspondent ground-truth map, the selected ones were including the intra-region and inter-region measures of Levine and Nazif, intra-region and inter-region measures of Rosenberger and Chehdi, Otsu's within-class and

between-class variances, Calinski-Harabasz criterion, Davies-Bouldin criterion and intra-region of Liu and Yang. To understand which of the unsupervised evaluation methods can have more success in correctly evaluating the segmentation results, a correlation study was done as in (Rosenberger et al. (2006)), which consists in analyzing the correlation factor between the results of the unsupervised measures and a supervised measure. The measurements were done for all the images of 1998 and 1999 that had associated to them a ground-truth map, and run with all the versions of the SEC algorithm, except for the fine-tuning version, and with all the SRG methods that were used in the comparative study. Using the images with ground-truth map has a learning platform, the robustness to correctly evaluate the segmentation results, by these unsupervised measures, can be registered and it can be seen how reliable they can be to evaluate the segmentation results for the SST images that have no ground-truth map.

In order to understand which of the unsupervised methods might be suited to evaluate more precisely the segmentation quality, the results of the F-measure, a reliable supervised evaluation measure, were compared with the results of these unsupervised methods, using a correlation measure.

It is important to note that for some of the unsupervised measures the correlation should be positive and for others it should be negative, because for the F-measure a higher score means a better score, which is also the same for some unsupervised measurers, but for others the lower the score is, the better is the segmentation result, according to their concept of quality of segmentation. Higher scores represent better segmentation results in the Inter_LN, Inter_FRC, Inter_Otsu and CalinskiHarabasz measures. Lower scores are better in measures like Intra_LN, Intra_Otsu, Intra_FRC, DaviesBouldin and Intra_Liu.

The results achieved with the inter-region measure of Levine and Nazif are equal to the ones achieved with the inter-region measure of Rosenberger and Chehdi, and the Otsu's within-class variance results are proportional to the ones of intra-region measure of Rosenberger and Chehdi.

Using the correlation coefficient to compare unsupervised evaluation methods with the F-measure, some of them were better than others for some sets of images, as seen in the Figure 4.18.

It was also necessary to do the same correlation study, but when applied to the SRG methods used in the comparative study. The best unsupervised methods were not always the same to all the sets of images. In the Figure 4.19 it is possible to see that none of the unsupervised measures has a good correlation factor to all the SRG methods, which makes it hard to trust any of these methods to, by itself, adequately evaluate the images with no ground-truth.

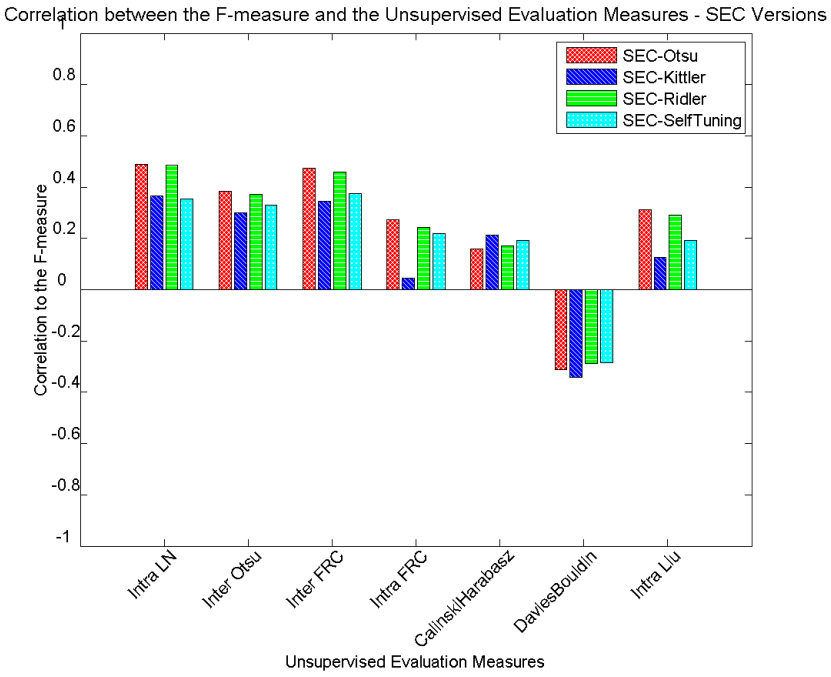

Figure 4.18: Correlation factors between the F-measure and the unsupervised evaluation measures, for each of the versions of the SEC algorithm. It is important to have into consideration which methods should have positive and negative correlation values.

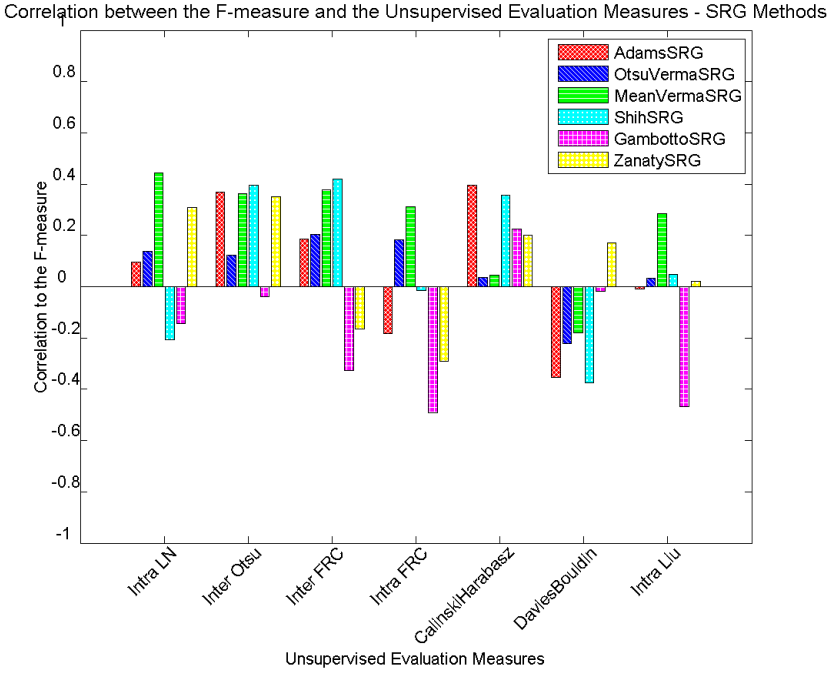

Figure 4.19: Correlation factors between the F-measure and the unsupervised evaluation measures, for each of the SRG methods. It is important to have into consideration which methods should have positive and negative correlation values.

In order to distinguish the good from the bad segmentation results of SST images with ground-truth map, a threshold value was defined and a F-measure higher than 0.7 represents a good segmentation, which was considered an accurate value after analyzing the results obtained. To tell the difference between the good and bad segmentation results for the SST images that have no ground-truth map, it was also necessary to define some threshold for each unsupervised evaluation measure, even if it is not expected to achieve the F-measure precision.

The thresholds for each measure and applied to each of the region growing methods was defined using the Information Gain as a supervised method, and the Otsu's method because it is an unsupervised automatic thresholding technique.

The Information Gain was used to find the best separation threshold that was equivalent to the 0.7 value of the F-measure. The input of the method consists in the values of the unsupervised evaluation measure that is attributed for each image and a ground-truth. So, the ground-truth that the Information Gain technique needs to find the threshold consists in mark as 1 the values for the images where the F-measure scored higher than 0.7, and 0 to the contrary, based on this the threshold value that better separates good from bad segmentation was calculated. The calculated thresholds for the Information Gain are displayed in the Table A.10.

The Otsu's method did not require the ground-truth, and it was also applied to test its effectiveness and as an alternative threshold. The thresholds generated by this method can be seen in the Table A.11.

After applying the thresholds, each unsupervised evaluation measure defined which segmentation results were good and which were not. However, because the unsupervised measures have their limitations, in order to measure how accurate they correctly distinguished the good from the bad segmentation results for the SST images without ground-truth map, the classifications made by each evaluation measure was compared with the classification made by visual inspection. It was created a ground-truth, which for all images segmented by all the SRG method, it was decided, visually, which cases there were clearly over-segmentation or under-segmentation. This made possible to compare the classification made by each unsupervised evaluation measure to the classification made by visual inspection. The percentage of times the classification made by the evaluation measures was coincident with the ground-truth is listed in the Table 4.5, for the Information Gain thresholds.

Table 4.5: Accuracy that each unsupervised evaluation measure had when applied to each SRG method. Underlined are the three most accurate evaluation measures for each of the SRG methods. In the bottom line it can be seen the percentage of times that each unsupervised evaluation measure was in the three most accurate for each SRG method (Success Rate). The values in bold are the ones where the correlation to the F-measure was better, meaning higher or lower than 0.2 or -0.2, depending if for the given unsupervised evaluation measure the ideal correlation should be positive or negative correspondingly.

	Intra_LN	Inter_Otsu	Inter_FRC	Intra_FRC	Intra_Liu	CalinskiHarabasz	DaviesBouldin
SEC-Otsu	0,54	**0,56**	**0,61**	0,60	0,56	0,32	**0,46**
SEC-Kittler	0,59	**0,50**	**0,60**	0,70	0,60	**0,51**	**0,68**
SEC-Ridler	0,30	**0,66**	**0,67**	0,63	0,58	0,38	**0,38**
SEC-SelfTuning	0,55	**0,54**	**0,62**	0,54	0,54	0,57	**0,46**
AdamsSRG	0,86	**0,89**	0,79	0,94	0,93	**0,89**	**0,87**
OtsuVermaSRG	0,37	0,57	**0,62**	0,46	0,60	0,59	**0,50**
MeanVermaSRG	0,42	**0,58**	**0,60**	0,46	0,47	0,50	0,57
ShihSRG	**0,46**	**0,74**	**0,71**	0,54	0,51	**0,76**	**0,39**
GambottoSRG	0,58	0,45	0,40	**0,73**	**0,50**	**0,57**	0,46
ZanatySRG	0,46	**0,57**	0,50	**0,54**	0,52	**0,52**	0,46
Success Rate	20%	60%	70%	60%	50%	60%	20%

Looking at the Table 4.5, four unsupervised measures were selected as the most suited to evaluate the segmentation results. The best methods are the Inter_Otsu, Inter_FRC, Intra_FRC and CalinskiHarabasz, by majority vote. The Intra_FRC is a method with low correlation to the F-measure for almost every SRG method, even so it was accurate. The other selected methods all have good correlation for most of the SRG methods.

4.5.2 SEC Automatic thresholding vs Self-tuning

The SST images from 1998, 2000, 2001 and 2002 without ground-truth map were evaluated using unsupervised measures. The limitations and accuracy of the unsupervised evaluation measures were studied in the Section 4.5.1. Complementary to the unsupervised evaluation, the segmentation results were visually inspected and compared to the unsupervised measurements, and as seen in the Table 4.5, the percentage of times that the measures were able to detect clear cases of over and under segmentation was not very high, and it was observed that the Inter_Otsu, Inter_FRC, Intra_FRC and CalinskiHarabasz measures would be the most adequate to use.

In the Table 4.6, it was registered the percentage of images that each unsupervised evaluation measure gave positive evaluations for each region growing method. The chosen evaluation measures classify the SEC-Ridler has a method with good results and has the best version of the SEC algorithm, with exception of the CalinskiHarabasz measure,

which is the only measure to give it a poor score. The problem is that through visual inspection it can be seen that the SEC-Otsu and SEC-Kittler versions of the SEC algorithm were in fact close to the segmentation results of the SEC-Ridler, and their segmentation results were also good, but the unsupervised evaluation measures do not agree between them in good scores or bad scores. The SEC-SelfTuning also achieved good scores and it follows the SEC-Ridler as the best SEC version.

Overall the mean rate of positive classifications, using the selected unsupervised evaluation measures, for each of the SEC versions was 72.4% (SEC-Riddler), 69.7% (SEC-SelfTuning), 61.4% (SEC-Kittler) and 47.2% (SEC-Otsu).

4.5.3 SEC versions vs other SRG Methods

Analyzing the box plots in the Appendix A.2.3, where the evaluation results for the Inter_Otsu, Inter_FRC, Intra_FRC and CalinskiHarabasz measures allow to compare the SEC algorithm versions with the other SRG methods, in the distribution of scores, and it can be seen that none of the measures classifies the SEC algorithm or the AdamsSRG the best methods, as it occurs on the SST images with ground-truth using the F-measure. However, using the threshold calculated by the Information Gain technique, in the study of the unsupervised evaluation measures, that are displayed in the Table A.10, it was possible to calculate the percentage of times that each unsupervised measure classified as good the segmentation done by the individual region growing methods.

In the Table 4.6, it can be seen that all the unsupervised evaluation measures agree that one SRG method performed very well in all the years, it was the AdamsSRG (with 89.5% of positive mean classifications overall), and this corresponds to what happened to the SST images with ground-truth and to what was visually inspected. The Inter_Otsu, Inter_FRC and CalinskiHarabasz gave the OtsuVermaSRG very good scores (with 84.2% of positive classifications), but the Intra_FRC measure does not give this SRG method great results. Crossing these results with visual inspection, it is possible to see that the results were generally good, but not has good as the Inter_Otsu, Inter_FRC and CalinskiHarabasz suggest. Looking at the MeanVermaSRG the results were good (with 80.9% of positive rate) using any of the measures, but bellow the OtsuVermaSRG, even so it is approximated to the reality. The SEC-Ridler was the best of the SEC versions (72.4% positive classifications), followed by the SEC-SelfTuning. Through visual inspection it can be seen that other two versions of the SEC got similar good segmentation results, even if they had lower scores with these measures. The ZanatySRG was also classified as a method with good scores (79% positive classifications). The evaluation measures mostly agree in a good evaluation for this method, but visually inspecting the segmentation results it can be seen that the method might have been overrated. For the ShihSRG and GambottoSRG the different evaluation measures do not reach a consensus for different years, but visually it can be seen that the results tended to have big over or under segmentation results, even if not in the majority of the images. However, the ShihSRG was better evaluated (74.6%

positive classifications) than the GambottoSRG (35.8% positive classifications).

The segmentation results are significant different depending on the year as seen in the Tables A.8 and A.9, meaning that for example the results from 2002 were generally better than the ones from 2000, because the year of 2002 has SST images with well defined upwelling boundaries, meaning that the SRG methods deal better with images with strong gradients than with weak gradients.

Table 4.6: Table that accounts for how frequent each version of the SEC algorithm and each SRG method had positive scores given by each unsupervised evaluation measures, when segmenting SST image without ground-truth. The best SRG methods scores are bold in the table. In the bottom lines it can be seen the mean rate of positive classifications given by the select four best unsupervised evaluation measures, and the correspondent standard deviation.

Image Set	Information	SEC-Otsu	SEC-Kittler	SEC-Ridler	SEC-SelfTuning	Adams SRG	OtsuVerma SRG	MeanVerma SRG	Shih SRG	Gambotto SRG	Zanaty SRG
All Images (No GT) #136	% Intra_LN	0,801	0,735	0,103	0,831	**0,875**	0,081	0,103	0,434	0,243	0,662
	% Inter_Otsu	0,375	0,382	0,846	0,324	0,904	**0,919**	0,735	0,691	0,096	0,610
	% Inter_FRC	0,426	0,515	**0,882**	0,838	0,831	0,875	0,779	0,831	0,728	0,868
	% Intra_FRC	0,919	0,919	0,926	0,735	**0,985**	0,581	0,728	0,772	0,463	0,868
	% Intra_Liu	0,801	0,794	0,824	0,750	0,971	**1,000**	0,757	0,243	0,088	0,801
	% Calinski Harabasz	0,169	0,640	0,243	0,890	0,860	**0,993**	**0,993**	0,691	0,147	0,816
	% Davies Bouldin	0,324	0,721	0,184	0,228	**0,912**	0,169	0,787	0,103	0,471	0,176
	Mean Rate Positive Classifications	0,472	0,614	0,724	0,697	**0,895**	0,842	0,809	0,746	0,358	0,790
	Standard Deviation	0,318	0,229	0,323	0,257	0,067	0,181	0,125	0,068	0,295	0,123

4.6 Tuning the Density Threshold of the SEC Algorithm

The density threshold of the SEC algorithm, by default was set to $\frac{1}{windowsSize \times windowsSize}$, but by doing fine-tuning of this parameter, the threshold that maximized the F-measure was usually higher than $\frac{1}{windowsSize \times windowsSize}$. So, analyzing the results some other values θ were considered, where $\frac{\theta}{windowsSize \times windowsSize}$ is the threshold.

For the Self-Tuning version of the algorithm, the best θ value was 16 (not the best for all, but the best overall). It can give good gains in the F-measure, but in three images it lowered significantly the quality and in another three this value as simply too high to allow the cluster to even grow.

Another value let the F-measure being improved compared to $\theta = 1$, and it was $\theta = 13$, but this one provided smaller gains, however no significant losses. Besides being a good value, like the 16 it was too high to two images and did not let the cluster grow beyond the neighbors of the initial seed.

So, a much more modest value, in terms of gains, but that works for all the tested images was $\theta = 10$. It has insignificant losses in some quality scores, but overall it can improve a little bit the majority of them, even if not much. The only disadvantage to $\theta = 10$ is that this value is not certain to not obstruct the growth of the clusters in some images outside the sets used in this study.

The differences in scores that these empirical threshold methods have in the can be seen in the Figure A.22, in which it can be seen differences between the best density threshold of the fine-tuning and the empirically selected thresholds. The smaller the differences better the thresholds were. But more important might be the Figure A.23, which has the differences between the empirically selected thresholds and the standard $\frac{1}{windowsSize \times windowsSize}$, with $windowsSize = 7$. It can be seen that sometimes an incorrect tuning of the threshold can lower the scores significantly.

The data shows that is difficult to establish a pre-defined density threshold that consistently improves the quality of the segmentation results of some images without deteriorating the segmentation quality of other images.

4.7 Outlook of the Results

The results of the experimental study for this dissertation were obtained using the software MATLAB R2014a and Java 7, in a computer with an Intel Core i5 CPU M460 @ 2.53GHz processor, 4GB of RAM memory and with the Windows 7 operating system.

The mean time to extract the upwelling regions of an SST image was: SEC-Otsu 30.99s, SEC-Kittler 28.08s, SEC-Ridler 43.39s, SEC-SelfTuning 53.89s, AdamsSRG 0.33s, OtsuVermaSRG 2.18s, MeanVermaSRG 1.62s, ShihSRG 0.45s, GambottoSRG 1690.30s, ZanatySRG 149.12s.

Overall the SEC algorithm proved to be effective in tackling the problem of delimiting the upwelling area, even if there are considerable differences in the results achieved by the many versions of the SEC algorithm. The SEC-Otsu and SEC-Ridler versions scored very close in all SST images with a few exceptions. However, comparing the SEC-Kittler version with SEC-Otsu and SEC-Ridler, it is obvious that the SEC-Kittler has a tendency to produce higher thresholds and in consequence constraining more the growth of the region. This can be good and can be bad, the SEC-Kittler achieves better segmentation results in images with weak gradients, because a high threshold is necessary to prevent the explosions that usually occur and cause over-segmentation. However, in images with strong gradients the SEC-Kittler usually has good segmentation results, but they are below the other SEC versions.

The SEC-SelfTuning version, which dynamically calculates a similarity threshold for each evaluated pixel, also achieved good results, many times similar to the SEC-Otsu and SEC-Ridler versions. Sometimes the segmentation results were even better than in the other versions, however in images with weak gradients, the SEC-SelfTuning version performance is affected.

Some of the SRG methods revealed to be reliable in delimiting the upwelling area, mainly the SEC algorithm versions, the AdamsSRG and the both VermaSRG versions for most of the times. Each of the methods has advantages and disadvantages. The AdamsSRG was overall the best, but its seeds had to be manually selected. The methods like the SEC and VermaSRG often provide well delimited upwelling regions and they are fully automated. The remaining SRG methods had difficulties to be accurate in delimit upwelling regions.

The SEC-SelfTuning, SEC-Otsu and SEC-Ridler generally performed well in most of the SST images, however in some of the images with weak gradients the performance was affected, because these methods tend to over-segment the image. In images with really weak gradients, the SEC-Kittler performed better.

The AdamsSRG method scored results of consistent high quality for all sets of images, even sometimes having success in images that other methods had poor results, like images with weak gradients. This method had the distinct advantage of manual seed selection, which benefited of human perception to provide adequate seeds that were meaningful placed and avoided noise.

The OtsuVermaSRG and MeanVermaSRG can be directly compared to the SEC-Otsu, SEC-Ridler and SEC-SelfTuning when it comes to its behavior, namely in its difficulties to correctly segment images with weak gradients and in its capabilities in achieving high quality segmentation results in images with stronger gradients. Overall it looks like there is equilibrium between the results of both versions of the VermaSRG, but the OtsuVermaSRG version tends to be the best of both, having better results than the SEC-SelfTuning and SEC-Otsu, except for the images of the Canary.

The ShihSRG is similar to the AdamsSRG, except it has an automatic seed selection

and merging procedure that try to segment the image in a meaningful way. The results of this method were generally not good, with some exceptions mainly in images with strong gradients. It is clear that the extra automation, relatively to the AdamsSRG method, has negative effects, however contrarily to AdamsSRG, this one processed images without human intervention in selecting good initial seeds.

The results of the GambottoSRG method were not good in most of the SST images, making poor segmentations, however the method revealed to be capable of achieving good scores in a few images with weak gradients. This is the only of the SRG methods that combines region growing with edge detection to control the growth. What happen in most of the images, was that even inside the cold waters there are areas that contain even colder waters, so when growing a region staring the coldest waters, rapidly an edge is found and the growth is constrained before the full upwelling area is extracted.

ZanatySRG performs relatively well in the images with strong gradients and not so much in images with weaker gradients. This happens because the results indicate that the method had a strong tendency to over-segmentation and creating large regions.

Chapter 5

Conclusion and Future Work

An iterative procedure that allows to extract more than one region of upwelling in the same SST image was developed. The process is composed by a set of criteria that were defined and tuned from experiments with a vast set of SST images and, it proved to be effective in correctly extract the exact number of regions of upwelling.

The segmentation results were evaluated using supervised measures, for images with ground-truth map, which provide very accurate information about the quality of the segmentation. In the comparative study that compared the different versions of the SEC algorithm for images of Portugal, the SEC-Kittler performed better in images with weak gradients in the upwelling boundaries than the other versions. However, the SEC-Otsu, SEC-Ridler and SEC-SelfTuning performed very well in images with stronger gradients. Overall, all the versions of the SEC algorithm were successful in correctly delimit the upwelling region. The rates of good segmentation results (F-measure score ≥ 0.7) were 67.2% (SEC-Otsu), 78.7% (SEC-Kittler), 70.5% (SEC-Ridler), 62.3% (SEC-SelfTuning). Moreover, the SEC-SelfTuning scored higher than the other versions in 47.5% of the images, followed by the SEC-Kittler that was the best in 32.8%.

Besides studying the behavior of the different versions of the SEC algorithm, it was also necessary to compare them to other SRG methods present in the literature. In this comparison it was possible to see that only the AdamsSRG method had good results (83.6% correct upwelling delimitations) more often then the SEC versions, which were also very good, just there was not a single version that was good in both SST images with strong and weak gradients. However, the AdamsSRG needed manual seed selection, so the SEC algorithm was the best of the fully automatic methods, being followed by the OtsuVermaSRG and MeanVermaSRG versions (59% and 54.1% success), which had some serious problems with explosions some times. The remaining SRG methods performed worst, because severe over or under segmentation results were common, meaning that

the good segmentation results never reached the 50% success rate.

For the SST images of the Canary, the SEC algorithm proved to be effective too, in this very distinct upwelling morphology. The SEC-SelfTuning achieved good results in all the images of this set, the SEC-Otsu and SEC-Ridler had good results in 90% of the images and the SEC-Kittler in 70%. The AdamsSRG was also very good and had a 90% success rate. The ShihSRG had good results in half the images and the remaining SRG methods had good segmentation rates of 20% (OtsuVermaSRG), 0% (MeanVermaSRG), 30% (GambottoSRG), and 10% (ZanatySRG).

To evaluate segmentation results of images without ground-truth map, unsupervised measures were used. It was necessary to make a study about the effectiveness of these measures, because it is described in the literature their limitations. The best measures for this context were selected and thresholds defined, in order to distinguish good from bad segmentation results, and it was possible to compare the performances of the SRG methods. Overall the mean rate of positive classifications, using the selected unsupervised evaluation measures, for each of the SRG methods was 89.5% (AdamsSRG), 84.2% (OtsuVermaSRG), 80.9% (MeanVermaSRG), 79% (ZanatySRG), 74.6% (ShihSRG), 72.4% (SEC-Riddler), 69.7% (SEC-SelfTuning), 61.4% (SEC-Kittler) and 47.2% (SEC-Otsu), 35.8% (GambottoSRG). It is important to state that through visual inspection it can be seen that the SEC-Otsu and SEC-Kittler were clearly underrated, and that the ZanatySRG and ShihSRG overrated.

It was also made a study that demonstrated that the correct tuning of the density threshold of the SEC algorithm can also allow a major improvement in the segmentation quality in some images or, at least delimit smoother boundaries to the upwelling region.

The future work following this dissertation can be made around finding a way to improve the segmentation results of the SEC algorithm. From what was determined in the study of the influence of the density condition of the SEC, it is hard to define, empirically, a density threshold that improves the results to all the images, so it would be a good improvement to find an automatic method to tune this parameter. Other way to improve the segmentation results of the SEC algorithm would be to find a strategy to control the explosion problem, which over-segments the images, and it is transversal to many other SRG methods too.

Bibliography

Adams, R. and L. Bischof (1994). "Seeded region growing". In: *Pattern Analysis and Machine Intelligence, IEEE Transactions on* 16(6), pp. 641–647.

Al-Faris, A. Q., U. K. Ngah, N. A. Isa, and I. L. Shuaib (2012). "Breast MRI tumour segmentation using modified automatic seeded region growing based on particle swarm optimization image clustering". In: *Soft Computing in Industrial Applications*. Springer, pp. 49–60.

Al-Faris, A. Q., U. K. Ngah, N. A. Isa, and I. L. Shuaib (2013). "Computer-Aided Segmentation System for Breast MRI Tumour using Modified Automatic Seeded Region Growing (BMRI-MASRG)". In: *Journal of digital imaging* 27(1), pp. 133–144.

Arriaza, J. A., F. G. Rojas, M. P. Lopez, and M. Cantón (2003). "Competitive neural-net-based system for the automatic detection of oceanic mesoscalar structures on AVHRR scenes". In: *Geoscience and Remote Sensing, IEEE Transactions on* 41(4), pp. 845–852.

Bagli, S., P. Soille, and E. Fermi (2004). "Automatic delineation of shoreline and lake boundaries from Landsat satellite images". In: *Proceedings of initial ECO-IMAGINE GI and GIS for Integrated Coastal Management, Seville*, pp. 13–15.

Bins, L. S., L. M. Fonseca, G. J. Erthal, and F. M. Ii (1996). "Satellite imagery segmentation: a region growing approach". In: *Simpósio Brasileiro de Sensoriamento Remoto* 8, pp. 677–680.

Caliński, T. and J. Harabasz (1974). "A dendrite method for cluster analysis". In: *Communications in Statistics-theory and Methods* 3(1), pp. 1–27.

Carvalho, E. A., D. M. Ushizima, F. N. Medeiros, I. O. Martins, C. P. Marques, and N. S. Oliveira (2010). "SAR imagery segmentation by statistical region growing and hierarchical merging". In: *Digital Signal Processing* 20(5), pp. 1365–1378.

Cayula, J. F. and P. Cornillon (1992). "Edge detection algorithm for SST images". In: *Journal of Atmospheric and Oceanic Technology* 9(1), pp. 67–80.

Chang, L. Y. and C. F. Chen (2007). "A Multi-Scale Region Growing Segmentation for High Resolution Remotely Sensed Images". In:

Chaudhari, S., R. Balasubramanian, and A. Gangopadhyay (2008). "Upwelling detection in AVHRR sea surface temperature (SST) images using neural-network framework". In: *Geoscience and Remote Sensing Symposium, 2008. IGARSS 2008. IEEE International*. Vol. 4. IEEE, pp. IV–926.

Chen, H. L., F. F. Samavati, M. C. Sousa, and J. R. Mitchell (2006). "Sketch-based volumetric seeded region growing". In: *Proceedings of the Third Eurographics conference on Sketch-Based Interfaces and Modeling*. Eurographics Association, pp. 123–130.

Dantulwar, S. and R. K. Krishna (2014). "Performance Analysis Using Single Seeded Region Growing Algorithm". In: *International Journal of Innovative Research in Advanced Engineering* 1(6), pp. 2349–2163.

Dass, R. and S. Devi (2012). "Image Segmentation Techniques 1". In:

Davies, D. and D. Bouldin (1979). "A cluster separation measure". In: *Pattern Analysis and Machine Intelligence, IEEE Transactions on*(2), pp. 224–227.

Espindola, G. M., G. Câmara, I. A. Reis, L. S. Bins, and A. M. Monteiro (2006). "Parameter selection for region-growing image segmentation algorithms using spatial autocorrelation". In: *International Journal of Remote Sensing* 27(14), pp. 3035–3040.

Fan, J., D. K. Yau, A. K. Elmagarmid, and W. G. Aref (2001). "Automatic image segmentation by integrating color-edge extraction and seeded region growing". In: *Image Processing, IEEE Transactions on* 10(10), pp. 1454–1466.

Fan, J., G. Zeng, M. Body, and M. S. Hacid (2005). "Seeded region growing: an extensive and comparative study". In: *Pattern Recognition Letters* 26(8), pp. 1139–1156.

Freixenet, J., X. Muñoz, D. Raba, J. Martí, and X. Cufí (2002). "Yet another survey on image segmentation: Region and boundary information integration". In: *Computer Vision—ECCV 2002*. Springer, pp. 408–422.

Gambotto, J. (1993). "A new approach to combining region growing and edge detection". In: *Pattern Recognition Letters* 14(11), pp. 869–875.

Gao, Y., J. F. Mas, N. Kerle, and J. A. Navarrete P. (2011). "Optimal region growing segmentation and its effect on classification accuracy". In: *International Journal of Remote Sensing* 32(13), pp. 3747–3763.

Hadwiger, M., F. Laura, C. Rezk-Salama, T. Hollt, G. Geier, and T. Pabel (2008). "Interactive volume exploration for feature detection and quantification in industrial CT data". In: *Visualization and Computer Graphics, IEEE Transactions on* 14(6), pp. 1507–1514.

Han, J. and M. Kamber (2001). "Data mining: concepts and techniques". In: *United States of America: Morgan Kauff mann Publishers*.

Haralick, R. M. (1983). "Image segmentation survey". In: *Fundamentals in computer vision, OD Faugeras, ed., Cambridge Univ. Press, Cambridge*, pp. 209–224.

Hojjatoleslami, S. A. and J. Kittler (1998). "Region growing: a new approach". In: *IEEE Transactions on Image processing* 7(7), pp. 1079–1084.

Hubert, L. and P. Arabie (1985). "Comparing partitions". In: *Journal of Classification* 2(1), pp. 193–218. ISSN: 0176-4268.

Jain, P. K. and S. Susan (2013). "An adaptive single seed based region growing algorithm for color image segmentation". In:

Kamdi, . and R. Krishna (2011). "Image Segmentation and Region Growing Algorithm". In: *International Journal of Computer Technology and Electronics Engineering (IJCTEE) Volume* 2.

Kittler, J. and J. Illingworth (1986). "Minimum error thresholding". In: *Pattern recognition* 19(1), pp. 41–47.

Kriebel, S. K., W. Brauer, and W. Eifler (1998). "Coastal upwelling prediction with a mixture of neural networks". In: *Geoscience and Remote Sensing, IEEE Transactions on* 36(5), pp. 1508–1518.

Lachance, S., R. Bauer, and A. Warkentin (2004). "Application of region growing method to evaluate the surface condition of grinding wheels". In: *International Journal of Machine Tools and Manufacture* 44(7), pp. 823–829.

Levine, M. and A. Nazif (1985). "Dynamic measurement of computer generated image segmentations". In: *Pattern Analysis and Machine Intelligence, IEEE Transactions on*(2), pp. 155–164.

Liu, J. and Y. Yang (1994). "Multiresolution color image segmentation". In: *Pattern Analysis and Machine Intelligence, IEEE Transactions on* 16(7), pp. 689–700.

Luccheseyz, L. and S. K. Mitray (2001). "Color image segmentation: A state-of-the-art survey". In: *Proceedings of the Indian National Science Academy (INSA-A)* 67(2), pp. 207–221.

Marcello, J., F. Marques, and F. Eugenio (2005). "Automatic tool for the precise detection of upwelling and filaments in remote sensing imagery". In: *Geoscience and Remote Sensing, IEEE Transactions on* 43(7), pp. 1605–1616.

Mat-Isa, N. A., M. Y. Mashor, and N. H. Othman (2005). "Seeded region growing features extraction algorithm; its potential use in improving screening for cervical cancer". In: *International Journal of The Computer, the Internet and Management* 13(1), pp. 61–70.

Mehnert, A. and P. Jackway (1997). "An improved seeded region growing algorithm". In: *Pattern Recognition Letters* 18(10), pp. 1065–1071.

Melouah, A. and R. Amirouche (2014). "Comparative study of automatic seed selection methods for medical image segmentation by region growing technique". In:

Mirkin, B. (1996). *Mathematical Classification and Clustering*. Kluwerr.

Mirkin, B. (2013). "Individual Approximate Clusters: Methods, Properties, Applications". In: *Rough Sets, Fuzzy Sets, Data Mining, and Granular Computing*. Springer, pp. 26–37.

Mishra, B. and J. Susaki (2013). "Coupling of Thresholding and Region Growing Algorithm for Change Detection in SAR Images". In: *Progress In Electromagnetics Research* 143, pp. 519–544.

Nascimento, S. and P. Franco (2009). "Segmentation of upwelling regions in sea surface temperature images via unsupervised fuzzy clustering". In: *Intelligent Data Engineering and Automated Learning-IDEAL 2009*. Springer, pp. 543–553.

Nascimento, S., F. Sousa, H. Casimiro, and D. Boutov (2005). "Applicability of fuzzy clustering for the identification of upwelling areas on sea surface temperature images".

In: *Procs. 2005 UK Workshop on Computational Intelligence, London, UK*. Citeseer, pp. 143–148.

Nascimento, S., P. Franco, F. Sousa, J. Dias, and F. Neves (2012). "Automated computational delimitation of SST upwelling areas using fuzzy clustering". In: *Computers & Geosciences* 43, pp. 207–216.

Nascimento, S., S. Casca, and B. Mirkin (2015). "A Seed Expanding Cluster Algorithm for Deriving Upwelling Areas on Sea Surface Temperature Images. Special issue on "Statistical learning in geoscience modelling: novel algorithms and challenging case studies" (to appear)." In: *Computers & Geosciences*.

Nieto, K., H. Demarcq, and S. McClatchie (2012). "Mesoscale frontal structures in the Canary Upwelling System: New front and filament detection algorithms applied to spatial and temporal patterns". In: *Remote Sensing of Environment* 123, pp. 339–346.

Otsu, N. (1979). "A Threshold Selection Method from Gray-Level Histograms". In: *Systems, Man and Cybernetics, IEEE Transactions on* 9(1), pp. 62–66. ISSN: 0018-9472. DOI: 10.1109/TSMC.1979.4310076.

Pal, N. R. and S. K. Pal (1993). "A review on image segmentation techniques". In: *Pattern recognition* 26(9), pp. 1277–1294.

Plattner, S., D. M. Mason, G. A. Leshkevich, D. J. Schwab, and E. S. Rutherford (2006). "Classifying and forecasting coastal upwellings in Lake Michigan using satellite derived temperature images and buoy data". In: *Journal of Great Lakes Research* 32(1), pp. 63–76.

Pohle, R. and K. D. Toennies (2001). "A new approach for model-based adaptive region growing in medical image analysis". In: *Computer Analysis of Images and Patterns*. Springer, pp. 238–246.

Pottmann, H., S. Leopoldseder, M. Hofer, T. Steiner, and W. Wang (2005). "Industrial geometry: recent advances and applications in CAD". In: *Computer-Aided Design* 37(7), pp. 751–766.

Preetha, M. J., L. P. Suresh, and M. J. Bosco (2012). "Image segmentation using seeded region growing". In: *Computing, Electronics and Electrical Technologies (ICCEET), 2012 International Conference on*. IEEE, pp. 576–583.

Prieto, E., P. Lecumberri, M. Pagola, M. Gómez, I. Bilbao, M. Ecay, I. Peñuelas, and J. M. Martí-Climent (2012). "Twelve automated thresholding methods for segmentation of PET images: a phantom study". In: *Physics in medicine and biology* 57(12), p. 3963.

Rai, G. N. and T. R. Nair (2010). "Gradient based seeded region grow method for CT angiographic image segmentation". In: *arXiv preprint arXiv:1001.3735*.

Ridler, T. W. and S. Calvard (1978). "Picture thresholding using an iterative selection method". In: *IEEE transactions on Systems, Man and Cybernetics* 8(8), pp. 630–632.

Rosenberger, C. and K. Chehdi (2000). "Genetic fusion: application to multi-components image segmentation". In: *Acoustics, Speech, and Signal Processing, 2000. ICASSP'00. Proceedings. 2000 IEEE International Conference on*. Vol. 6. IEEE, pp. 2223–2226.

Rosenberger, C., S. Chabrier, H. Laurent, and B. Emile (2006). "Unsupervised and supervised image segmentation evaluation". In: *Advances in image and video segmentation*, pp. 365–393.

Sezgin, M. and B. Sankur (2004). "Survey over image thresholding techniques and quantitative performance evaluation". In: *Journal of Electronic imaging* 13(1), pp. 146–168.

Shih, F. Y. and S. Cheng (2005). "Automatic seeded region growing for color image segmentation". In: *Image and Vision Computing* 23(10), pp. 877–886.

Stokking, R., K. L. Vincken, and M. A. Viergever (2000). "Automatic morphology-based brain segmentation (MBRASE) from MRI-T1 data". In: *NeuroImage* 12(6), pp. 726–738.

Stroppiana, D., G. Bordogna, P. Carrara, M. Boschetti, L. Boschetti, and P. A. Brivio (2012). "A method for extracting burned areas from Landsat TM/ETM+ images by soft aggregation of multiple Spectral Indices and a region growing algorithm". In: *ISPRS Journal of Photogrammetry and Remote Sensing* 69, pp. 88–102.

Szeliski, R. (2010). *Computer vision: algorithms and applications*. Springer.

Tamim, A., K. Minaoui, K. Daoudi, H. Yahia, A. Atillah, M. F. Smiej, and D. Aboutajdine (2013). "A simple and efficient approach for coarse segmentation of Moroccan coastal upwelling". In: *Signal Processing Conference (EUSIPCO), 2013 Proceedings of the 21st European*. IEEE, pp. 1–5.

Tang, J. (2010). "A color image segmentation algorithm based on region growing". In: *Computer Engineering and Technology (ICCET), 2010 2nd International Conference on*. Vol. 6. IEEE, pp. V6–634.

Tilton, J. C., Y. Tarabalka, P. M. Montesano, and E. Gofman (2012). "Best merge region-growing segmentation with integrated nonadjacent region object aggregation". In: *Geoscience and Remote Sensing, IEEE Transactions on* 50(11), pp. 4454–4467.

Urschler, M., A. Bornik, E. Scheurer, K. Yen, H. Bischof, and D. Schmalstieg (2012). "Forensic-case analysis: From 3D imaging to interactive visualization". In: *IEEE computer graphics and applications* 32(4), pp. 79–87.

Van Rijsbergen, C. J. (1979). *Information Retrieval. 1979*.

Verma, O. P., M. Hanmandlu, S. Susan, M. Kulkarni, and P. K. Jain (2011). "A simple single seeded region growing algorithm for color image segmentation using adaptive thresholding". In: *Communication Systems and Network Technologies (CSNT), 2011 International Conference on*. IEEE, pp. 500–503.

Wan, S. Y. and W. E. Higgins (2003). "Symmetric region growing". In: *Image Processing, IEEE Transactions on* 12(9), pp. 1007–1015.

Wang, C. M. and R. M. Chen (2012). "Automatic Vector Seeded Region Growing for Parenchyma Classification in Brain MRI". In:

Wong, S. J. and T. Zrimec (2006). "Classification of lung disease pattern using seeded region growing". In: *AI 2006: Advances in Artificial Intelligence*. Springer, pp. 233–242.

Wu, J., S. Poehlman, M. D. Noseworthy, and M. V. Kamath (2008). "Texture feature based automated seeded region growing in abdominal MRI segmentation". In: *BioMedical Engineering and Informatics, 2008. BMEI 2008. International Conference on*. Vol. 2. IEEE, pp. 263–267.

Xue, J. H. and Y. J. Zhang (2012). "Ridler and Calvard's, Kittler and Illingworth's and Otsu's methods for image thresholding". In: *Pattern Recognition Letters* 33(6), pp. 793–797.

Zanaty, E. A. and A. Asaad (2013). "Probabilistic region growing method for improving magnetic resonance image segmentation". In: *Connection Science* 25(4), pp. 179–196.

Zhang, H., J. E. Fritts, and S. A. Goldman (2008). "Image segmentation evaluation: A survey of unsupervised methods". In: *computer vision and image understanding* 110(2), pp. 260–280.

Zhang, T., X. Yang, S. Hu, and F. Su (2013). "Extraction of Coastline in Aquaculture Coast from Multispectral Remote Sensing Images: Object-Based Region Growing Integrating Edge Detection". In: *Remote Sensing* 5(9), pp. 4470–4487.

Zhang, Y. J. (1996). "A survey on evaluation methods for image segmentation". In: *Pattern recognition* 29(8), pp. 1335–1346.

Zhengtao, Z., Y. Xiongyi, H. Liuqian, and W. De (2011). "Fast capsule image segmentation based on linear region growing". In: *Computer Science and Automation Engineering (CSAE), 2011 IEEE International Conference on*. Vol. 2. IEEE, pp. 99–103.

Appendix A

Analysis of Experimental Results

A.1 Discontinuity in the Upwelling Region

For each image set it was verified which of the SST images have discontinuities that require an iterative version of the region growing algorithms that only grows one cluster at a time. The reason for the each discontinuity is described in the Table A.1. There are three possible reasons that make the upwelling area be in more than one continuous region of space, for these SST image. The first cause is *Natural Upwelling Discontinuity* which is an example of how the upwelling phenomenon can occur in more than one region near the continental coast, has seen in the image of 3.1. However there are another cause of spacial discontinuity of the region of upwelling, and that can be cause by noise, described simply has *Noise*, which is generally clouds above the ocean that did not allow to capture the sea surface temperature bellow, has seen in A.1, or described by *Noise Related Cut* for a type of noise common in some images that does not allow the region growing algorithm to fully extract the complete upwelling area, has seen in the image A.2.

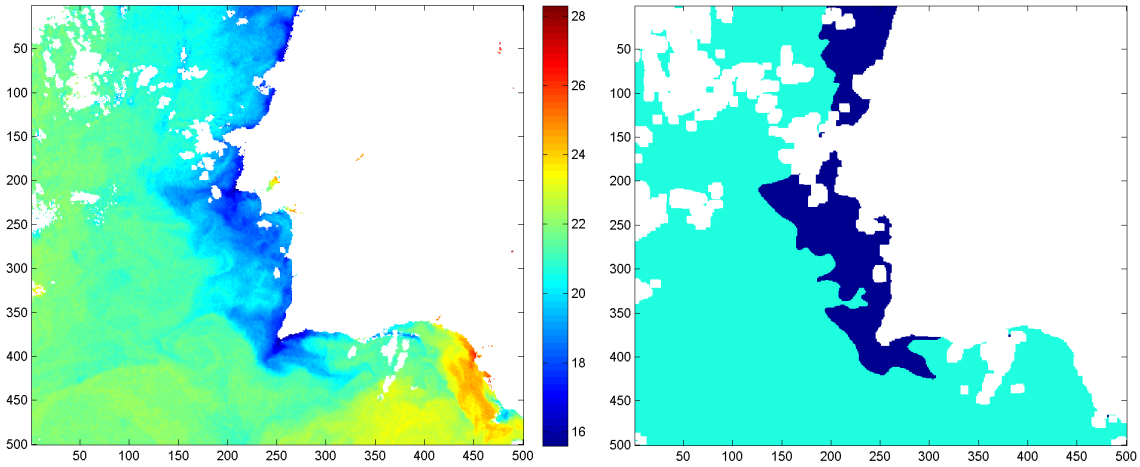

Figure A.1: SST Image from 29 of July 1999, in the left, and the correspondent ground-truth in the right. It is an example of how noise, in this case clouds, can interfere and make necessary to the region growing algorithms to extract more than one cluster for just one continuous upwelling area. In this case, there are only one upwelling region, but the algorithm must extract two continuous regions.

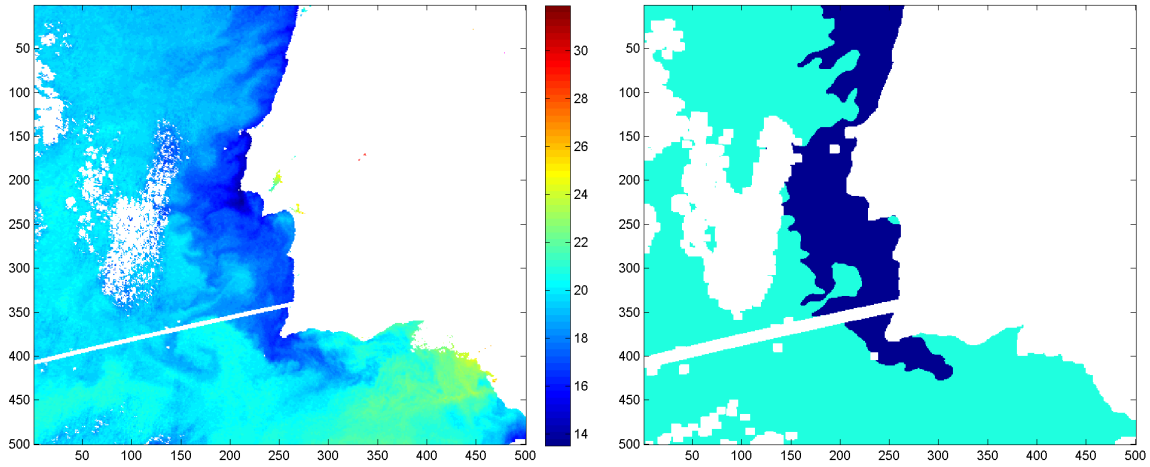

Figure A.2: SST Image from 21 of July 1999, in the left, and the correspondent ground-truth in the right. This image has a type of noise that is not caused by clouds, which cuts the upwelling area in two and make it necessary to the region growing algorithms to extract more than one cluster. There are only one upwelling region, but the algorithm must extract two continuous regions.

Table A.1: Images with discontinuity that need more than one iteration to extract the full upwelling area and the correspondent cause of the discontinuity.

Image Set	**Image Name**	**Discontinuity Factor**
Strong Gradients (1998)	1998-08-05	Natural Upwelling Discontinuity
	1998-08-19	Noise Related Cut
Weak Gradients (1998)	1998-06-12	Natural Upwelling Discontinuity
	1998-09-24	Natural Upwelling Discontinuity
Noisy (1998)	1998-07-07	Noise
1999	1999-06-30	Natural Upwelling Discontinuity
	1999-07-21	Noise Related Cut
	1999-07-29	Noise
	1999-08-01	Noise
	1999-08-26	Natural Upwelling Discontinuity
	1999-09-28	Natural Upwelling Discontinuity
	1999-09-30	Noise
1998 (No Ground-Truth)	1998-06-10	Noise
	1998-06-11	Natural Upwelling Discontinuity
	1998-06-16	Noise
	1998-07-02	Noise Related Cut
	1998-07-16	Noise Related Cut
	1998-08-03	Noise Related Cut
	1998-08-18	Noise
	1998-08-19	Noise Related Cut
	1998-08-21	Noise Related Cut
	1998-08-24	Noise
2000 (No Ground-Truth)	2000-07-11	Noise Related Cut
	2000-08-17	Noise Related Cut
	2000-09-06	Noise Related Cut
2001 (No Ground-Truth)	2001-07-01	Noise
	2001-07-26	Noise
	2001-07-15	Noise Related Cut

A.2 Validation of SRG methods

A.2.1 Validation of SRG methods with the F-measure

Table A.2: Table with the F-measure results for the comparative study between the SEC algorithm and the SRG methods applied to the extraction of upwelling context. The segmentation results are from the SST images of the portuguese coast from the year 1998, with strong gradients in the frontier of the upwelling area. The best scores for each SST image are highlighted in bold.

Image Name	SEC-Otsu	SEC-Kittler	SEC-Ridler	SEC-SelfTuning	Adams SRG	OtsuVerma SRG	MeanVerma SRG	Shih SRG	Gambotto SRG	Zanaty SRG
1998-06-28	**0,948**	0,805	0,926	0,792	0,747	0,579	0,729	0,577	0,616	0,579
1998-07-03	**0,939**	0,897	0,938	0,791	0,904	0,613	0,736	0,589	0,872	0,587
1998-07-18	0,948	0,948	0,949	**0,955**	0,931	0,933	0,919	0,623	0,475	0,921
1998-07-21	0,873	0,873	0,875	0,885	0,892	**0,894**	0,872	0,693	0,668	0,874
1998-07-24	0,872	0,872	0,872	0,893	0,925	**0,971**	0,837	0,813	0,675	0,841
1998-07-28	0,934	0,823	0,930	0,896	**0,980**	0,662	0,871	0,627	0,451	0,662
1998-08-01	0,978	0,978	**0,980**	0,974	0,865	0,917	0,978	0,761	0,361	0,978
1998-08-02	0,979	0,979	0,977	0,956	0,865	0,869	0,979	0,927	0,434	**0,979**
1998-08-05	**0,894**	0,768	0,882	0,884	0,708	0,783	0,849	0,668	0,486	0,805
1998-08-12	**0,973**	**0,973**	0,973	0,942	0,870	0,867	0,971	0,709	0,768	0,973
1998-08-19	0,863	0,843	0,861	**0,898**	0,834	0,780	0,887	0,744	0,666	0,780
1998-08-21	**0,942**	**0,942**	0,929	0,717	0,909	0,574	0,654	0,574	0,599	0,573
1998-08-30	0,919	0,919	0,919	0,935	**0,941**	0,928	0,907	0,909	0,917	0,908
1998-09-05	0,694	0,694	0,703	0,714	0,879	**0,880**	0,665	0,837	0,771	0,681
1998-09-15	0,832	0,851	**0,903**	0,891	0,770	0,873	0,812	0,763	0,597	0,822

Table A.3: Table with the F-measure results for the comparative study between the SEC algorithm and the SRG methods applied to the extraction of upwelling context. The segmentation results are from the SST images of the portuguese coast from the year 1998, with weak gradients in the frontier of the upwelling area. The best scores for each SST image are highlighted in bold.

Image Name	SEC-Otsu	SEC-Kittler	SEC-Ridler	SEC-SelfTuning	Adams SRG	OtsuVerma SRG	MeanVerma SRG	Shih SRG	Gambotto SRG	Zanaty SRG
1998-06-09	0,706	**0,770**	0,693	0,628	0,706	0,528	0,584	0,390	0,767	0,563
1998-06-12	0,331	0,370	0,319	0,256	0,598	0,204	0,232	0,150	**0,627**	0,204
1998-06-14	0,898	0,874	**0,916**	0,647	0,812	0,412	0,522	0,373	0,761	0,719
1998-06-18	0,567	**0,932**	0,619	0,590	0,752	0,509	0,509	0,603	0,688	0,511
1998-06-23	0,743	0,743	0,743	0,787	**0,944**	0,814	0,741	0,773	0,904	0,743
1998-06-25	**0,962**	0,822	0,951	0,682	0,874	0,515	0,631	0,516	0,632	0,516
1998-07-11	**0,955**	0,885	0,948	0,627	0,884	0,426	0,568	0,430	0,551	0,426
1998-07-15	0,757	0,757	0,758	0,781	**0,783**	0,782	0,757	0,474	0,641	0,757
1998-08-23	0,840	0,793	0,826	0,729	**0,873**	0,496	0,690	0,682	0,149	0,497
1998-09-08	0,652	**0,976**	0,704	0,695	0,950	0,869	0,609	0,934	0,812	0,838
1998-09-24	0,592	**0,797**	0,603	0,624	0,780	0,626	0,591	0,372	0,684	0,600

Table A.4: Table with the F-measure results for the comparative study between the SEC algorithm and the SRG methods applied to the extraction of upwelling context. The segmentation results are from the SST images of the portuguese coast from the year 1998, with noise interfering with the segmentation process. The best scores for each SST image are highlighted in bold.

Image Name	SEC-Otsu	SEC-Kittler	SEC-Ridler	SEC-SelfTuning	Adams SRG	OtsuVerma SRG	MeanVerma SRG	Shih SRG	Gambotto SRG	Zanaty SRG
1998-07-07	0,803	0,818	0,803	0,827	**0,866**	0,822	0,797	0,816	0,761	0,798
1998-08-10	0,665	**0,669**	0,667	0,584	0,495	0,667	0,665	0,549	0,391	0,665
1998-09-11	0,809	0,809	0,816	0,838	0,836	**0,896**	0,807	0,450	0,796	0,567
1998-09-30	0,787	0,787	0,797	0,824	**0,876**	0,712	0,787	0,835	0,766	0,079

Table A.5: Table with the F-measure results for the comparative study between the SEC algorithm and the SRG methods applied to the extraction of upwelling context. The segmentation results are from the SST images of the portuguese coast from the year 1999. The best scores for each SST image are highlighted in bold. (Part 1/2)

Image Name	SEC-Otsu	SEC-Kittler	SEC-Ridler	SEC-SelfTuning	Adams SRG	OtsuVerma SRG	MeanVerma SRG	Shih SRG	Gambotto SRG	Zanaty SRG
1999-06-02	**0,717**	**0,717**	0,711	0,694	0,644	0,698	0,656	0,284	0,700	0,664
1999-06-08	0,493	0,808	0,494	0,512	**0,860**	0,493	0,493	0,474	0,655	0,493
1999-06-10	0,348	**0,572**	0,335	0,342	0,400	0,359	0,361	0,280	0,339	0,359
1999-06-14	0,806	0,806	0,804	0,402	**0,807**	0,316	0,383	0,322	0,790	0,376
1999-06-19	0,384	0,404	0,388	0,329	0,669	0,272	0,323	0,262	**0,764**	0,273
1999-06-20	0,418	0,397	0,434	0,283	0,784	0,242	0,263	0,242	**0,873**	0,242
1999-06-27	0,377	0,718	0,387	0,299	**0,749**	0,239	0,260	0,147	0,384	0,337
1999-06-30	0,389	0,389	0,390	0,422	0,672	**0,682**	0,302	0,115	0,356	0,375
1999-07-06	0,685	0,697	0,882	0,852	0,657	**0,904**	0,665	0,571	0,627	0,670
1999-07-08	0,869	0,869	0,879	0,905	0,785	**0,944**	0,839	0,591	0,540	0,623
1999-07-14	0,605	0,609	0,607	0,600	**0,698**	0,527	0,567	0,524	0,623	0,527
1999-07-15	0,602	0,620	0,608	0,629	0,750	0,602	0,602	**0,765**	0,619	0,604
1999-07-19	0,833	0,833	0,832	0,834	**0,935**	0,902	0,809	0,787	0,734	0,810
1999-07-21	0,759	0,750	0,760	0,791	0,924	**0,947**	0,751	0,863	0,665	0,675
1999-07-29	0,670	0,670	0,671	0,696	**0,925**	0,810	0,670	0,843	0,452	0,671
1999-07-31	0,842	0,719	0,840	0,856	0,847	**0,917**	0,785	0,520	0,620	0,786

Table A.6: Table with the F-measure results for the comparative study between the SEC algorithm and the SRG methods applied to the extraction of upwelling context. The segmentation results are from the SST images of the portuguese coast from the year 1999. The best scores for each SST image are highlighted in bold. (Part 2/2)

Image Name	SEC-Otsu	SEC-Kittler	SEC-Ridler	SEC-SelfTuning	Adams SRG	OtsuVerma SRG	MeanVerma SRG	Shih SRG	Gambotto SRG	Zanaty SRG
1999-08-01	0,759	0,782	0,765	0,818	0,836	**0,934**	0,759	0,565	0,697	0,647
1999-08-10	0,679	0,679	0,694	0,706	**0,845**	0,781	0,660	0,374	0,761	0,681
1999-08-14	0,532	0,532	0,534	0,546	**0,856**	0,558	0,527	0,520	0,728	0,708
1999-08-17	0,795	0,795	0,796	0,821	0,915	**0,954**	0,781	0,730	0,800	0,782
1999-08-21	**0,882**	**0,882**	0,882	0,874	0,763	0,817	0,874	0,806	0,558	0,875
1999-08-23	0,814	0,814	0,811	0,837	0,897	**0,983**	0,811	0,805	0,237	0,252
1999-08-26	0,750	0,750	0,743	0,780	0,916	**0,938**	0,734	0,910	0,730	0,735
1999-08-30	0,815	0,815	0,816	0,820	0,851	**0,917**	0,833	0,455	0,868	0,836
1999-09-01	0,921	0,921	0,922	0,941	0,916	**0,960**	0,918	0,236	0,733	0,770
1999-09-08	0,737	0,737	0,749	0,770	0,792	**0,842**	0,735	0,736	0,758	0,656
1999-09-10	0,910	0,910	0,910	**0,931**	0,798	0,881	0,890	0,887	0,695	0,013
1999-09-14	0,950	0,950	0,950	**0,960**	0,959	0,944	0,950	0,941	0,642	0,950
1999-09-28	0,448	**0,721**	0,446	0,428	0,604	0,445	0,453	0,491	0,357	0,453
1999-09-30	0,634	0,727	0,634	0,618	0,663	0,707	0,567	0,758	**0,764**	0,579
1999-10-03	0,786	0,838	0,804	0,802	**0,867**	0,792	0,779	0,504	0,807	0,780

Table A.7: Table with the F-measure results for the comparative study between the SEC algorithm and the SRG methods applied to the extraction of upwelling context. The segmentation results are from the SST images of the Canary. The best scores for each SST image are highlighted in bold.

Image Name	SEC-Otsu	SEC-Kittler	SEC-Ridler	SEC-SelfTuning	Adams SRG	OtsuVerma SRG	MeanVerma SRG	Shih SRG	Gambotto SRG	Zanaty SRG
img58	**0,810**	0,721	0,809	0,781	0,781	0,657	0,552	0,712	0,770	0,596
img117	**0,852**	**0,852**	0,851	0,810	0,837	0,808	0,650	0,356	0,558	0,658
img152	0,762	0,692	0,762	**0,780**	0,750	0,704	0,618	0,575	0,728	0,588
img177	**0,827**	0,496	0,826	0,810	0,712	0,689	0,509	0,592	0,608	0,511
img214	**0,864**	0,628	0,864	0,847	0,800	0,434	0,433	0,786	0,650	0,643
img237	0,820	0,820	0,829	**0,830**	0,733	0,578	0,516	0,700	0,727	0,594
img262	0,845	**0,848**	0,844	0,814	0,791	0,539	0,438	0,790	0,539	0,703
img310	**0,825**	0,790	0,825	0,809	0,811	0,440	0,393	0,762	0,651	0,651
img334	0,756	0,724	0,761	0,724	**0,799**	0,301	0,311	0,778	0,476	0,334
img336	0,643	0,718	0,649	0,724	**0,844**	0,449	0,398	0,640	0,422	0,433

A.2.2 Validation of SRG methods with ARI index

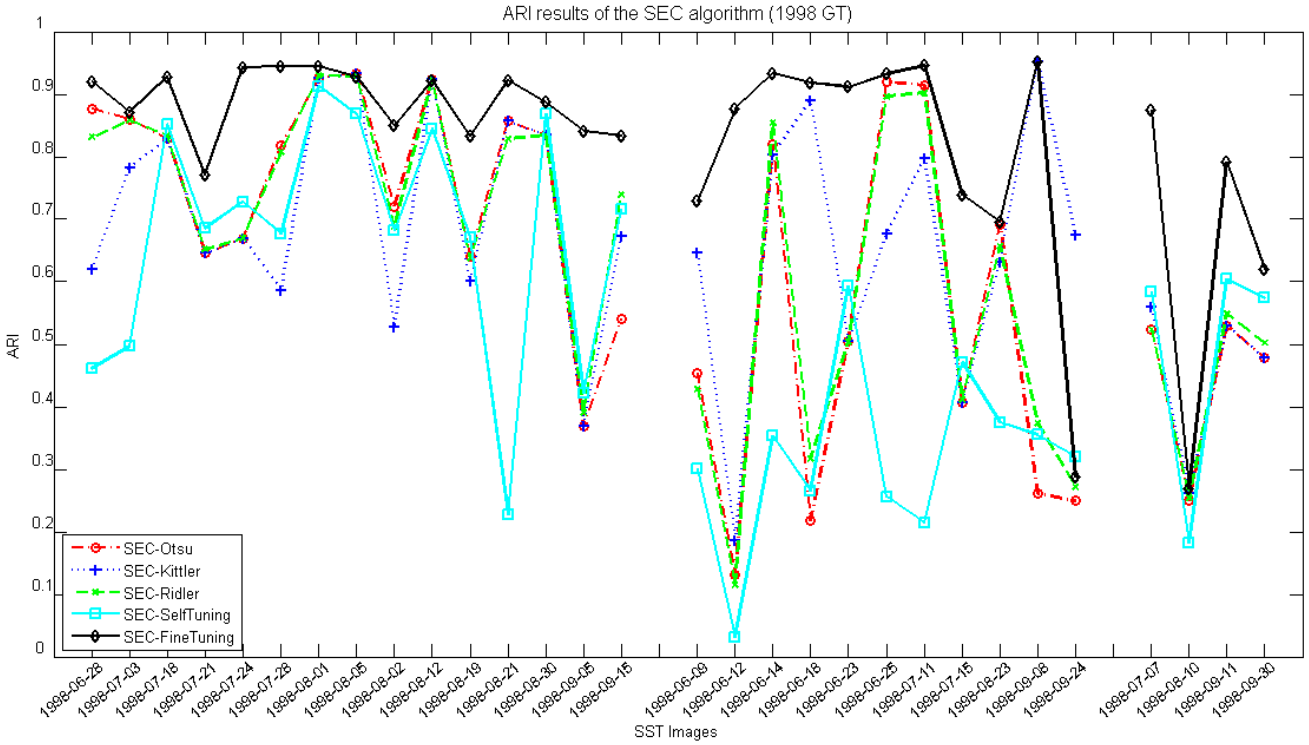

Figure A.3: ARI results for the comparative study between the SEC algorithm versions. The segmentation results are from the SST images of the portuguese coast from the year 1998, which was divided into subsets of images with strong gradients in the frontier of the upwelling area, weak gradients and images with noise, from left to right in the graphic correspondingly.

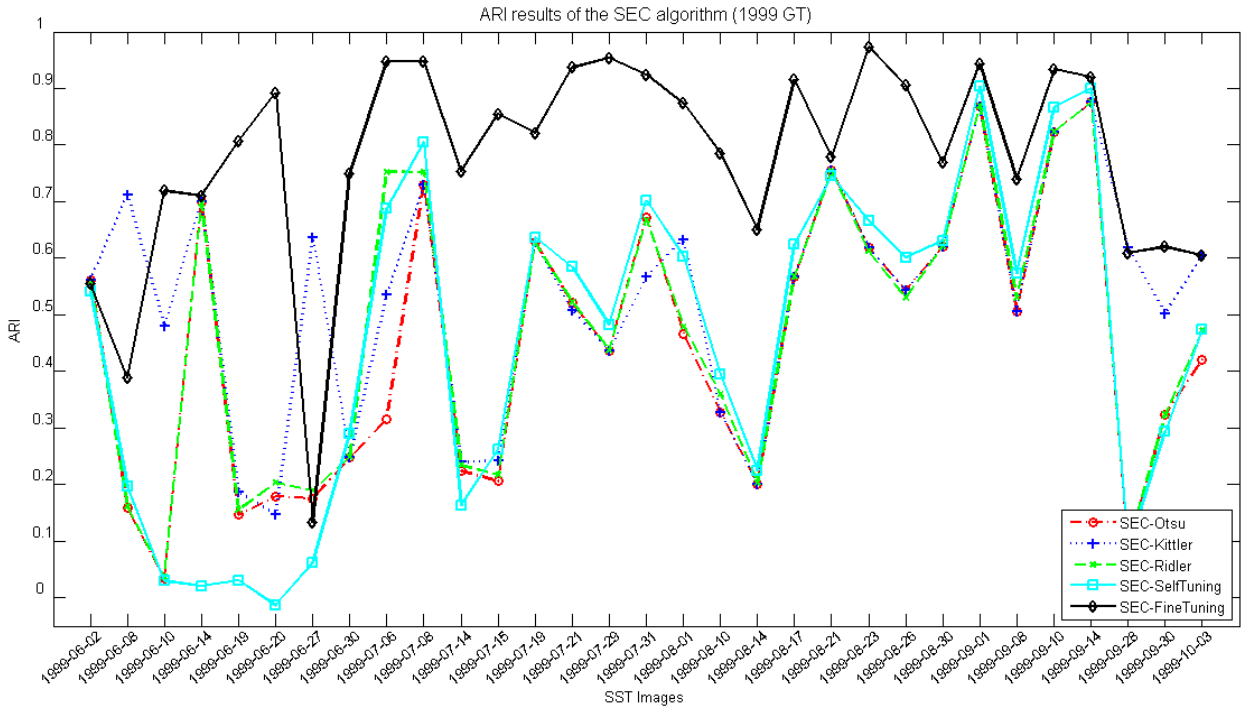

Figure A.4: ARI results for the comparative study between the SEC algorithm versions. The segmentation results are from the SST images of the portuguese coast from the year 1999.

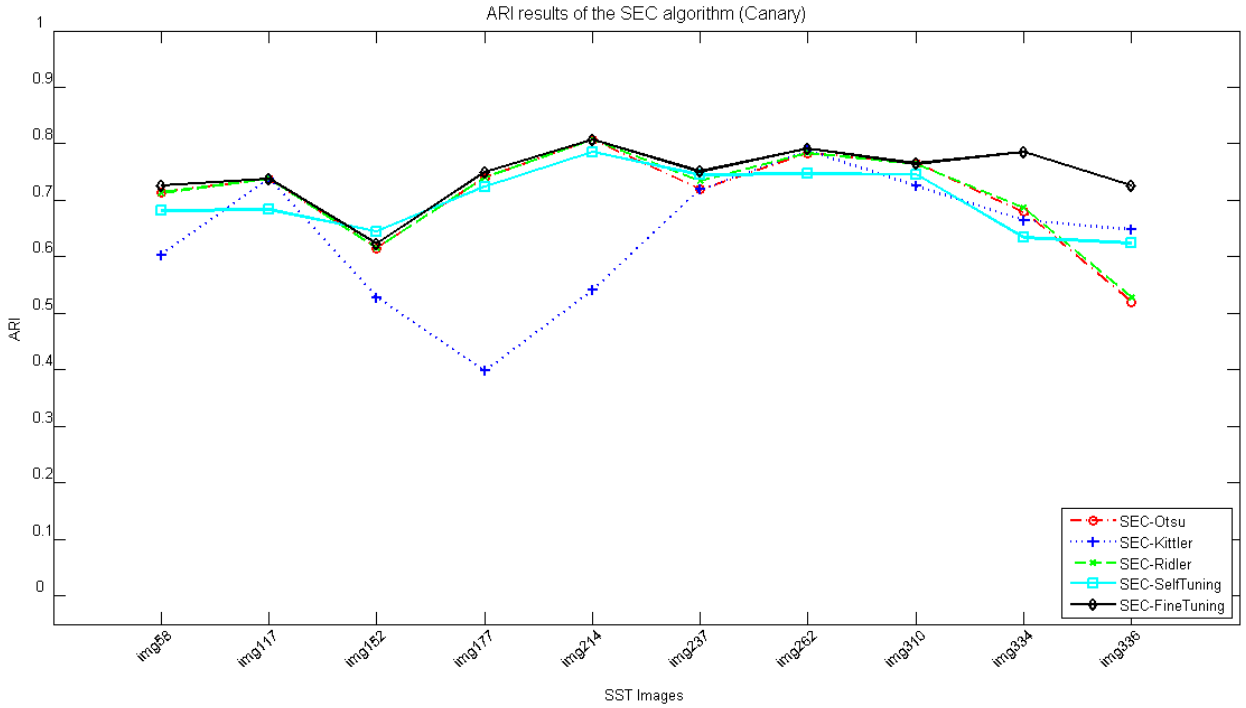

Figure A.5: ARI results for the comparative study between the SEC algorithm versions. The segmentation results are from the SST images of the Canary.

A.2.3 Validation of SRG methods with unsupervised evaluation measures

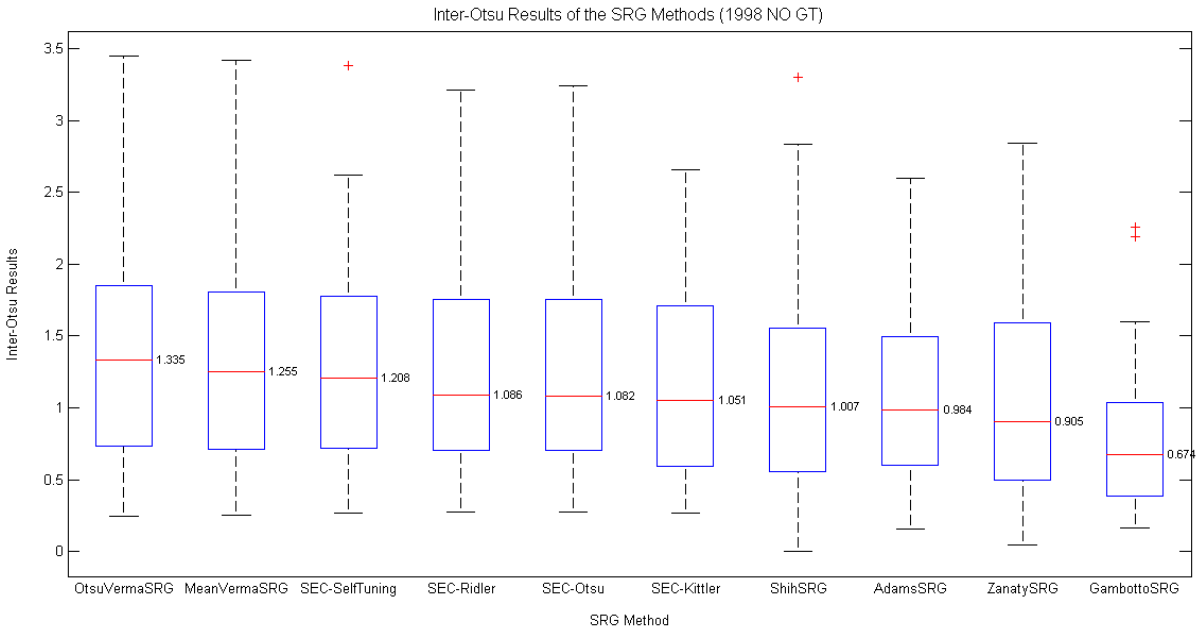

Figure A.6: Inter-Otsu results for each of the SRG methods visualized in a box plot, making it possible to understand the variation of the results in the set of SST images from 1998 with no ground-truth map.

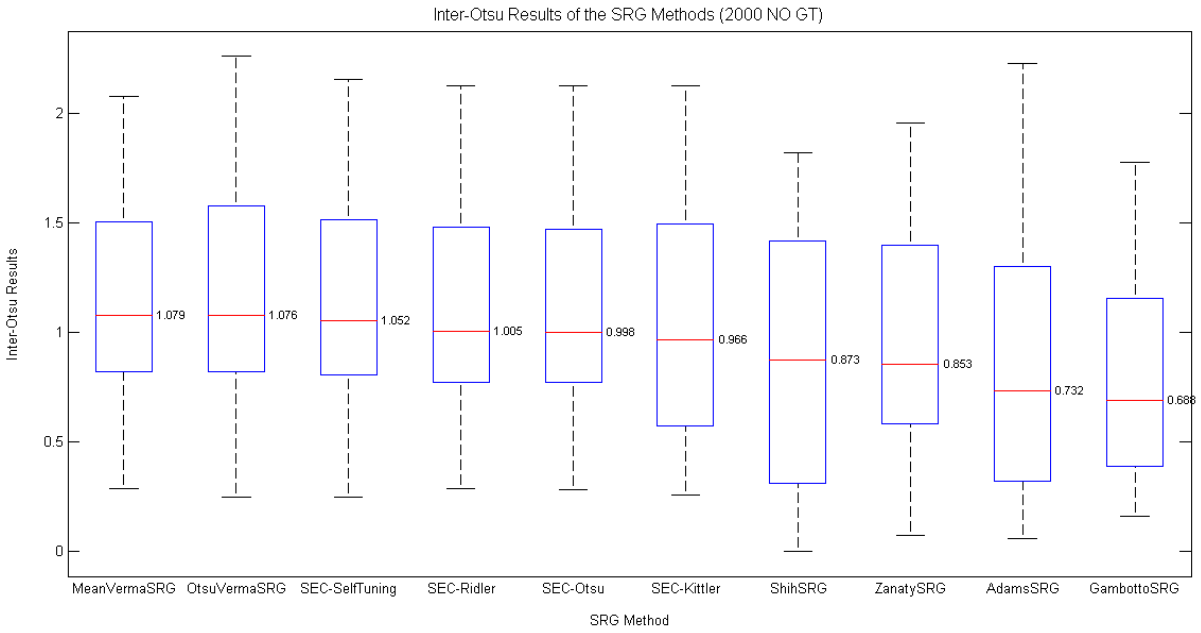

Figure A.7: Inter-Otsu results for each of the SRG methods visualized in a box plot, making it possible to understand the variation of the results in the set of SST images from 2000 with no ground-truth map.

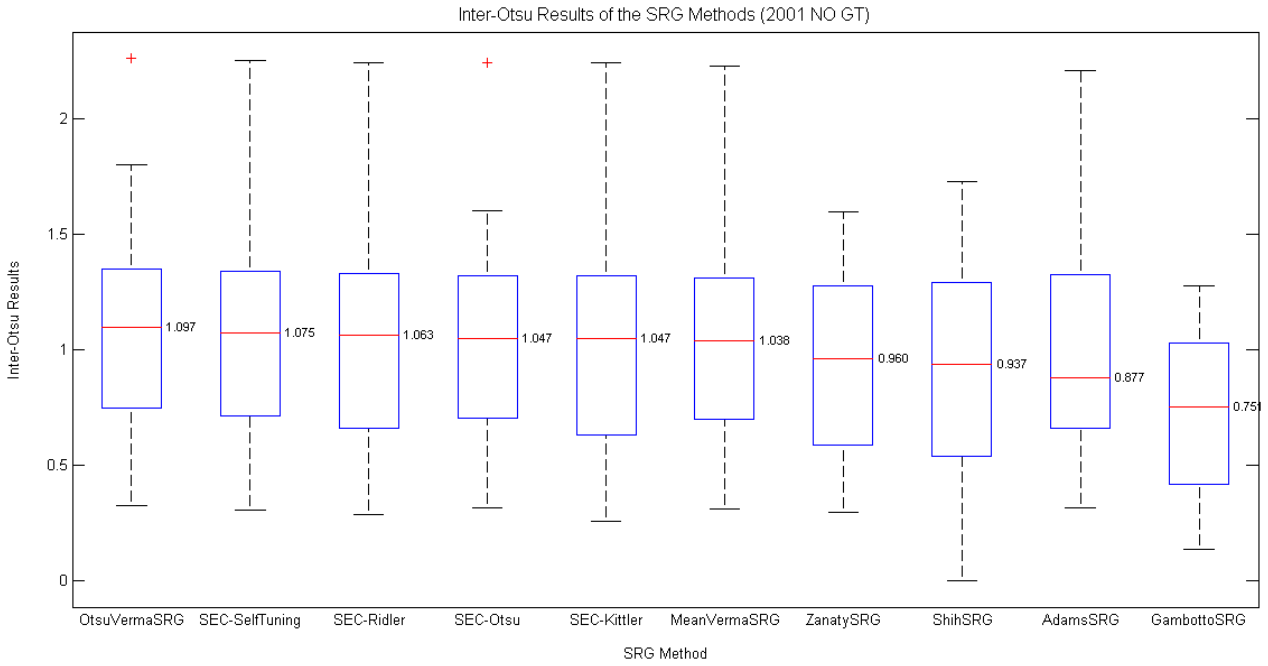

Figure A.8: Inter-Otsu results for each of the SRG methods visualized in a box plot, making it possible to understand the variation of the results in the set of SST images from 2001 with no ground-truth map.

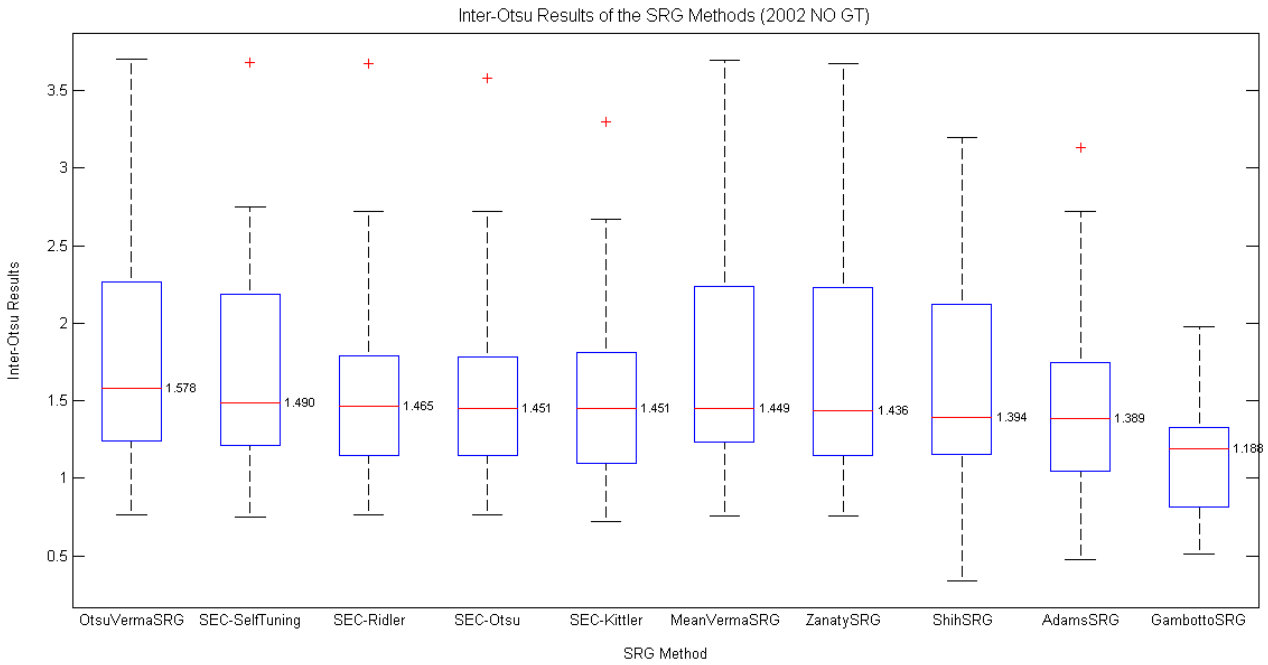

Figure A.9: Inter-Otsu results for each of the SRG methods visualized in a box plot, making it possible to understand the variation of the results in the set of SST images from 2002 with no ground-truth map.

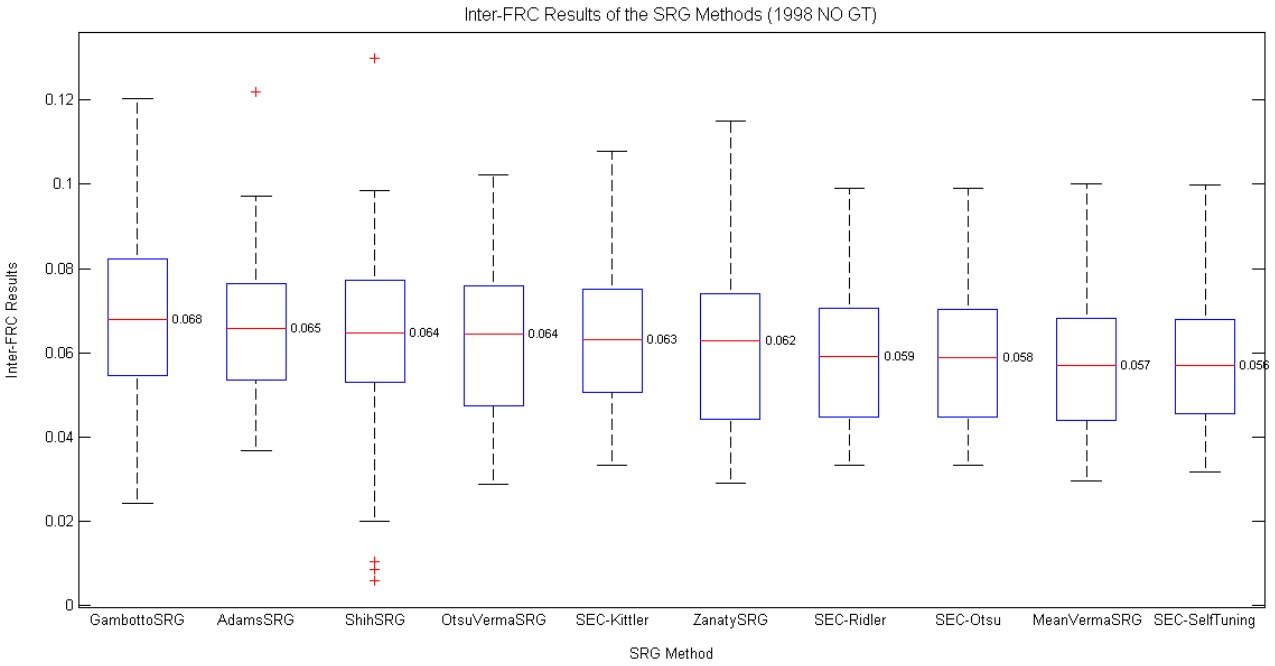

Figure A.10: Inter-FRC results for each of the SRG methods visualized in a box plot, making it possible to understand the variation of the results in the set of SST images from 1998 with no ground-truth map.

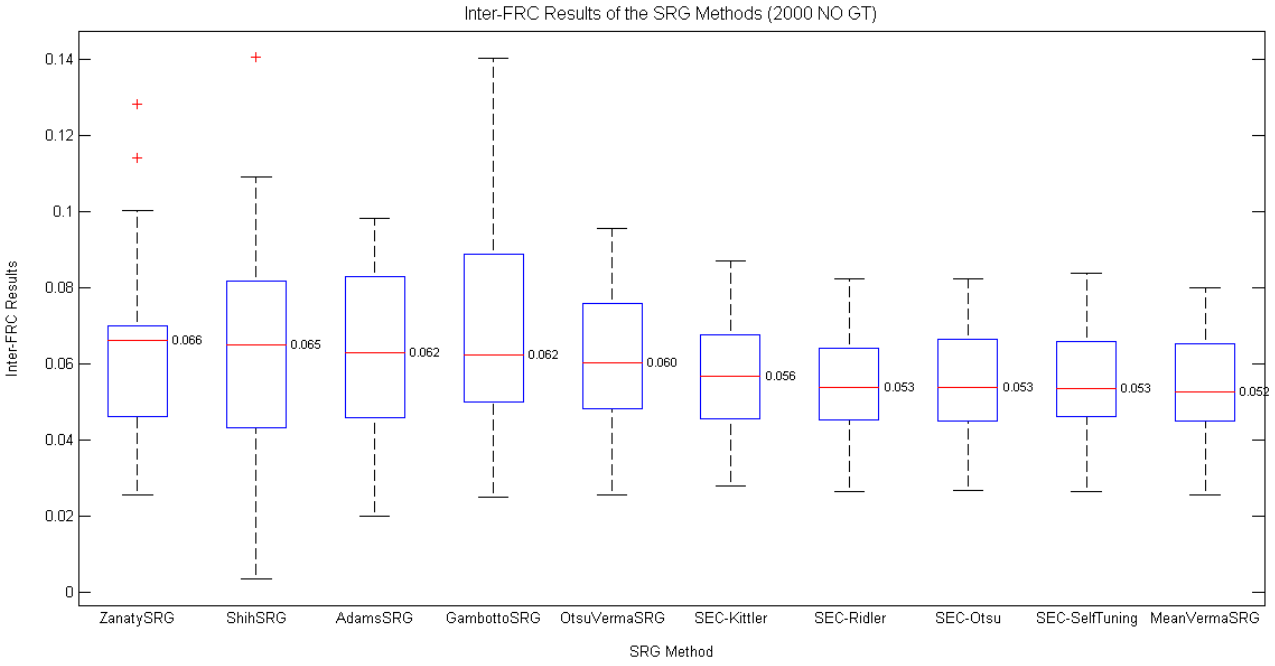

Figure A.11: Inter-FRC results for each of the SRG methods visualized in a box plot, making it possible to understand the variation of the results in the set of SST images from 2000 with no ground-truth map.

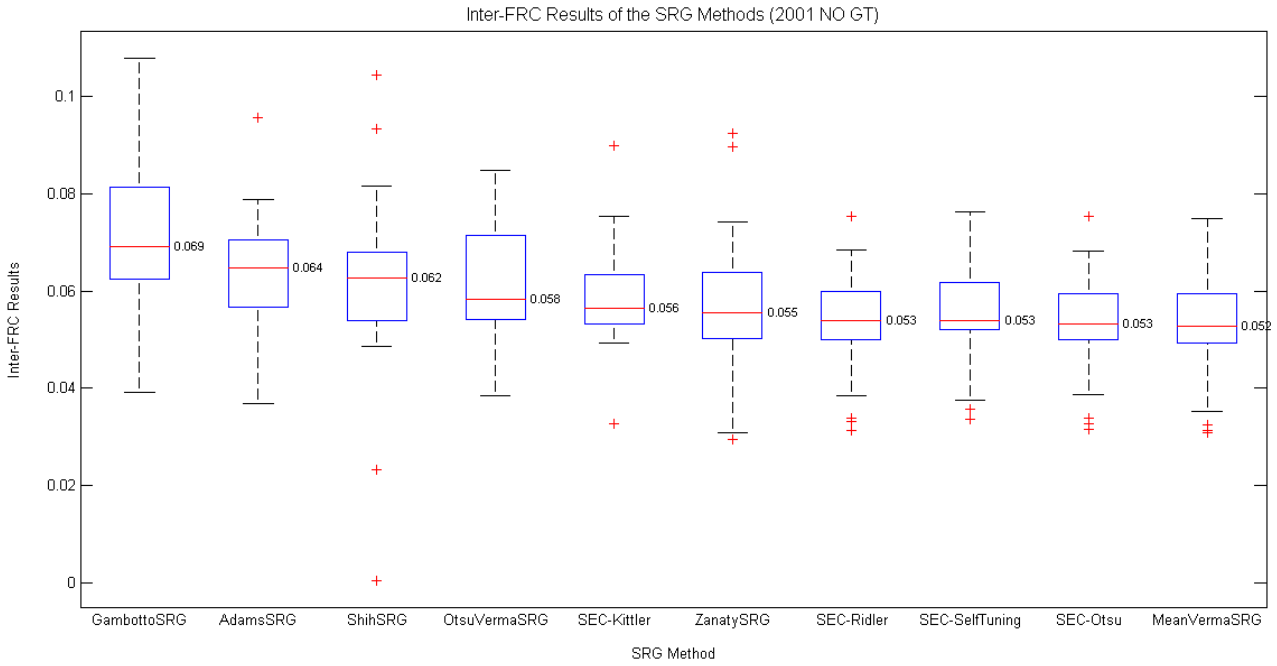

Figure A.12: Inter-FRC results for each of the SRG methods visualized in a box plot, making it possible to understand the variation of the results in the set of SST images from 2001 with no ground-truth map.

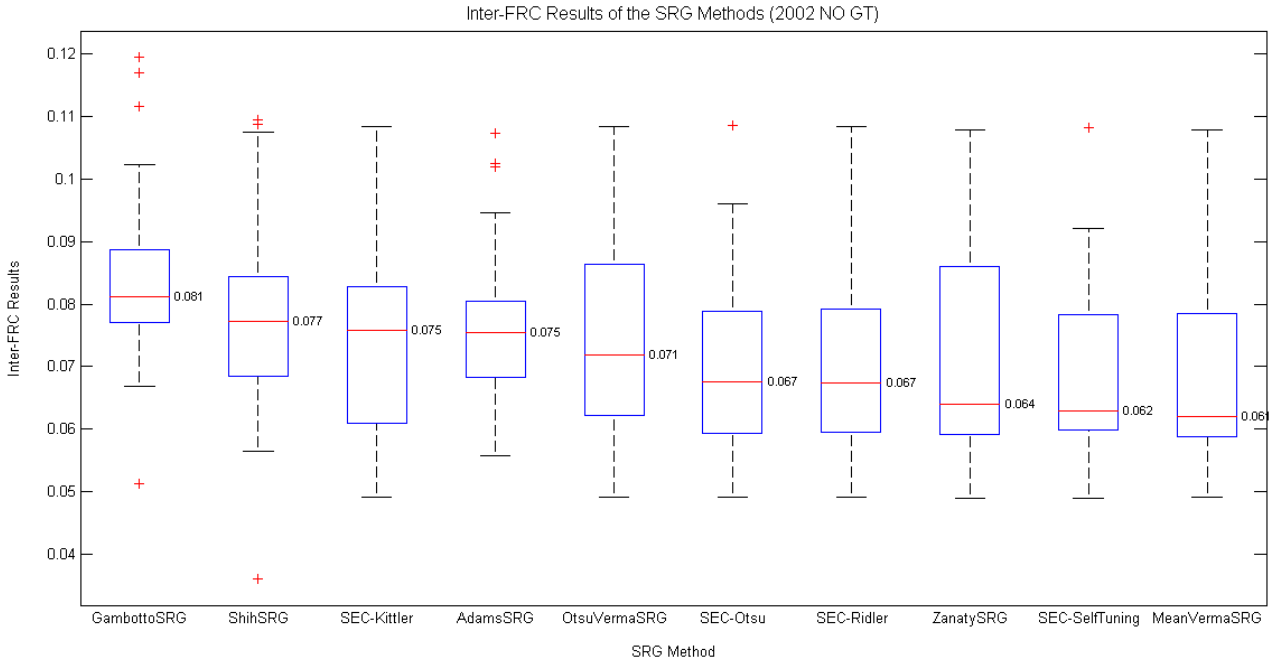

Figure A.13: Inter-FRC results for each of the SRG methods visualized in a box plot, making it possible to understand the variation of the results in the set of SST images from 2002 with no ground-truth map.

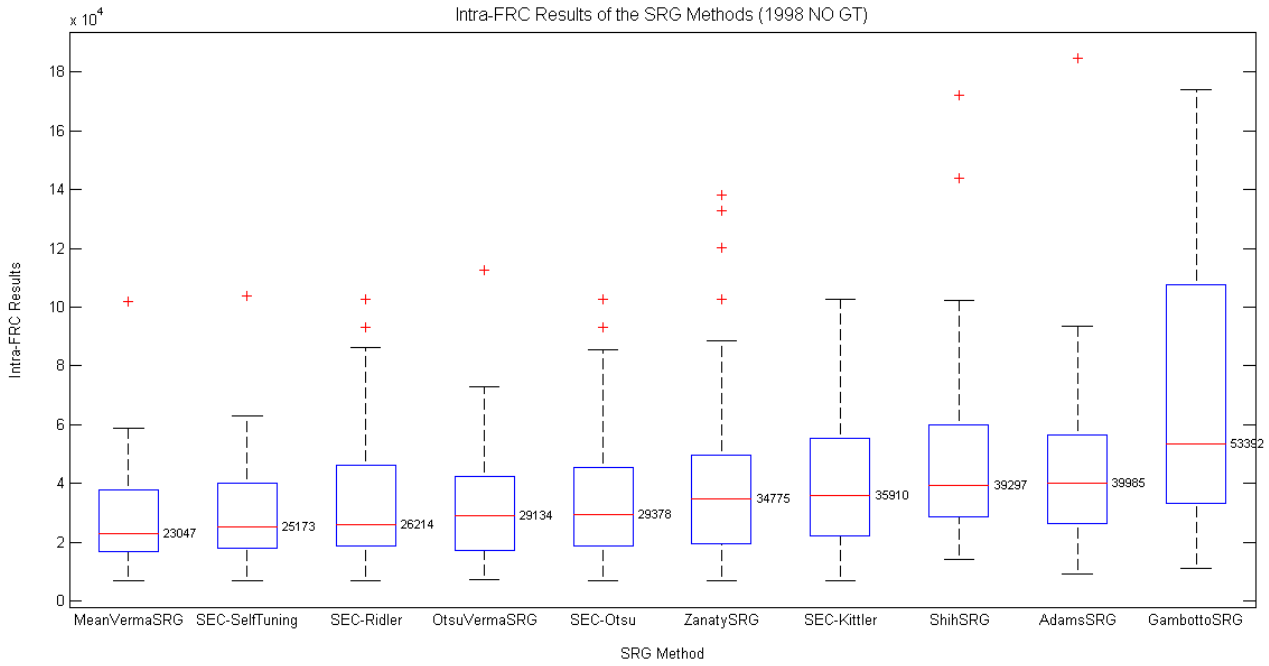

Figure A.14: Intra-FRC results for each of the SRG methods visualized in a box plot, making it possible to understand the variation of the results in the set of SST images from 1998 with no ground-truth map.

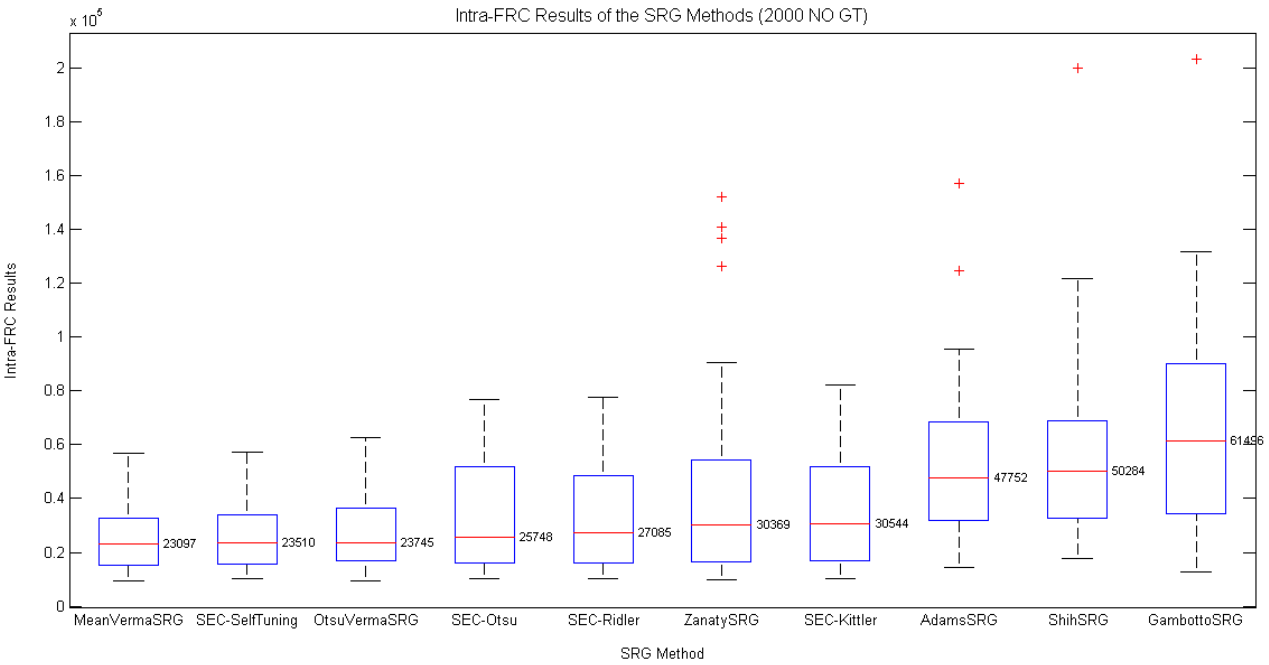

Figure A.15: Intra-FRC results for each of the SRG methods visualized in a box plot, making it possible to understand the variation of the results in the set of SST images from 2000 with no ground-truth map.

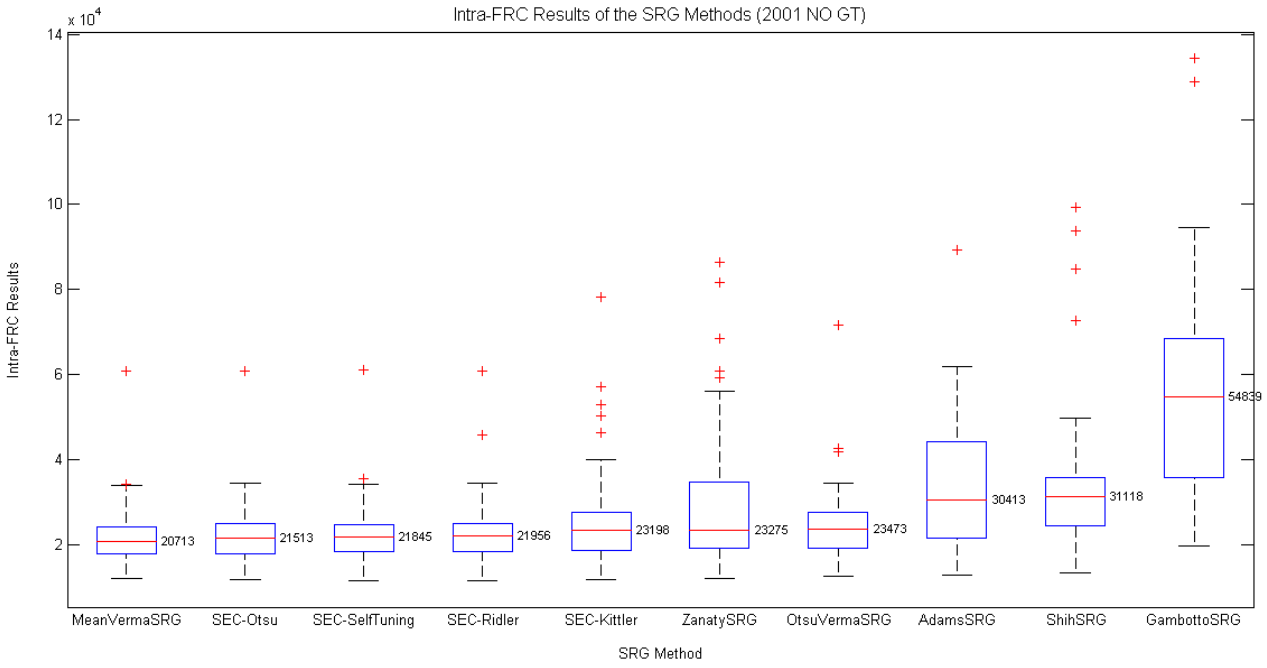

Figure A.16: Intra-FRC results for each of the SRG methods visualized in a box plot, making it possible to understand the variation of the results in the set of SST images from 2001 with no ground-truth map.

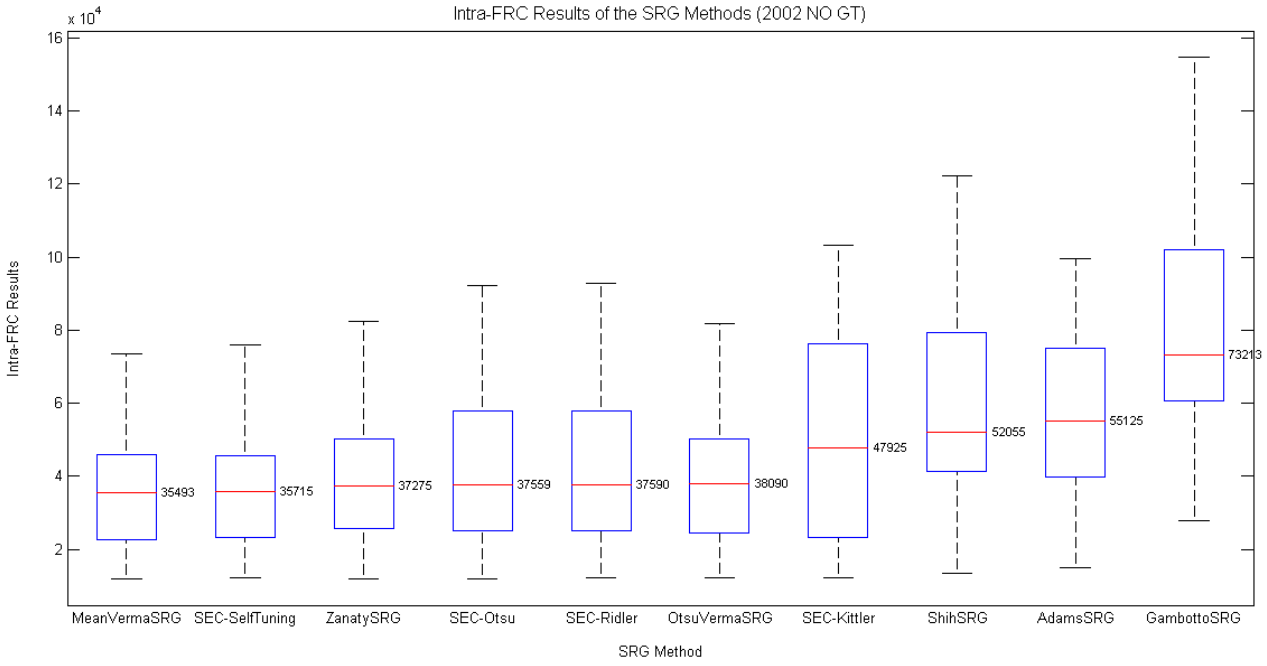

Figure A.17: Intra-FRC results for each of the SRG methods visualized in a box plot, making it possible to understand the variation of the results in the set of SST images from 2002 with no ground-truth map.

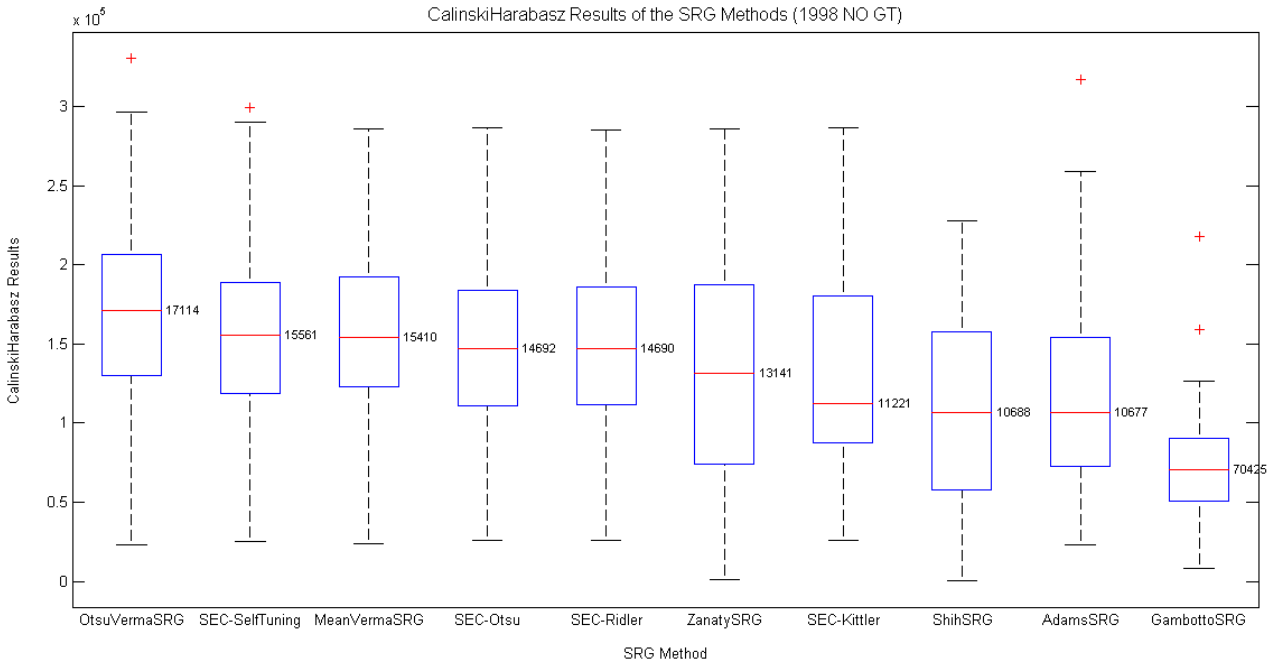

Figure A.18: CalinskiHarabasz results for each of the SRG methods in a box plot, making it possible to understand the variation of the results in the set of SST images from 1998 with no ground-truth map.

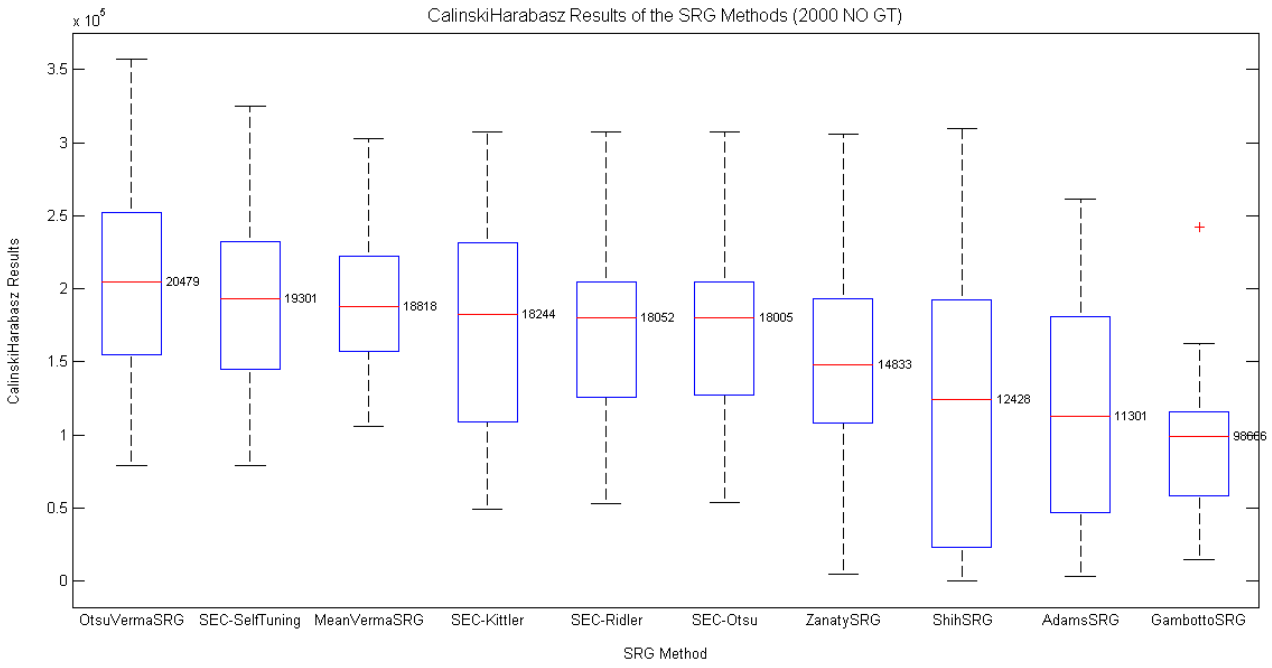

Figure A.19: CalinskiHarabasz results for each of the SRG methods in a box plot, making it possible to understand the variation of the results in the set of SST images from 2000 with no ground-truth map.

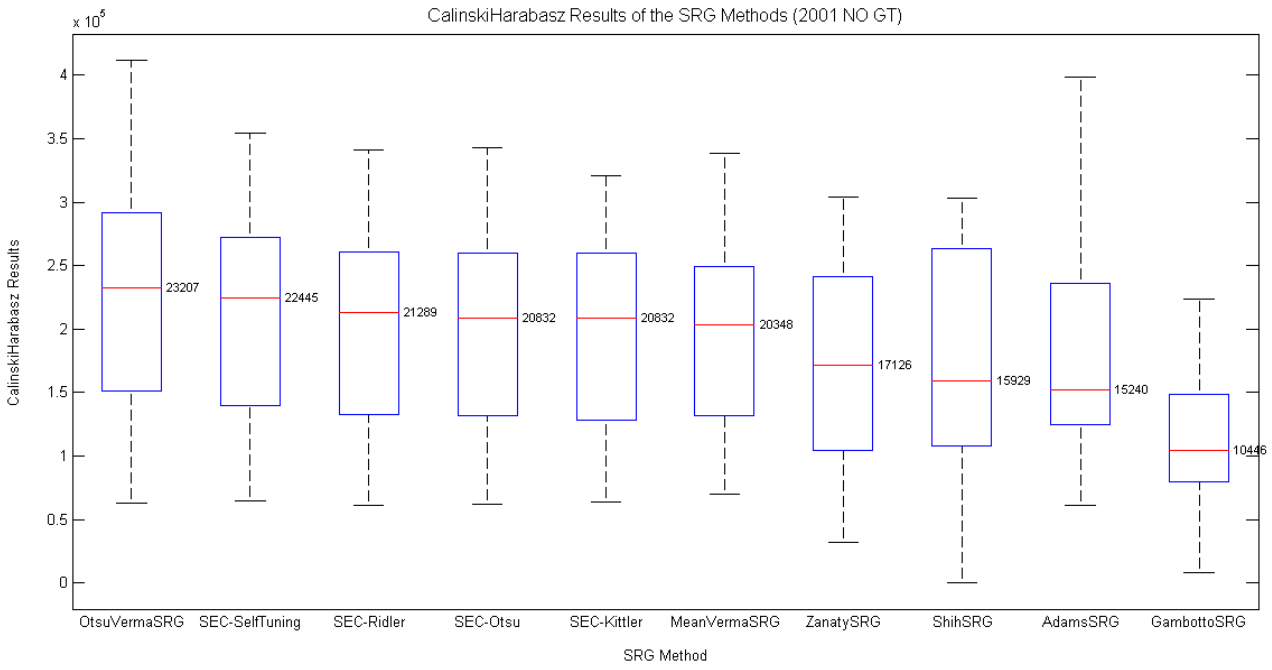

Figure A.20: CalinskiHarabasz results for each of the SRG methods in a box plot, making it possible to understand the variation of the results in the set of SST images from 2001 with no ground-truth map.

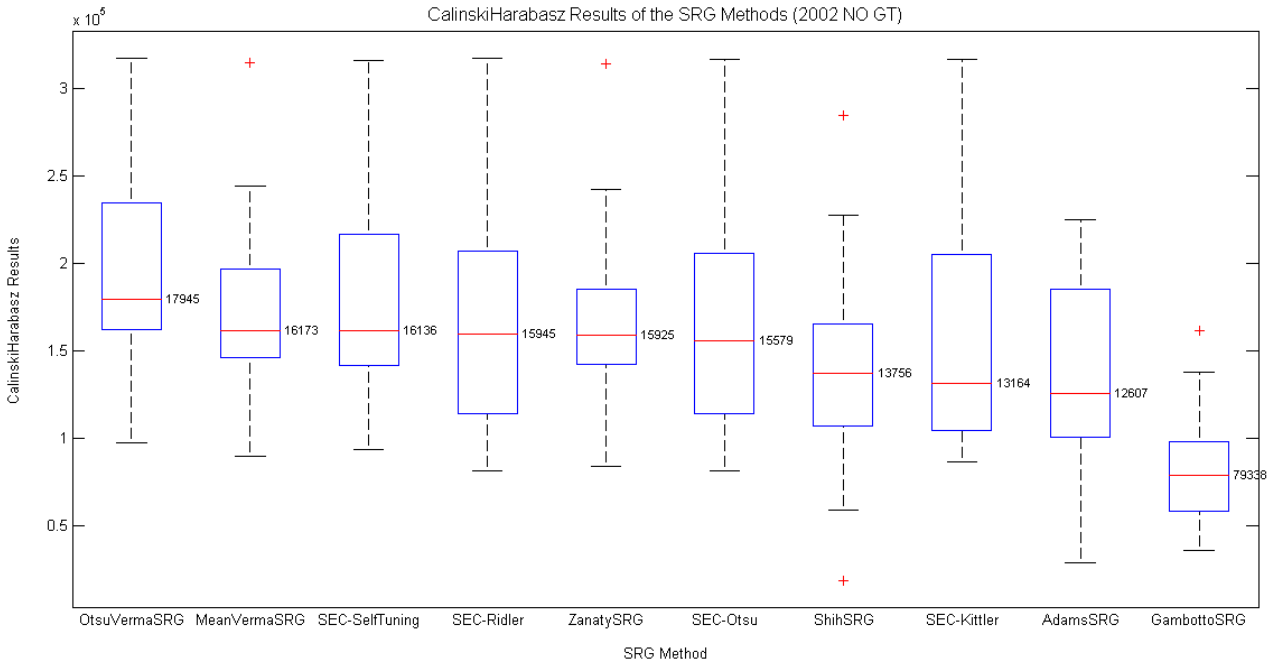

Figure A.21: CalinskiHarabasz results for each of the SRG methods in a box plot, making it possible to understand the variation of the results in the set of SST images from 2002 with no ground-truth map.

Table A.8: Table that accounts for how frequent each version of the SEC algorithm, excluding the fine-tuning version, and each SRG method had good score, relatively to the correspondent threshold, when segmenting SST image without ground-truth. The best SRG methods scores are bold in the table, for each of the sets of images and information that is being analyzed. (Part 1/2)

Image Set	Information	SEC-Otsu	SEC-Kittler	SEC-Ridler	SEC-SelfTuning	Adams SRG	OtsuVerma SRG	MeanVerma SRG	Shih SRG	Gambotto SRG	Zanaty SRG
1998 #52	% Intra_LN	0,750	0,673	0,115	0,788	**0,846**	0,135	0,154	0,365	0,192	0,538
	% Inter_Otsu	0,442	0,423	0,808	0,404	0,885	**0,904**	0,654	0,673	0,135	0,538
	% Inter_FRC	0,481	0,577	**0,865**	0,788	0,827	0,827	0,712	0,808	0,654	0,827
	% Intra_FRC	0,923	0,904	0,923	0,673	**0,981**	0,538	0,654	0,788	0,500	0,865
	% Intra_Liu	0,750	0,731	0,808	0,673	**0,962**	1,000	0,692	0,288	0,096	0,788
	% Calinski Harabasz	0,058	0,481	0,115	0,846	0,846	**0,981**	**0,981**	0,596	0,038	0,692
	% Davies Bouldin	0,250	0,750	0,115	0,154	**0,923**	0,115	0,788	0,096	0,365	0,135
2000 #32	% Intra_LN	0,813	0,750	0,219	0,875	**0,906**	0,094	0,156	0,375	0,281	0,750
	% Inter_Otsu	0,281	0,344	0,781	0,250	0,781	**0,906**	0,750	0,594	0,031	0,500
	% Inter_FRC	0,344	0,406	**0,844**	0,781	0,688	0,813	0,750	0,719	0,625	**0,844**
	% Intra_FRC	0,938	**0,969**	**0,969**	0,781	**0,969**	0,594	0,781	0,688	0,500	0,844
	% Intra_Liu	0,813	0,813	0,813	0,781	0,969	**1**	0,781	0,156	0,156	0,750
	% Calinski Harabasz	0,156	0,719	0,219	0,938	0,719	**1**	**1**	0,594	0,188	0,844
	% Davies Bouldin	0,219	0,531	0,094	0,125	0,781	0,125	**0,875**	0,156	0,500	0,281

Table A.9: Table that accounts for how frequent each version of the SEC algorithm, excluding the fine-tuning version, and each SRG method had good score, relatively to the correspondent threshold, when segmenting SST image without ground-truth. The best SRG methods scores are bold in the table, for each of the sets of images and information that is being analyzed. (Part 2/2)

Image Set	Information	SEC-Otsu	SEC-Kittler	SEC-Ridler	SEC-SelfTuning	Adams SRG	OtsuVerma SRG	MeanVerma SRG	Shih SRG	Gambotto SRG	Zanaty SRG
2001 #30	% Intra_LN	0,967	0,900	0,033	0,967	**1**	0,033	0,033	0,633	0,367	0,867
	% Inter_Otsu	0,233	0,233	0,867	0,133	**1**	0,900	0,733	0,667	0	0,633
	% Inter_FRC	0,233	0,333	0,867	0,867	0,867	0,933	0,767	**0,900**	0,800	0,867
	% Intra_FRC	**1**	0,967	**1**	0,967	**1**	0,800	0,967	0,867	0,533	0,900
	% Intra_Liu	0,967	0,967	0,967	0,967	**1**	**1**	0,967	0,300	0,033	0,933
	% Calinski Harabasz	0,400	0,833	0,500	0,900	0,967	**1**	**1**	0,800	0,300	0,867
	% Davies Bouldin	0,533	0,800	0,367	0,467	**1**	0,333	0,700	0,100	0,500	0,133
2002 #22	% Intra_LN	0,682	0,636	0	0,682	**0,727**	0	0	0,409	0,136	0,545
	% Inter_Otsu	0,545	0,545	**1**	0,500	**1**	**1**	0,909	0,909	0,227	0,909
	% Inter_FRC	0,682	0,773	**1**	**1**	**1**	**1**	**1**	0,955	0,955	**1**
	% Intra_FRC	0,773	0,818	0,773	0,500	**1**	0,364	0,500	0,727	0,227	0,864
	% Intra_Liu	0,682	0,682	0,682	0,591	0,955	**1**	0,591	0,182	0,045	0,727
	% Calinski Harabasz	0,136	0,636	0,227	0,909	0,955	**1**	**1**	0,909	0,136	**1**
	% Davies Bouldin	0,364	0,818	0,227	0,227	**0,955**	0,136	0,773	0,045	0,636	0,182

A.3 Thresholds of the Unsupervised Evaluation Measures

Table A.10: Table with the produced thresholds using the Information Gain method. For each region growing algorithm, different thresholds were calculated for the many unsupervised evaluation measures. The values in bold text are the ones where the correlation to the F-measure was better, meaning higher or lower than 0.2 or -0.2, depending if for the given unsupervised evaluation measure the ideal correlation should be positive or negative correspondingly.

	Intra_LN	Inter_Otsu	Inter_FRC	Intra_FRC	Intra_Liu	CalinskiHarabasz	DaviesBouldin
SEC-Otsu	0,3180	**1,3319**	**0,0599**	62510,63	891,06	233071,27	**0,6176**
SEC-Kittler	0,2804	**1,3319**	**0,0602**	77168,53	893,63	**116957,63**	**0,6455**
SEC-Ridler	0,1407	**0,5763**	**0,0410**	63231,26	921,46	212350,91	**0,5752**
SEC-SelfTuning	0,3376	**1,4877**	**0,0430**	37464,63	842,34	101504,56	**0,5777**
AdamsSRG	0,3136	**0,3022**	0,0499	140588,46	1309,11	**64152,01**	**0,7799**
OtsuVermaSRG	0,1291	0,4578	**0,0436**	29822,34	1475,17	46472,76	**0,5029**
MeanVermaSRG	0,1391	**0,8421**	**0,0453**	34898,00	834,21	44435,02	0,7456
ShihSRG	**0,2073**	**0,7050**	**0,0489**	66255,94	472,38	**84478,47**	**0,4534**
GambottoSRG	0,1732	1,4528	0,0581	**56296,24**	**326,93**	**129025,82**	0,5197
ZanatySRG	0,2872	**0,8478**	0,0410	**64226,22**	964,94	**77181,12**	0,5420

Table A.11: Table with the produced thresholds using the Otsu's method. For each region growing algorithm, different thresholds were calculated for the many unsupervised evaluation measures. The values in bold text are the ones where the correlation to the F-measure was better, meaning higher or lower than 0.2 or -0.2, depending if for the given unsupervised evaluation measure the ideal correlation should be positive or negative correspondingly.

	Intra_LN	Inter_Otsu	Inter_FRC	Intra_FRC	Intra_Liu	CalinskiHarabasz	DaviesBouldin
SEC-Otsu	0,2550	**1,2763**	**0,0578**	42937,29	767,86	157976,37	**0,7174**
SEC-Kittler	0,2536	**1,2756**	**0,0603**	56116,16	781,36	**161731,19**	**0,7279**
SEC-Ridler	0,2545	**1,2781**	**0,0578**	45284,29	766,93	158331,01	**0,7374**
SEC-SelfTuning	0,2729	**1,3210**	**0,0584**	32758,12	723,51	181830,74	**0,6773**
AdamsSRG	0,2365	**1,2421**	0,0656	63570,62	791,97	**168246,04**	**0,7131**
OtsuVermaSRG	0,2576	1,4276	**0,0652**	34327,27	699,06	210257,37	**0,6784**
MeanVermaSRG	0,2812	**1,2754**	**0,0544**	32778,61	765,34	169041,64	0,7147
ShihSRG	**0,2588**	**1,1733**	**0,0585**	56152,45	775,19	**159882,62**	**2,7433**
GambottoSRG	0,2295	1,0012	0,0725	**86009,24**	**923,46**	**104595,87**	0,6621
ZanatySRG	0,2798	**1,1741**	0,0663	**104939,10**	635,19	**165309,76**	0,6667

A.4 Empirical Study of Density Threshold

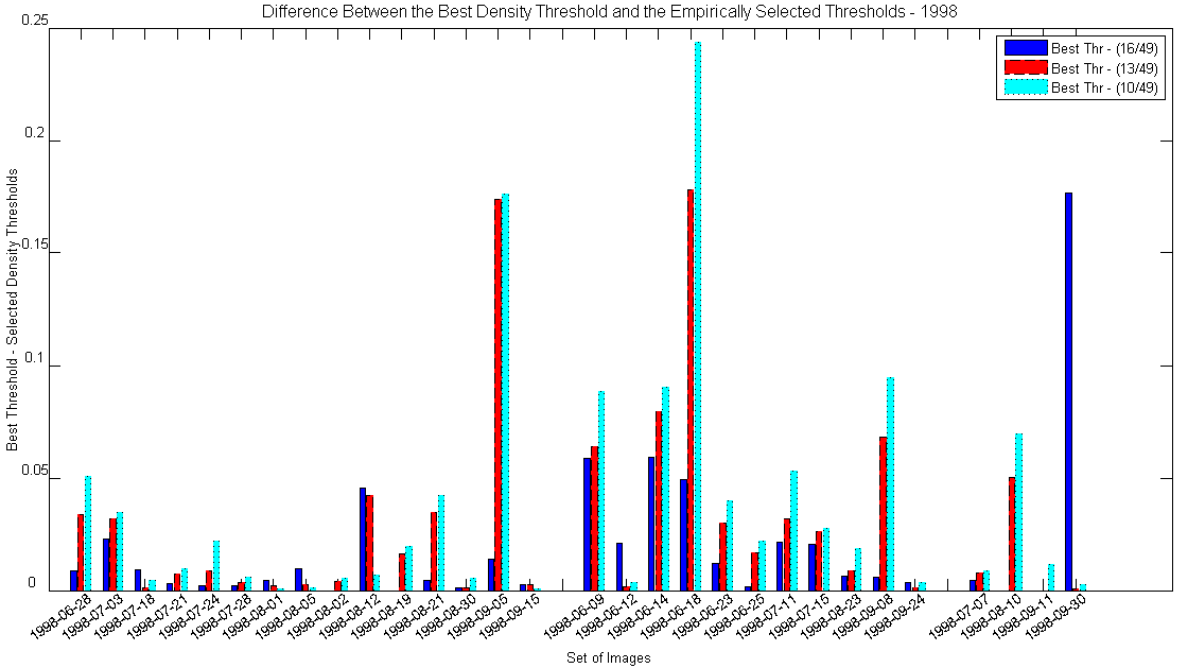

Figure A.22: Differences between the best density threshold and the empirically selected thresholds for the SEC-SelfTuning in 1998 images. Lower differences are best.

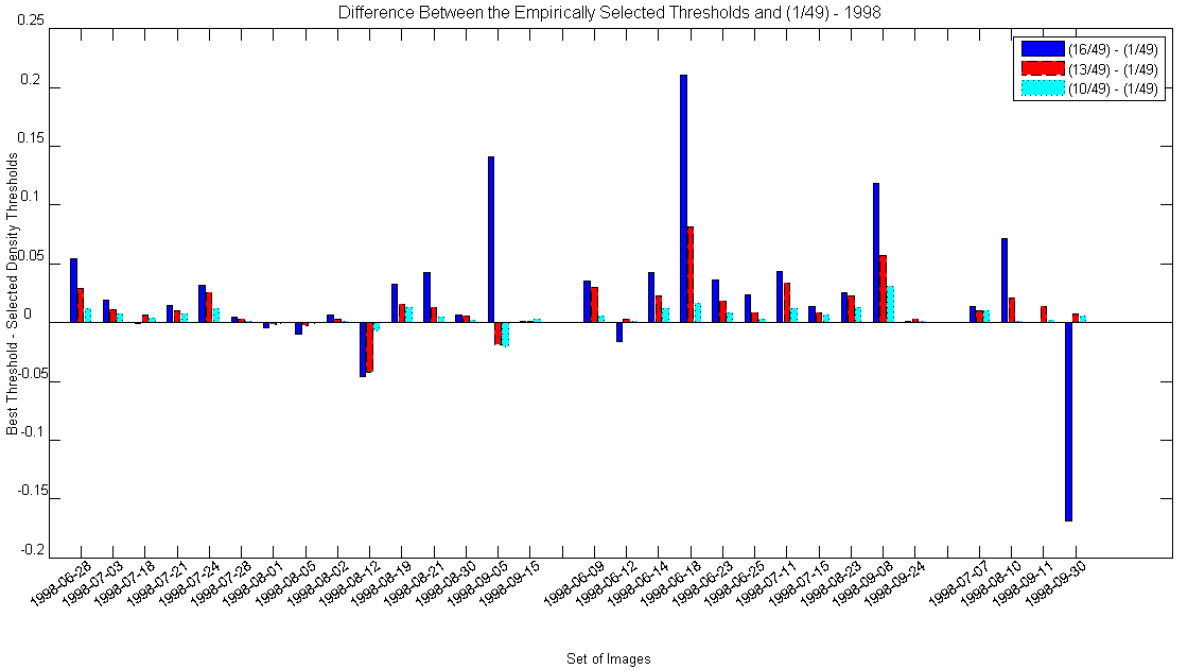

Figure A.23: Differences between the empirically selected thresholds and 0.0204 for the SEC-SelfTuning in 1998 images. Higher differences are best.

A.5 Iterative Procedure Segmentation Study

The graphics include the values for the difference between the mean of the first region and the minimum of one relevant cluster, the relevant cluster has different meanings depending of which category described in the legend. It also includes, for each SST image, the number of the iteration that the last region of upwelling was extracted and the reason why the iterative procedure ended.

A.5.1 Iterative Procedure for the SEC-Otsu

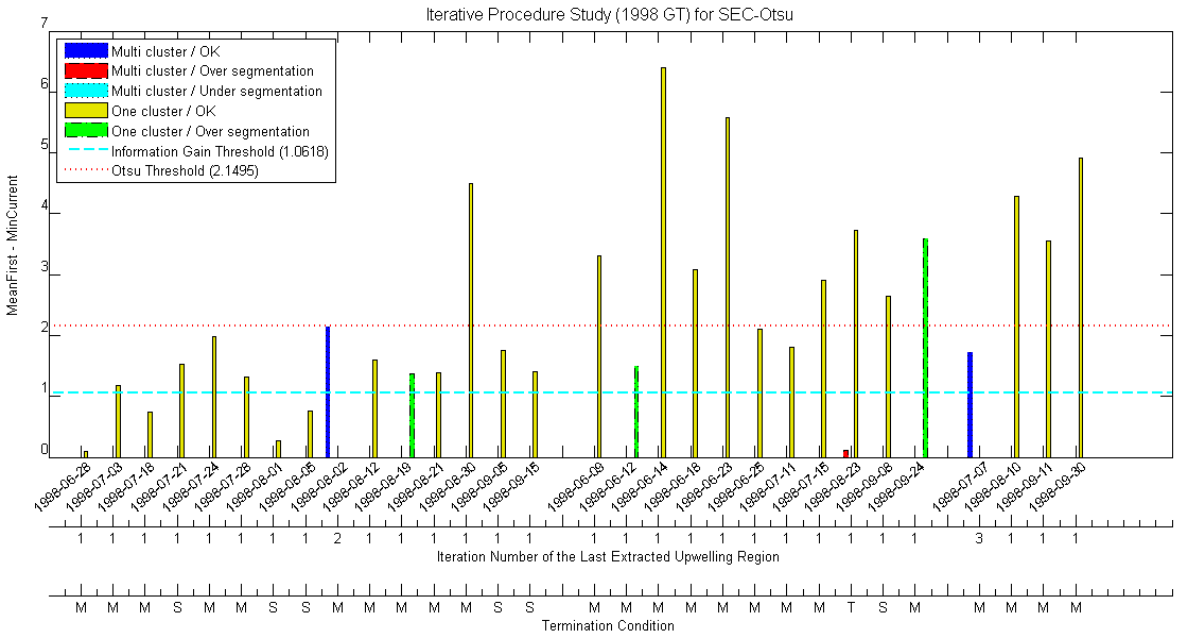

Figure A.24: Data related to the iterative procedure applied to the SEC-Otsu for the SST images from 1998 with ground-truth.

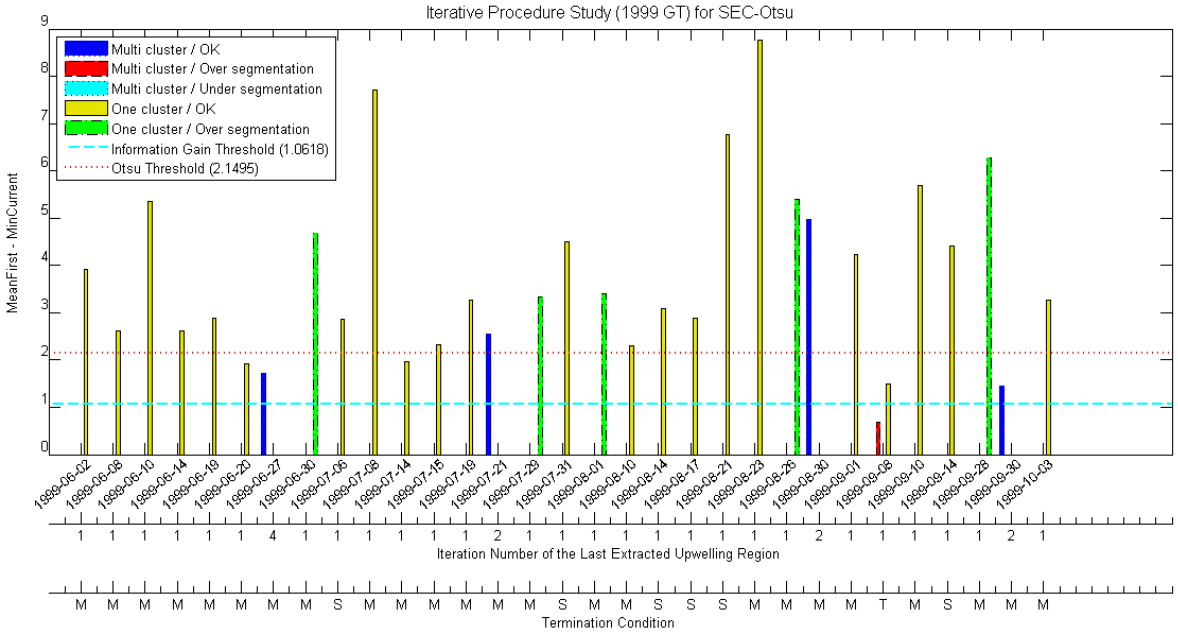

Figure A.25: Data related to the iterative procedure applied to the SEC-Otsu for the SST images from 1999 with ground-truth.

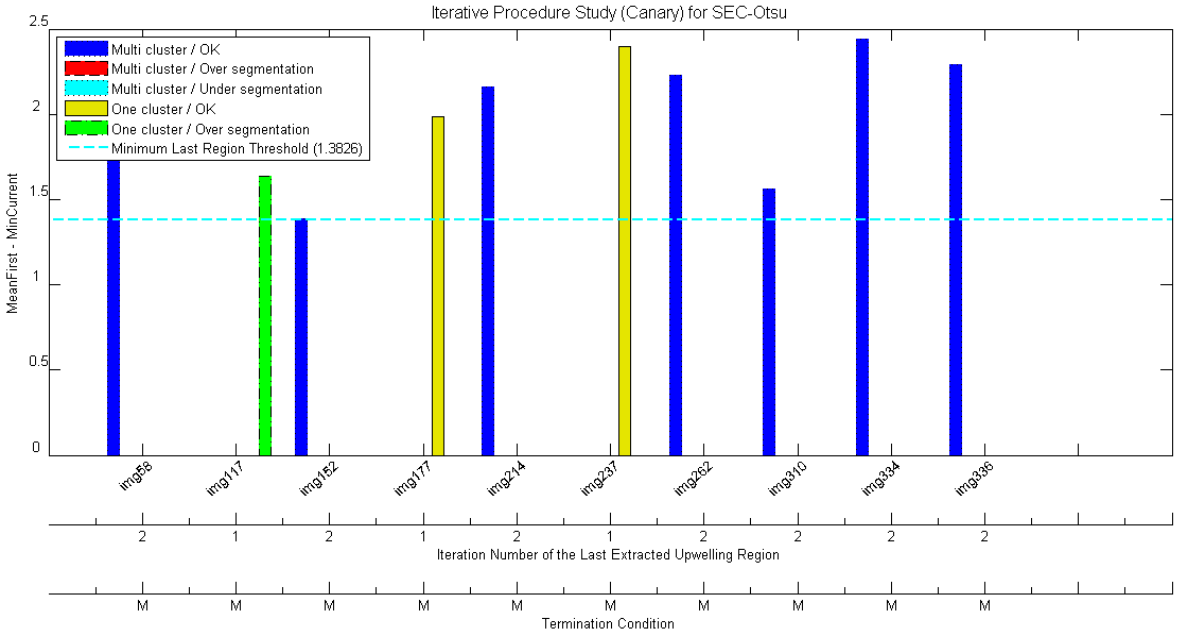

Figure A.26: Data related to the iterative procedure applied to the SEC-Otsu for the SST images of the Canary with ground-truth.

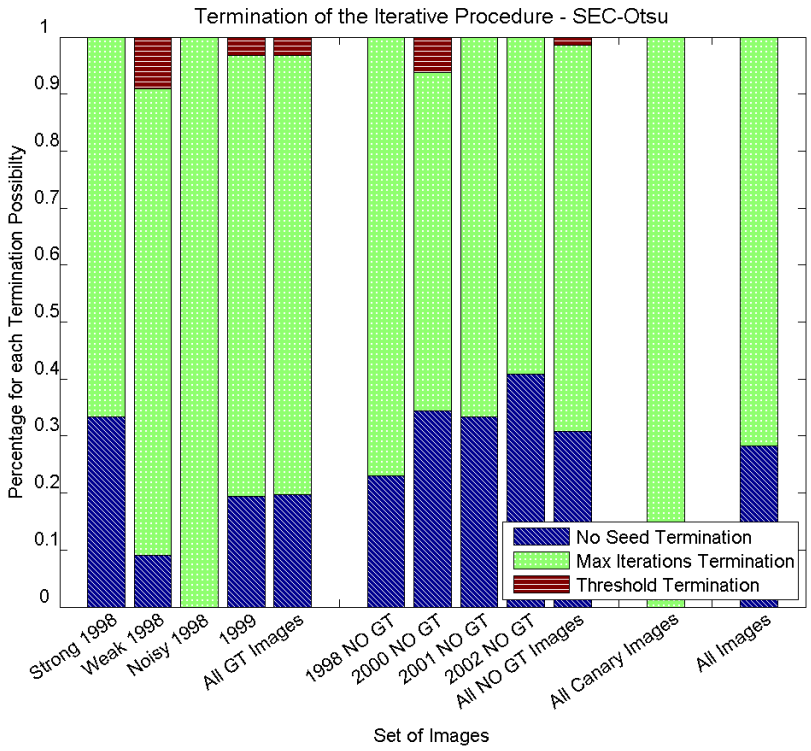

Figure A.27: The plot shows the percentage for each termination possibility of the iterative procedure, organized by sets of images, in this case for the results of the SEC-Otsu.

A.5.2 Iterative Procedure for the SEC-Kittler

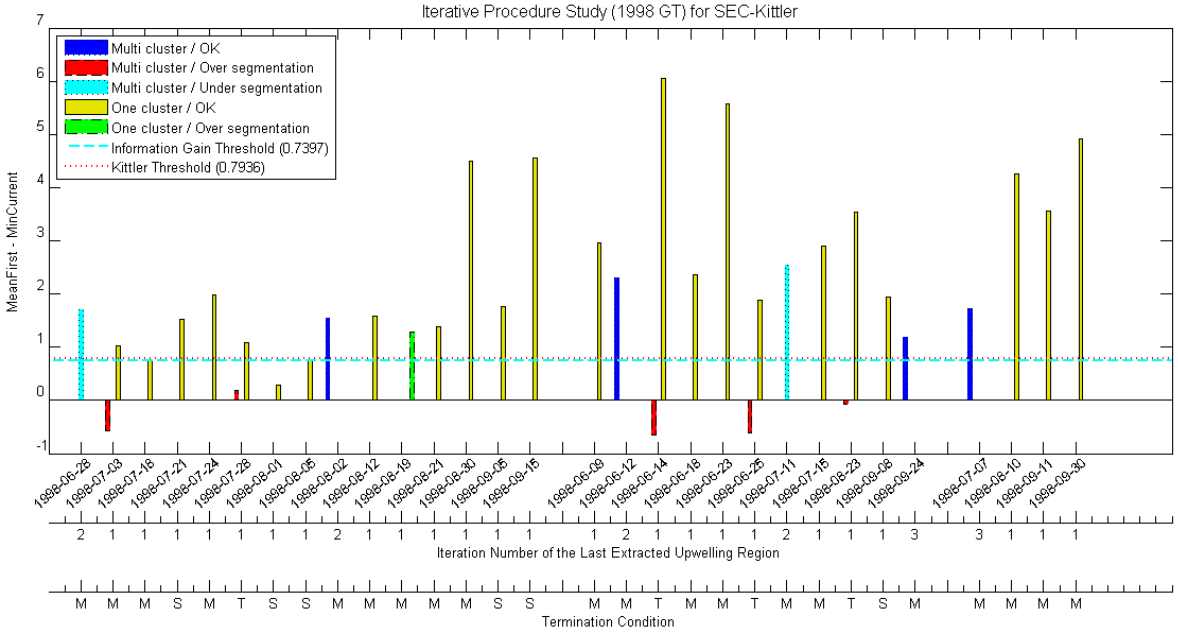

Figure A.28: Data related to the iterative procedure applied to the SEC-Kittler for the SST images from 1998 with ground-truth.

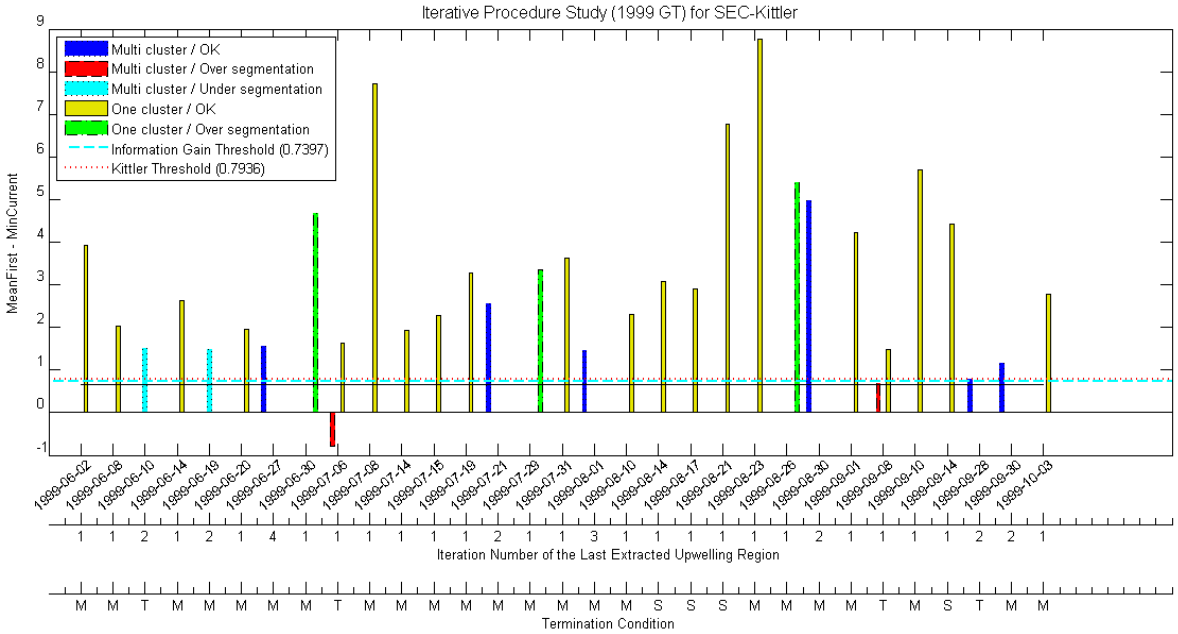

Figure A.29: Data related to the iterative procedure applied to the SEC-Kittler for the SST images from 1999 with ground-truth.

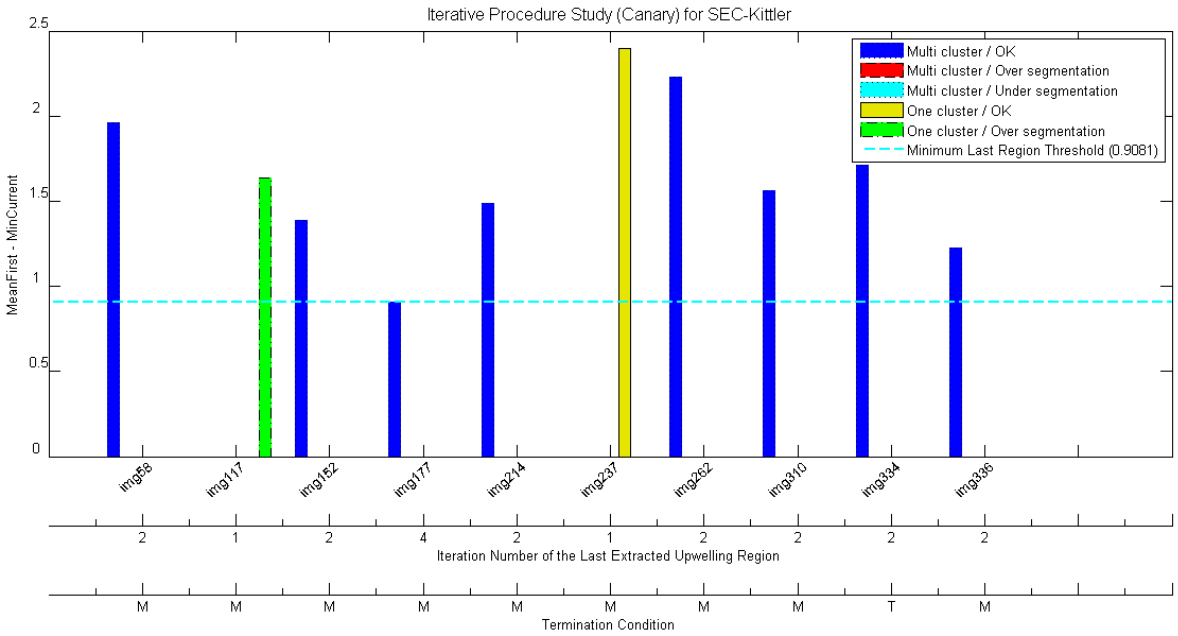

Figure A.30: Data related to the iterative procedure applied to the SEC-Kittler for the SST images of the Canary with ground-truth.

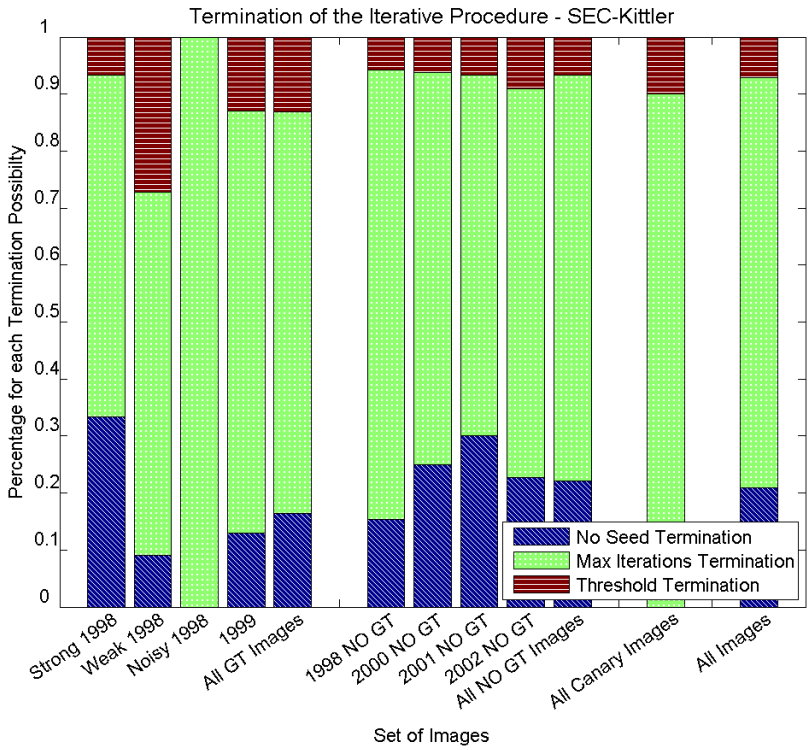

Figure A.31: The plot shows the percentage for each termination possibility of the iterative procedure, organized by sets of images, in this case for the results of the SEC-Kittler.

A.5.3 Iterative Procedure for the SEC-Ridler

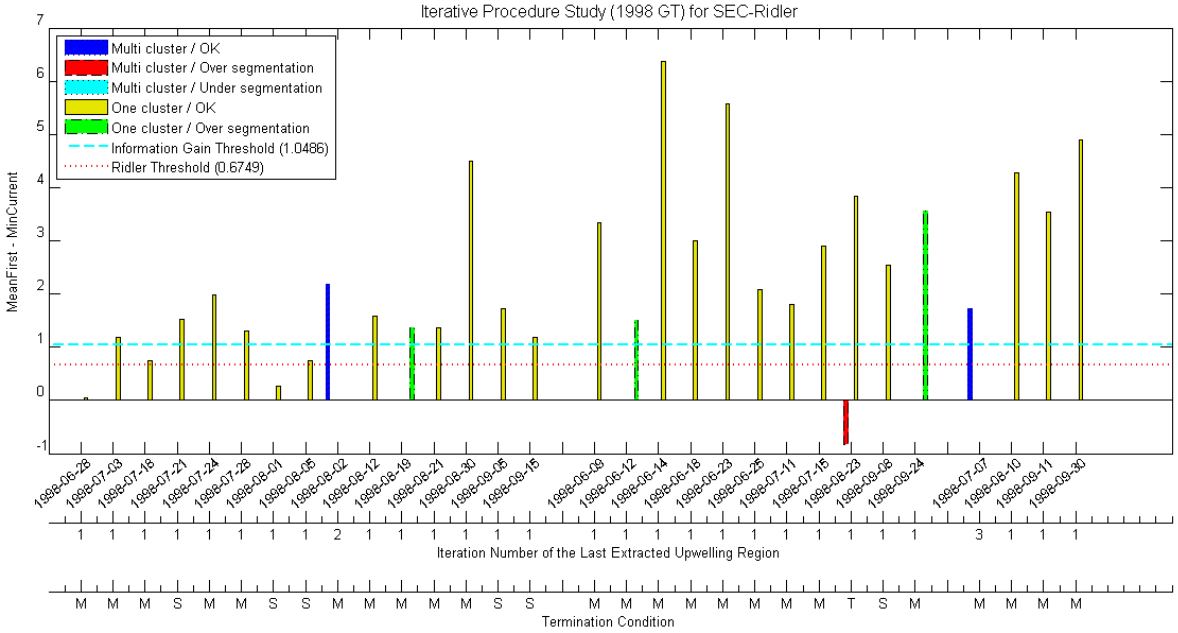

Figure A.32: Data related to the iterative procedure applied to the SEC-Ridler for the SST images from 1998 with ground-truth.

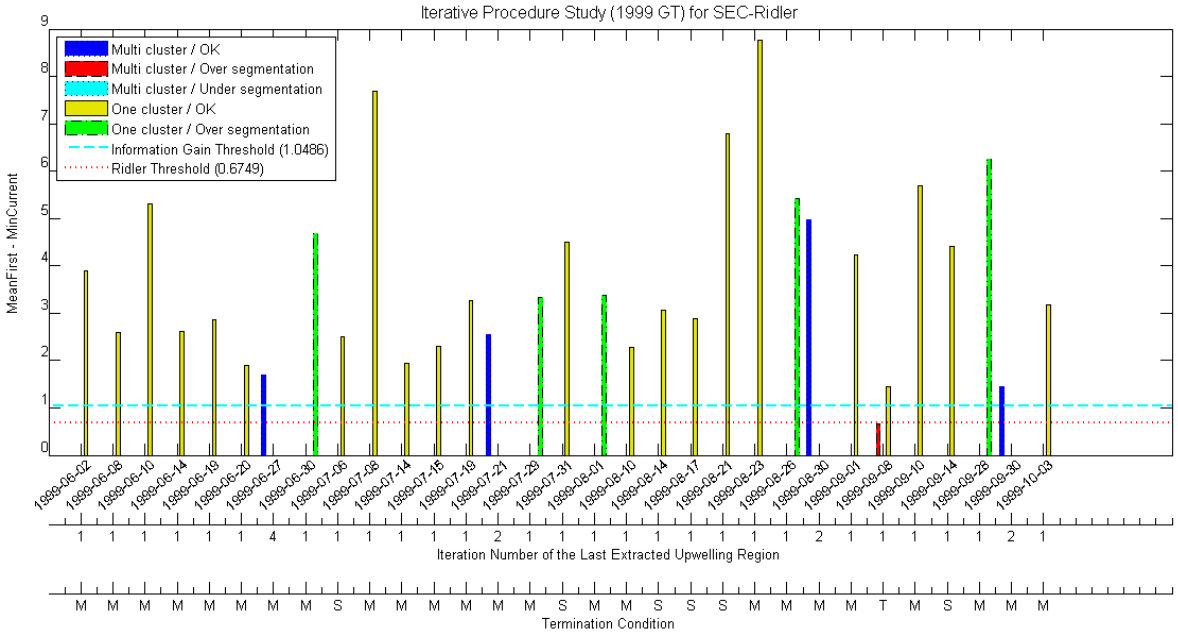

Figure A.33: Data related to the iterative procedure applied to the SEC-Ridler for the SST images from 1999 with ground-truth.

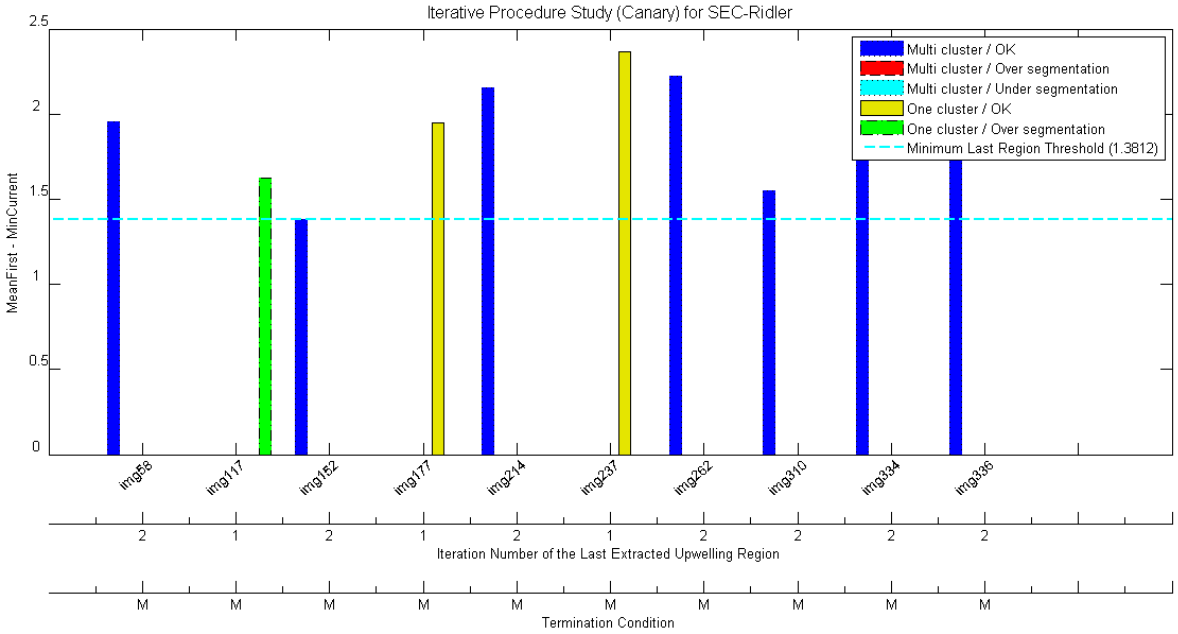

Figure A.34: Data related to the iterative procedure applied to the SEC-Ridler for the SST images of the Canary with ground-truth.

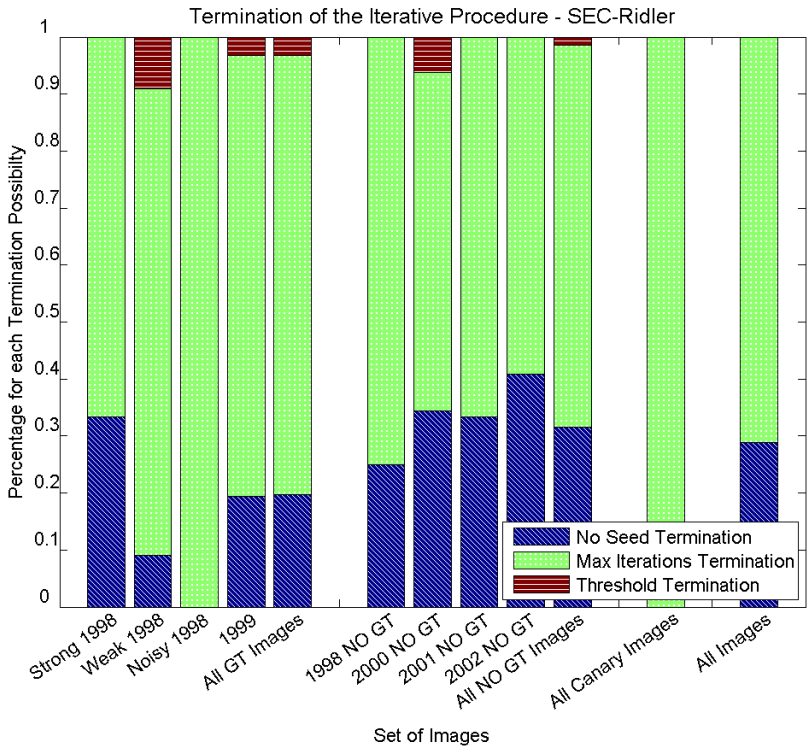

Figure A.35: The plot shows the percentage for each termination possibility of the iterative procedure, organized by sets of images, in this case for the results of the SEC-Ridler.

A.5.4 Iterative Procedure for the SEC-SelfTuning

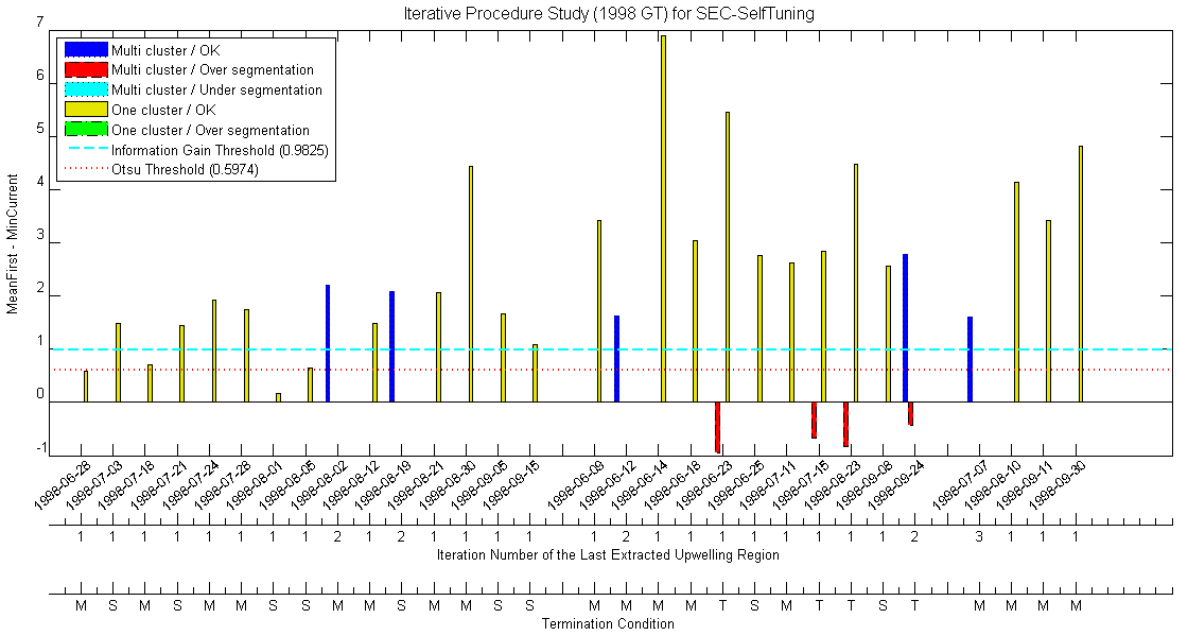

Figure A.36: Data related to the iterative procedure applied to the SEC-SelfTuning for the SST images from 1998 with ground-truth.

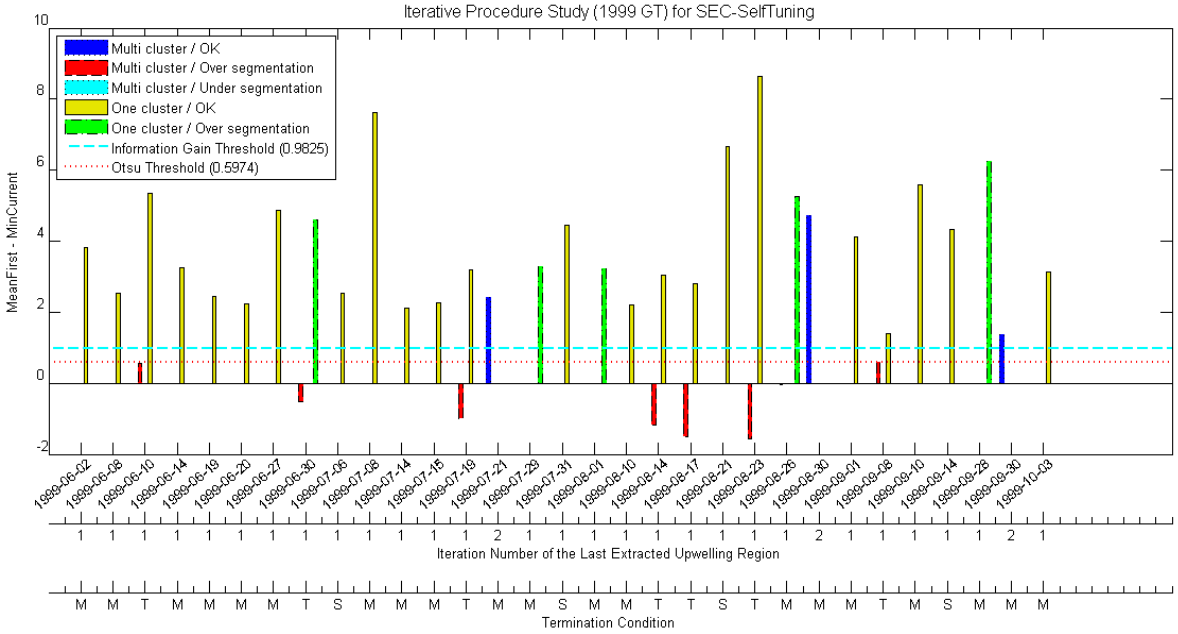

Figure A.37: Data related to the iterative procedure applied to the SEC-SelfTuning for the SST images from 1999 with ground-truth.

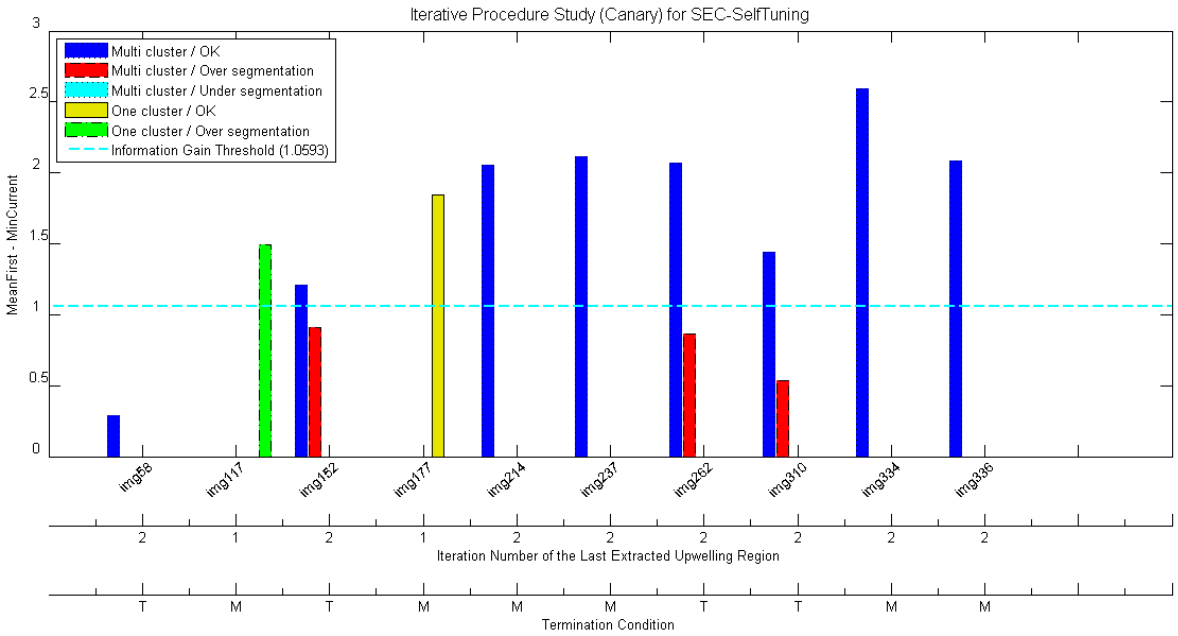

Figure A.38: Data related to the iterative procedure applied to the SEC-SelfTuning for the SST images of the Canary with ground-truth.

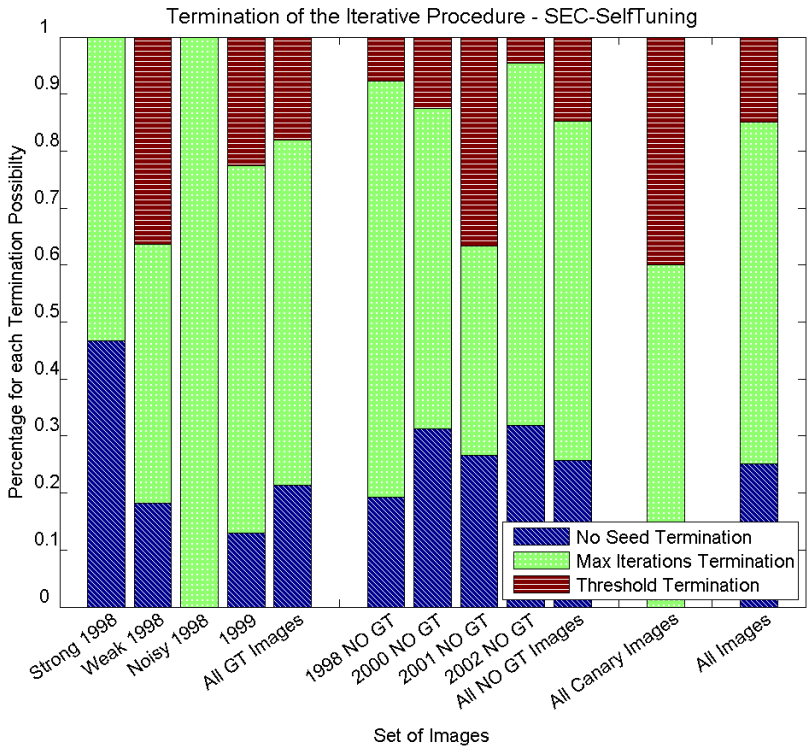

Figure A.39: The plot shows the percentage for each termination possibility of the iterative procedure, organized by sets of images, in this case for the results of the SEC-SelfTuning.

A.5.5 Iterative Procedure for the OtsuVermaSRG

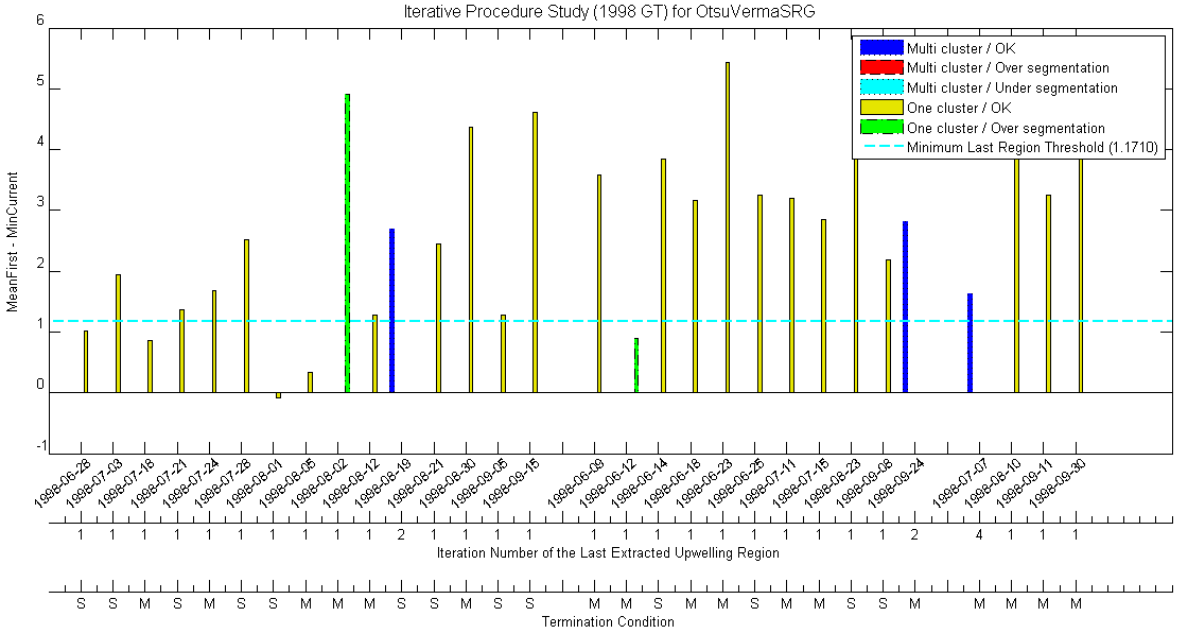

Figure A.40: Data related to the iterative procedure applied to the OtsuVermaSRG for the SST images from 1998 with ground-truth.

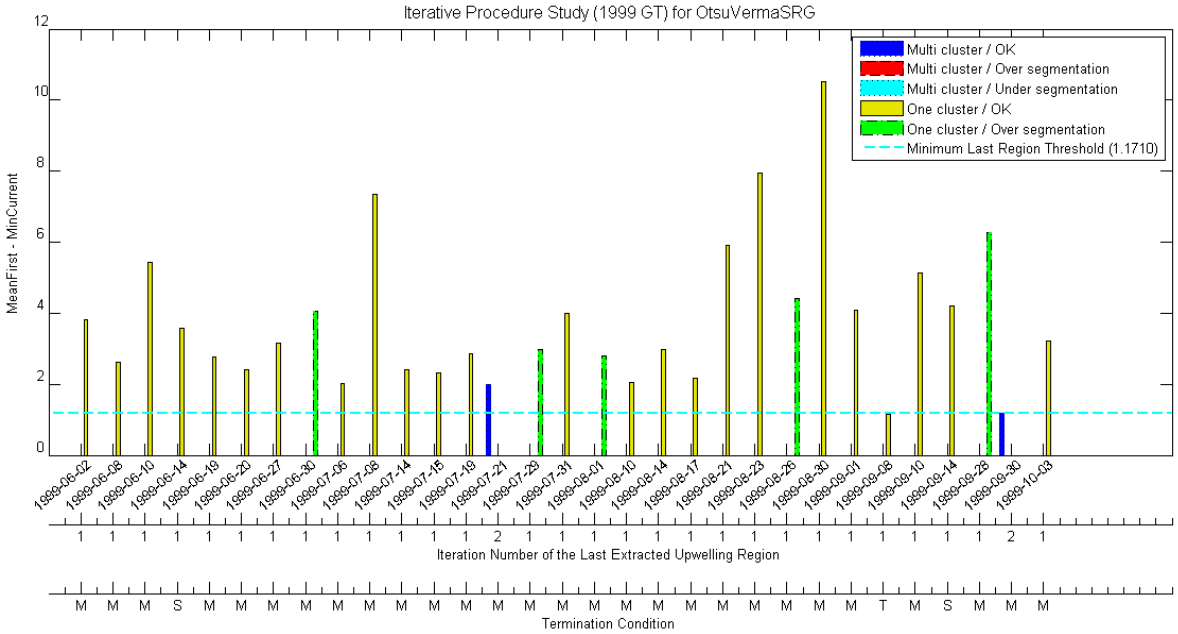

Figure A.41: Data related to the iterative procedure applied to the OtsuVermaSRG for the SST images from 1999 with ground-truth.

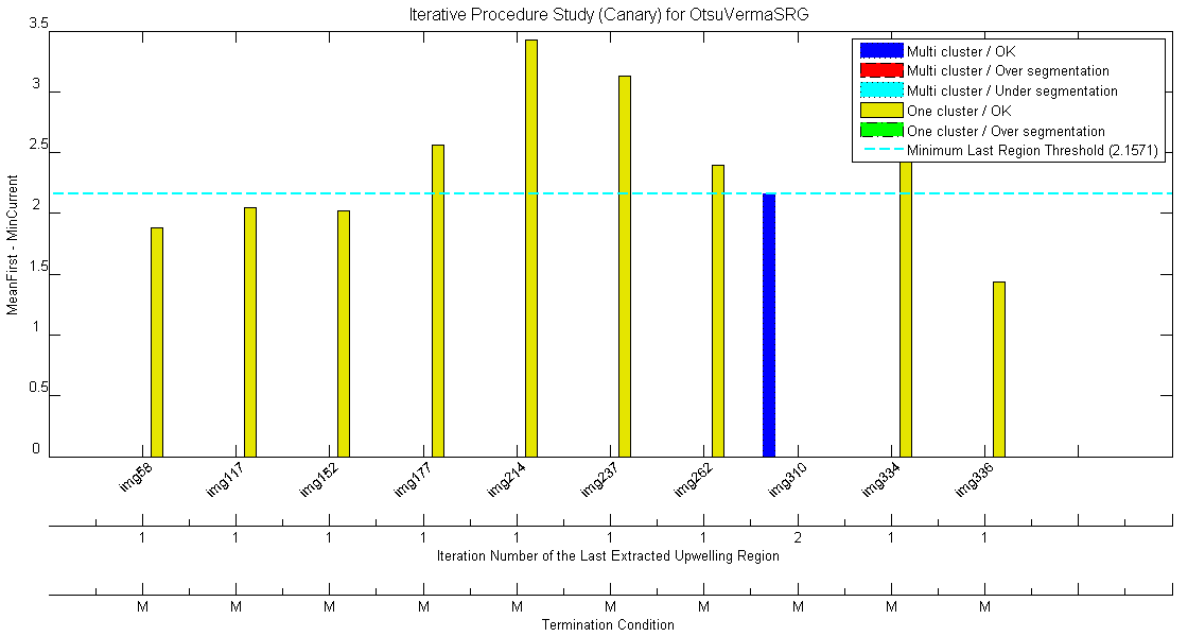

Figure A.42: Data related to the iterative procedure applied to the OtsuVermaSRG for the SST images of the Canary with ground-truth.

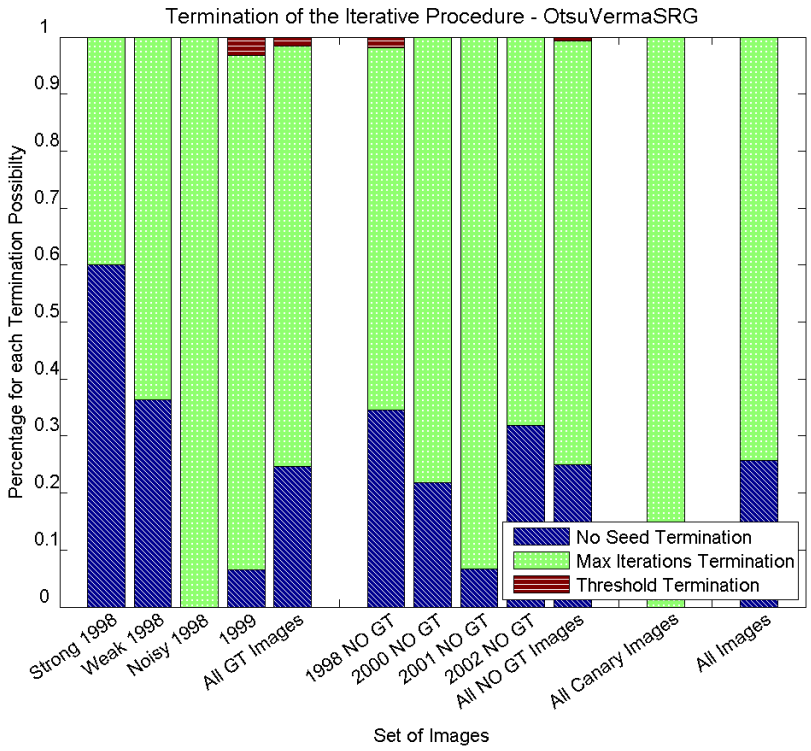

Figure A.43: The plot shows the percentage for each termination possibility of the iterative procedure, organized by sets of images, in this case for the results of the OtsuVermaSRG.

A.5.6 Iterative Procedure for the MeanVermaSRG

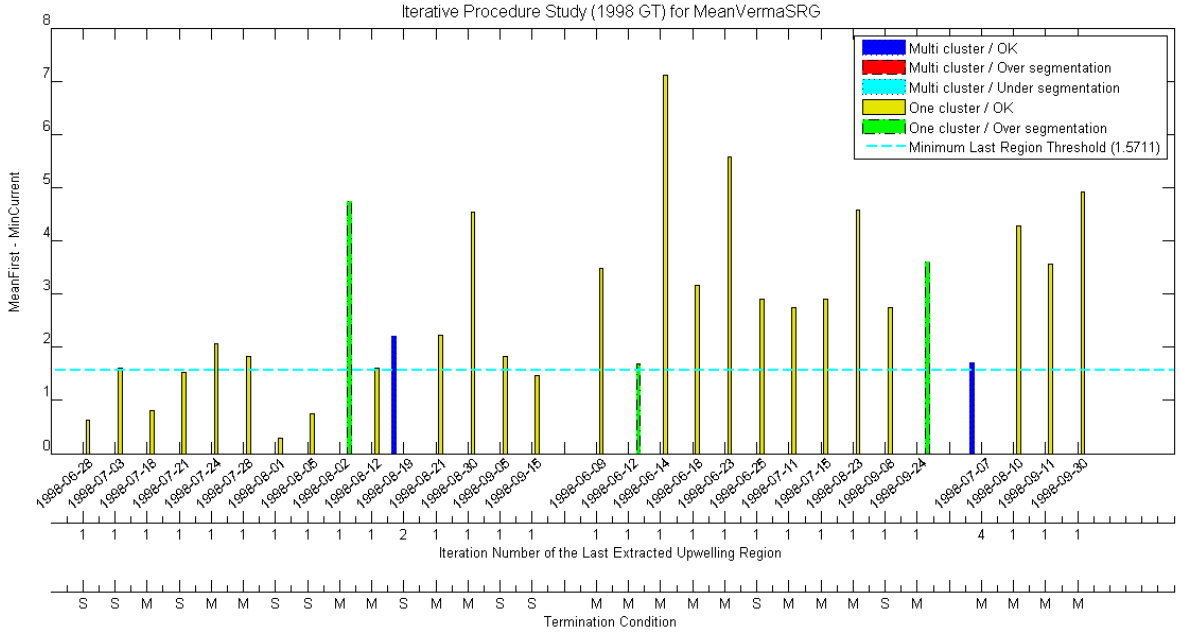

Figure A.44: Data related to the iterative procedure applied to the MeanVermaSRG for the SST images from 1998 with ground-truth.

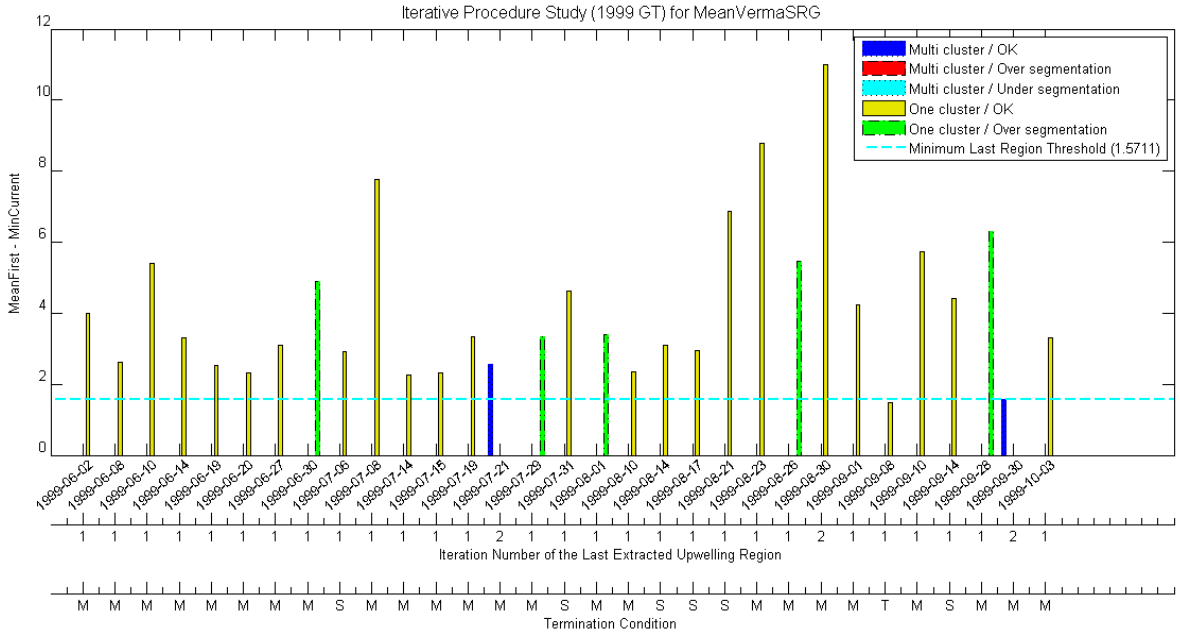

Figure A.45: Data related to the iterative procedure applied to the MeanVermaSRG for the SST images from 1999 with ground-truth.

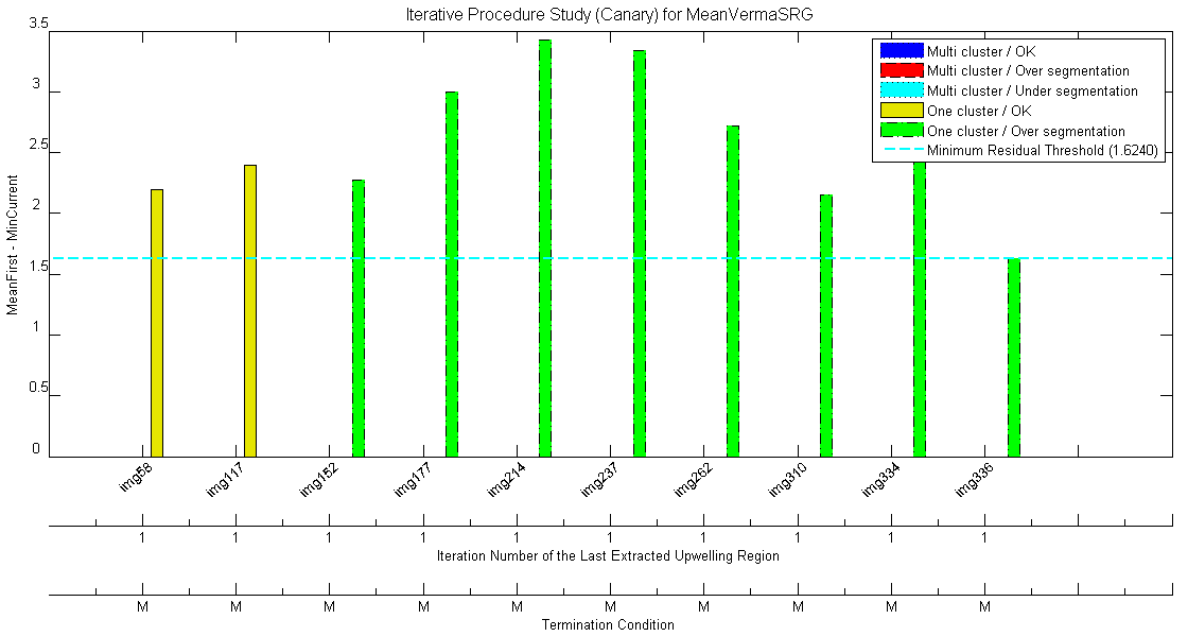

Figure A.46: Data related to the iterative procedure applied to the MeanVermaSRG for the SST images of the Canary with ground-truth.

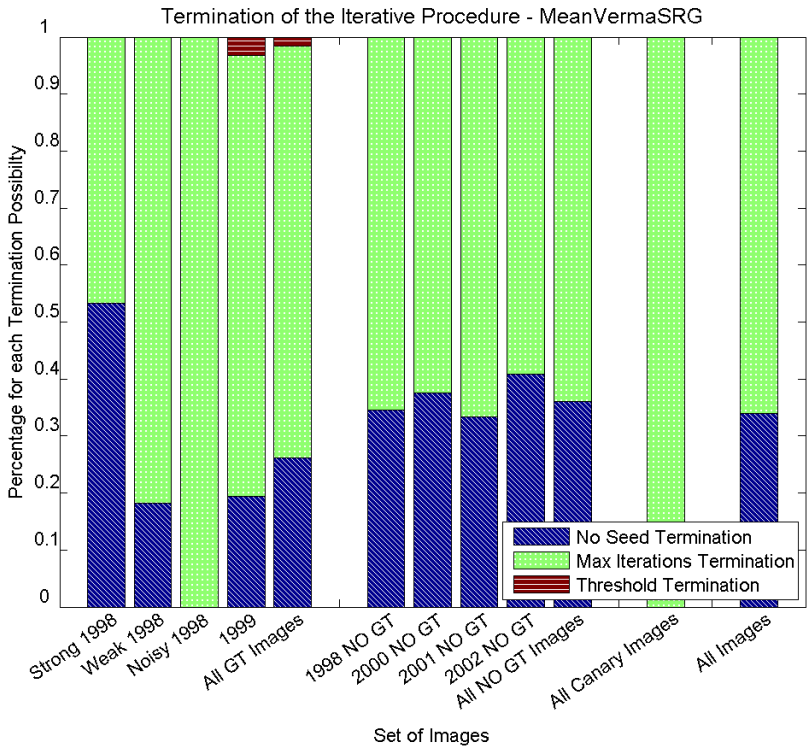

Figure A.47: The plot shows the percentage for each termination possibility of the iterative procedure, organized by sets of images, in this case for the results of the MeanVermaSRG.

A.5.7 Iterative Procedure for the ShihSRG

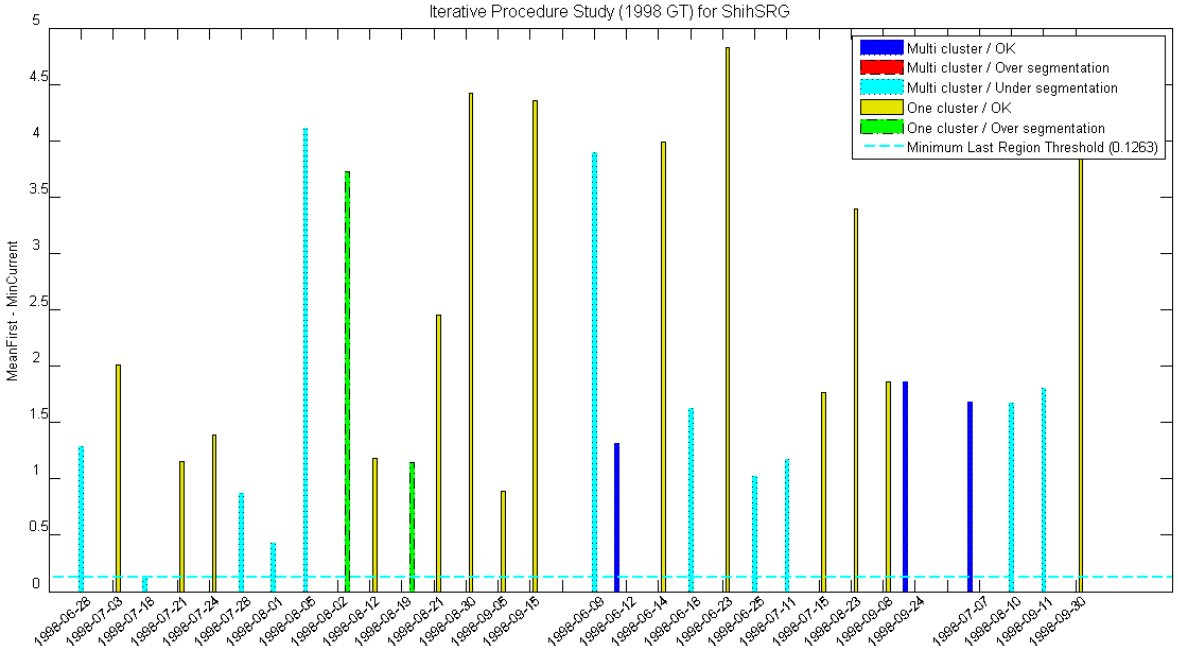

Figure A.48: Data related to the iterative procedure applied to the ShihSRG for the SST images from 1998 with ground-truth.

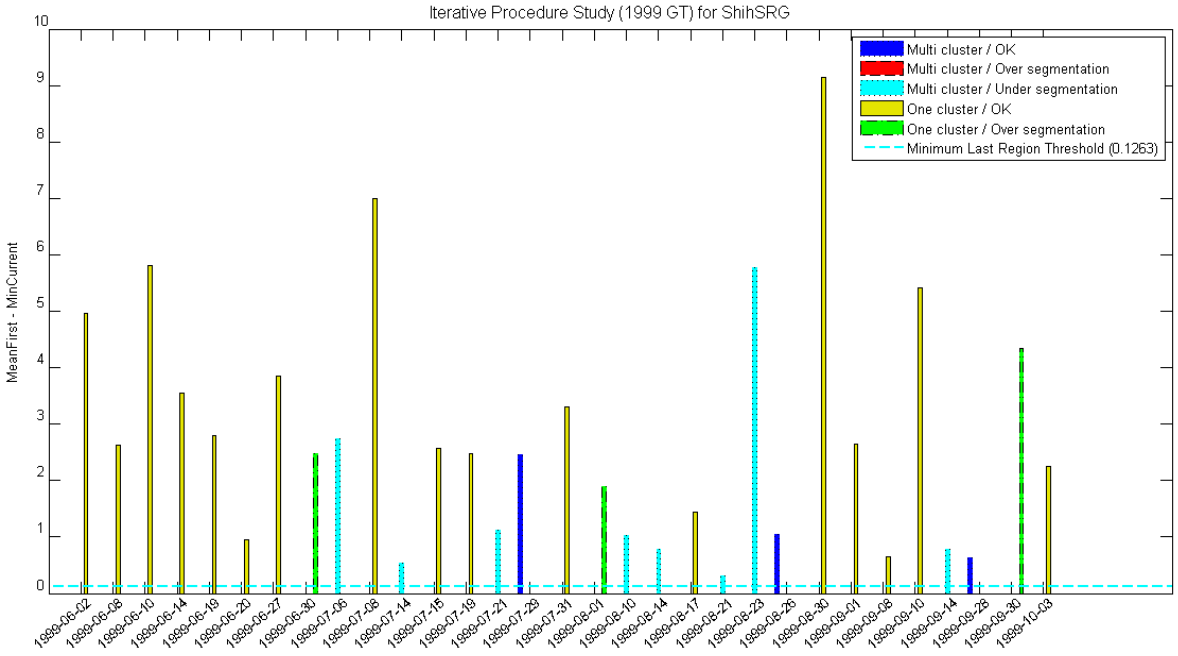

Figure A.49: Data related to the iterative procedure applied to the ShihSRG for the SST images from 1999 with ground-truth.

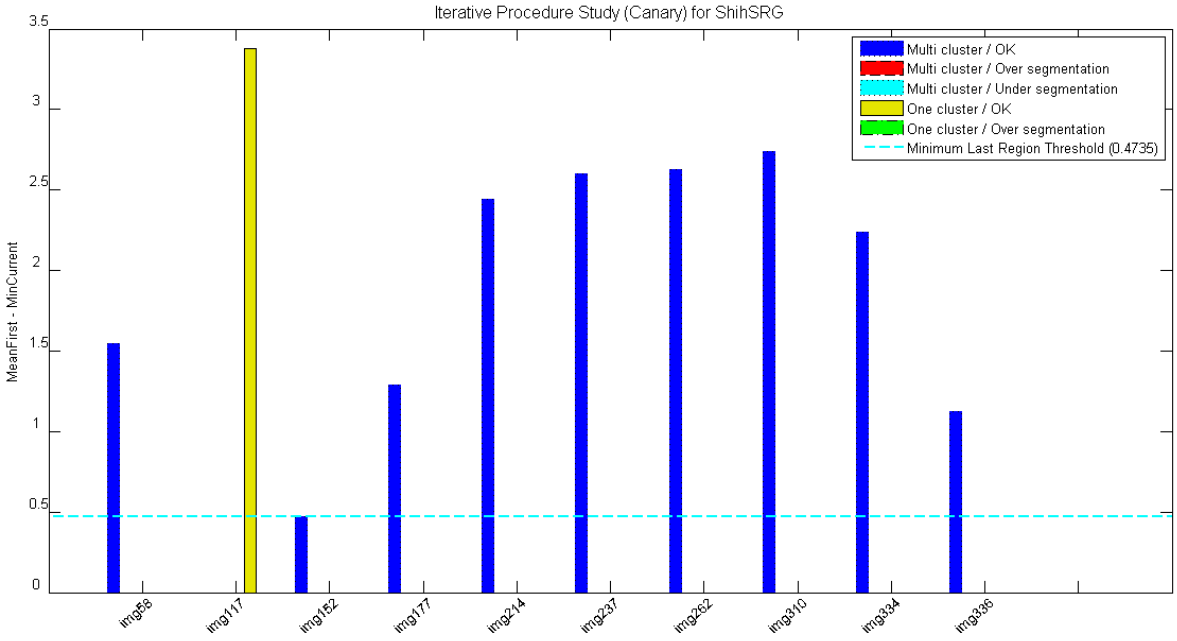

Figure A.50: Data related to the iterative procedure applied to the ShihSRG for the SST images of the Canary with ground-truth.

A.5.8 Iterative Procedure for the GambottoSRG

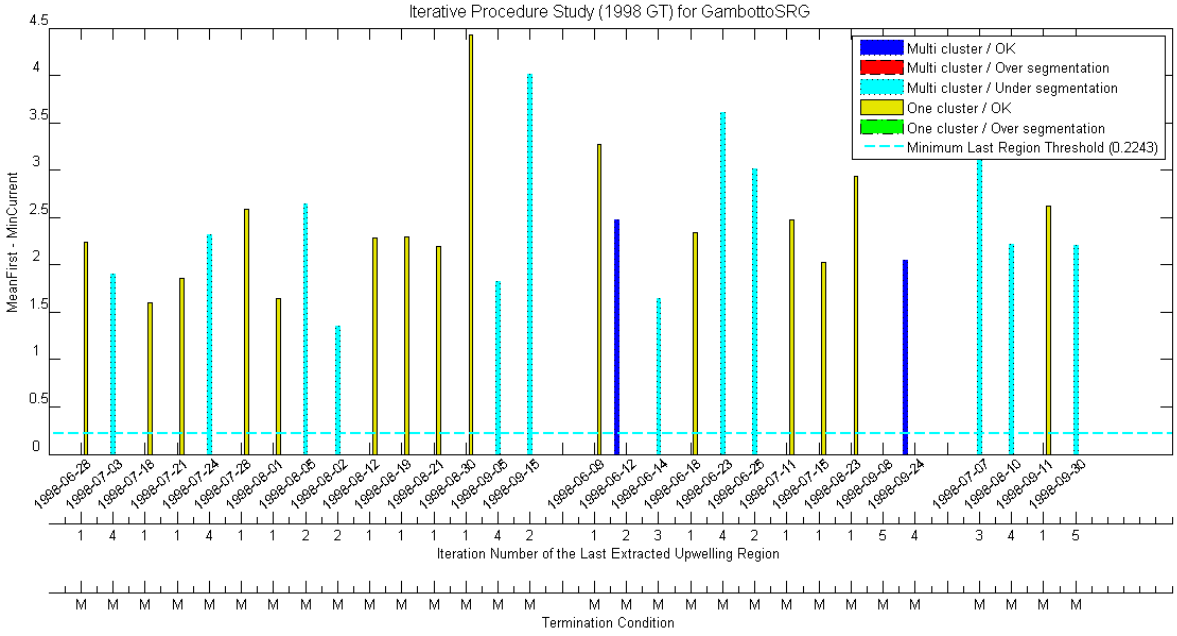

Figure A.51: Data related to the iterative procedure applied to the GambottoSRG for the SST images from 1998 with ground-truth.

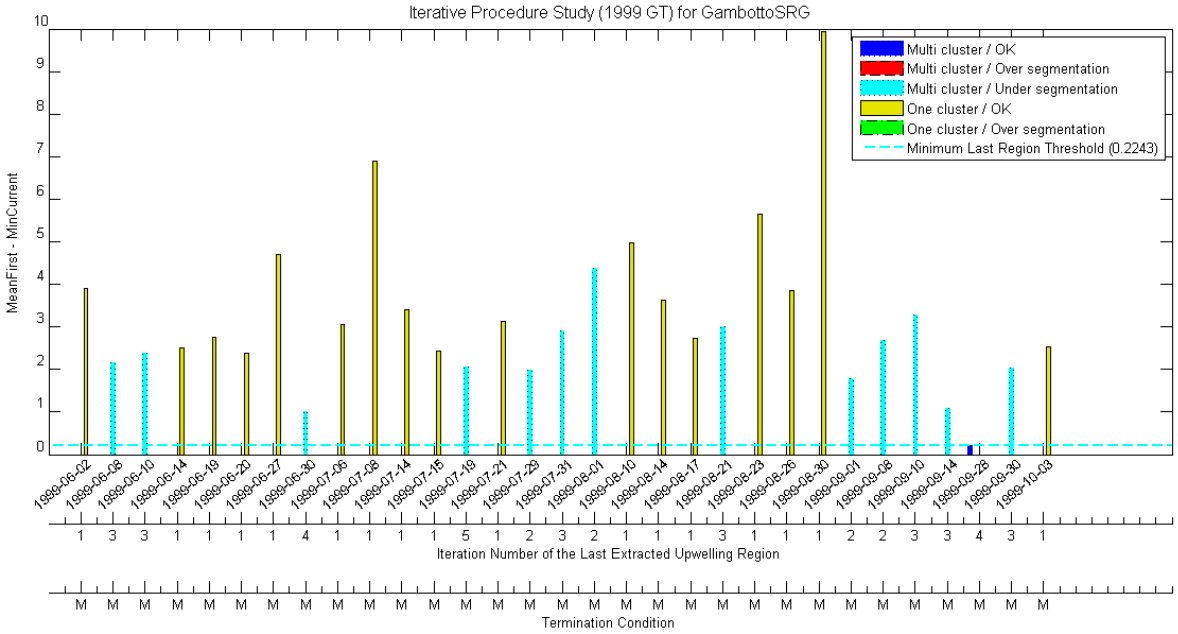

Figure A.52: Data related to the iterative procedure applied to the GambottoSRG for the SST images from 1999 with ground-truth.

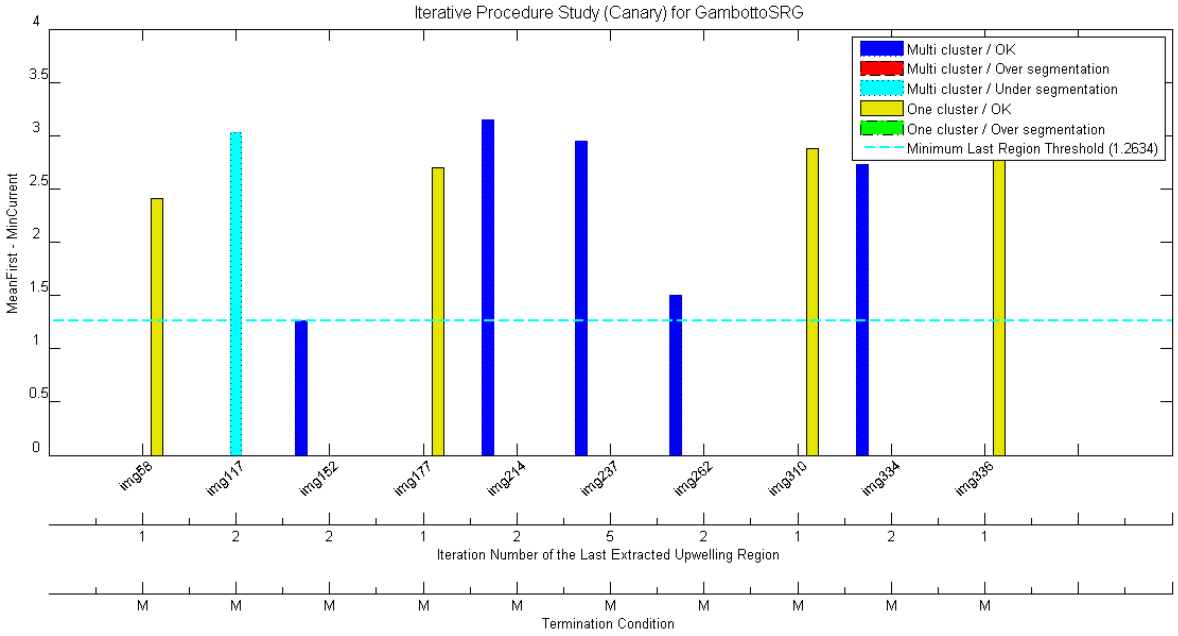

Figure A.53: Data related to the iterative procedure applied to the GambottoSRG for the SST images of the Canary with ground-truth.

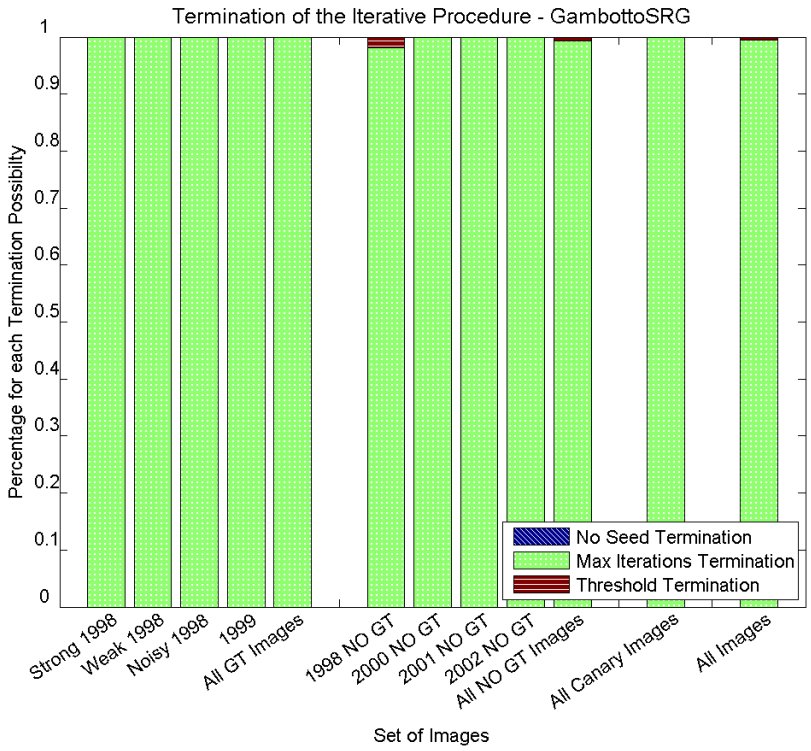

Figure A.54: The plot shows the percentage for each termination possibility of the iterative procedure, organized by sets of images, in this case for the results of the GambottoSRG.

A.5.9 Iterative Procedure for the ZanatySRG

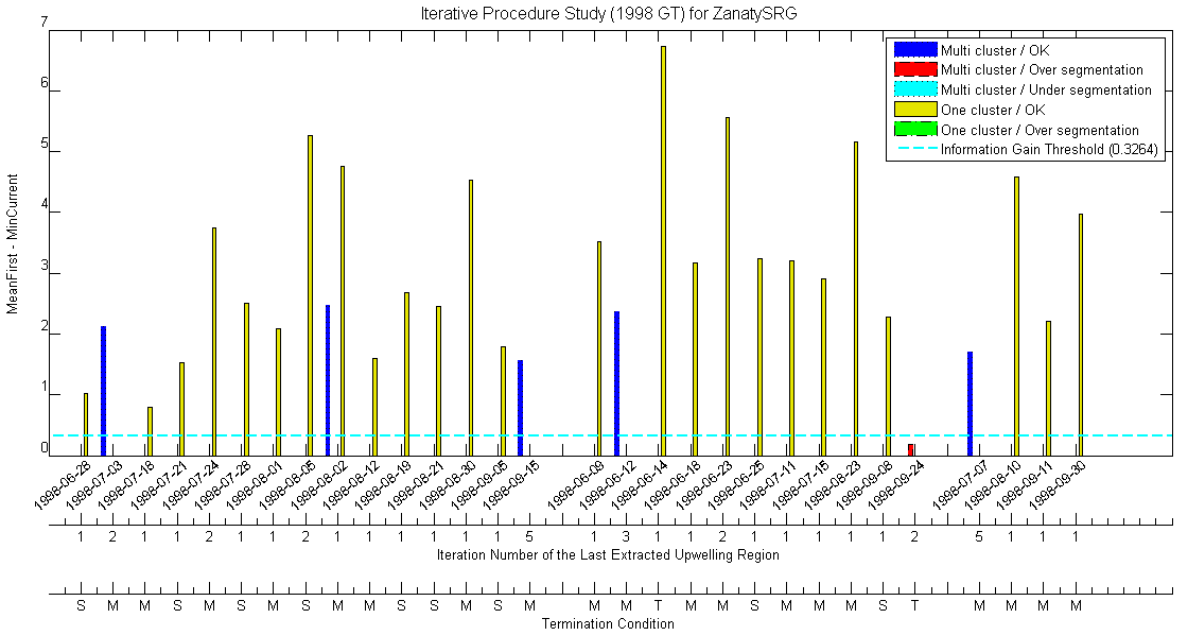

Figure A.55: Data related to the iterative procedure applied to the ZanatySRG for the SST images from 1998 with ground-truth.

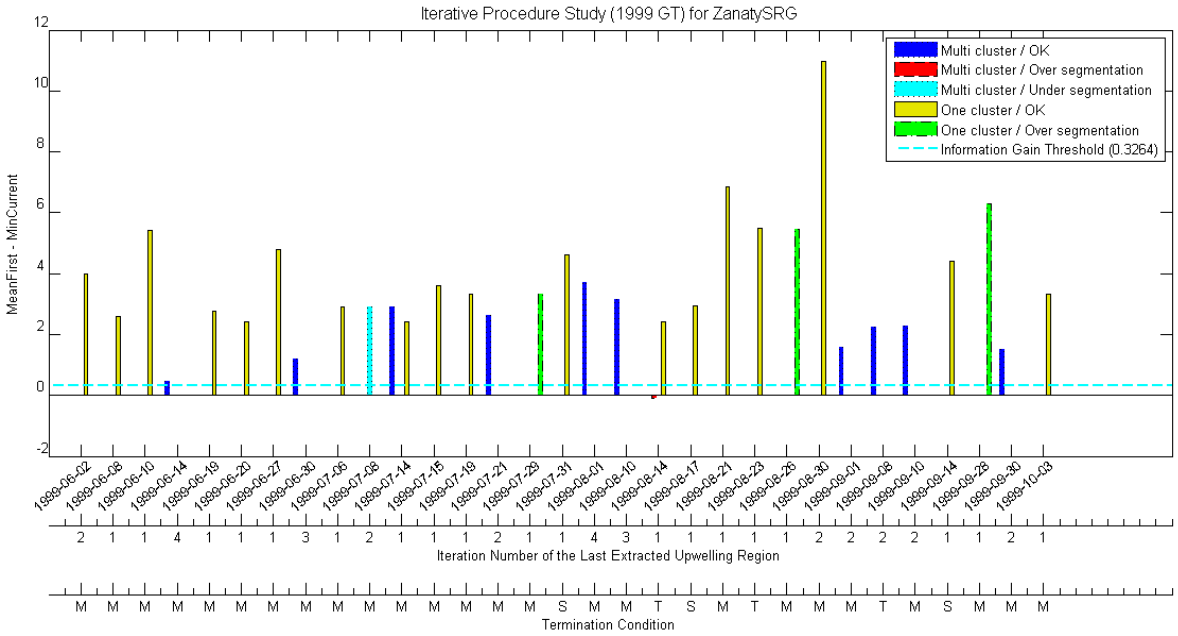

Figure A.56: Data related to the iterative procedure applied to the ZanatySRG for the SST images from 1999 with ground-truth.

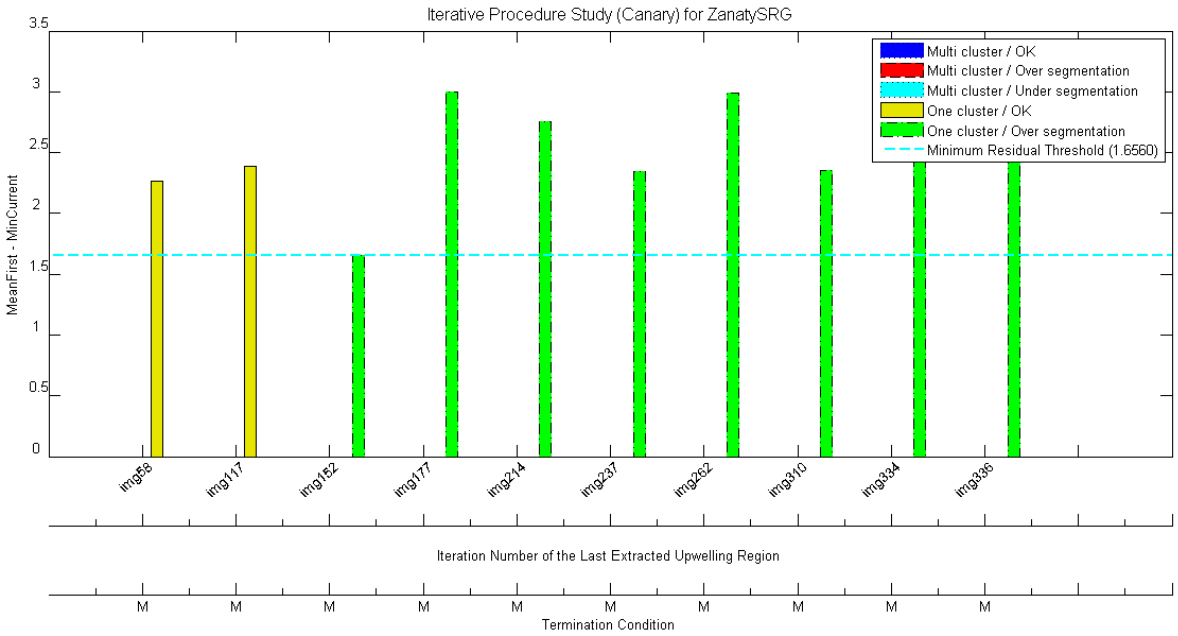

Figure A.57: Data related to the iterative procedure applied to the ZanatySRG for the SST images of the Canary with ground-truth.

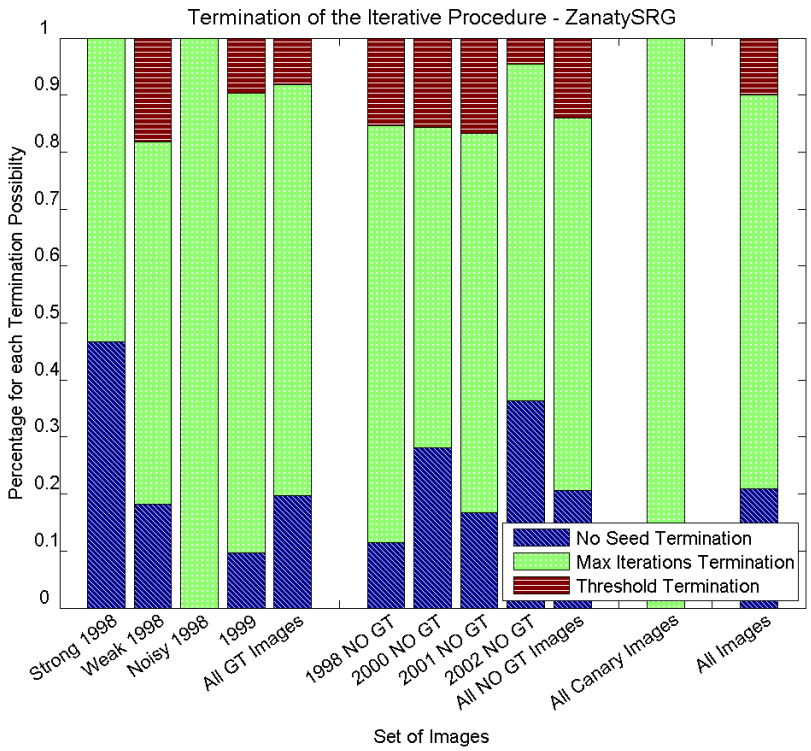

Figure A.58: The plot shows the percentage for each termination possibility of the iterative procedure, organized by sets of images, in this case for the results of the ZanatySRG.

Appendix B

Segmentation Results

B.1 SST Images with GT / Strong Gradients from 1998

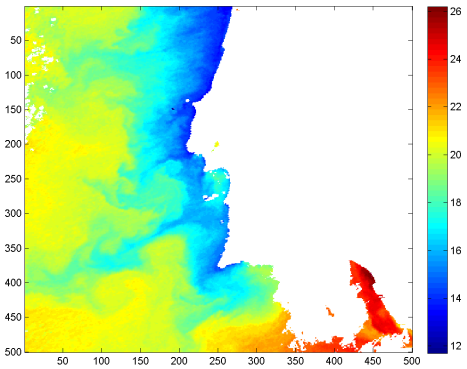

Figure B.1: 1998-08-02

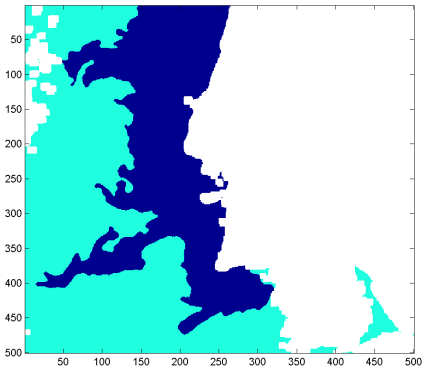

Figure B.2: 1998-08-02 ground-truth map

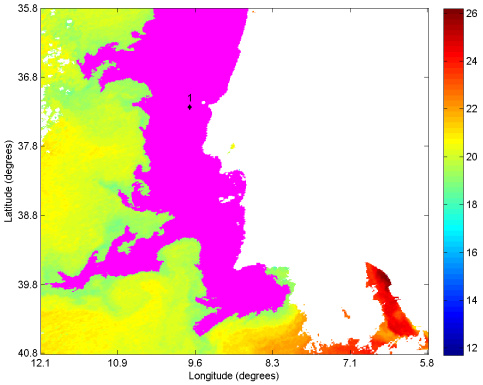

Figure B.3: 1998-08-02 SEC-Otsu

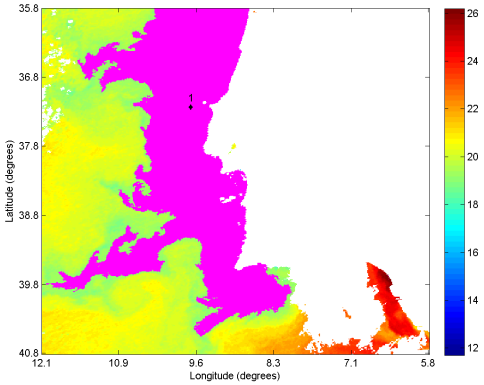

Figure B.4: 1998-08-02 SEC-Kittler

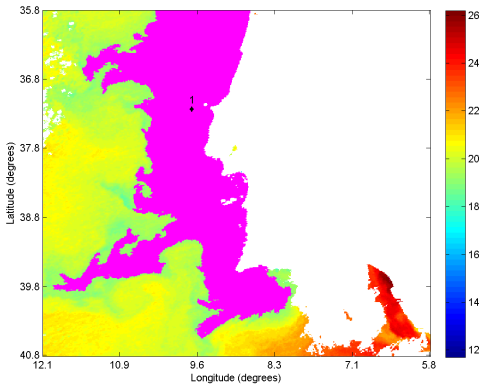

Figure B.5: 1998-08-02 SEC-Ridler

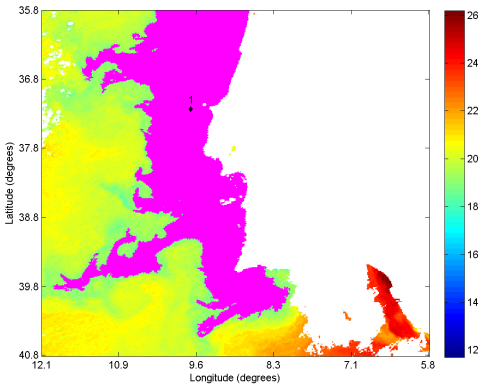

Figure B.6: 1998-08-02 SEC-SelfTuning

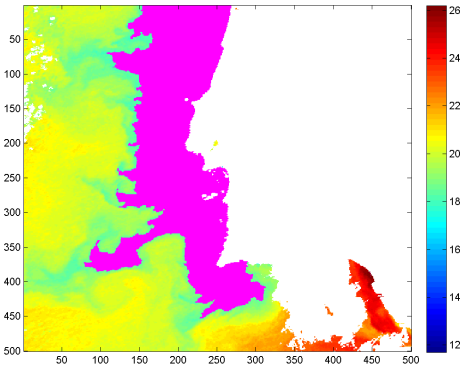

Figure B.7: 1998-08-02 AdamsSRG

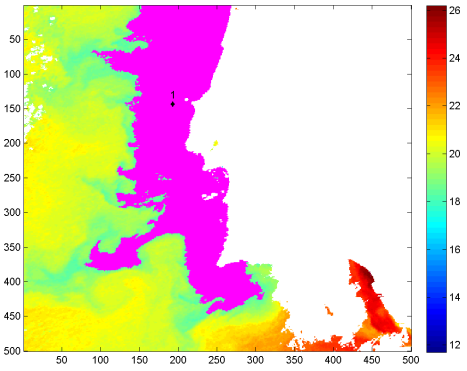

Figure B.8: 1998-08-02 OtsuVermaSRG

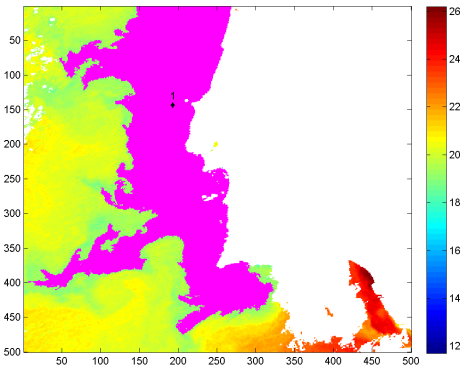

Figure B.9: 1998-08-02 MeanVermaSRG

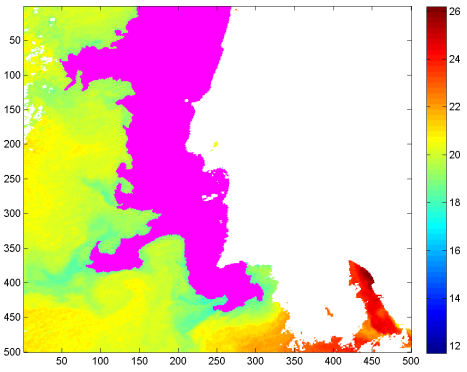

Figure B.10: 1998-08-02 ShihSRG

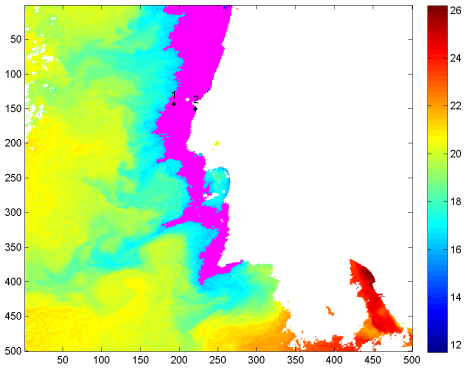

Figure B.11: 1998-08-02 GambottoSRG

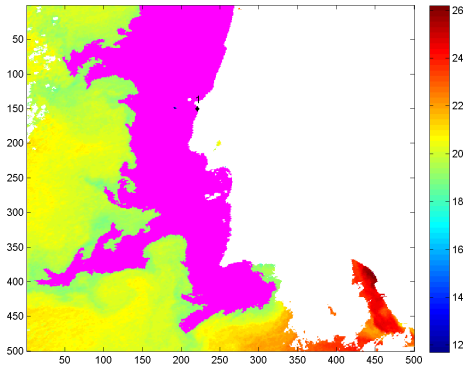

Figure B.12: 1998-08-02 ZanatySRG

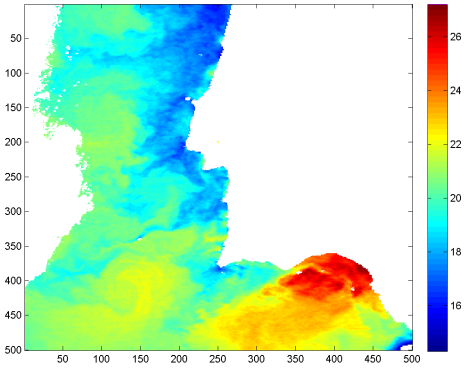

Figure B.13: 1998-08-05

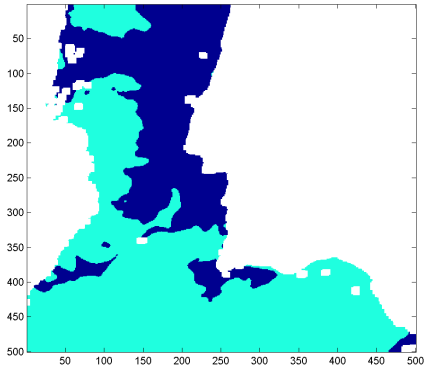

Figure B.14: 1998-08-05 ground-truth map

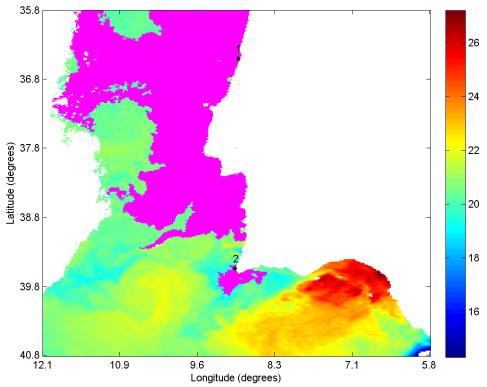

Figure B.15: 1998-08-05 SEC-Otsu

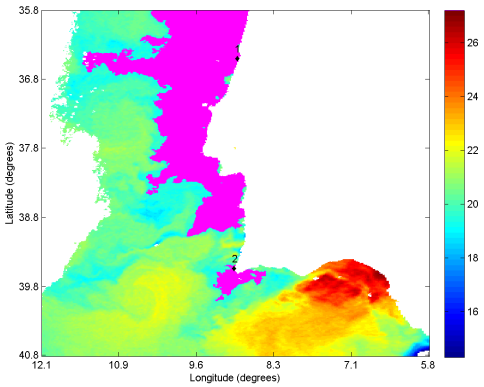

Figure B.16: 1998-08-05 SEC-Kittler

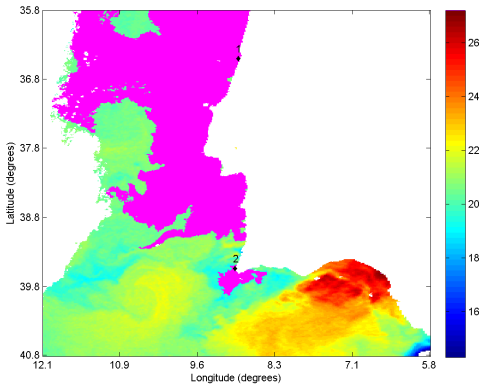

Figure B.17: 1998-08-05 SEC-Ridler

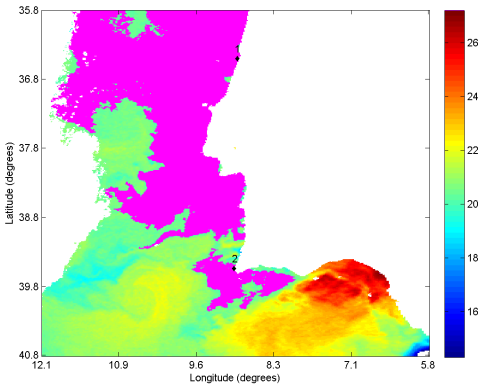

Figure B.18: 1998-08-05 SEC-SelfTuning

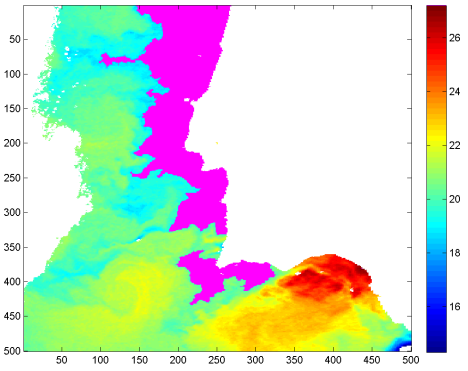

Figure B.19: 1998-08-05 AdamsSRG

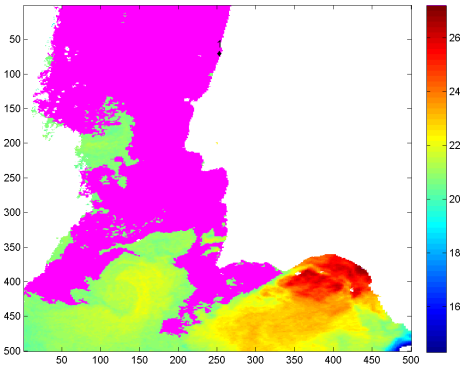

Figure B.20: 1998-08-05 OtsuVermaSRG

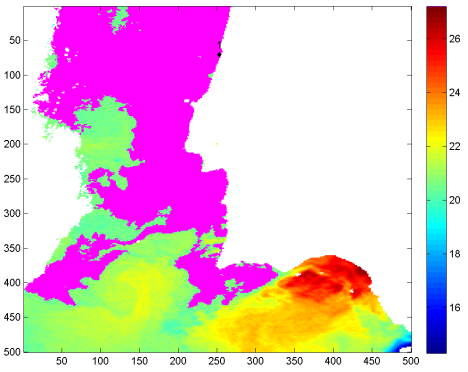

Figure B.21: 1998-08-05 MeanVermaSRG

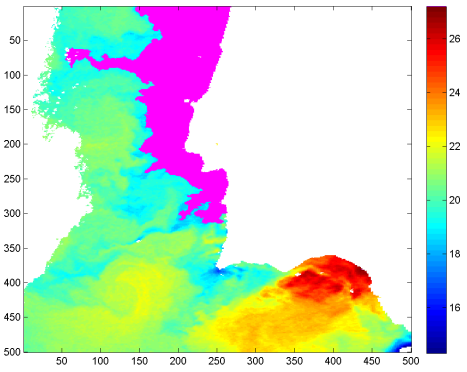

Figure B.22: 1998-08-05 ShihSRG

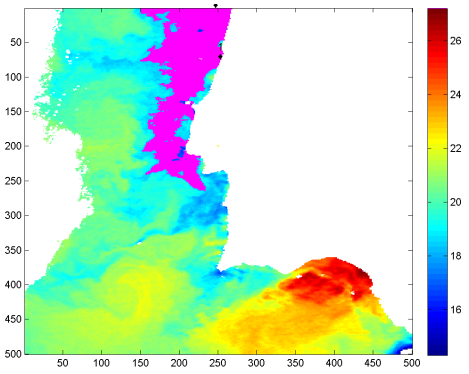

Figure B.23: 1998-08-05 GambottoSRG

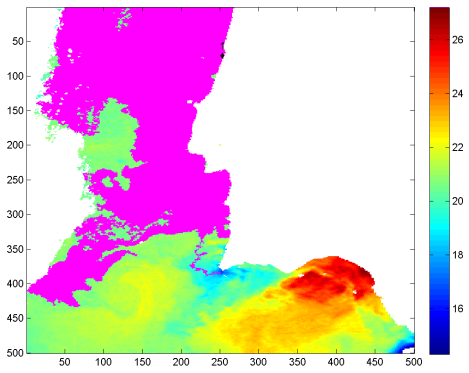

Figure B.24: 1998-08-05 ZanatySRG

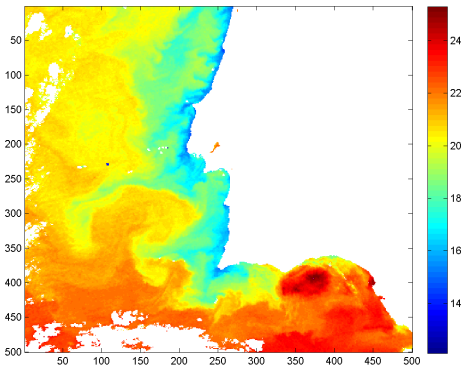

Figure B.25: 1998-09-15

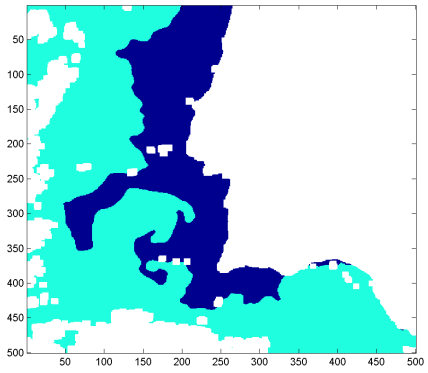

Figure B.26: 1998-09-15 ground-truth map

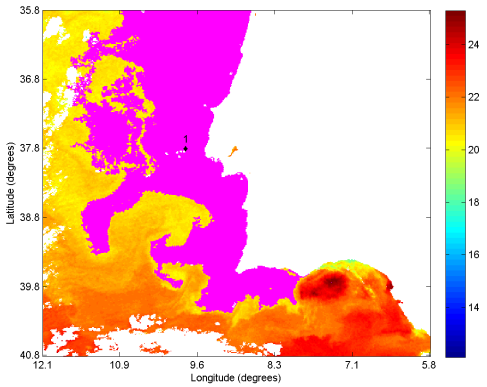

Figure B.27: 1998-09-15 SEC-Otsu

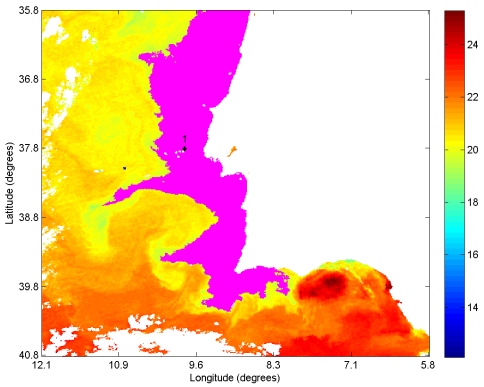

Figure B.28: 1998-09-15 SEC-Kittler

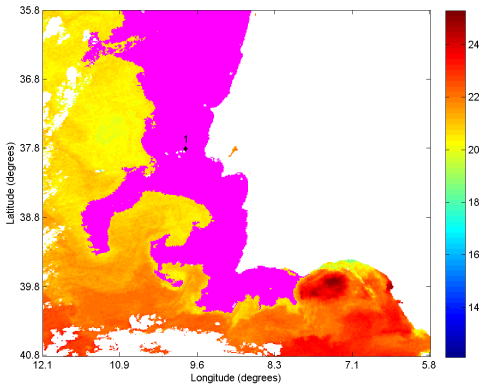

Figure B.29: 1998-09-15 SEC-Ridler

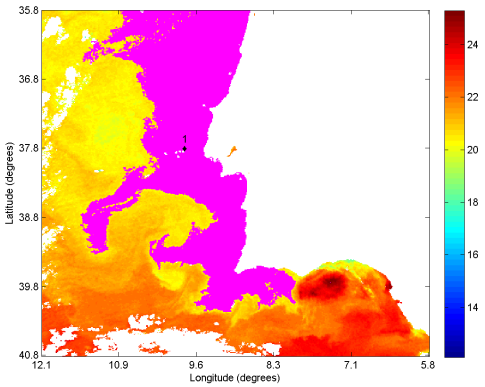

Figure B.30: 1998-09-15 SEC-SelfTuning

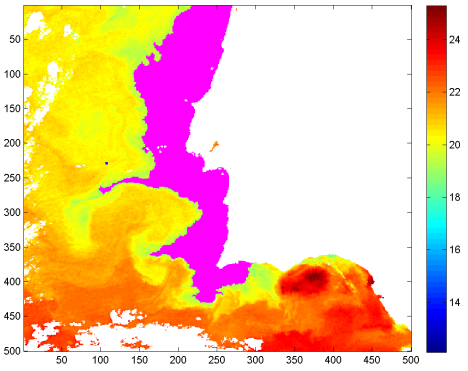

Figure B.31: 1998-09-15 AdamsSRG

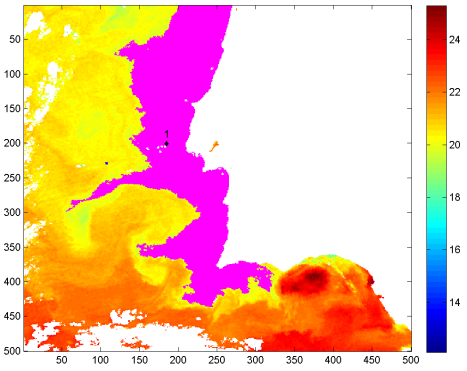

Figure B.32: 1998-09-15 OtsuVermaSRG

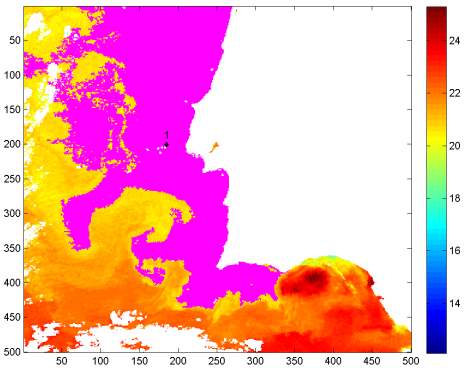

Figure B.33: 1998-09-15 MeanVermaSRG

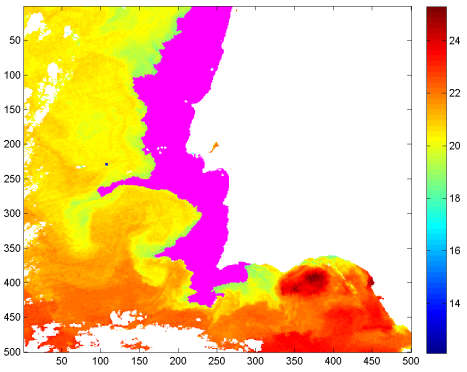

Figure B.34: 1998-09-15 ShihSRG

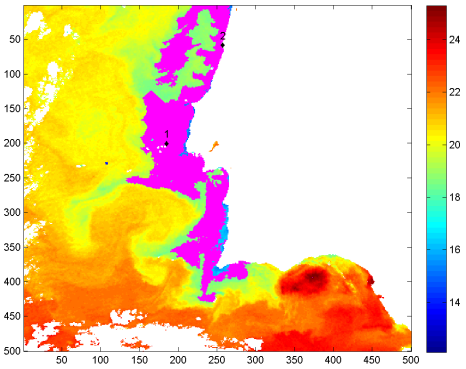

Figure B.35: 1998-09-15 GambottoSRG

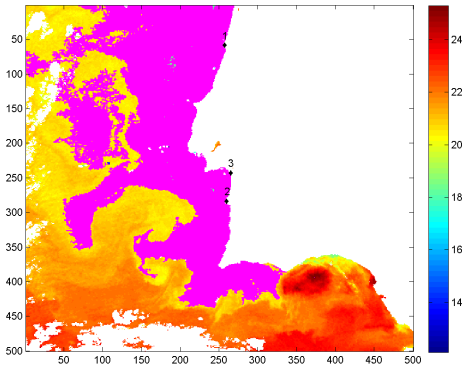

Figure B.36: 1998-09-15 ZanatySRG

B.2 SST Images with GT / Weak Gradients from 1998

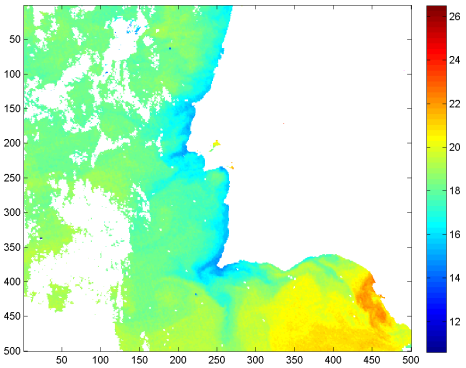

Figure B.37: 1998-06-14

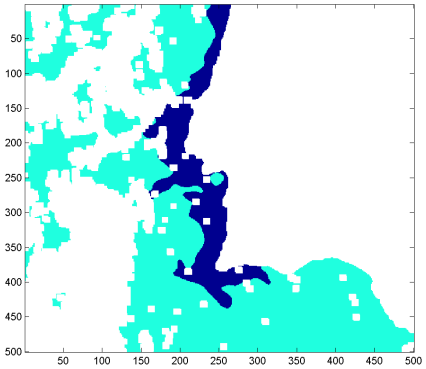

Figure B.38: 1998-06-14 ground-truth map

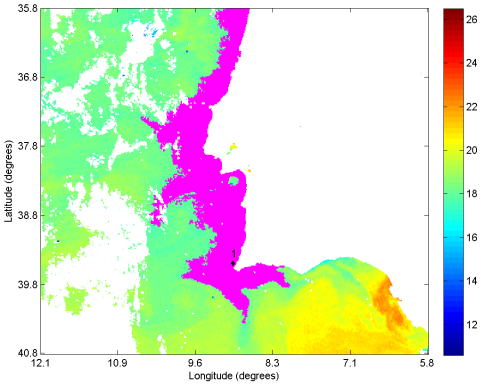

Figure B.39: 1998-06-14 SEC-Otsu

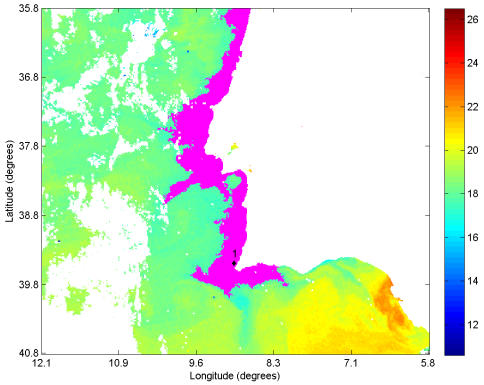

Figure B.40: 1998-06-14 SEC-Kittler

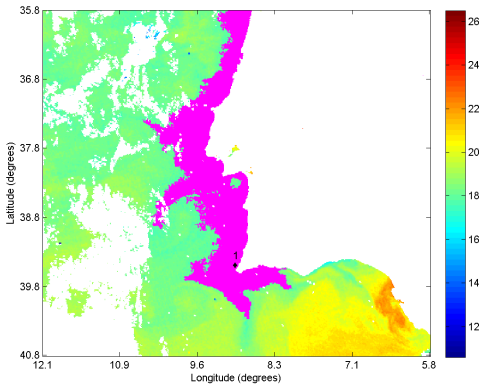

Figure B.41: 1998-06-14 SEC-Ridler

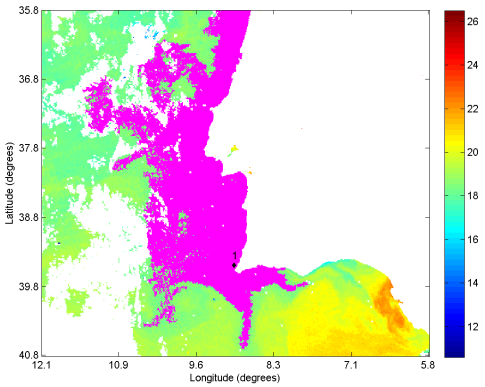

Figure B.42: 1998-06-14 SEC-SelfTuning

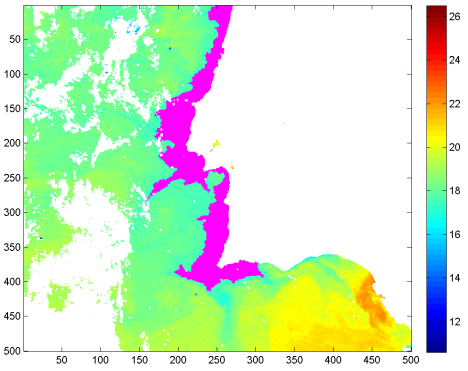

Figure B.43: 1998-06-14 AdamsSRG

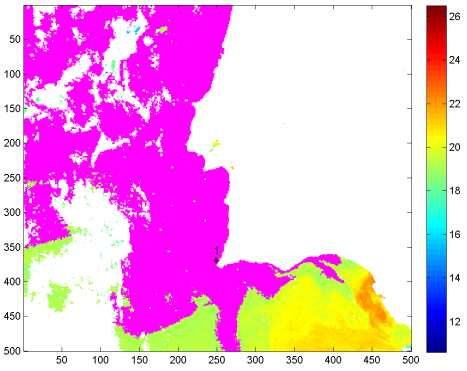

Figure B.44: 1998-06-14 OtsuVermaSRG

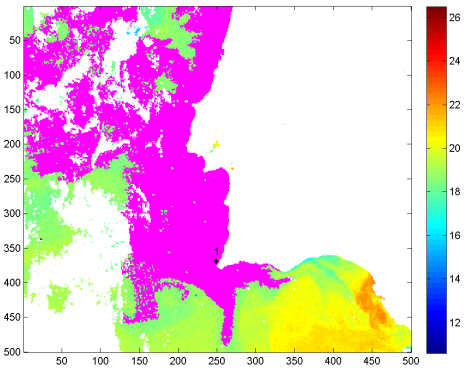

Figure B.45: 1998-06-14 MeanVermaSRG

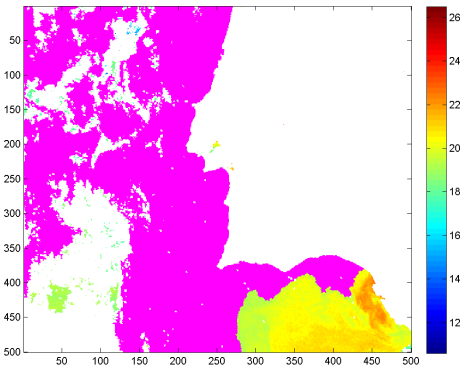

Figure B.46: 1998-06-14 ShihSRG

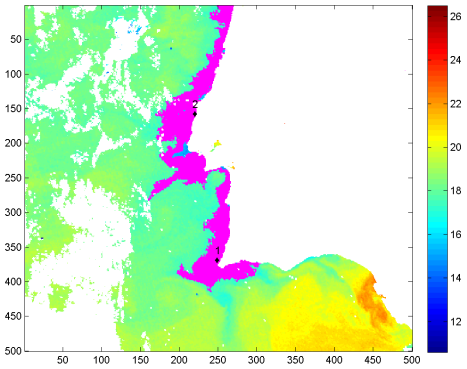

Figure B.47: 1998-06-14 GambottoSRG

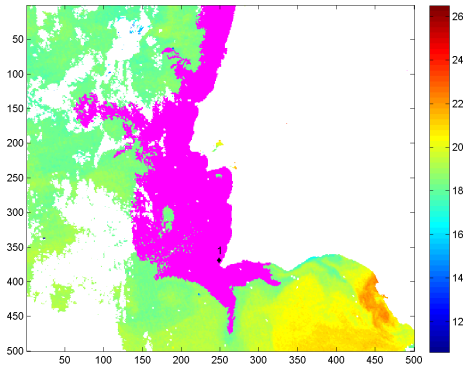

Figure B.48: 1998-06-14 ZanatySRG

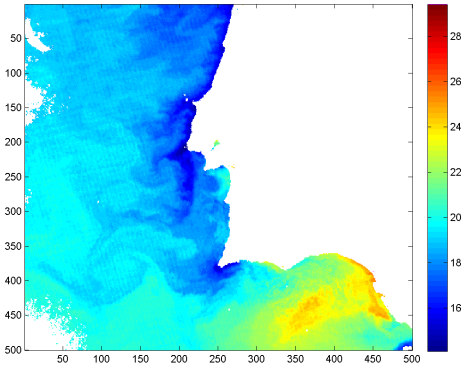

Figure B.49: 1998-07-11

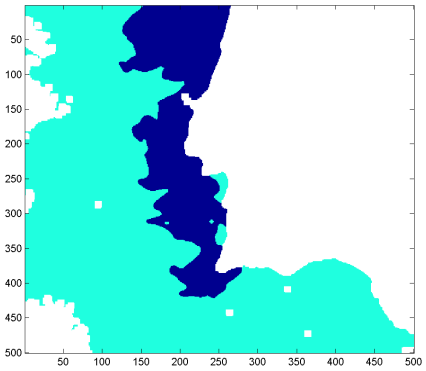

Figure B.50: 1998-07-11 ground-truth map

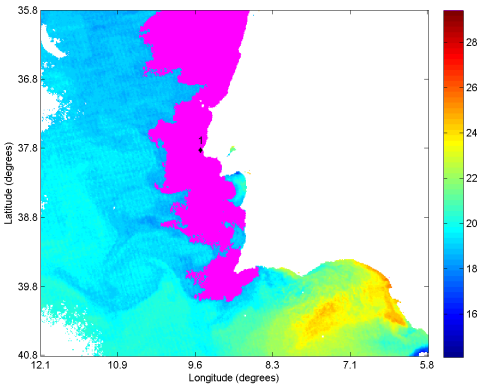

Figure B.51: 1998-07-11 SEC-Otsu

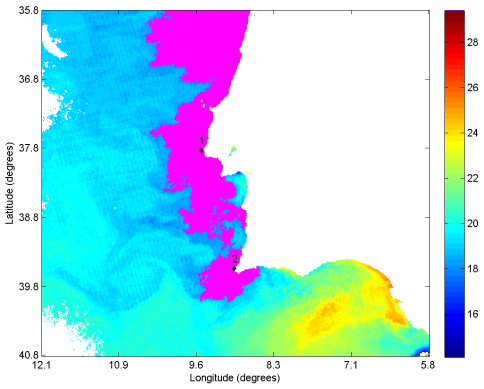

Figure B.52: 1998-07-11 SEC-Kittler

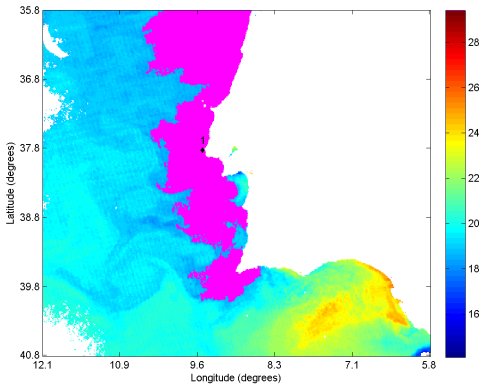

Figure B.53: 1998-07-11 SEC-Ridler

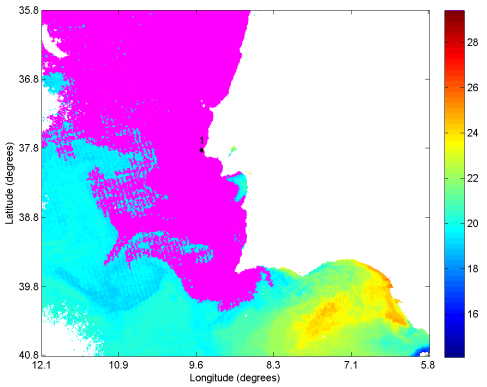

Figure B.54: 1998-07-11 SEC-SelfTuning

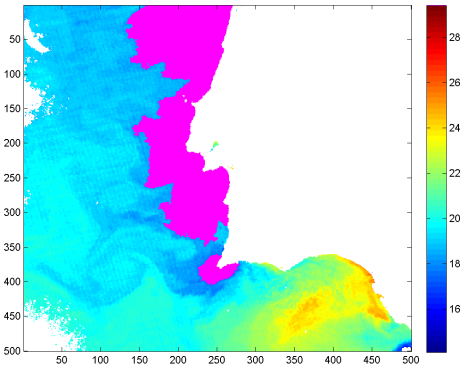

Figure B.55: 1998-07-11 AdamsSRG

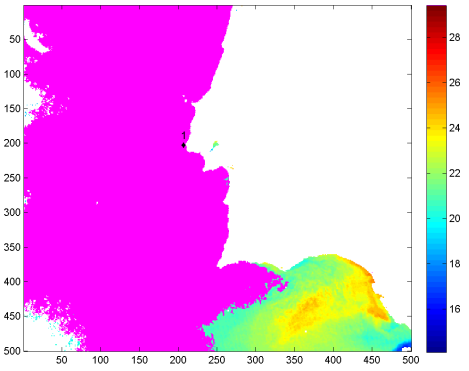

Figure B.56: 1998-07-11 OtsuVermaSRG

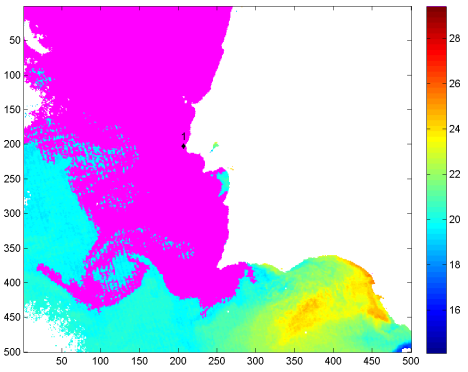

Figure B.57: 1998-07-11 MeanVermaSRG

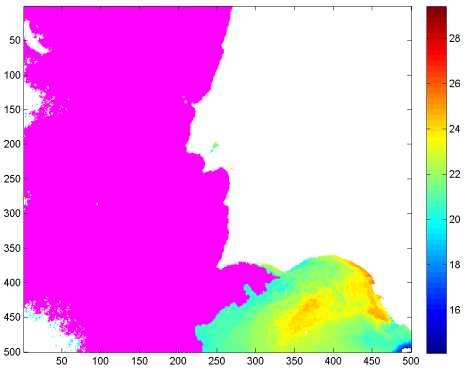

Figure B.58: 1998-07-11 ShihSRG

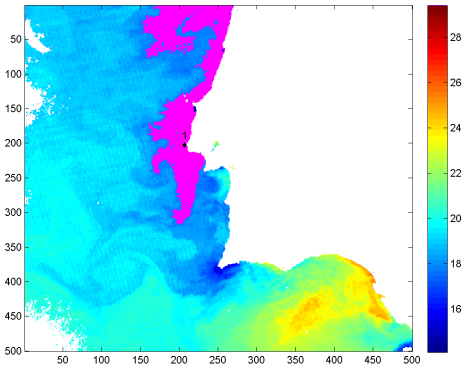

Figure B.59: 1998-07-11 GambottoSRG

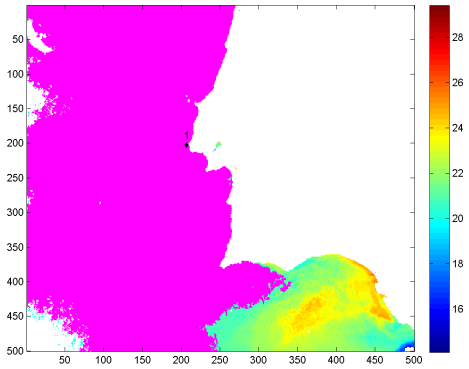

Figure B.60: 1998-07-11 ZanatySRG

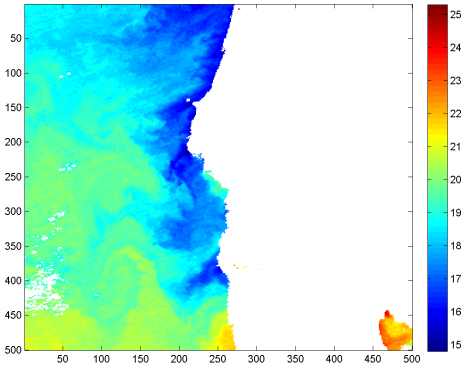

Figure B.61: 1998-07-15

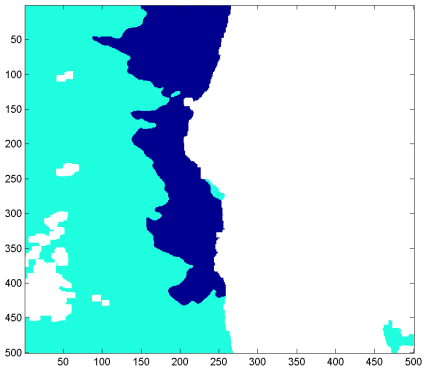

Figure B.62: 1998-07-15 ground-truth map

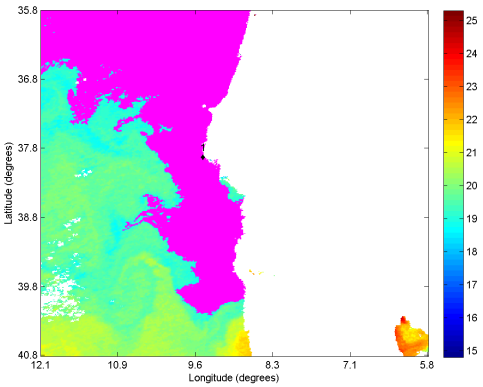

Figure B.63: 1998-07-15 SEC-Otsu

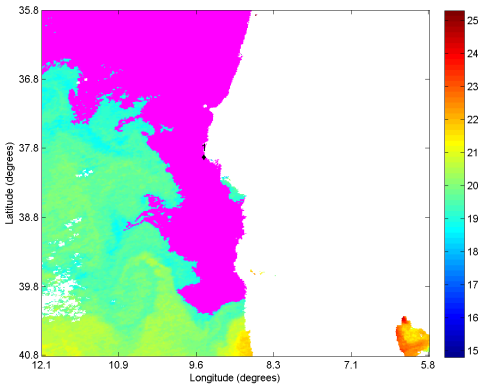

Figure B.64: 1998-07-15 SEC-Kittler

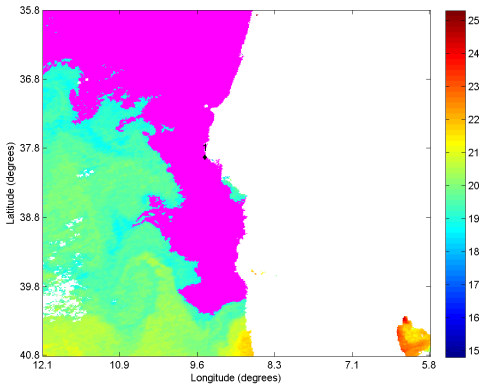

Figure B.65: 1998-07-15 SEC-Ridler

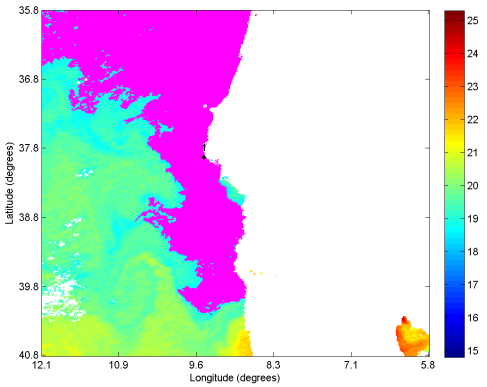

Figure B.66: 1998-07-15 SEC-SelfTuning

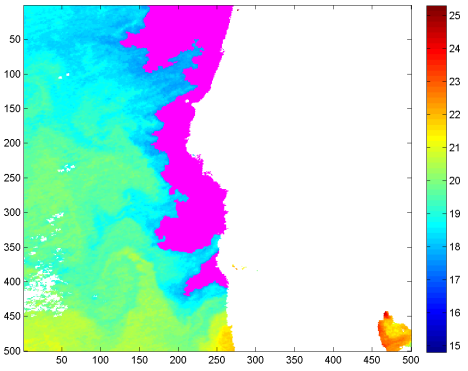

Figure B.67: 1998-07-15 AdamsSRG

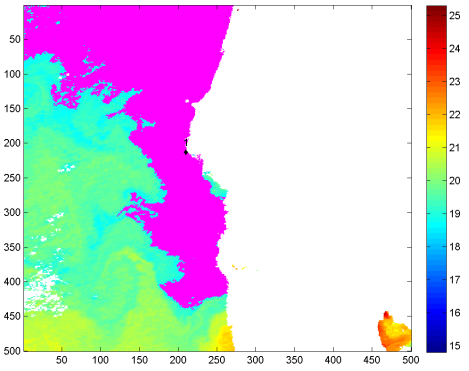

Figure B.68: 1998-07-15 OtsuVermaSRG

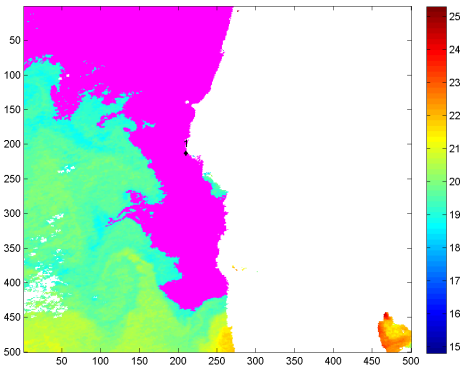

Figure B.69: 1998-07-15 MeanVermaSRG

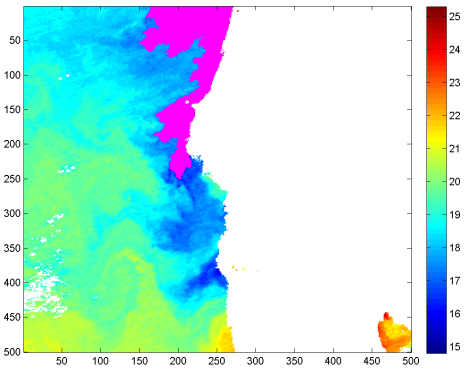

Figure B.70: 1998-07-15 ShihSRG

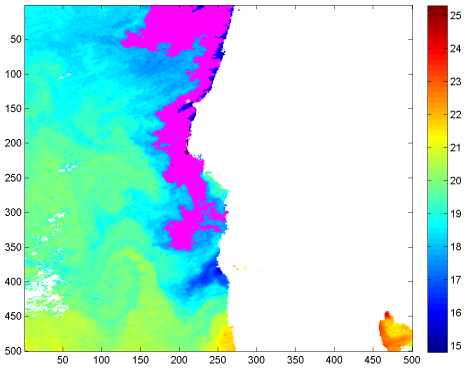

Figure B.71: 1998-07-15 GambottoSRG

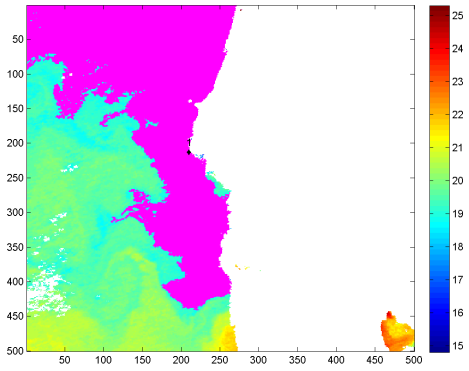

Figure B.72: 1998-07-15 ZanatySRG

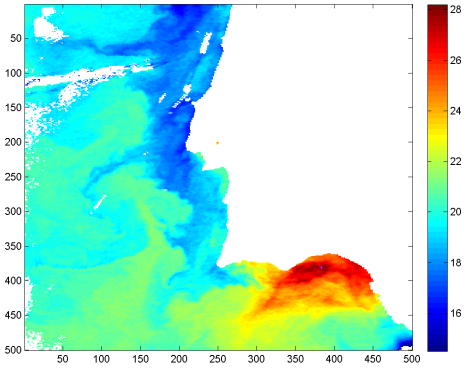

Figure B.73: 1998-08-23

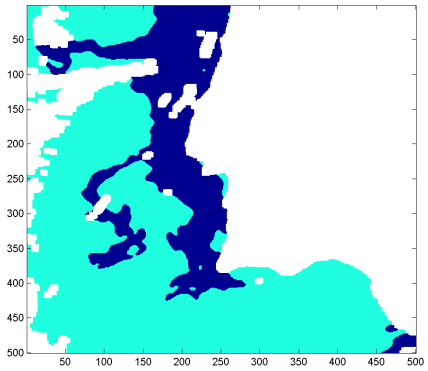

Figure B.74: 1998-08-23 ground-truth map

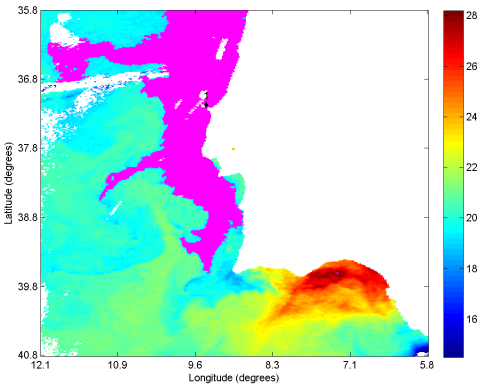

Figure B.75: 1998-08-23 SEC-Otsu

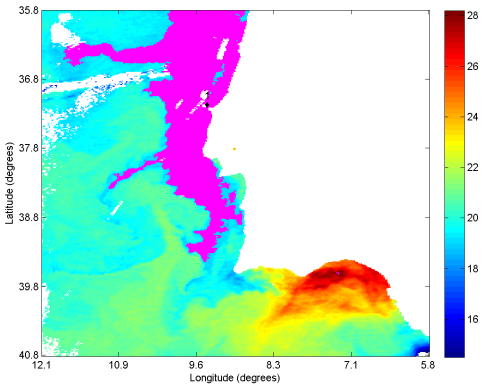

Figure B.76: 1998-08-23 SEC-Kittler

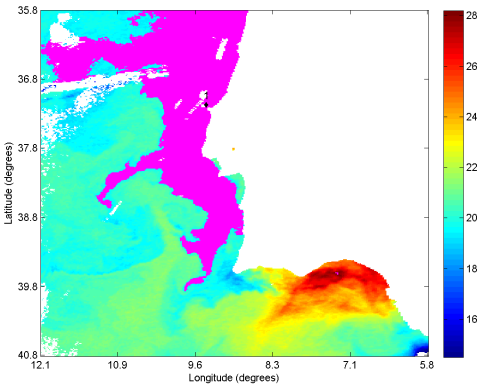

Figure B.77: 1998-08-23 SEC-Ridler

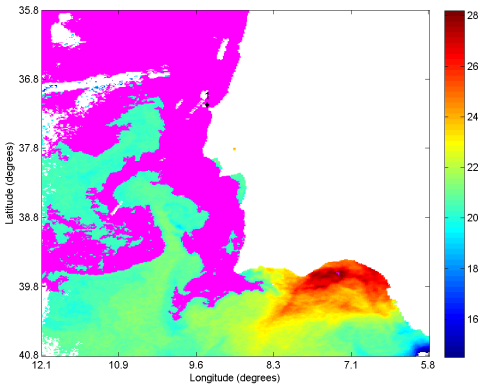

Figure B.78: 1998-08-23 SEC-SelfTuning

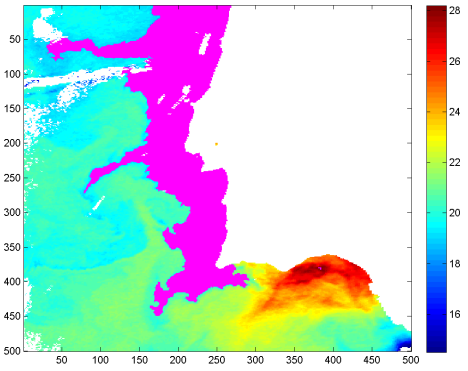

Figure B.79: 1998-08-23 AdamsSRG

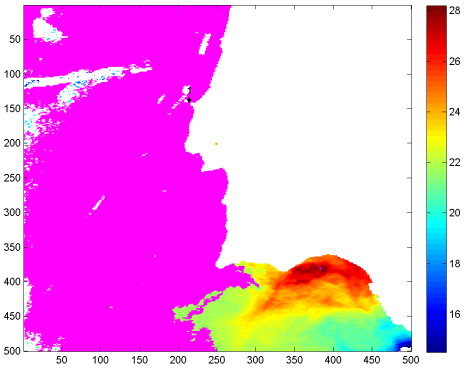

Figure B.80: 1998-08-23 OtsuVermaSRG

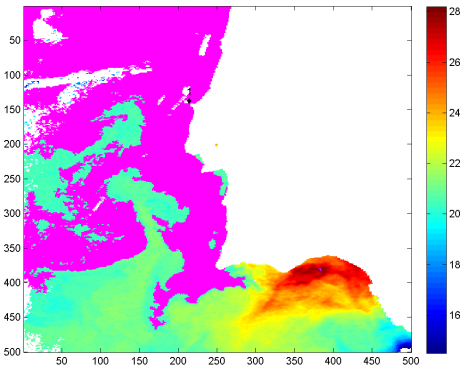

Figure B.81: 1998-08-23 MeanVermaSRG

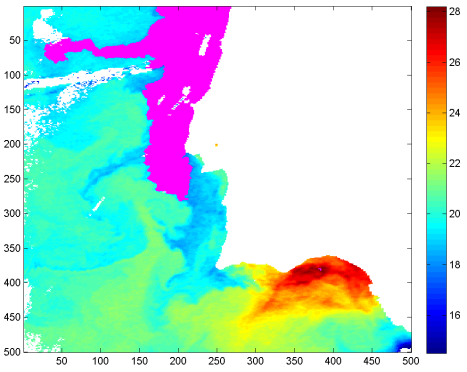

Figure B.82: 1998-08-23 ShihSRG

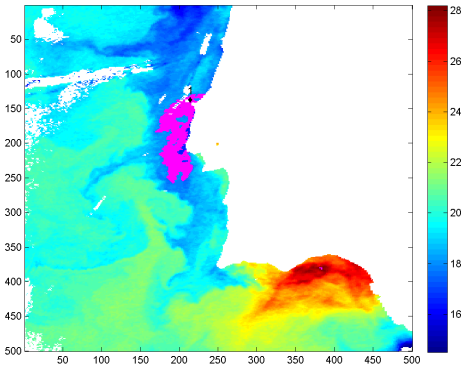

Figure B.83: 1998-08-23 GambottoSRG

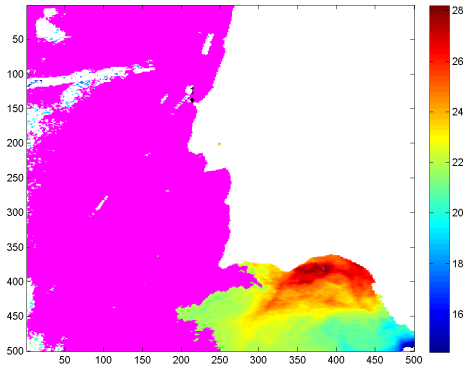

Figure B.84: 1998-08-23 ZanatySRG

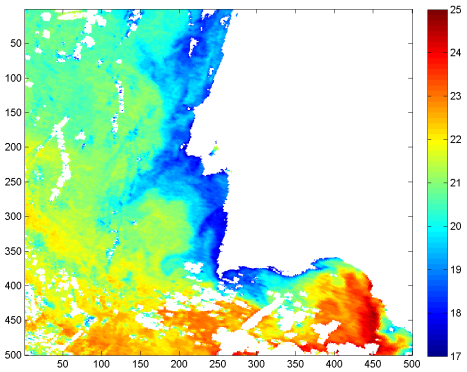

Figure B.85: 1998-09-08

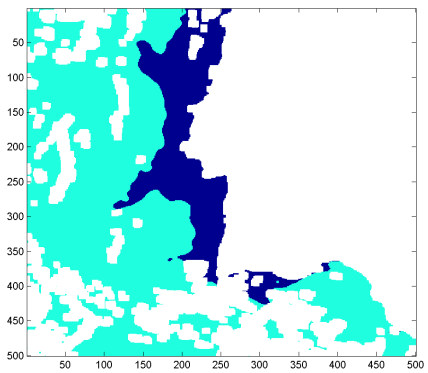

Figure B.86: 1998-09-08 ground-truth map

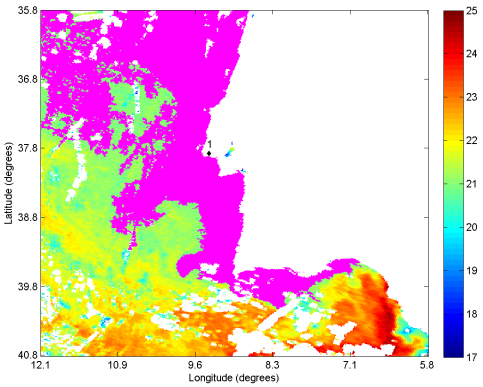

Figure B.87: 1998-09-08 SEC-Otsu

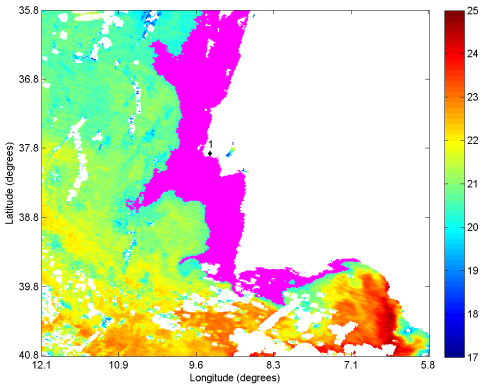

Figure B.88: 1998-09-08 SEC-Kittler

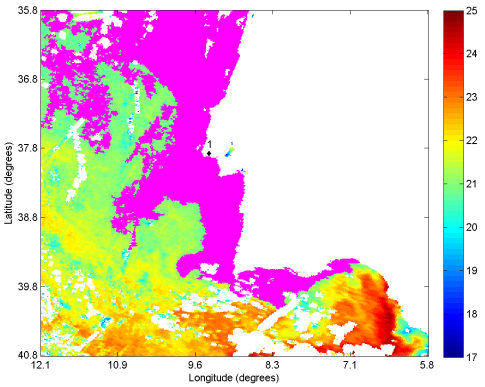

Figure B.89: 1998-09-08 SEC-Ridler

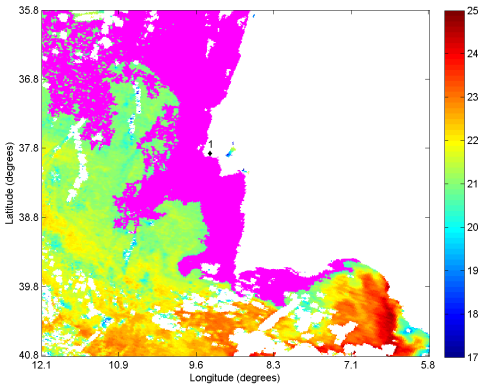

Figure B.90: 1998-09-08 SEC-SelfTuning

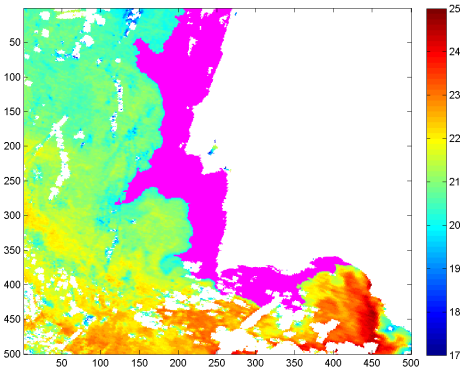

Figure B.91: 1998-09-08 AdamsSRG

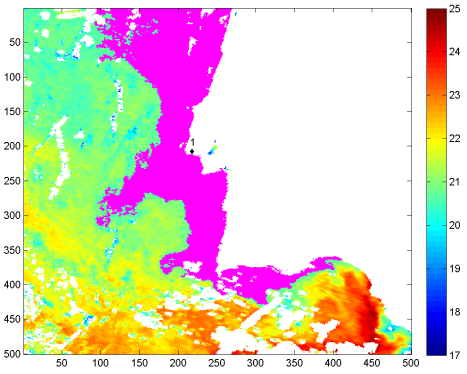

Figure B.92: 1998-09-08 OtsuVermaSRG

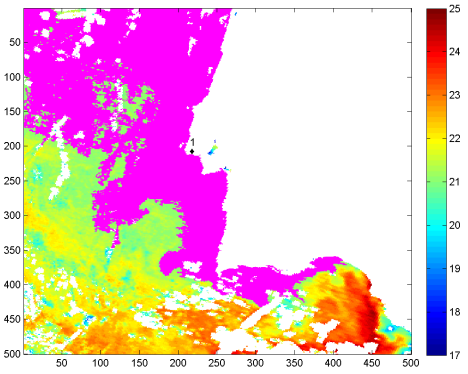

Figure B.93: 1998-09-08 MeanVermaSRG

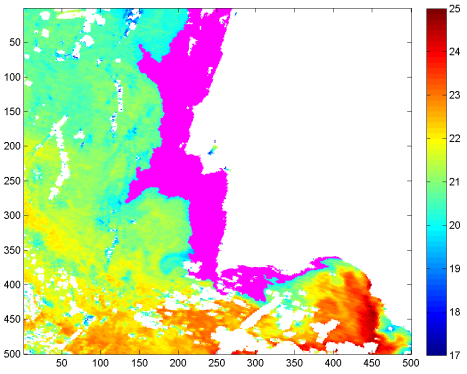

Figure B.94: 1998-09-08 ShihSRG

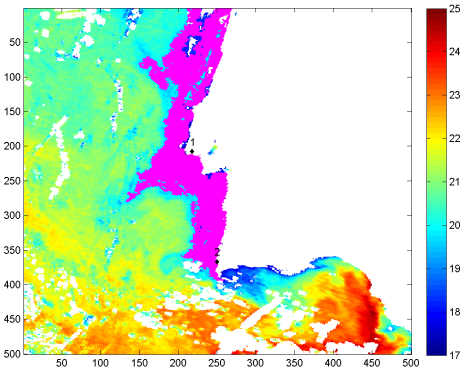

Figure B.95: 1998-09-08 GambottoSRG

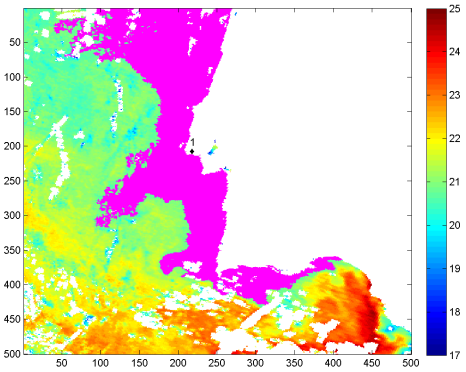

Figure B.96: 1998-09-08 ZanatySRG

B.3 SST Images with GT / Noisy from 1998

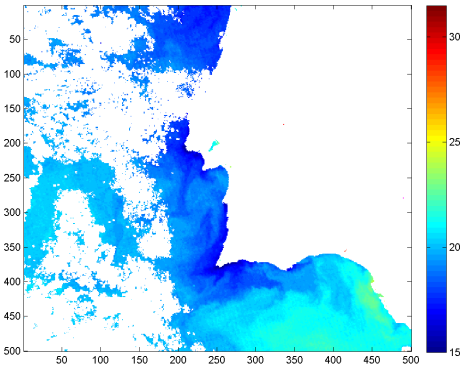

Figure B.97: 1998-07-07

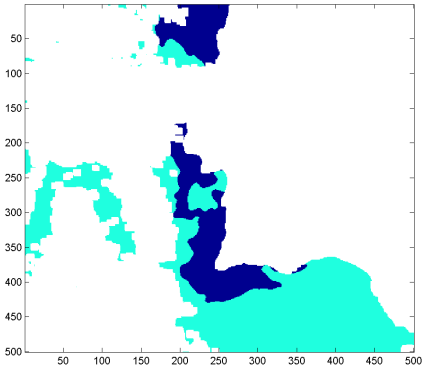

Figure B.98: 1998-07-07 ground-truth map

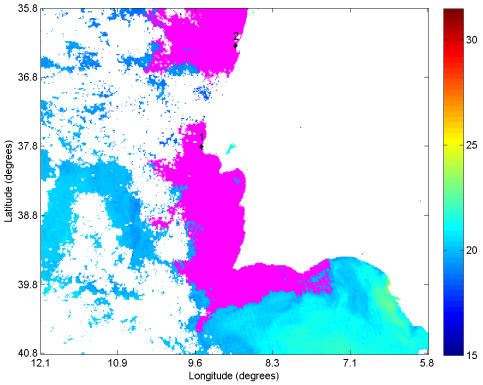

Figure B.99: 1998-07-07 SEC-Otsu

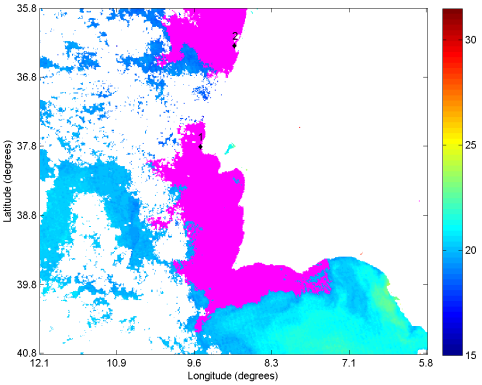

Figure B.100: 1998-07-07 SEC-Kittler

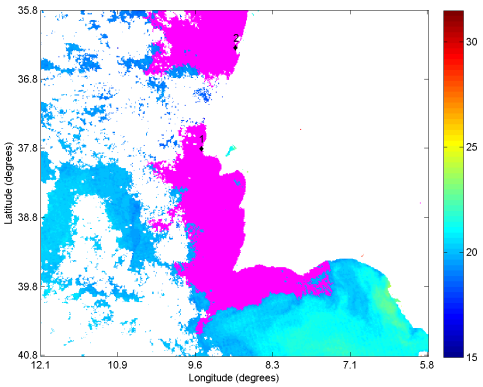

Figure B.101: 1998-07-07 SEC-Ridler

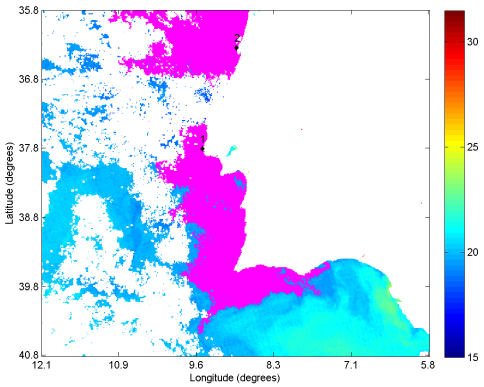

Figure B.102: 1998-07-07 SEC-SelfTuning

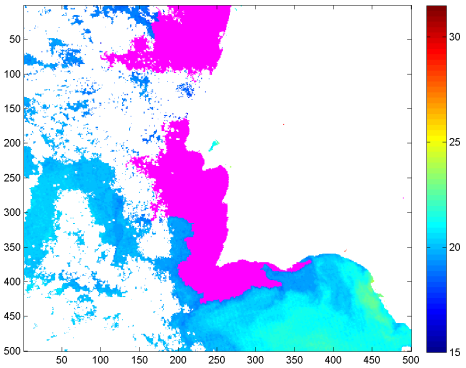

Figure B.103: 1998-07-07 AdamsSRG

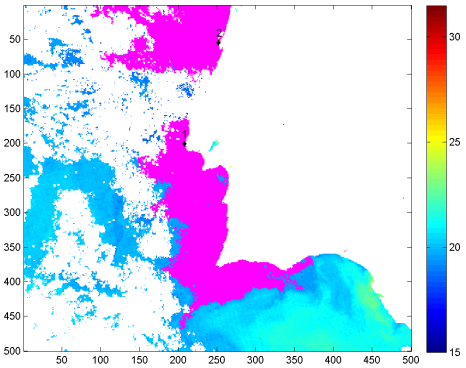

Figure B.104: 1998-07-07 OtsuVermaSRG

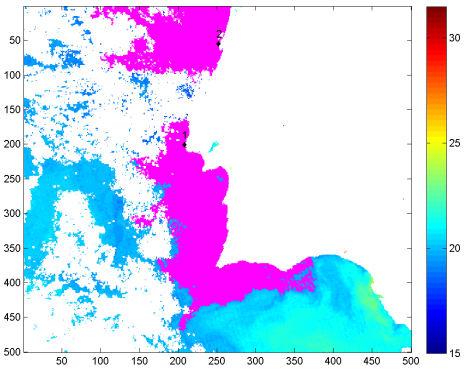

Figure B.105: 1998-07-07 MeanVermaSRG

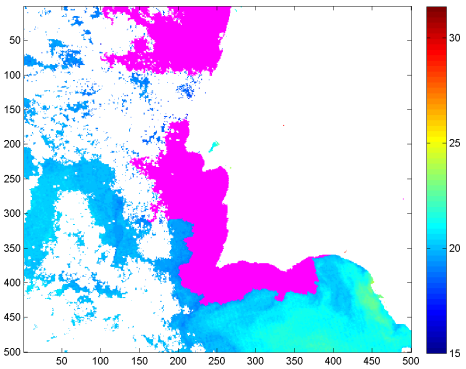

Figure B.106: 1998-07-07 ShihSRG

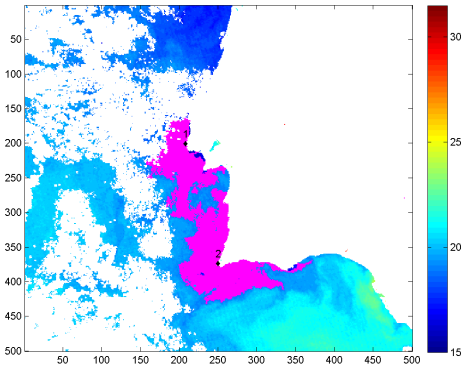

Figure B.107: 1998-07-07 GambottoSRG

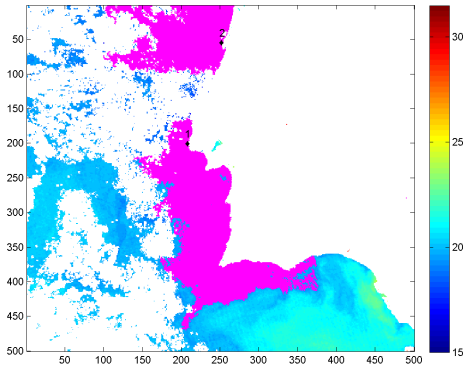

Figure B.108: 1998-07-07 ZanatySRG

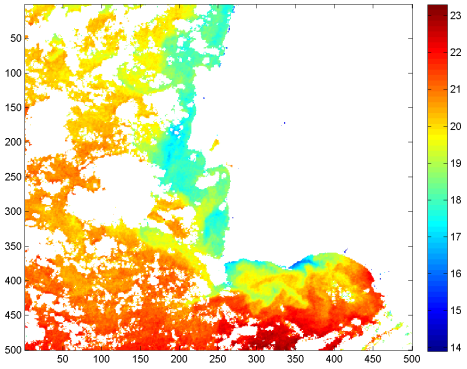

Figure B.109: 1998-09-30

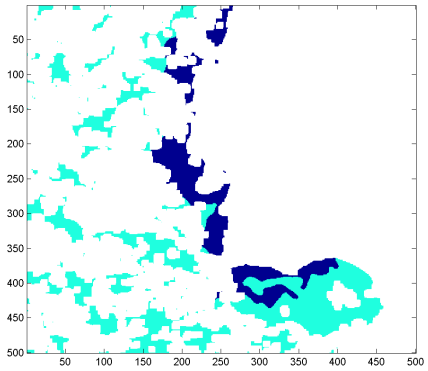

Figure B.110: 1998-09-30 ground-truth map

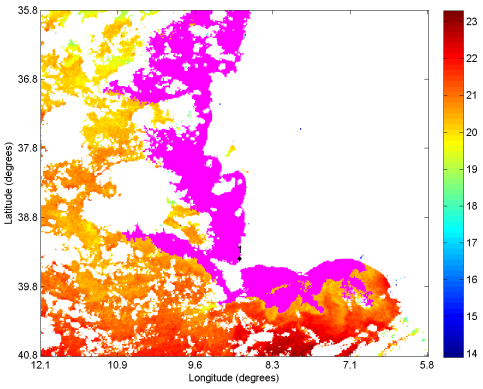

Figure B.111: 1998-09-30 SEC-Otsu

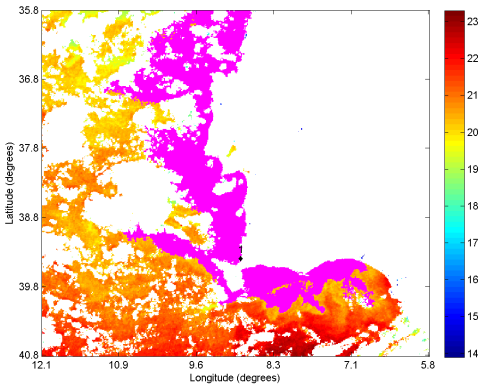

Figure B.112: 1998-09-30 SEC-Kittler

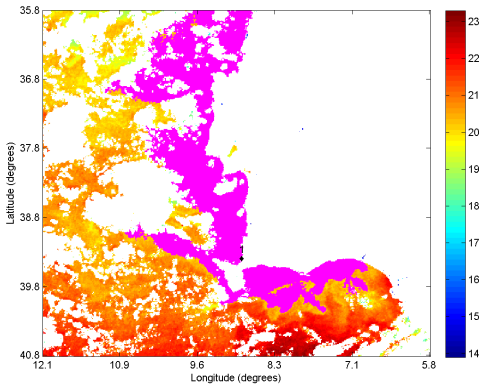

Figure B.113: 1998-09-30 SEC-Ridler

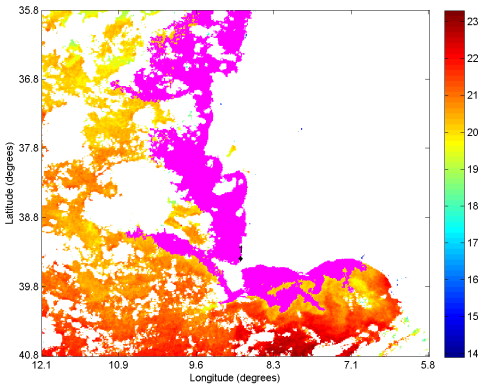

Figure B.114: 1998-09-30 SEC-SelfTuning

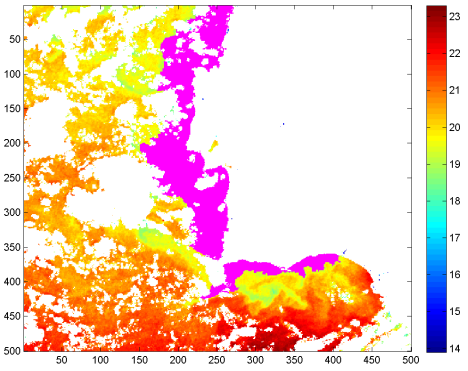

Figure B.115: 1998-09-30 AdamsSRG

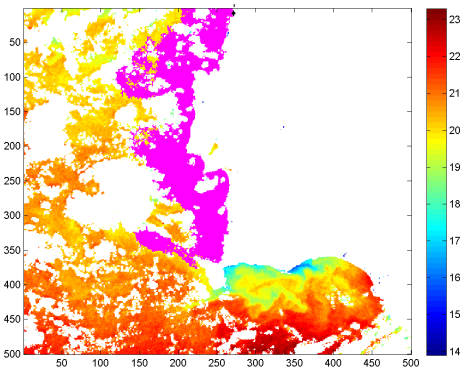

Figure B.116: 1998-09-30 OtsuVermaSRG

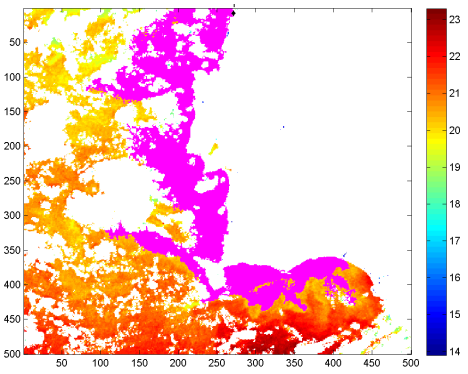

Figure B.117: 1998-09-30 MeanVermaSRG

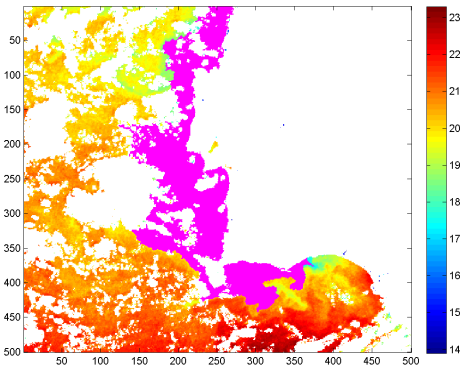

Figure B.118: 1998-09-30 ShihSRG

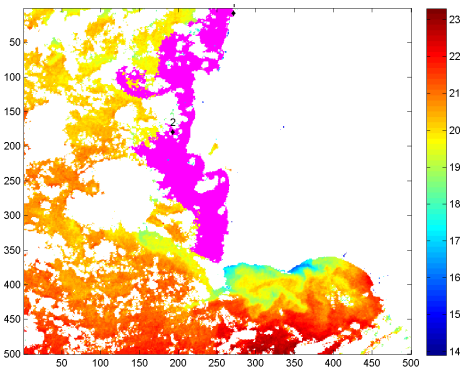

Figure B.119: 1998-09-30 GambottoSRG

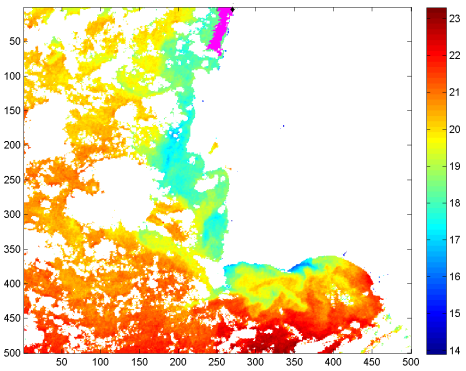

Figure B.120: 1998-09-30 ZanatySRG

B.4 SST Images with GT from 1999

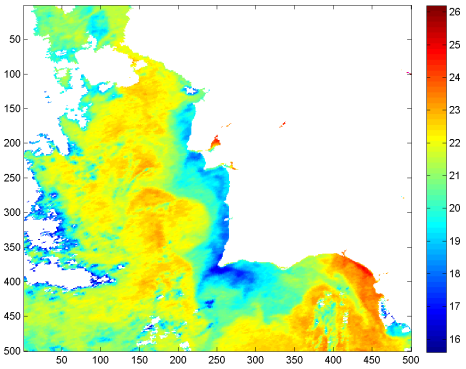

Figure B.121: 1999-09-01

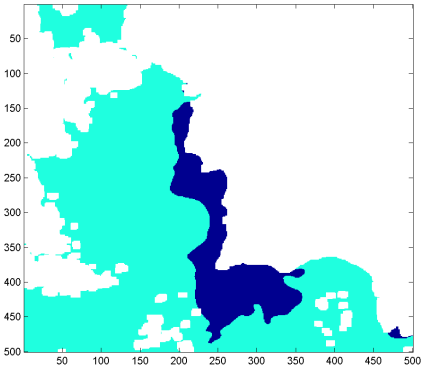

Figure B.122: 1999-09-01 ground-truth map

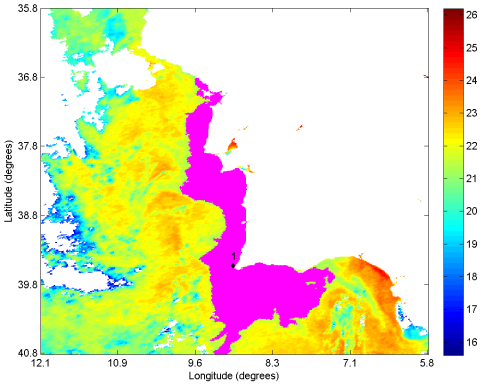

Figure B.123: 1999-09-01 SEC-Otsu

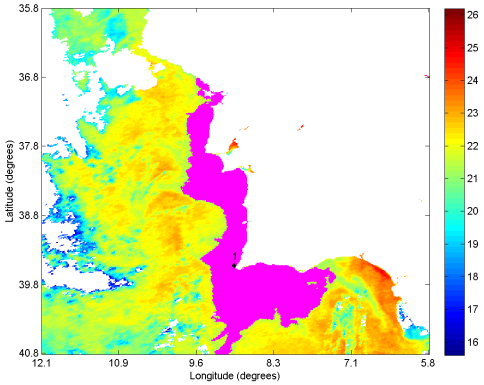

Figure B.124: 1999-09-01 SEC-Kittler

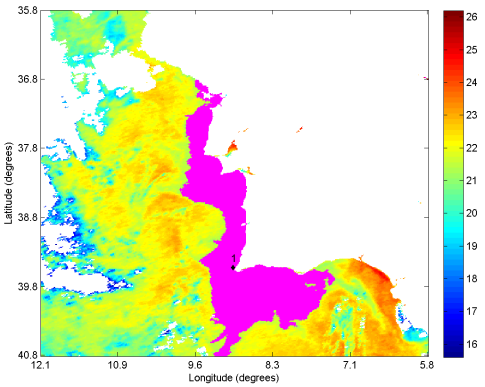

Figure B.125: 1999-09-01 SEC-Ridler

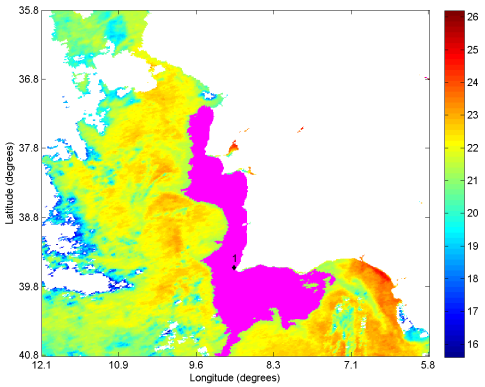

Figure B.126: 1999-09-01 SEC-SelfTuning

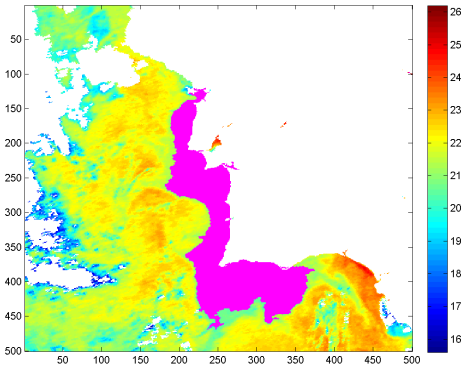

Figure B.127: 1999-09-01 AdamsSRG

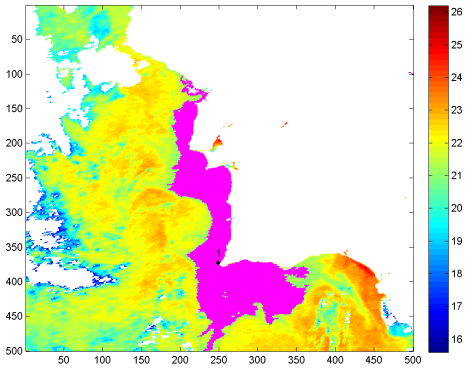

Figure B.128: 1999-09-01 OtsuVermaSRG

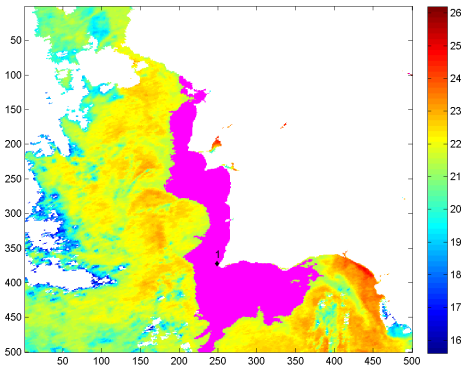

Figure B.129: 1999-09-01 MeanVermaSRG

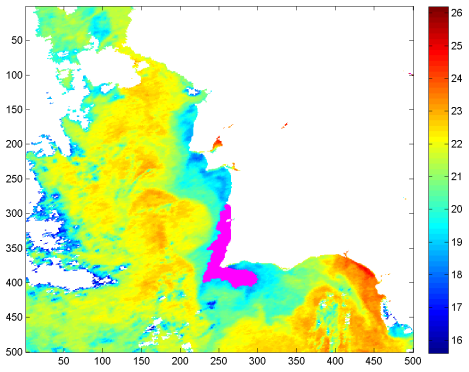

Figure B.130: 1999-09-01 ShihSRG

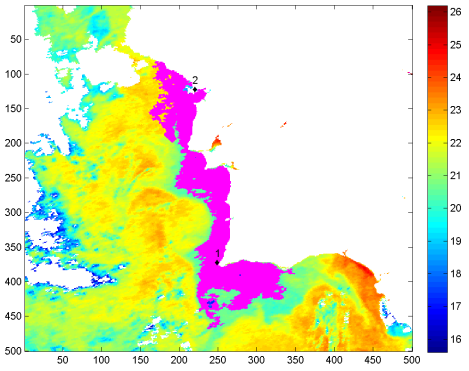

Figure B.131: 1999-09-01 GambottoSRG

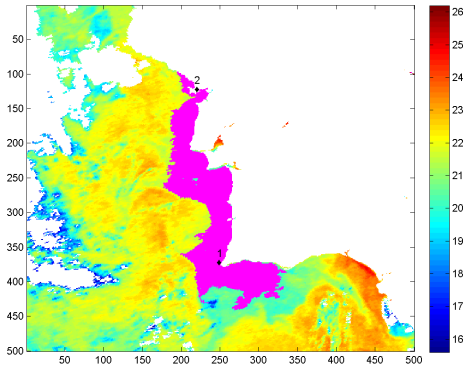

Figure B.132: 1999-09-01 ZanatySRG

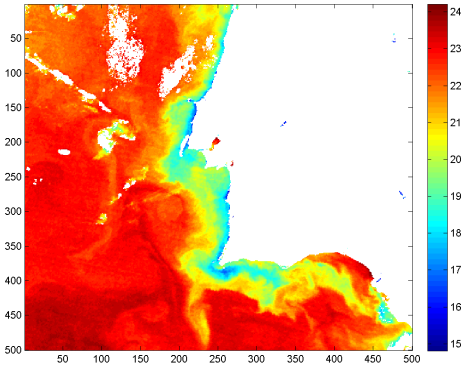

Figure B.133: 1999-09-10

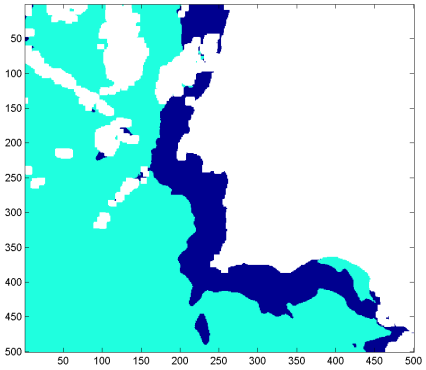

Figure B.134: 1999-09-10 ground-truth map

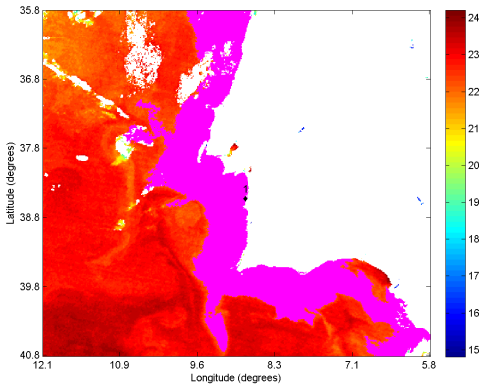

Figure B.135: 1999-09-10 SEC-Otsu

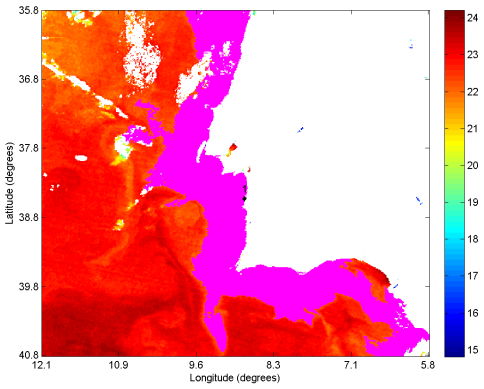

Figure B.136: 1999-09-10 SEC-Kittler

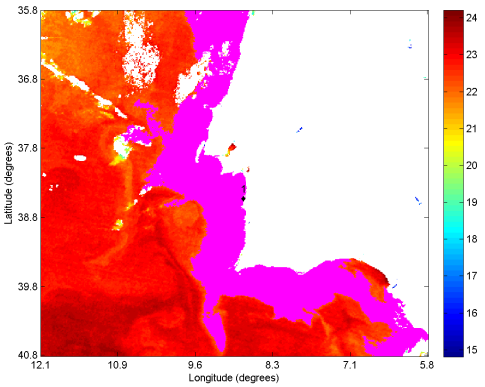

Figure B.137: 1999-09-10 SEC-Ridler

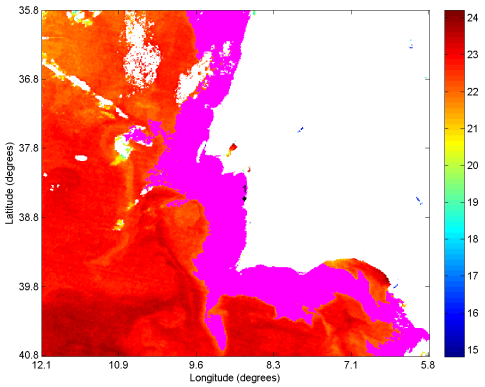

Figure B.138: 1999-09-10 SEC-SelfTuning

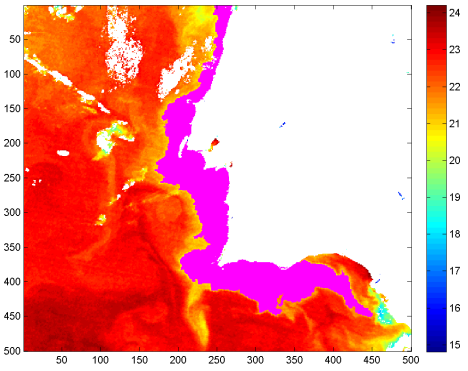

Figure B.139: 1999-09-10 AdamsSRG

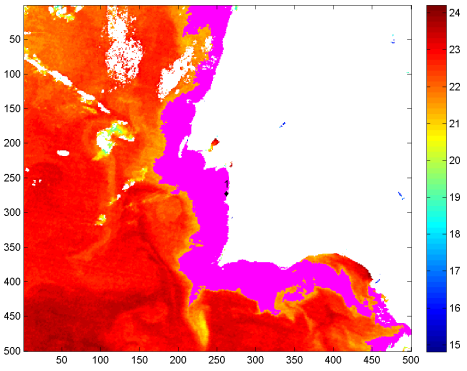

Figure B.140: 1999-09-10 OtsuVermaSRG

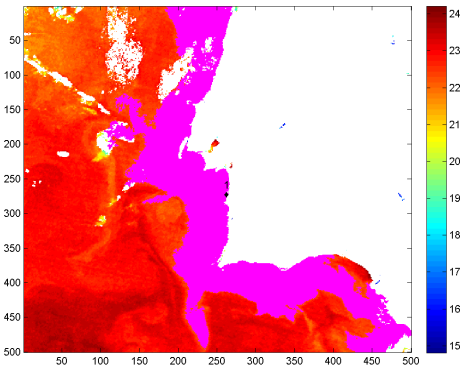

Figure B.141: 1999-09-10 MeanVermaSRG

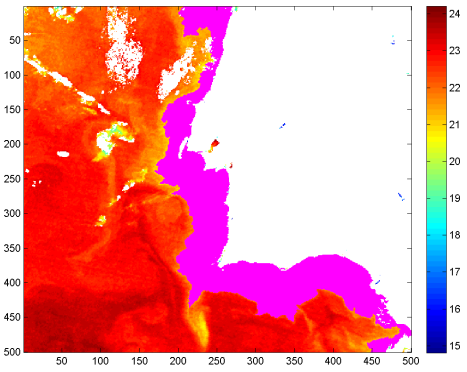

Figure B.142: 1999-09-10 ShihSRG

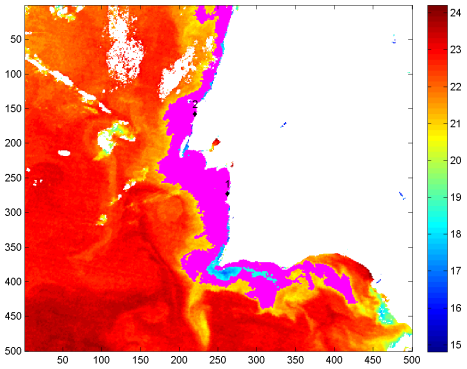

Figure B.143: 1999-09-10 GambottoSRG

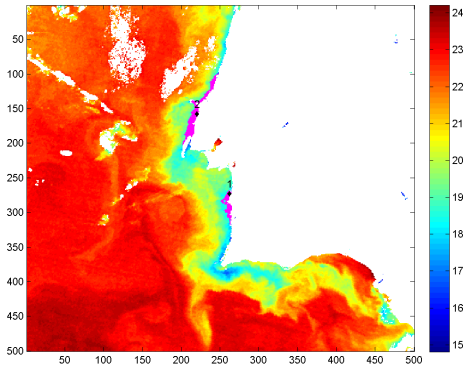

Figure B.144: 1999-09-10 ZanatySRG

B.5 SST Images without ground-truth (NGT) from 1998

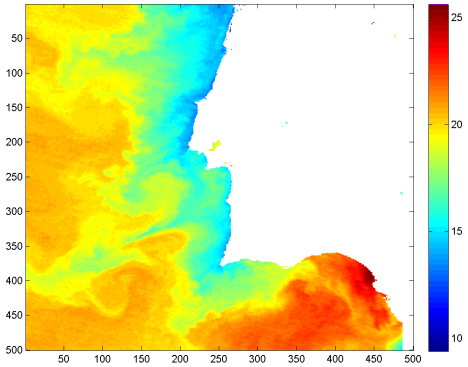

Figure B.145: 1998-08-04

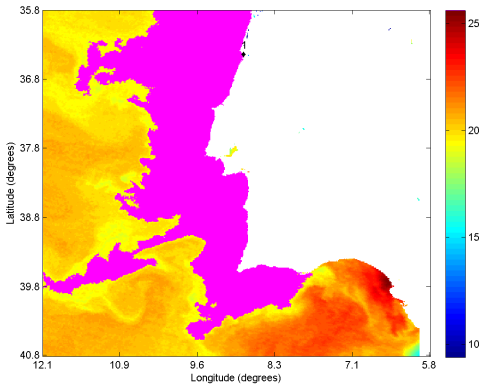

Figure B.146: 1998-08-04 SEC-Otsu

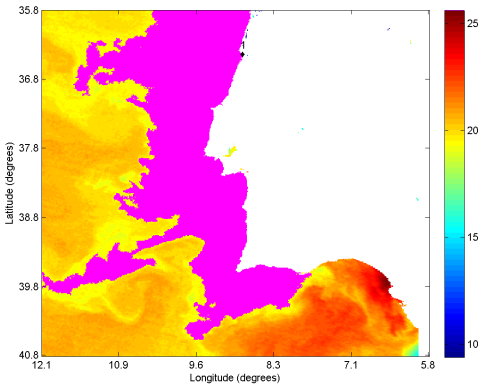

Figure B.147: 1998-08-04 SEC-Kittler

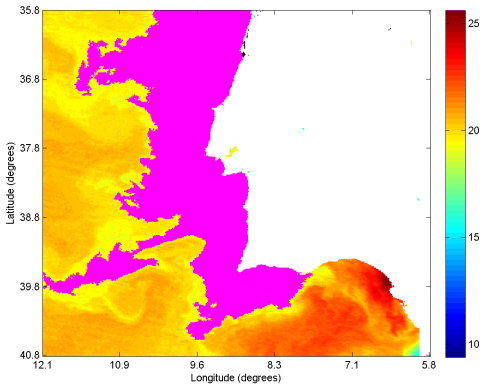

Figure B.148: 1998-08-04 SEC-Ridler

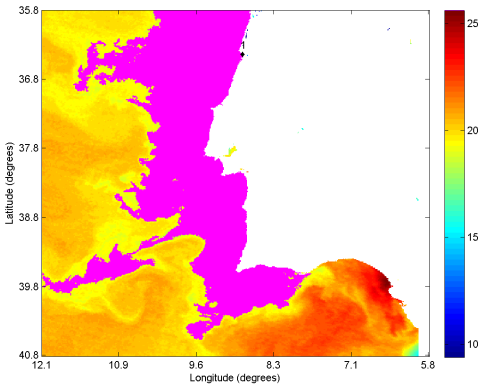

Figure B.149: 1998-08-04 SEC-SelfTuning

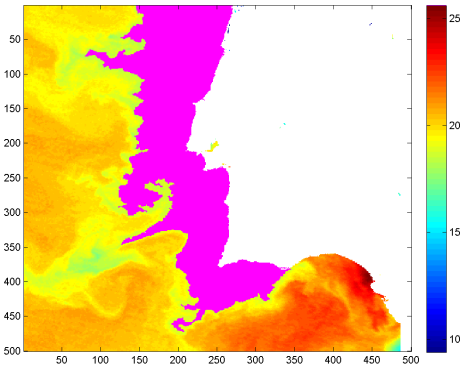

Figure B.150: 1998-08-04 AdamsSRG

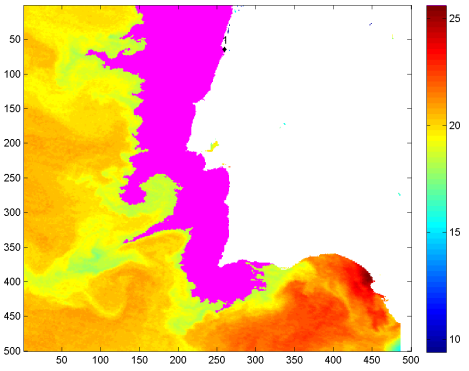

Figure B.151: 1998-08-04 OtsuVermaSRG

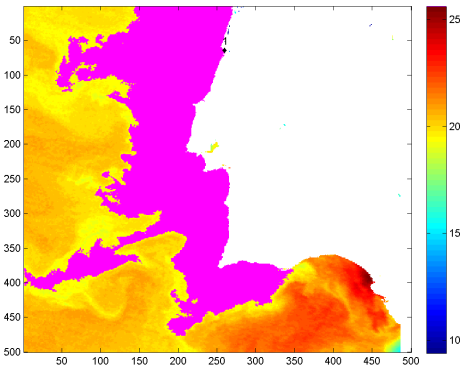

Figure B.152: 1998-08-04 MeanVermaSRG

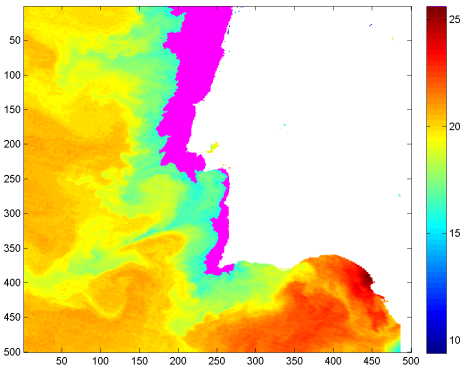

Figure B.153: 1998-08-04 ShihSRG

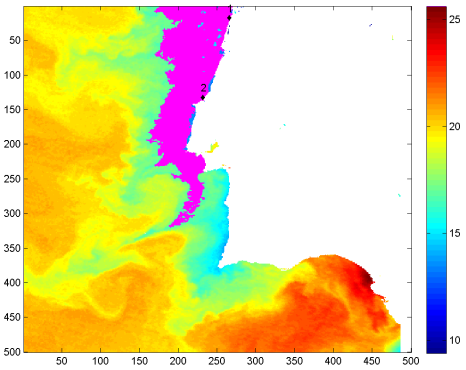

Figure B.154: 1998-08-04 GambottoSRG

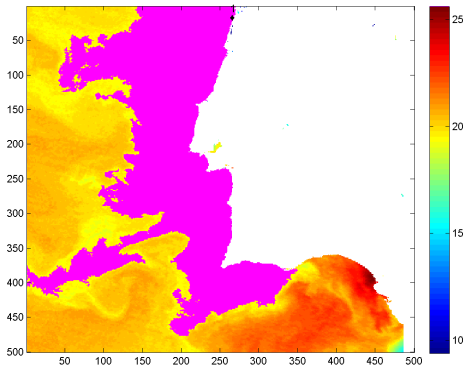

Figure B.155: 1998-08-04 ZanatySRG

B.6 SST Images NGT from 2000

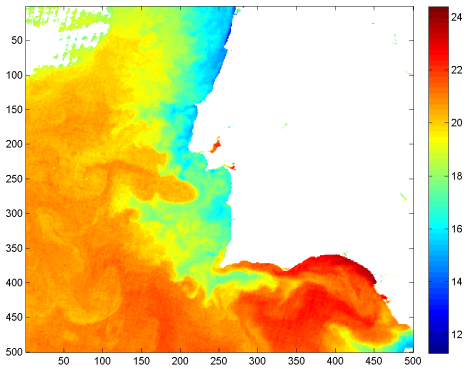

Figure B.156: 2000-08-08

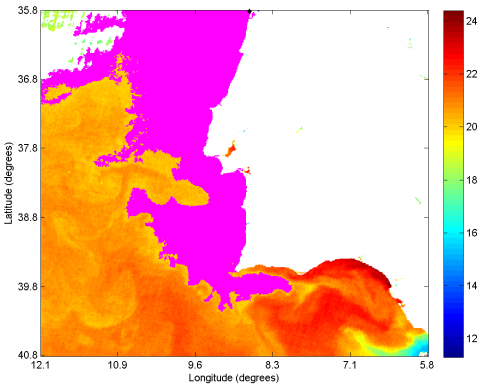

Figure B.157: 2000-08-08 SEC-Otsu

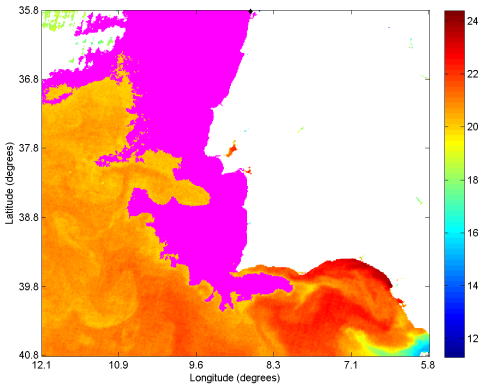

Figure B.158: 2000-08-08 SEC-Kittler

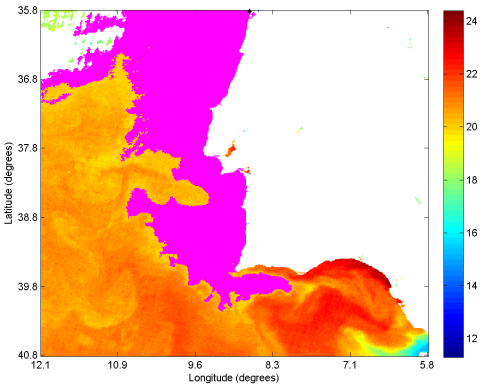

Figure B.159: 2000-08-08 SEC-Ridler

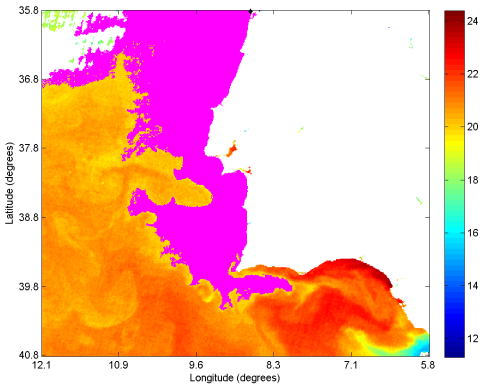

Figure B.160: 2000-08-08 SEC-SelfTuning

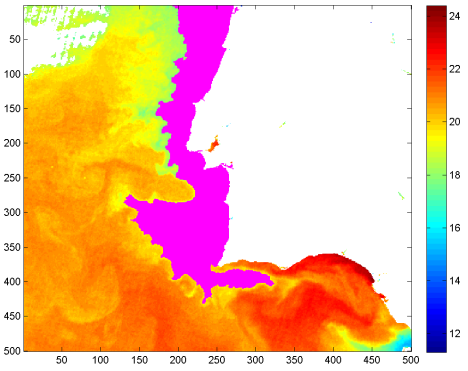

Figure B.161: 2000-08-08 AdamsSRG

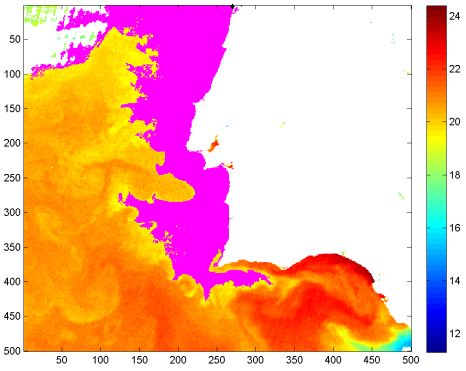

Figure B.162: 2000-08-08 OtsuVermaSRG

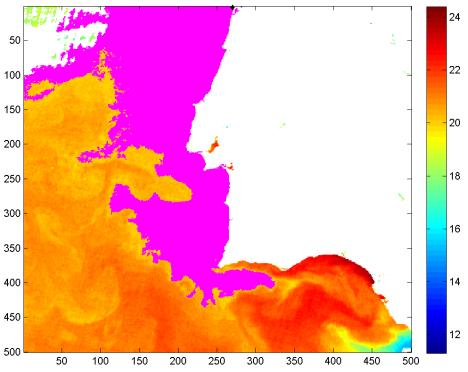

Figure B.163: 2000-08-08 MeanVermaSRG

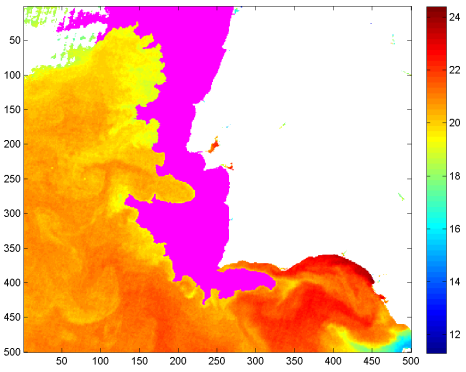

Figure B.164: 2000-08-08 ShihSRG

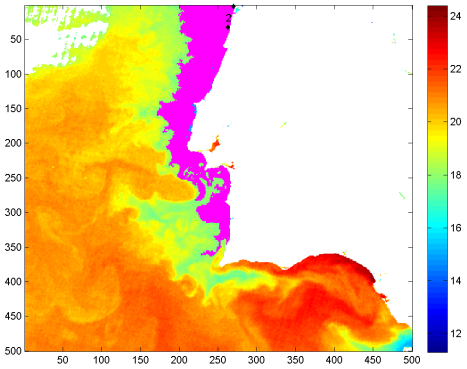

Figure B.165: 2000-08-08 GambottoSRG

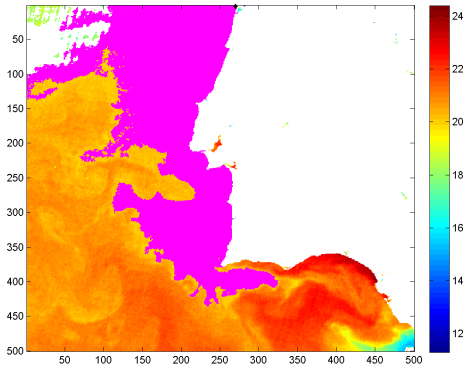

Figure B.166: 2000-08-08 ZanatySRG

B.7 SST Images NGT from 2001

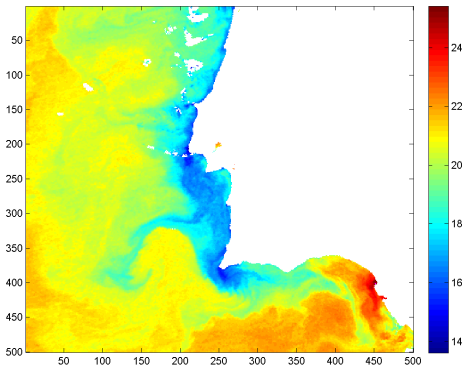

Figure B.167: 2001-08-04

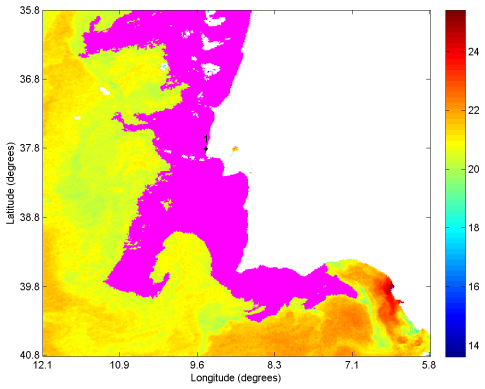

Figure B.168: 2001-08-04 SEC-Otsu

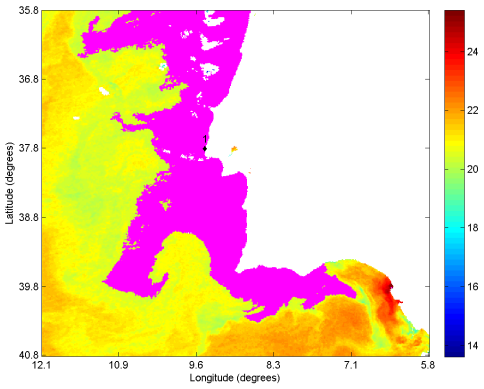

Figure B.169: 2001-08-04 SEC-Kittler

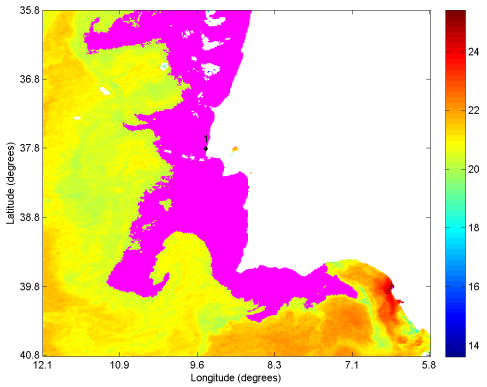

Figure B.170: 2001-08-04 SEC-Ridler

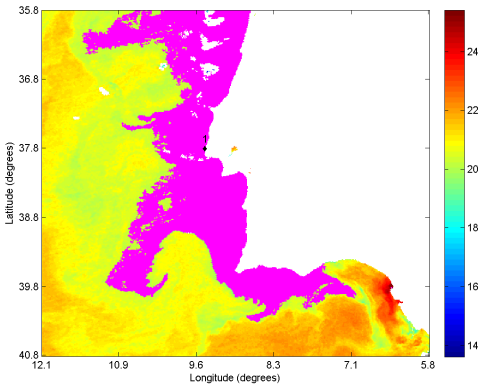

Figure B.171: 2001-08-04 SEC-SelfTuning

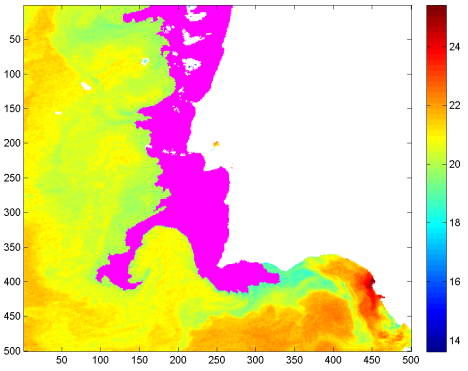

Figure B.172: 2001-08-04 AdamsSRG

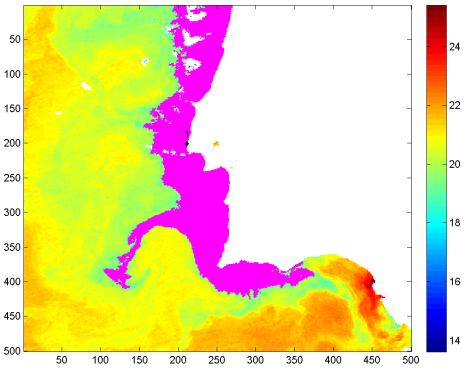

Figure B.173: 2001-08-04 OtsuVermaSRG

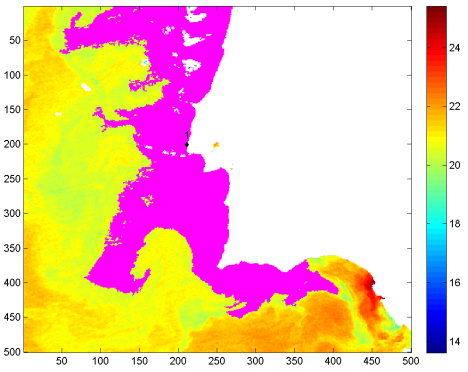

Figure B.174: 2001-08-04 MeanVermaSRG

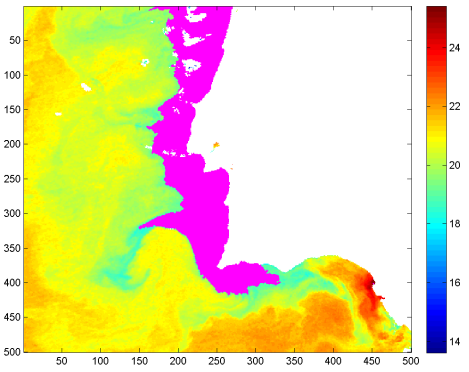

Figure B.175: 2001-08-04 ShihSRG

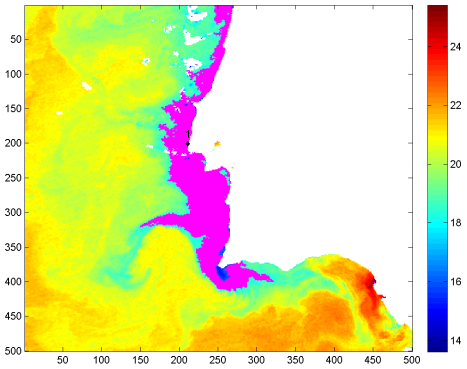

Figure B.176: 2001-08-04 GambottoSRG

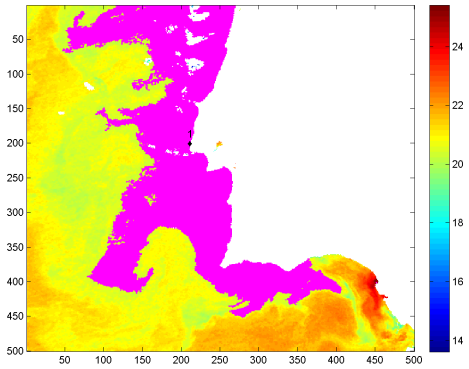

Figure B.177: 2001-08-04 ZanatySRG

B.8 SST Images NGT from 2002

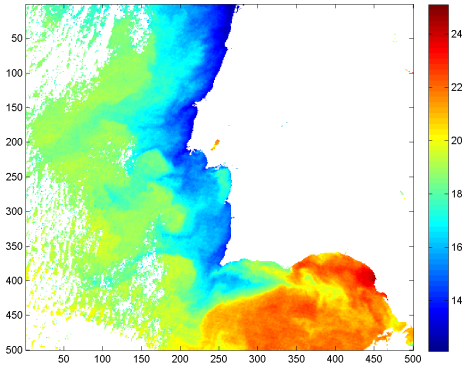

Figure B.178: 2002-07-31

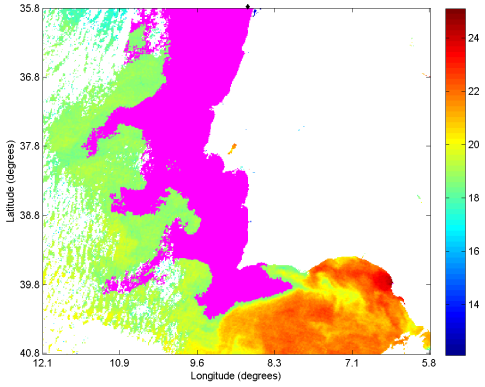

Figure B.179: 2002-07-31 SEC-Otsu

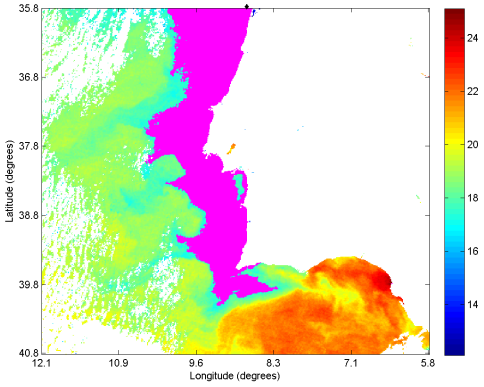

Figure B.180: 2002-07-31 SEC-Kittler

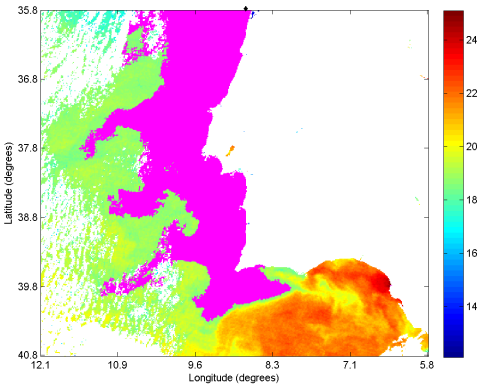

Figure B.181: 2002-07-31 SEC-Ridler

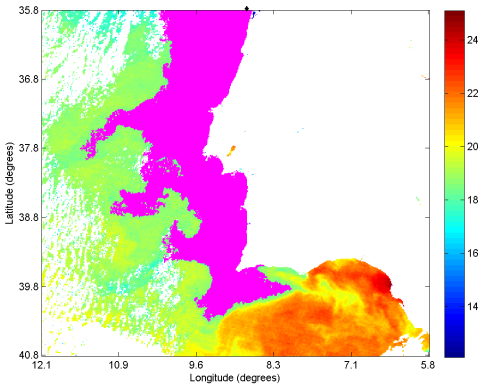

Figure B.182: 2002-07-31 SEC-SelfTuning

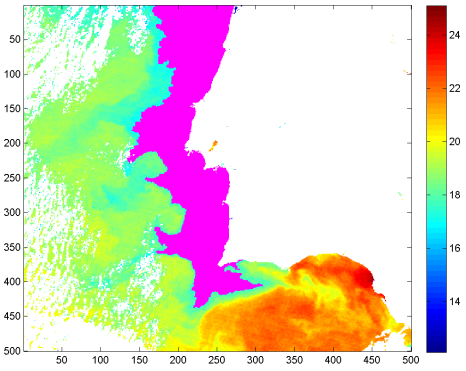

Figure B.183: 2002-07-31 AdamsSRG

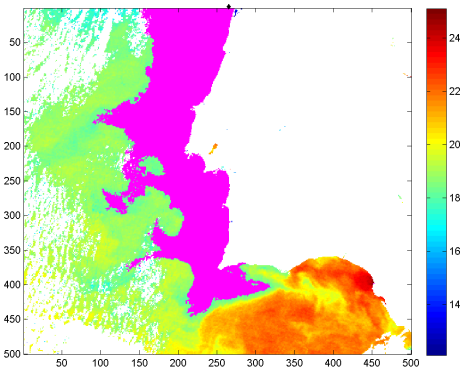

Figure B.184: 2002-07-31 OtsuVermaSRG

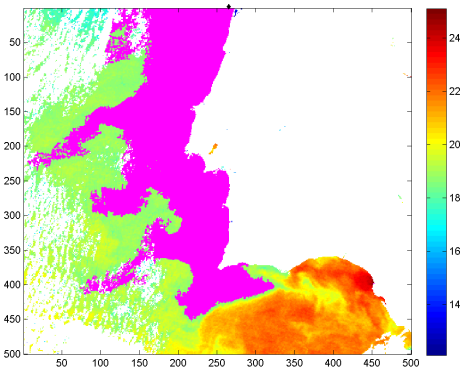

Figure B.185: 2002-07-31 MeanVermaSRG

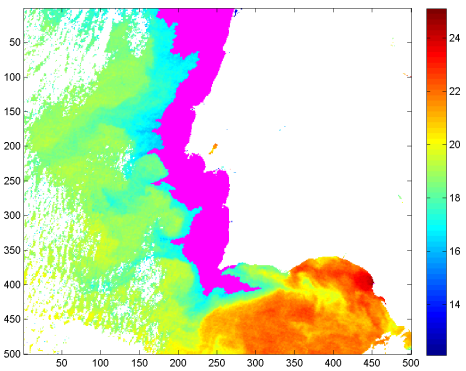

Figure B.186: 2002-07-31 ShihSRG

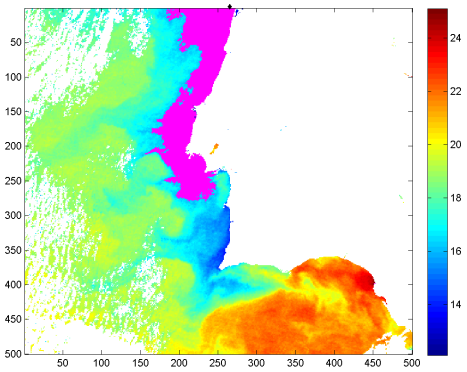

Figure B.187: 2002-07-31 GambottoSRG

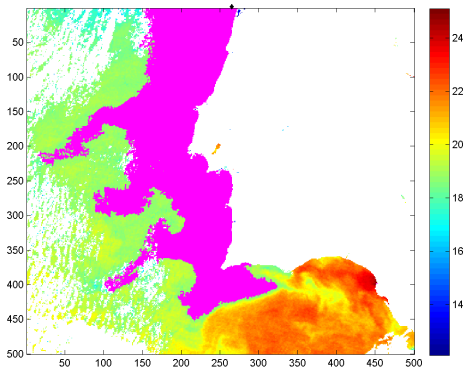

Figure B.188: 2002-07-31 ZanatySRG

B.9 SST Images from the Canary

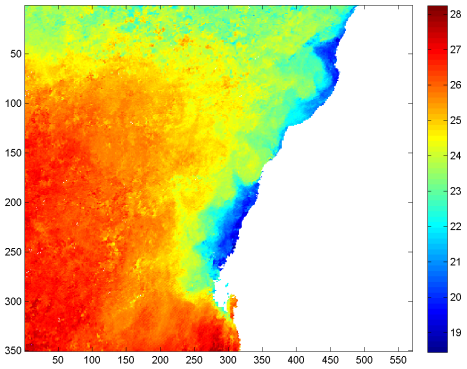

Figure B.189: *img*_262

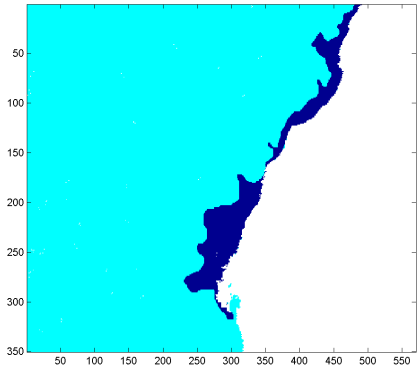

Figure B.190: *img*_262 ground-truth map

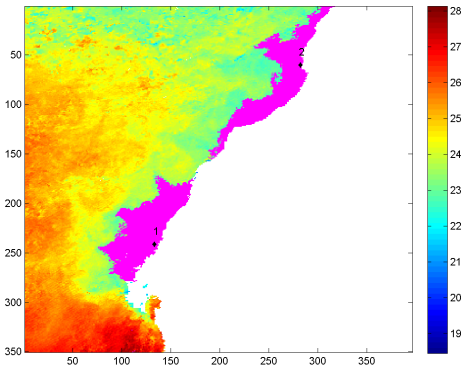

Figure B.191: *img*_262 SEC-Otsu

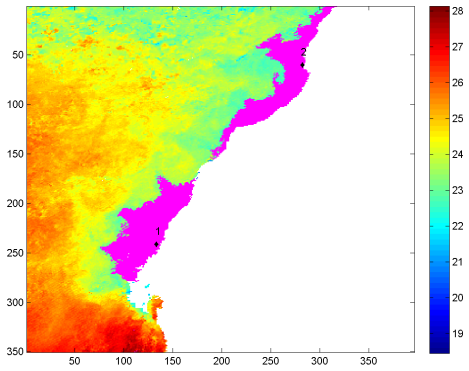

Figure B.192: *img*_262 SEC-Kittler

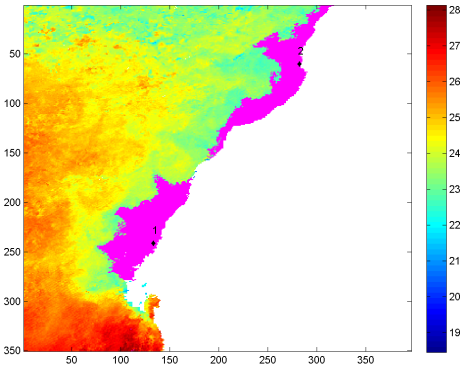

Figure B.193: *img*_262 SEC-Ridler

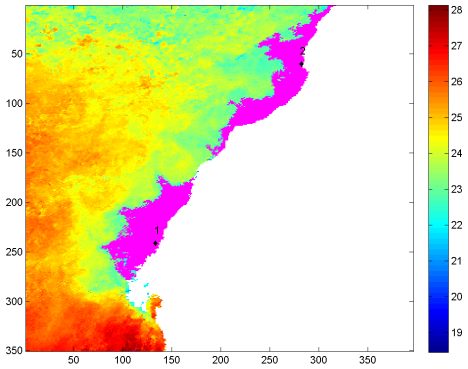

Figure B.194: *img*_262 SEC-SelfTuning

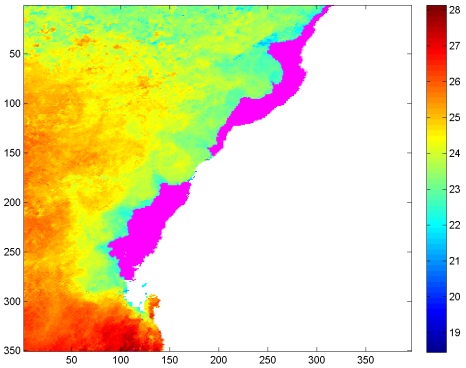

Figure B.195: *img*_262 AdamsSRG

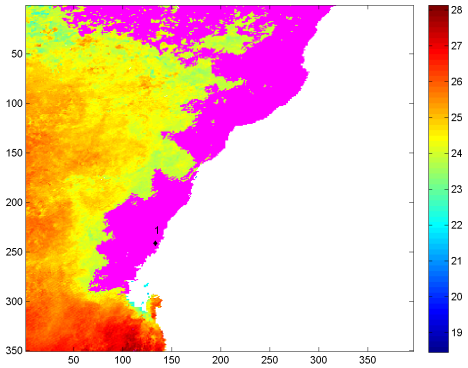

Figure B.196: *img*_262 OtsuVermaSRG

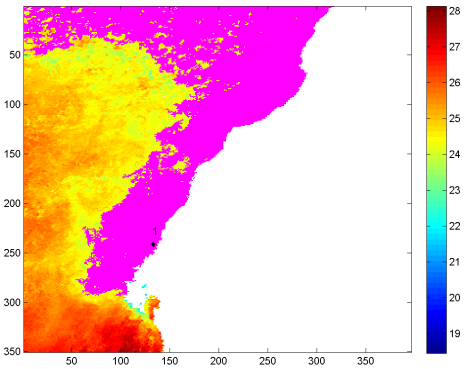

Figure B.197: *img*_262 MeanVermaSRG

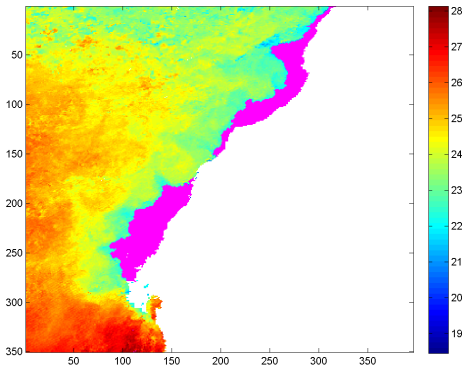

Figure B.198: *img*_262 ShihSRG

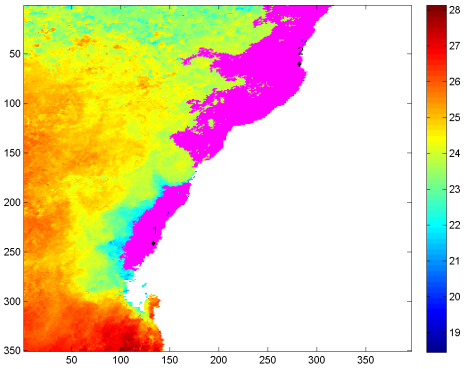

Figure B.199: *img*_262 GambottoSRG

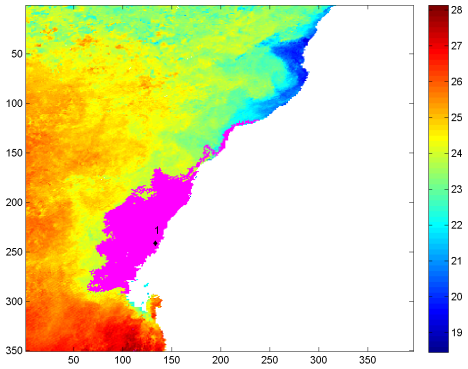

Figure B.200: *img*_262 ZanatySRG

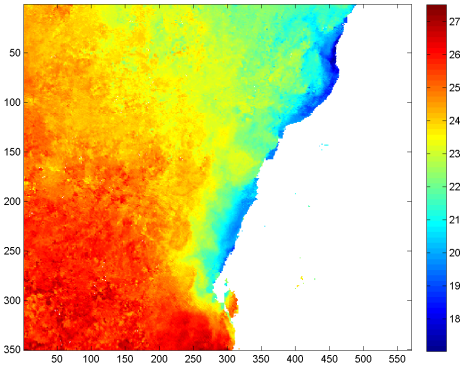

Figure B.201: *img*_336

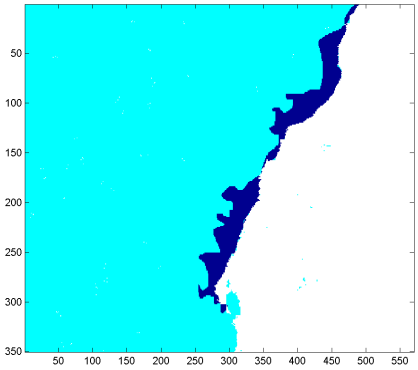

Figure B.202: *img*_336 ground-truth map

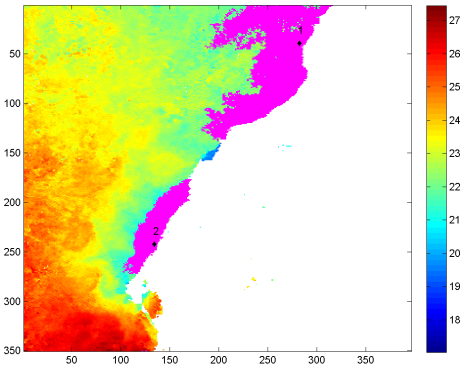

Figure B.203: *img*_336 SEC-Otsu

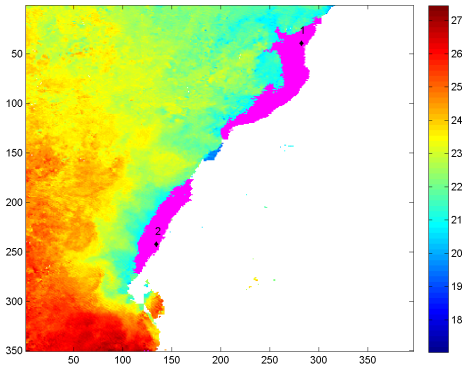

Figure B.204: *img*_336 SEC-Kittler

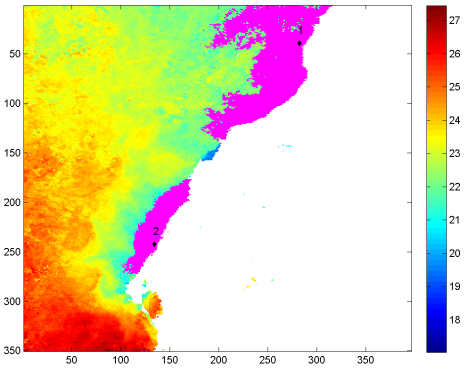

Figure B.205: *img*_336 SEC-Ridler

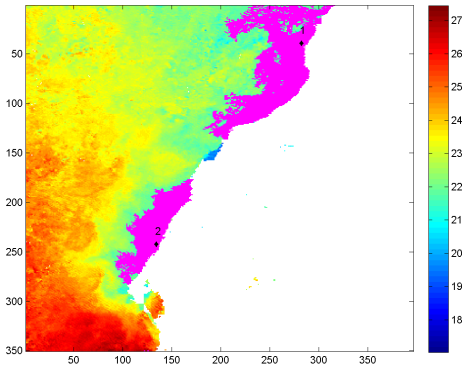

Figure B.206: *img*_336 SEC-SelfTuning

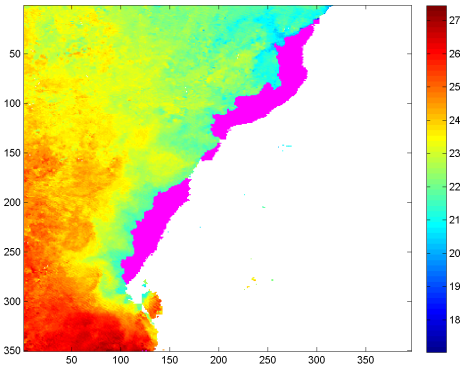

Figure B.207: *img*_336 AdamsSRG

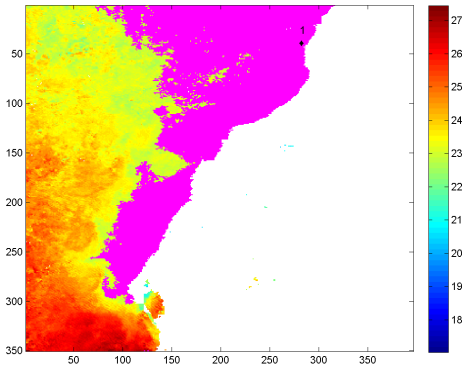

Figure B.208: *img*_336 OtsuVermaSRG

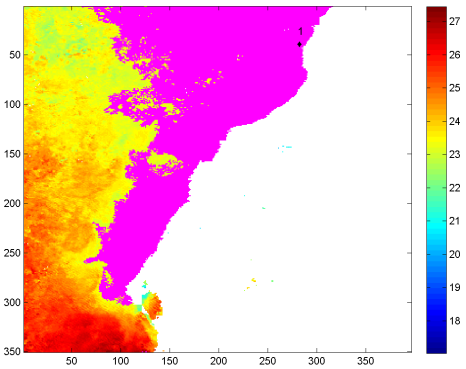

Figure B.209: *img*_336 MeanVermaSRG

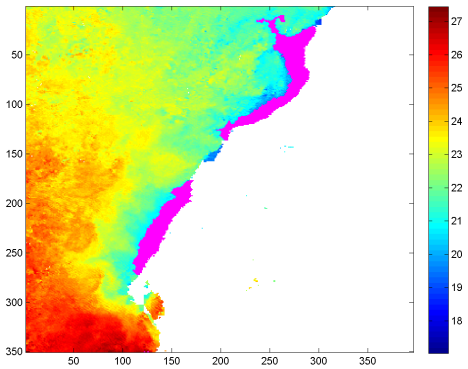

Figure B.210: *img*_336 ShihSRG

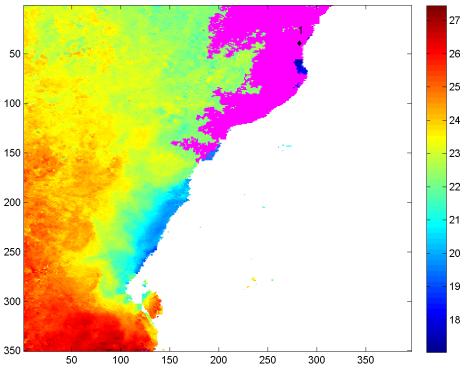

Figure B.211: *img*_336 GambottoSRG

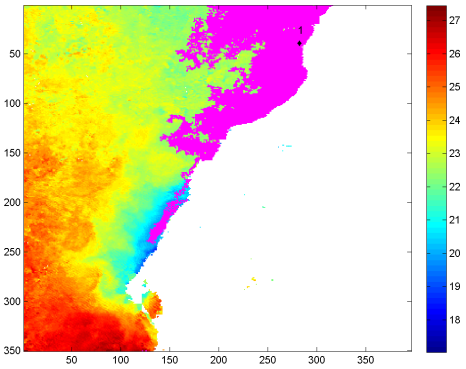

Figure B.212: *img*_336 ZanatySRG